Carbon fluxes along the European land-to-ocean continuum estimated by models and observations

Céline Gommet

THESE DE DOCTORAT

NNT : 2022UPASJ004

Carbon fluxes along the European land-to-ocean continuum estimated by models and observations

Les flux de carbone le long du continuum terre-océan Européen estimés par modèles et observations

Thèse de doctorat de l'université Paris-Saclay et de l'université Libre de Bruxelles

École doctorale n° 129 : sciences de l'environnement d'Île-de-France (SEIF)
Spécialité de doctorat : Océan, atmosphère, climat et observations spatiales
Graduate School : Géosciences, climat, environnement et planètes
Référent : Université de Versailles-Saint-Quentin-en-Yvelines

Thèse préparée dans l'unité de recherche **LSCE (Université Paris-Saclay, CNRS, CEA, UVSQ)** et dans le département, **Biogeochemistry and Earth System Modeling (Université libre de Bruxelles, faculté des sciences)**, sous la direction de **Philippe CIAIS**, docteur, la co-direction de **Pierre Regnier**, professeur, le co-encadrement de **Ronny Lauerwald**, docteur

Thèse soutenue à Bruxelles, le 17 mars 2022, par

Céline GOMMET

Composition du Jury

Sandra ARNDT Professeur, Université Libre de Bruxelles	Présidente
Sebastian SOBEK Professeur, Uppsala University	Rapporteur & Examinateur
Kristof VAN OOST Professeur, Université catholique de Louvain	Rapporteur & Examinateur
Olivier EVRARD Docteur, Université Paris-Saclay	Examinateur
Vincent THIEU Docteur, Université Pierre et Marie Curie	Examinateur

université PARIS-SACLAY

ÉCOLE DOCTORALE
Sciences de l'Environnement d'Île-de-France (SEIF)

Titre : Les flux de carbone le long du continuum terre-océan Européen estimés par modèles et observations

Mots clés : Carbone, modélisation, rivières, dégradation, Europe

Résumé : Depuis la révolution industrielle, les émissions de dioxyde de carbone (CO2) vers l'atmosphère dues à l'activité humaine ont fortement augmentées, perturbant le cycle naturel du carbone (C). Les océans et l'écosystème terrestre ont vu leur stock en C augmenter. Afin de mieux comprendre la dynamique de ces puits, il est essentiel de s'intéresser au lien antre le puits terrestre et les océans, c'est-à-dire les eaux continentales. Dans ma thèse, j'ai utilisé trois méthodes différentes afin d'améliorer notre compréhension de la dynamique du C dans le réseau hydrographique Européen et avec un focus sur le C organique dissous (COD). Tout d'abord, j'ai appliqué un modèle du système terre à l'échelle Européenne pour estimer et étudier la variabilité spatio-temporelle du transfert du C des terres jusqu'aux rivières. J'ai estimé qu'en moyenne environ 14.3 TgC par an sont transférés des terres vers le système hydrographique Européen, ce qui représente envrion 0.6% de la productivité primaire nette (NPP). J'ai observé également une importante variabilité spatio-temporelle avec un maximum en hiver et un minimum en été sauf dans les régions nordiques où le maximum a lieu au printemps lors de la fonte des neiges. Mes résultats montrent que la fraction de NPP transférée en tant que COD vers les rivières est principalement contrôlé par le ruissellement et le drainage. Ensuite, j'ai effectué des campagnes d'échantillonnage sur la Meuse afin d'étudier la biodégradation du COD. J'ai estimé un temps de demi-vie à environ 10 jours, valeur inférieure au temps de résidence de l'eau de la Meuse estimé sur tout le bassin à 24 jours, ce qui signifie que la majorité du COD aura été décomposé avant d'atteindre l'estuaire. Et finalement, sur base de la littérature, j'ai construit un budget C pour les eaux continentales pour chaque pays Européen pour évalue les imports et exports de C à travers les frontières via les rivières. J'ai estimé que sur toute l'Europe en moyenne environ 2.3 gC m-2 an-1 sont importés et 4.4 gC m-2 an-1 sont exportés entraînant un bilan net de C dans les rivières (RNCB) de 2.1 gC m-2 an-1. A l'exception des Pays-Bas, du Portugal, de l'Estonie et de l'Ukraine, tous les pays ont un RNCB positif, ils exportent plus de C qu'ils n'en importent. J'ai comparé le RNCB avec d'autres composants du budget national de C et ainsi qu'avec un autre flux latéral de C d'un pays vers un autre, les émissions liées aux échanges de récoltes de bois et d'agriculture. J'ai montré que certains pays le RNCB est du même ordre de grandeur que les échanges de récoltes et devraient donc être inclus dans les budget nationaux de C.

Title : Carbon fluxes along the European land-to-ocean continuum estimated by models and observations.

Keywords : carbon, modelling, rivers, decay, Europe

Abstract : Since the industrial revolution, emissions of carbon dioxide (CO2) due to human activities have drastically increased carbon concentration in the atmosphere, perturbing the natural cycle of carbon (C). Oceans and the land biosphere have seen their C stocks increase. In order to better understand the dynamics of those sinks, it is essential to understand the link between them, the inland waters. In my thesis, I used three different methods to improve our understanding if the C dynamics in the European inland waters, with a focus on the fate of dissolved organic C (DOC) in the river network. First I applied a land surface model at the European scale to estimate and study the spatio-temporal variability of DOC leaching from land to rivers. I estimated that around 14 TgC per year are leached into the European river network, about 0.6% of the net primary production (NPP). I observed an important spatio-temporal variability with a maximum during winter and minimum in summer with the exception of nordic region where the maximum occurs in spring after the snow melt. My results showed that the fraction of NPP that is leached as DOC in the river primarly depends on the runoff and drainage while temperature only plays a secondary role.

Secondly, I sampled the Meuse in order to study the biodegradability of DOC in the river. I estimated a half-life time around 10 days, value inferior to the calculated water residence time in the Meuse, meaning that most of the DOC will be degraded before reaching the sea. Thirdly, based on literature, I built a C budget for European inland waters at the country scale in order to evaluate the import and export of C through border via rivers. I estimated that over Europe around 2.3 m-2 per year an-1 are imported and 4.4 gC m-2 per year exported leading to a net river C balance (RNCB) of 2.1 gC m-2 per year. With the exception of the Netherlands, Portugal, Estonia and Ukraine, all countries have a positive RNCB meaning that the export more C than they import. I compared the RNCB against other components of the national C budget and against a other lateral flux of C between countries, the emissions related to wood and crop harvest trades. I showed that for some countries, the RNCB can be around the same order of magnitudes as harvest trades and thus should be included in national budget.

Remerciements

Un tout grand merci à mes promoteurs, Pierre Regnier, Philippe Ciais et Ronny Lauerwald sans qui ma thèse n'aurait pas pu se faire.

Merci à tous mes collègues qui m'ont aidé dans la réalisation de ma thèse, Steeve Bonneville, Lei Chou, Alizée Roobaert, Silvia Placitu, Haicheng Zhang, Goulven Laruelle, Sandra Arndt, Nathalie Roevros et Emily Mainetti.

Merci à ma famille, Blaise et mes amis qui m'ont soutenu pendant ces quatre années.

CONTENU

1 INTRODUCTION

1.1 GENERAL CONTEXT

Concentrations of carbon dioxide (CO_2) in the atmosphere have drastically increased due to human activities from a pre-Industrial level of approximately 277 parts per million (ppm) in 1750 (Joos and Spahni, 2008) to 410 ppm in 2019 (Dlugokencky and Tans, 2020). Until the middle of the 20th century, anthropogenic CO_2 emissions were mainly related to land use change (LUC), and in particular to deforestation (Ciais et al., 2013). Then, the fast-increasing fossil fuel (FF) emissions became the dominant source. For the last decade (2010-2019), 81% of the anthropogenic emissions were caused by FF emissions (9.6 ± 0.5 GtC yr^{-1}, Gtonnes = 10^{15} grams), the remaining 19% by LUC (1.6 ± 0.7 GtC yr^{-1}; Friedlingstein et al., 2020). Figure 1.1 shows the evolution of the sources and sinks for CO_2 fluxes since 1850, when industrialization started to have a significant effect on the global carbon (C) budget.

The growth in atmospheric CO_2 concentration directly affects the Earth climate through radiative forcing. Nowadays, we observe numerous consequences such as increase in global air temperature, modification of oceanic currents, change in precipitation patterns, deglaciation, increasing sea level, etc. (IPCC 2021). These numerous consequences are synthesized by the intergovernmental panel on climate change (IPCC 2021), which was formed in 1988 by the United Nations to gather scientific knowledge about climate change, its economic impact and risks, and to propose eventual solutions. The consequences of climate change do not only affect the environment but also have social-economic impacts such as diseases, poverty, conflicts, etc.

It is well established that only about half (5.1 ± 0.02 GtC yr^{-1}, 2010-2019) of the anthropogenic CO_2 emissions are accumulated in the atmosphere, the remainder being absorbed in roughly equal parts by the ocean (2.5 ± 0.6 GtC yr^{-1}, 2010-2019) and terrestrial ecosystems (3.4 ± 0.9 GtC yr^{-1}, 2010-2019; Friedlingstein et al., 2020). With the steady increase in anthropogenic CO_2 emissions, the different sinks (ocean uptake, land uptake and atmospheric accumulation) also increased. However, the quantification of the sinks by observational datasets and carbon models do not exactly match the total emissions, leading to an imbalance in the C cycle (BIM, -0.1 GtC yr^{-1}, 2010-2019), as represented by the purple line in figure 1.1. The budget imbalance is defined as the difference between the estimated emissions (FF and LUC) and the estimated changes in atmospheric growth rate, land and ocean uptakes according to equation 1.1 (Friedlingstein et al., 2020):

$$E_{FFF} + E_{LUC} = G_{ATM} + S_{LAND} + S_{OCEAN} + B_{IM} \quad (1.1)$$

where E_{FF} is the CO_2 emissions from fossil fuel combustion and oxidation from all energy and industrial processes, also including cement production and carbonation (GtC yr^{-1}), E_{LUC} the emissions from land use changes (GtC yr^{-1}), G_{ATM} the growth of atmospheric CO_2 concentrations (GtC yr^{-1}), S_{LAND} the terrestrial sink (GtC yr^{-1}), S_{OCEAN} the ocean sink (GtC yr^{-1}) and B_{IM} the imbalance of the budget (GtC yr^{-1}).

The imbalance (B_{IM}) highlights that there are still knowledge gaps in our understanding and quantification of the global C budget, in particular regarding the sinks. Because of their importance for the climate system and human wellbeing, it is important to improve the quantification of those sinks, their spatio-temporal variability and how they will respond to climate change, land use change, etc.

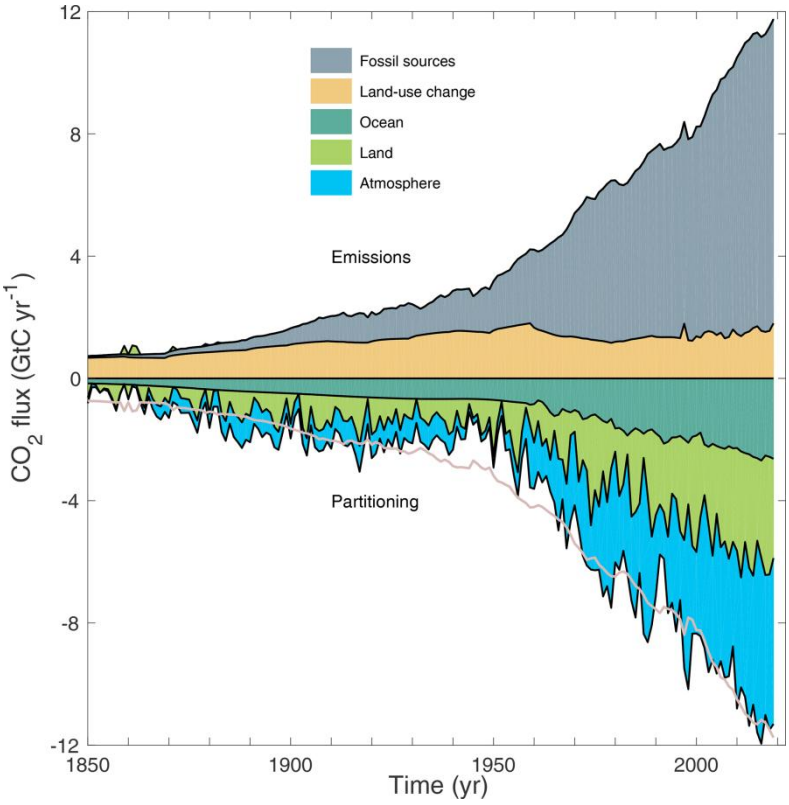

Figure 1.1 *The global carbon budget for the period 1850-2019 in GtC yr^{-1}. Sources: fossil CO_2 emissions (grey) and emissions from land-use change (brown). Sinks: the atmosphere (blue), ocean (turquoise), and land (green). The partitioning is based on nearly independent estimates from observations (for the atmosphere) and from process model ensembles constrained by data (for the ocean and the land) and does not exactly add up to the sum of emissions, resulting in a budget imbalance which is represented by the difference between the bottom pink line (reflecting total emissions) and the sum of the ocean, land, and atmospheric sinks. Figure from Friedlingstein et al., 2020.*

1.2 THE GLOBAL CARBON CYCLE

To improve the assessment and representation of C sinks, it is essential to first study the global C cycle in a more complete and detailed way. The global C cycle describes the exchange of C between the three main reservoirs of the Earth System - the atmosphere, the land, and the ocean - and is controlled by biogeochemical and physical processes operating at different spatial and temporal scales. It is important to note that here we discuss only one part of the C cycle, the short-term C cycle, where the reservoir turnover times ranges from years to millennia. The other part, the long-term C cycle, concerns the C exchanges between the short-term cycle and the large geological reservoirs of C such as carbonates rocks and organic matter in sediments where exchanges are much slower, at least at timescales longer than 10 000 years and beyond (Ciais et al., 2013). A graphical representation of the global C cycle is shown in Figure 1.2. The quantification of the fluxes typically distinguishes between the pre-industrial state and for the anthropogenic perturbation, which in this example corresponds to the decade 2000-2009.

Changes in the global C cycle are characterized by the accumulation or liberation of C in each reservoir, changes in the flux rates between them and in the C turnover times. The ecosystem C turnover time is the average time that a C atom resides in an ecosystem from entrance to the exit (Barrett, 2002) and has a typical global value of about two-three decades for the terrestrial ecosystem (23 years in Carvalhais et al., 2014). Since we aim to investigate the terrestrial C sink, we are mainly interested in the parts of the global C cycle that affect the terrestrial accumulation, and we now zoom on this specific portion of the cycle.

The terrestrial C cycle is largely controlled by the fluxes of C between the atmosphere and the terrestrial biosphere. Plants, which contribute by far the largest portion of terrestrial biomass, take up atmospheric C through the process of photosynthesis (Fig. 1.2). A part of this C is respired back by the plants to the atmosphere to gain energy needed for growth and maintenance, while the rest of the C is accumulated in the biomass as organic C (OC). The plant biomass is either grazed or burned, and when dead, is mineralized into inorganic C by heterotrophic organisms (including bacteria and fungi) and respired back to the atmosphere. In addition to the organic form of C, there are inorganic C inputs from CO_2 uptake by chemical rock weathering and dissolution of lithogenic carbonates, as well as transport of free dissolved CO_2 due to respiration in soils and wetlands.

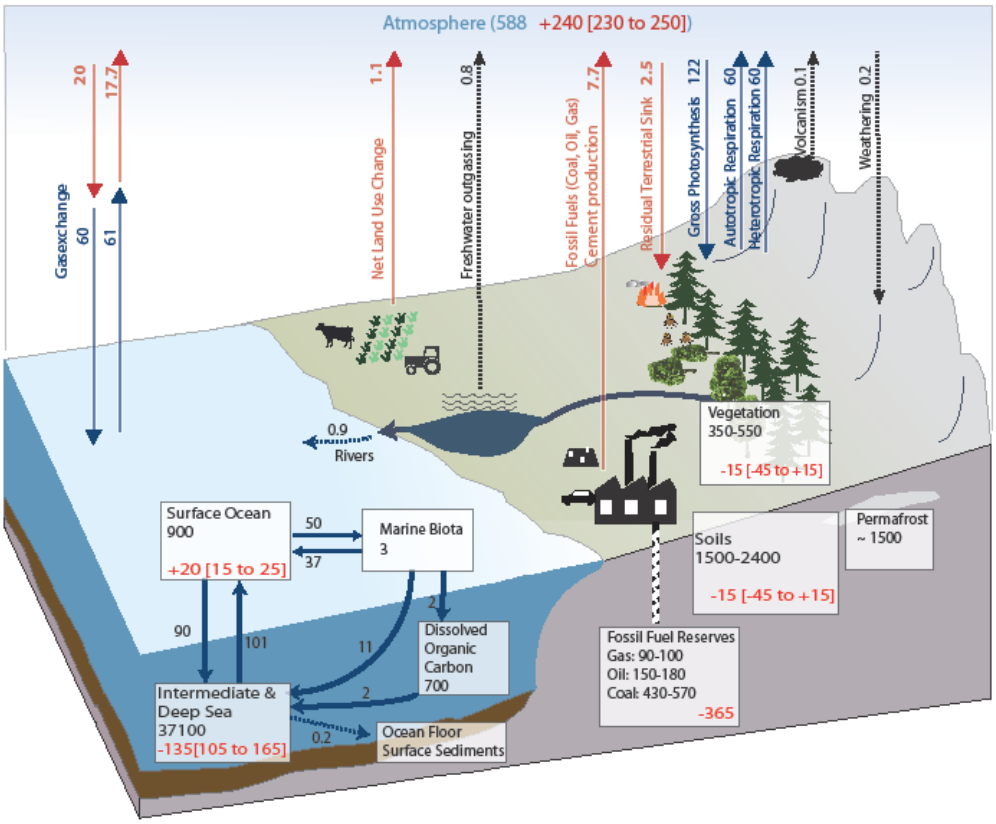

Figure 1.2 *Simplified schematic of the global carbon cycle. Numbers represent reservoir sizes (in GtC), and carbon exchange fluxes (in GtC yr^{-1}). Dotted arrow lines denote carbon fluxes between the fast and the slow carbon cycle domain (see text). Dark blue numbers and arrows indicate reservoir sizes and natural exchange fluxes estimated for the time prior to the Industrial Era. Red arrows and numbers indicate fluxes averaged over 2000–2009 time period resulting from the emissions of CO_2 from fossil fuel combustion, cement production, and changes in land use, and their partitioning among atmosphere, ocean and terrestrial reservoirs. Red numbers in the reservoirs denote cumulative changes over the Industrial Period, define here as 1750–2011. Figure from Ciais et al., 2013.*

For a long time, the exchange of C between biosphere and atmosphere through the balance of photosynthesis and respiration was assumed to control the temporal changes in terrestrial biosphere C stocks under natural conditions. Two other fluxes have also long been recognized to impact the terrestrial C stocks: fires and crop and wood harvests by humans. However, it is only a few decades ago that scientists pointed to an important missing flux in the terrestrial C balance (Schlesinger and Melack 1981; Degens et al., 1991). Indeed, part of the C in the soil is not recycled within the terrestrial realm but is instead brought to the inland water system by runoff and drainage. In addition, inland waters were usually considered as a passive pipe transferring C from land to ocean. However, in 2007, Cole et al. demonstrated that C burial and re-emission to the atmosphere are substantial components of the inland water C budget, suggesting that the amount of terrestrial C transferred to inland waters is considerably larger than the fluvial C export to the sea (Figure 1.3). These land-to-inland water C transfers remain nevertheless poorly constrained even

today, as they are still based on a budget closure using estimates of fluvial C exports to the seas, C burial in aquatic sediments, and CO_2 emissions from inland waters, all of which can be impacted by autochthonous C production within the inland water system. The flux from land to inland waters is of potential importance in the global terrestrial C budget, especially regarding the anthropogenic perturbation fluxes. If this flux is not accounted for, the net-C uptake by the plant-soil system in response to anthropogenic CO_2 emissions could indeed be significantly overestimated, the land C sink being not easily constrained from observations alone (Regnier et al., 2013).

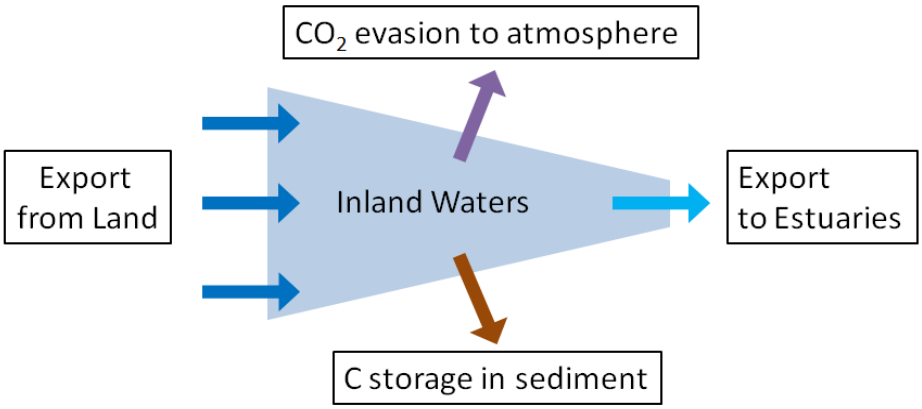

Figure 1.3 *Schematic view of the inland water C budget. The C inputs from land are significant larger than the exports to the ocean due to significant inland water outgassing and burial (modified from Cole et al. (2007).*

1.3 ESTIMATION OF THE INLAND WATER C FLUXES

1.3.1 Upscaling and empirical approaches

As for concern of the inland water C budget, the first estimation of C transport from land to ocean by rivers goes back to 1963 (Table 1.1), with an estimate by Livingstone (1963) of 0.38 PgC yr^{-1} (PgC = 10^{15} gC) of inorganic C only based on actual data of C chemistry for a still relatively small number of rivers. Almost a decade later, the first estimation for organic C was realised by Skopinstev (1971) with 0.18 PgC yr^{-1} of organic C. The same year, Garrels and Mackenzie (1971) differentiated dissolved inorganic C (DIC) and particulate (PIC) with respectively 0.37 and 0.16 PgC yr^{-1} and provided also an estimation for organic C exports of 0.3 PgC yr^{-1}. The differentiation between dissolved organic C (DOC) and particulate (POC) was realised by Kempe (1979), with respectively 0.12 and 0.066 PgC yr^{-1}, and 0.45 PgC yr^{-1} for inorganic C. Meybeck (1982) used global literature data of discharge and C concentration in the river system around the globe to estimate a C transport of 0.38 (DIC), 0.18 (PIC), 0.215 (DOC) and 0.18 (POC) PgC yr^{-1} confirming the order of magnitude of the previous assessments. Since then, estimations of global C transport in rivers have not significantly changed with values between 0.38 and 0.53 PgC yr^{-1} for organic C and from 0.21 to 0.3 PgC yr^{-1} for DIC (Degens et al., 1991; Suchet and Probst 1995; Ludwig

et al., 1996; Stallard 1998; Gaillard et al., 1999; Beusen et al., 2005; Hartmann et al., 2009).

Table 1.1 *Synthesis of C export to estuaries estimates: inorganic C (IC), organic C (OC).*

Studies	**Export to estuaries (Pg C yr^{-1})**	
Livingstone et al., 1963	0.38	IC
Skopinstev, 1971	0.18	OC
Garrels and Mackenzie 1971	0.37 0.16 0.3	DIC PIC OC
Kempe et al., 1979	0.12 0.066 0.45	DOC POC IC
Meybeck, 1982	0.38 0.18 0.215 0.18	DIC PIC DOC POC
Cole et al., 2007	0.9	Total
Bauer et al., 2013	0.9	Total

As of today, the C export to the coast is considered well constrained and estimated at global scale at 0.9 PgC yr^{-1} (Bauer et al., 2013, Drake et al., 2018). This export to estuaries comprises the river flow and the subsurface discharge from groundwater (Cole et al., 2007). By formulating a simple mass balance (import to the aquatic system equals the sum of storage in sediment, gas efflux to the atmosphere and

export to the sea), Cole et al. 2007 further estimated a total C import from the land to the aquatic system of 1.9 PgC yr^{-1} at the global scale, a value more than twice the export to the sea. Since then, values of land to river fluxes have been revised while the export to the sea have remained the same, indicating that the C accumulation in sediments and the CO_2 emissions are still not very well constrained. For instance, Tranvik et al. (2009) applied the active pipe concept to investigate the impact of lakes on the global C cycle. Their study suggested higher values for both CO_2 emissions and C storage compared to Cole et al. (2007) for a total import to inland waters of 2.4 PgC yr^{-1}.

The most recent synthesis of estimates of terrestrial C inputs to inland waters at the global scale is the one by Drake et al. 2018 (Table 1.2). In this review, the land to inland water flux was estimated using the value of 0.6 PgC yr^{-1} for the storage in sediments reported by Tranvik et al., 2009. However, in 2017 a study estimated a much lower global burial in lakes and reservoirs of 0.15 PgC yr^{-1} (range 0.06–0.25 PgC yr^{-1}), derived from a comprehensive compilation of literature data (Mendonca et al., 2017). Yet this value does not encompass all component fluxes and in particular exclude the contribution of burial in floodplains and inland deltas. The CO_2 evasion from inland waters is also subject to significant uncertainties. In particular, floodplains are an important part of the inland water C budget of tropical systems (Hastie et al., 2019 and 2021), but it is still debated as to whether those fluxes should be incorporated in inland water budgets or not. During the last decade, major progress has nevertheless been achieved regarding global CO_2 emissions from rivers and lakes, especially with respect to the contribution of small inland water bodies: streams (Raymond et al., 2013; Marx et al., 2017) and ponds (Holgerson and Raymond 2016). For large rivers, recent empirically derived estimates also account for the impact of the seasonal variability in the assessment of CO_2 evasion (Lauerwald et al., 2015). Note that autochthonous CO_2 fixation by aquatic algae and macrophytes contributes to the net CO_2 flux from water to the atmosphere and needs to be subtracted for the assessment of the allochthonous C inputs from land to inland waters. All those components put together, a present-day total C import from land to inland water can be estimated at about 3.0-4.0 PgC yr^{-1}, confirming that this massive flux is an important component of the global C budget.

Table 1.2 Synthesis of recent CO_2 evasion and burial estimates.

Studies	**CO2 evasion (Pg C yr^{-1})**	**Burial (Pg C yr^{-1})**

Cole et al., 2007	0.75	0.23
Tranvik et al. (2009)	1.4	0.6
Raymond et al. (2013)	2.2	-
Lauerwald et al. (2015)	0.65 (only large rivers)	-
Holgerson and Raymond (2016)	3.1	-
Mendonca et al. (2017)	-	0.15

Even more uncertain is the quantification of the anthropogenic perturbation on the inland water C budget. Regnier et al. (2013) investigated the global scale perturbation of the land-to-ocean C fluxes and suggested that human activities may have increased C fluxes from land to the river network by up to 1.0 PgC yr^{-1} since the pre-industrial period. This anthropogenic perturbation mostly sustains enhanced outgassing and the burial along the inland water network while the change in C exports to the sea are marginal, maybe not exceeding 0.1 PgC yr^{-1}. This view of the inland water C cycle perturbation is in line with regional studies, both observational (e.g. Lapierre et al., 2013) or model-derived (e.g. Lauerwald et al., 2020).

A different approach to a budget closure approach for determining the land to inland water C flux is direct field observations. Unfortunately, only few local and regional studies have attempted a quantification of the export from land to inland waters directly and its underlying environmental controls. For instance, Brye et al. (2001) reported a local increase in DOC leaching upon conversion of grasslands to cultivated land. Vinther et al. (2006) studied the effect of agriculture on DOC leaching and found that higher quantities of DOC are leached from crops than from bare soils. At regional scale, Kindler et al. (2010) attempted a quantification of the flux of dissolved C from land to river directly based on field observations. To carry this assessment, various land cover types across Europe were sampled and an average total C flux (DOC and DIC) of 19.4 ± 4 gC m^{-2} yr^{-1} was estimated. Integrated at the European scale, this value corresponds to a leaching flux of around 0.08 PgC yr^{-1} or about 1-5% of the global C fluxes from land to river estimated from the budget closure approach. However, due to the scarcity of observational data and strong methodological limitations to carry the extrapolation, it remains extremely challenging to quantify the C leaching from soil to river based on empirical methods only.

1.3.2 Process-based modelling

A complementary approach to observational studies consists in using process-based models to constrain the regional-scale C budget at the land-inland water interface. Among those, land surface models (LSMs), the land component of Earth system models, are suitable tools because they represent the terrestrial C cycle and simulate water and energy balances. LSMs allow to elucidate the different processes driving the transport and transformations of C and to test how the C fluxes will respond to future climate and land use change.

In the past, no LSMs explicitly included a representation of the terrestrial C losses to the inland water network. Recent progress in this area has however been achieved over the last decade, with novel LSM schemes that represent the export of C from soils to the river network (Smith et al. 2010; Kicklighter et al. 2013; Nakhavali et al., 2018), and in some cases even the transport and cycling of these terrestrial C loads along the river network down to the coast (Tian et al., 2015; Lauerwald et al., 2017). Constructing such a representation of the river C budget that can then be compared to observational estimates of leaching fluxes, C concentrations in river and soil water, and process rates from empirical studies allows us to better constrain the response of fluvial C fluxes to environmental drivers, whether natural or anthropogenic. Process based models are also powerful tools to extrapolate in space and time, a critical advantage taken the scarcity of direct observations. In addition to present-day simulations, they can also simulate trends over the historical period and carry projections into the future, as well as conduct attribution analyses to identify the dominant drivers of changes (e.g. climate, atmospheric composition and LU changes). These LSMs enabled for land-to-inland water fluxes have so far mostly been applied to simulate the coupled terrestrial-inland water C cycle in different regions across the globe. In what follows, we summarize the main characteristics of these LSMs as well as the key findings of these modeling studies.

In 2015, Tian et al. published a seminal study on carbon fluxes from eastern North America to the Atlantic Ocean using the Dynamic Land Ecosystem Model, Version 2.0 (DLEM 2.0), an explicit, process-based model that couples vegetation dynamics to the cycles of water, carbon, nitrogen, and phosphorus. Their study encompassed DIC, POC and DOC fluxes in the river network, including the contribution from bedrock weathering. Tian et al. investigated the spatial and temporal variability due to climate, CO_2 fertilization, land-use change and management and showed that riverine DIC had significantly decreased from 1901 to 2008 while DOC and POC fluxes showed no significant trend.

ORCHILEAK, a new branch of the LSM ORCHIDEE (Organizing Carbon and Hydrology in Dynamic Ecosystem) (Krinner et al. 2005), was developed by Lauerwald et al. (2017) to simulate terrestrial DOC and soil CO_2 leaching fluxes. ORCHILEAK was first

calibrated and applied to the Amazon basin to estimate the fluxes from C fixation by the vegetation to the C exports to the sea, including their historical and future evolution. Hastie et al. (2019) extended the study by improving the representation of the floodplain dynamics in the Amazon basin. With this new model, Hastie et al. found that around 12 % of the terrestrial NPP was lost to the river–floodplain system on average (both as DOC and CO_2), but that this leaching was highly variable at the interannual timescale. In a recent modeling study, Lauerwald et al. (2020), found that CO_2 emissions from the river-floodplain network of the Amazon basin could increase by 23% and the export to the coast by 27% from present day till 2100 under climate scenario RCP 6.0 (Meinshausen et al., 2011). ORCHILEAK was then applied to another tropical basin, the Congo, to estimate the historical and future changes in lateral C fluxes and the underlying drivers responsible for these changes (Hastie et al., 2021). It was found that around 4% of the Congolese tropical forest NPP is leached from soils to the LOAC. Furthermore, the results suggested that CO_2 evasion and C export to the coast have already increased by around 25% from 1861 till today. Under climate scenario RCP 6.0, the evasion and export fluxes are predicted to further increase by 79% and 67% by the end of the century, respectively. The ORCHILEAK model has also been applied to a high-latitude basin, the Lena (Bowring et al., 2019), for which it was found that only about 1.5% of the boreal/arctic NPP is exported to the LOAC. More recently, POC transfers have also been implemented in ORCHILEAK, with a first application to the Rhine catchment (Zhang et al., 2020) and another underway at the scale of the entire European river network (Zhang et al., submitted).

Another LSM, JULES (Joint UK Land Environment Simulator) has been upgraded with the simulation of DOC fluxes (JULES-DOCM) in the soil system. The model has been applied at the global scale, after calibration using a large collection of site data (n = 109) across different ecosystems (Nakhavali et al., 2020). JULES-DOCM provides a representation of DOC production in terrestrial ecosystems based on the incomplete decomposition of organic matter, DOC decomposition within the soil column, and DOC export to the river network via leaching (Nakhavali et al., 2018). The simulations led to a global terrestrial DOC leaching flux of 0.28 ± 0.07 Pg C y^{-1}, corresponding to about 0.3% of the global terrestrial NPP.

The TRIPLEX-HYDRA model (TRIPLEX-hydrological routing algorithm) simulates the global fluvial C transport focusing on the production and consumption of non-anthropogenic DOC leached from soil to river ecosystems (Li et al., 2019). This model was validated against data for 26 major rivers across the globe. The DOC yields to the river were well captured and the results were able to explain more than 50% of the temporal variability in DOC fluxes. Furthermore, Li et al. (2019) retraced the evolution of DOC yields and suggested a slight global decrease in riverine DOC export flux to the sea from 1951 to 2015. This decrease in DOC fluxes was mostly located in

intermediate and high latitudes while in the tropical regions, DOC fluxes increased.

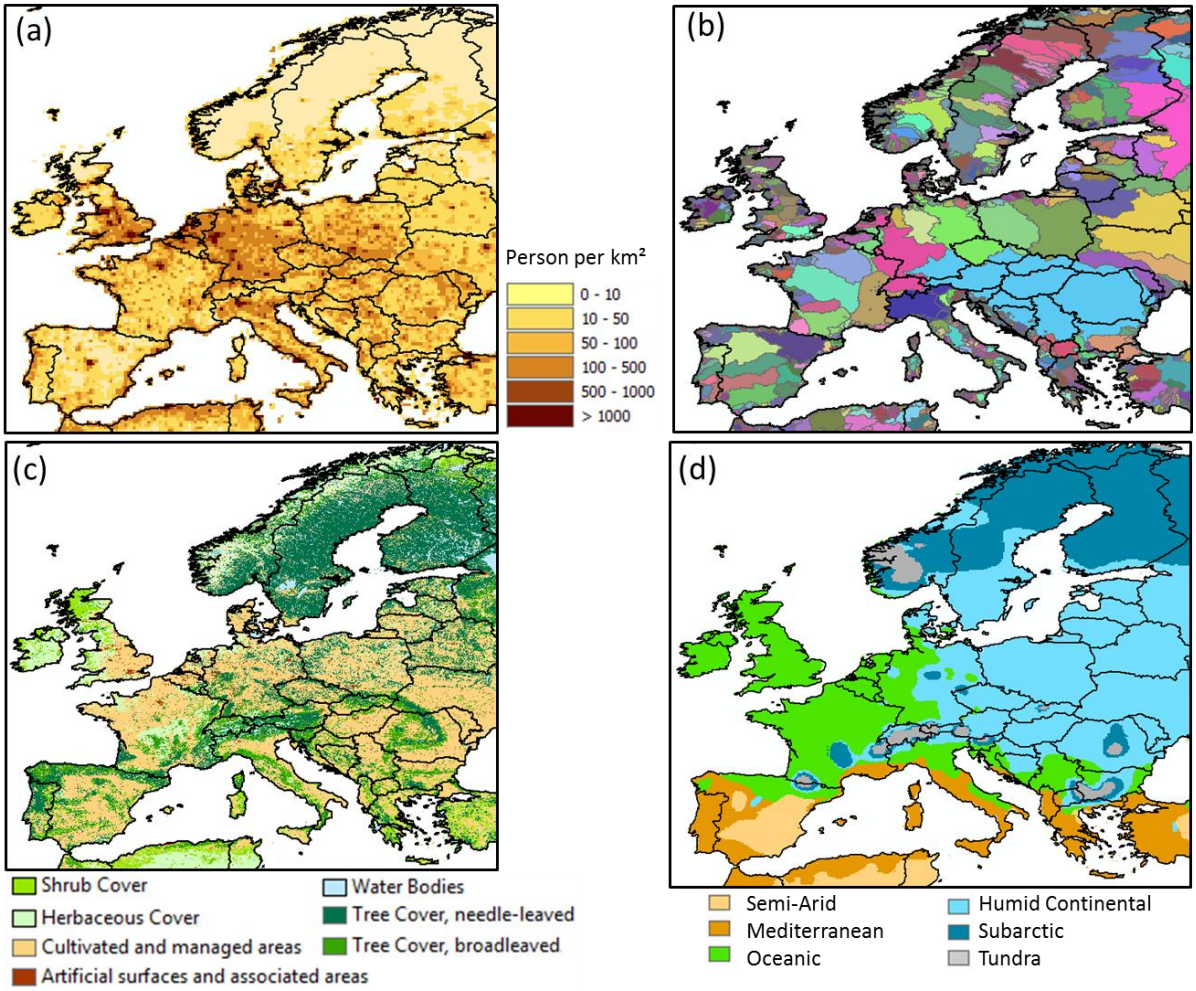

Figure 1.4 *Geographical characteristics of the European domain which are key to this work (a) population density (person per km^{-2}) ; (b) delineation of European catchments; (c) dominant land cover types (Adapted from the Global land cover 2000, Hartley et al., 2006); (d) climatic regions according to the Koppen-Geiger classification (Peel et al., 2017).*

So far, no modeling study has addressed specifically the terrestrial-inland water C budget of the European region. LOAC fluxes in Europe are expected to be quite different compared to those of tropical and boreal ecosystems. Firstly, because Europe is heavily urbanized (fig 1.4a) and has been subject to tremendous land management over the past centuries. Secondly, the European domain is fragmented in many catchments of small to intermediate size, as shown in Fig 1.4b. Thirdly, many land-cover types are found in Europe (grassland, cropland, boreal and temperate forests) with a large proportion (about 42%) dedicated to agricultural activities (fig.1.4c). Furthermore, compared to tropical and boreal regions characterized by one type of ecosystem and climate, Europe experiences a patchwork of environmental conditions, with boreal forests and boreal climate in the North, a temperate climate (oceanic and continental) for its major part and a Mediterranean and semi-arid

climate in the South (fig 1.4d). As a result, the terrestrial-inland water C budget of Europe is expected to show significant spatio-temporal variability across climate zones, national boundaries, and individual catchments.

1.4 THE EUROPEAN CARBON BUDGET

With climate change and environmental degradation, constraining the C budget for Europe has become a priority of the European Commission (EC). The EC presented the European Green Deal at the end of 2019 which consists in a set of policies to transform the EU into a climate neutral zone by 2050, including an intermediate step by 2030 which targets a reduction in greenhouse gases (GHG's) emissions by 55%. To be able to institute new policies, the EC needs to gather knowledge from various organizations, including research institutes that can help monitor the GHG's budget of Europe and conduct future scenarios of emission reduction. Several ongoing projects aim to answer these needs. One of them, the project VERIFY funded by the EC's Horizon 2020 program, develops a system for monitoring and verification of greenhouse gas emissions based on land, ocean and atmospheric observations. The project focuses on the three major greenhouse gases responsible for global warming: carbon dioxide, methane (CH_4), and nitrous oxide (N_2O).

However, at the European scale, policy relevant GHG budgets generally ignores the C fluxes in inland waters. The inland water C budget encompasses the inputs from uplands to inland waters and the exports of C to estuaries and further downstream to shelf seas, the CO_2 (and CH_4) emissions from rivers, lakes and reservoirs as well as the C burial in sediments of lakes and reservoirs. Several studies already suggested that these fluxes may nevertheless be significant for the European C balance. One important reason to focus on "lateral" fluxes though the river network relates to the need to reconcile methodologies to establish regional C budgets. Indeed, regional C budgets can be established via two approaches: "top-down" estimates from atmospheric inversions and "bottom up" estimates based on C stocks inventories, process- and data-oriented models. These two methods will however diverge due to the existence of lateral fluxes at the land surface and from land to the ocean, which displace C from one region to another. Consequently, the CO_2 flux diagnosed by an inversion is not equal to the change of stock in a region (Ciais et al., 2020). Therefore, estimating and understanding lateral fluxes through rivers is a necessary step for the comparison of "bottom up" and "top down" approaches.

The first assessment of the role of lateral C fluxes for the European C budget was performed by Ciais et al. (2008). This study not only addressed the role of riverine C transport from land to the ocean but also the contribution of lateral fluxes from trades of food, feed and wood as well as those from non-CO_2 compounds laterally transported in the atmosphere on the European C balance. In this study, the total lateral CO_2 fluxes outside of the EU-25 domain (25 EU countries and their associated

coastal seas) was estimated at 165 TgC yr^{-1}, of which 15% (about 25 TgC yr^{-1}) was attributed to riverine transport. This value was later used by several studies to build improved C budgets for Europe. For instance, Schulze et al. (2010) used this assessment in their own C budget for geographic Europe (10^7 km^2) and also applied the 141-178 TgC yr^{-1} C flux (DIC+DOC+POC) exported from land to inland waters (about 6 times larger than the export to the sea) reported by Ciais et al. (2008). In 2012, Luyssaert et al. compiled a new GHG balance for a smaller European region (EU-27 plus Albania, Bosnia and Herzegovina, Croatia, Iceland, Kosovo, Macedonia, Norway, Serbia, Montenegro and Switzerland, for a total surface area of around $5x10^6$ km^2) for the period 2001-2005 based on (1) inversion-derived net land to atmosphere GHG fluxes and (2) Eddy-covariance and inventory-based net land to atmosphere GHG fluxes (figure 1.5). This budget was again closed using the lateral transport of C (excluding DIC) from terrestrial ecosystems to freshwater ecosystems of 72 TgC yr^{-1} and an export to the sea of 36 TgC yr^{-1} estimated by Ciais et al. (2008) (note that the domain covered by Luyssaert et al. (2012) is not the same as in Ciais et al. (2008)). This figure shows the importance of the leaching fluxes for the terrestrial C balance of Europe because it represents about 7.5% of the net ecosystem exchange, the difference between NPP and soil heterotrophic respiration.

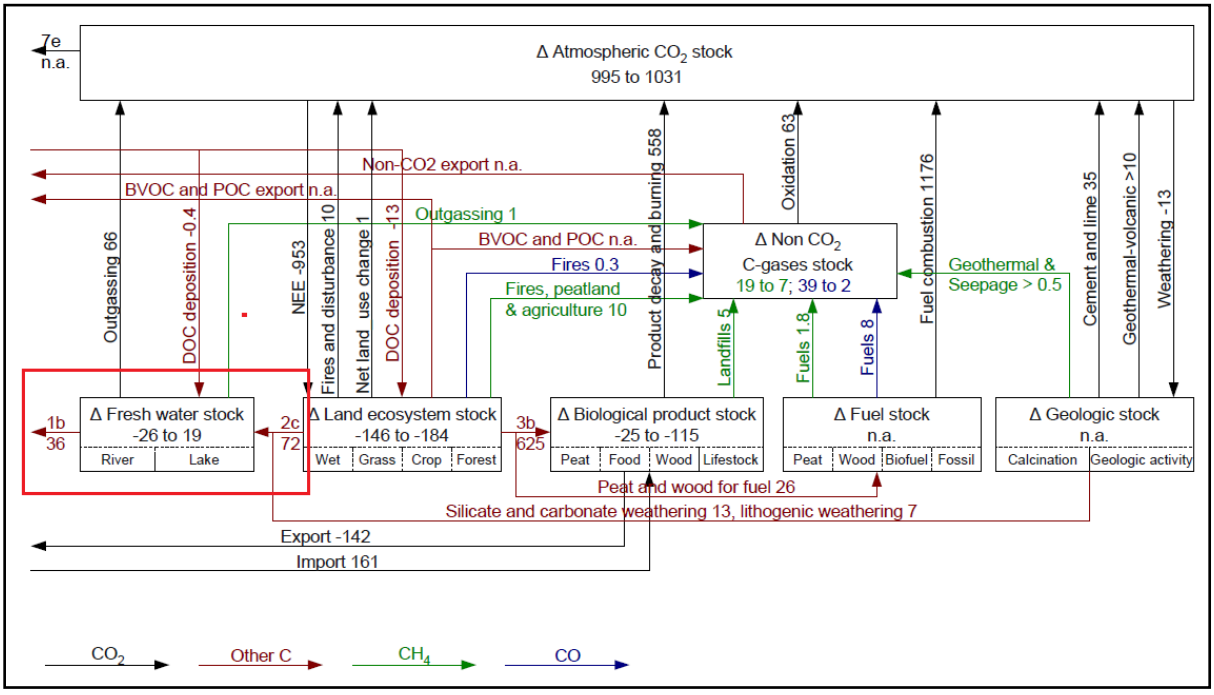

Figure 1.5 *European C-balance for CO_2, CH_4, CO and other C-compounds (Tg C yr^{-1}) based on diverse data sources including atmospheric inversions, flux measurements and stock inventories. Black arrows indicate CO_2 fluxes, green CH4 fluxes, blue CO and red indicates other C-fluxes. Labeling: 1b is the lateral transport to the ocean; 2c is the lateral transport from land to freshwater (excluding DIC); 3b is the peat, wood and crop harvest + grazing for other uses than fuel production; 7e is the net atmospheric CO_2 transport to adjacent regions. (Figure from Luyssaert et al., 2012). The portion of the*

budget highlighted by the red box corresponds to the contribution of inland waters to the terrestrial C balance.

In all the above budgets, the export from terrestrial ecosystems to the river network was calculated by budget closure based on export to estuaries, CO_2 emissions from rivers and lakes to the atmosphere and C burial in sediments. However, a budget closure approach does not provide much information about the spatial and temporal variability in lateral C fluxes, about the potential drivers of C leaching from terrestrial ecosystems, and about the fate of the various C pools within the river network. From a policy relevant perspective, the European C budget with river C fluxes included has not yet been downscaled to the country level despite its relevance for national C inventories. Those limitations can be answered by combining new LSMs, process-based experiments and geostatistical approaches and form the cornerstone of my PhD goals.

1.5 RESEARCH QUESTIONS

The purpose of my thesis is to better understand the role of the river network in the European C cycle. Previous research has established the potential role of aquatic C fluxes in the terrestrial C cycle. However, there are still major gaps regarding C fluxes to and within the river network, especially regarding their spatial and temporal variability. In this thesis, I address those gaps using three distinct methodological approaches. Because we build on the existing modeling tool ORCHILEAK (that ignored POC at the start time of my thesis), I put more emphasis on the fate of terrestrial DOC in this work:

- Physically-based modeling to advance our quantitative understanding of the DOC exports from land to river;
- Field observations and laboratory experiments to investigate the degradation of C within the river system, focusing here again on DOC;
- Budget analysis based on literature data and geostatistical tools to assess how national C budgets are impacted by lateral C fluxes (DOC, DIC and POC) through the European river network.

Chapter 2

"Spatio-temporal patterns and drivers of terrestrial Dissolved Organic Carbon (DOC) leaching to the European river network."

The first step consists in using a modeling approach to estimate the DOC transfers at the terrestrial-aquatic system's interface for Europe. The transfer of C from land to the river network is simulated with the LSM ORCHILEAK (Lauerwald et al. 2017). I then investigate the impact of this lateral C transfer on the terrestrial C budget in Europe. To my knowledge, only one study (Kindler et al., 2011) estimated the soil DOC leaching flux based on runoff and direct observations of DOC concentrations in the soil water for various locations across Europe. I thus use this study to evaluate the simulated leaching fluxes, along with a larger set of observational data of DOC fluxes at river mouths. Making full use of the capabilities of the ORCHILEAK model, I assess in detail the spatio-temporal patterns in DOC leaching, its environmental controls, and its impact on the European terrestrial C budget. I investigate how specific climate zones in Europe differ with regard to seasonality in DOC leaching fluxes, which are hypothesized to be controlled by hydrology, litter fall and temperature effects on litter and SOC decomposition. I further quantify the effect of these controls in the different climate zones of Europe. Finally, I strive to find out in which climate zone DOC leaching affects the terrestrial C budget the most. The key research questions addressed in this chapter are:

- *At the European scale, what quantities of DOC are leached for the soil to the river network and how does it vary in time and space?*
- *What are the controlling factors of the spatio-temporal distribution of DOC leaching and how do they impact the leaching fluxes?*

Chapter 3

"Controlling factors of the degradation kinetics of dissolved organic carbon: An experimental study in the Meuse catchment"

Once in the river system, part of the DOC degrades and is released back to the atmosphere as carbon dioxide. In ORCHILEAK, the model used in the first chapter, C degradation is described using two distinct pools, one "labile" and one "refractory", each following linear kinetics with their own decay constant. These decay constants are identical within a catchment and for all catchments within the European domain. This is obviously a simplification and this chapter aims to investigate the temporal and spatial variability of the degradation kinetics within a given catchment under the influence of different land-use types (The Meuse in France and Belgium). To achieve this goal, I calculate DOC decay rate constants according to three different models (one pool following a first order kinetic, two pools with one following a first order kinetic and the other being non-degradable, and the reactive continuum model). I first compare the ability of each model formulation to capture the DOC degradation kinetics. Then, I investigate whether DOC degradability, as represented by the values in kinetic rate constants, is correlated to land use, seasonality and/or organic matter

quality. This chapter revolves around the following research questions:

- *Do we observe any spatial or temporal patterns in DOC decay rate constants within the Meuse catchment?*
- *How do the land use type, the seasons and the DOM quality influence DOC decay rate constants in the river network?*
- *How can we best represent DOC degradation in a model?*

Chapter 4

"Lateral carbon fluxes in Europe: quantification and implication for national carbon budgets."

In the fourth chapter, I quantify the riverine C fluxes at the European scale and investigate how those fluxes can be integrated in the overall C budget, with a focus on national C budgets. Because rivers cross borders, C is transferred "laterally" from one country to another, and those fluxes are thus important in the re-assessment of national C inventories. Gathering data from the literature, I develop and apply a mass balance approach relying on geostatistical tools to estimate riverine C imports and exports through the borders of each country of the EU-27+UK. Hypothesizing that those lateral transfers are significant at the country scale, I establish a methodology that allows for including them in national inventories and address the following research questions:

- *How much carbon is imported and exported through countries via the European river network?*
- *How important are the riverine carbon fluxes compared to the lateral carbon fluxes associated with wood and crop harvesting and to other components of the national greenhouse gas budgets such as direct anthropogenic emissions and land use change?*
- *Should lateral C flows through rivers be accounted for in national C budgets?*

Chapter 5 closes this thesis. It comes back to the above questions and summarizes the main findings of my research. Finally, we conclude by identifying several priorities for future research to be conducted within the next 5-10 years.

2 SPATIO-TEMPORAL PATTERNS AND DRIVERS OF TERRESTRIAL DISSOLVED ORGANIC CARBON (DOC) LEACHING TO THE EUROPEAN RIVER NETWORK.

Gommet, C., Lauerwald, R., Ciais, P., Guenet, B., Zhang, H., and Regnier, P.: Spatiotemporal patterns and drivers of terrestrial dissolved organic carbon (DOC) leaching into the European river network, Earth Syst. Dynam., 13, 393–418, https://doi.org/10.5194/esd-13-393-2022, 2022.

Abstract

Leaching of dissolved organic carbon (DOC) from soils to the river network is an important component of the land carbon (C) budget. At regional to global scales, its significance has been estimated through simple mass budgets, often using multi-year averages of observed fluvial DOC fluxes as proxy of DOC leaching due to the limited availability of observations of the leaching flux itself. This procedure leads to a systematic underestimation of the leaching flux because of the decay of DOC during fluvial transport. Moreover, this procedure does not allow revealing spatio-temporal variability in DOC leaching from soils, which is vital to better understand the drivers of DOC leaching and its impact on the local soil C budget. In this study, we use the land surface model ORCHILEAK to simulate the terrestrial C budget including leaching of DOC from the soil and its subsequent reactive transport through the river network of Europe. The model performance is evaluated not only against the sparse observations of soil DOC leaching rate, but also against the more abundant observations of fluxes and reactivity of DOC in rivers, providing further evidence that our simulated DOC fluxes are realistic. The model is then used to simulate the spatio-temporal patterns of DOC leaching across Europe over the period 1972–2012, quantifying both the environmental drivers of these patterns as well as the impact of DOC leaching on the land C budget. Over the simulation period, we find that, on average, 14.3 TgC yr^{-1} of DOC is leached from land to European rivers, which is only about 0.6% of the terrestrial net primary production, a fraction significantly lower than that reported for tropical river networks. On average, 12.3 TgC yr^{-1} of the leached DOC is finally exported to the coast via the river network, and the rest is respired during transit. DOC leaching presents a large seasonal variability, with the maximum occurring in winter and the minimum in summer, except for most part of the Northern Europe where the maximum occurs in spring due to the snow melt. DOC leaching rate is generally low in warm and dry regions, and high in cold and wet regions of Europe. Furthermore, runoff, and the ratio between runoff from shallower flow paths vs. deep drainage and groundwater flow, are the main drivers of the spatio-temporal variation of DOC leaching. Temperature, as a major control of DOC production and decomposition rates in the soils, only plays a secondary role.

2.1 INTRODUCTION

Terrestrial ecosystems are an important carbon sink as they absorb about one fourth of anthropogenic CO_2 emissions and store these C in plant biomass and soil carbon pools (Friedlingstein et al., 2020). This terrestrial C sink mitigates the growth rate of atmospheric CO_2 concentration and thus plays an important role in regulating climate change (Ciais et al., 2013). However, the efficiency of that sink is partly alleviated by the permanent, lateral leaching of C from soils, through the river network down to the ocean (Regnier et al., 2013). An accurate understanding of lateral C fluxes through the river network is thus necessary to better understand global C cycling and to inform policies of climate change mitigation (Le Quéré et al., 2018).

The identification of riverine C transfers as a key component of the continental C budget constituted an important paradigm shift in our understanding of the global C cycle (Cole et al., 2007). More recently, riverine C cycling was also shown to be affected by anthropogenic perturbation and thus to be an element of the anthropogenic CO_2 budget (Regnier et al., 2013; Le Quéré et al. 2015). Anthropogenic perturbations of riverine C fluxes are manifold and comprise direct impacts through changing C and nutrient inputs following land-use change and agricultural activities, wastewater discharge, and hydraulic management (e.g. Tian et al., 2015; Lauerwald et al., 2020; Hastie et al., 2021; Maavara et al., 2017). There are also indirect impacts following climate change and changes in atmospheric composition. Together, these perturbations have accelerated the turnover of C along the terrestrial-inland water continuum. The terrestrial C sink, which is classically estimated without taking into account the C exports through the river network, is thus generally overestimated (Regnier et al., 2013; Lauerwald et al., 2020).

The integration of riverine C transfers into the terrestrial C budget requires the quantification of the amount of C lost from soils to the river network. Due to the scarcity of observational data, this flux is not easy to estimate based on empirical methods. At global scale, this flux was constrained through budget closure based on estimates of riverine C exports to the coast and estimates of C losses to the atmosphere and aquatic sediments during transport. The existing global estimates of these soil C exports to the river network, as synthesized by Drake et al. (2018), range from 1.1 to 5.1 PgC yr^{-1} – a huge uncertainty range reflecting the limitations of empirical estimation approaches and the paucity of underlying data. Over the past decade, a new generation of land surface models (LSMs) have been developed, which represent the export of C from soils to the river network, and in some cases even the transport and cycling of these terrestrial C loads along the river network down to the coast (Smith et al. 2010; Kicklighter et al. 2013; Tian et al., 2015; Lauerwald et al., 2017; Nakhavali et al., 2018). With the exception of the study by Tian et al. 2015, all these studies focus on the lateral export of dissolved organic C (DOC) which is a product of the incomplete decomposition of plant litter and soil organic carbon (SOC). These

mechanistically based models allow to predict the leaching of DOC in unmonitored regions and to assess the spatial and temporal variability which, to date, can only be poorly resolved by empirical methods. Moreover, these approaches link the C exports from soils to the river network to the terrestrial C cycle, and thus allow to directly assess the role of these C exports in the terrestrial C budget, its perturbation through land use, land use change and changes in climate and atmospheric chemistry, and its impact on the terrestrial sink for anthropogenic CO_2 emissions.

In this study, we use the LSM ORCHILEAK (Lauerwald et al. 2017), a branch of the IPSL-LSCE LSM ORCHIDEE (Krinner et al. 2005), to quantify the DOC leaching from soils and its effects on the terrestrial C budget in Europe. ORCHILEAK not only simulates the vertical C cycling between vegetation, soils and atmosphere in response to climate, atmospheric CO_2 concentrations, and land use change, but also represents the lateral exports of DOC from soils to the river network as well as the reactive transport of that DOC through the river network. To our knowledge, only one study (Kindler et al., 2011) has estimated the soil DOC leaching flux based on runoff and direct observations of DOC concentrations in the soil water for various locations across Europe. Thus, this empirical assessment will be used for evaluating the simulated DOC leaching fluxes in this study. Further, we evaluate simulated against observed riverine DOC fluxes, which are obtained from different water quality surveys and scientific publications. Assuming a realistic representation of DOC reactivity in the river network, which is to be evaluated against observations as well, this model-data comparison of riverine DOC fluxes represents a valuable and additional possibility to assess the validity of simulated soil DOC leaching.

So far, ORCHILEAK has been successfully tested and applied on large, near-natural river systems such as the Amazon (Lauerwald et al. 2017, Hastie et al. 2019, Lauerwald et al. 2020), the Congo (Hastie et al. 2021) and the Lena Rivers with a version also including some specific permafrost related mechanisms (Bowring et al. 2019, 2020). In this study, for the first time, ORCHILEAK is applied to, and evaluated for, the European river network which is subject to direct impacts of agricultural land use, in contrast to more natural river basins. For this reason, we devote special attention to manure application as an anthropogenic non-point source of DOC to the river network, while we assume that for the period of simulation (1979-2012), due to the quality of sewage water treatment, anthropogenic point sources of DOC are now negligible for most parts of Europe. Moreover, as shown for instance by Meybeck (1986), DOC from sewage is highly labile and only affects concentration within short distances downstream of water processing plants. Avoiding observational data from sites that are known to be directly impacted by sewage inputs, we are able to evaluate model performance with regard to fluvial transfers of soil derived DOC, which is the focus of our study.

Making full use of the capabilities of the ORCHILEAK model, we study in detail the

spatio-temporal patterns in DOC leaching and its quantitative contribution to the terrestrial C budget across Europe. We investigate how specific climate zones in Europe differ with regard to seasonality in DOC leaching fluxes, which are hypothesized to be controlled by hydrology, litter fall and temperature effects on litter and SOC decomposition. We will further try to quantify the effect of these controls in the different climate zones of Europe. Finally, we strive to find out in which climate zone DOC leaching affects the terrestrial C budget the most.

2.2 METHODOLOGY

2.2.1 ORCHILEAK

2.2.1.1 Model overview

ORCHILEAK (Lauerwald et al., 2017) is a branch of the model ORCHIDEE (Organizing Carbon and Hydrology in Dynamic Ecosystems) (Krinner et al., 2005), the land surface component of the Institut Pierre-Simon Laplace (IPSL) Earth system model (ESM). ORCHIDEE simulates energy, water and C fluxes between the atmosphere and the land at a global scale. This LSM is based on four sub-modules. The first one, SECHIBA, simulates the energy budget (energy, carbon and water) between the atmosphere and the biosphere as well as the hydrology, which in the default set-up used here, are both represented using a 30 minute time-step. The second sub-module, adapted from the LPJ model (Sitch et al., 2003), represents the dynamics of vegetation distribution on long time scales (1 year), while the third one (STOMATE) simulates the C dynamics in vegetation and soils at a daily to sub-daily step (Krinner et al., 2005). Finally, the fourth sub-module handles the routing of water that is lost via surface runoff and drainage from soils to the ocean through the global river network (Polcher 2003, Guimberteau et al.,2012), for which a daily time-step is used. All processes are simulated on a horizontal model grid, the resolution of which can be adapted to that of the meteorological forcing files. In this study, simulations are run at a spatial resolution of 0.5°. Moreover, in the default set-up, up to 13 plant function types (PFTs; bare soil, eight types of forest, two types of grassland and two types of cropland) can be distinguished for each cell, for which C budgets are simulated individually, while energy and water budgets are simulated at the grid cell level.

ORCHIDEE represents the soil C dynamics distinguishing different pools of plant litter and soil organic C over a 2 m profile. A branch of ORCHIDEE, called ORCHIDEE-SOM (Camino et al. 2018), added a vertical discretization of these carbon pools over 11 layers and included the representation of DOC production and cycling within the soil column (see section 2.1.2 for more details). ORCHILEAK was built on this branch and accounts for the coupled reactive transport processes impacting the dissolved C inputs from soils to the river network, including both DOC leaching from soils and CO_2 produced by soil respiration, into the hydrologic routing scheme. Besides

advective transport of carbon with the water flow, ORCHILEAK simulates the decomposition of DOC during riverine transport, the gas exchange of CO_2 at the interface between the inland water and the atmosphere, and the exchange of C between water column and soil column in inundated floodplains. For the representation of in-river DOC decomposition, two pools with different basic decay rates are distinguished, a slow (refractory DOC) and a fast (labile DOC) pool. All those fluxes are closely coupled to the model representation of hydrology that comprises interception of precipitation, throughfall, infiltration, percolation, surface runoff, drainage, and the routing of discharge along the river-floodplain network.

2.2.1.2 Soil carbon module

The soil carbon module of ORCHILEAK (Fig. 2.1) is derived from the CENTURY soil carbon model of Parton et al. (1988). In the standard scheme (Krinner et al., 2005), C in the soil of each model grid cell, and for each PFT, is represented by four different litter and three different soil organic carbon (SOC) pools with different turnover rates. The four litter pools correspond to metabolic aboveground and belowground litter, structural aboveground and belowground litter (Fig. 2.1). The SOC is subdivided into three pools, an active, a slow and a passive, which have default decomposition rates that are further modified at each time-step according to the evolving soil moisture and soil temperature. In the CENTURY scheme, C from the decomposed structural litter enters the active and the slow pools with the fraction allocated to each pools depending on lignin content of the litter, while the entire metabolic litter pool and the remaining part of structural litter is allocated to the active SOC pool. The SOC pools then feed into each other with the main C flux going from active to slow and passive to represent microbial decomposition of detrital organic matter, and a small return flux of slow and passive C back to the active pool to represent implicitly the C supply in the form of dead microbial biomass.

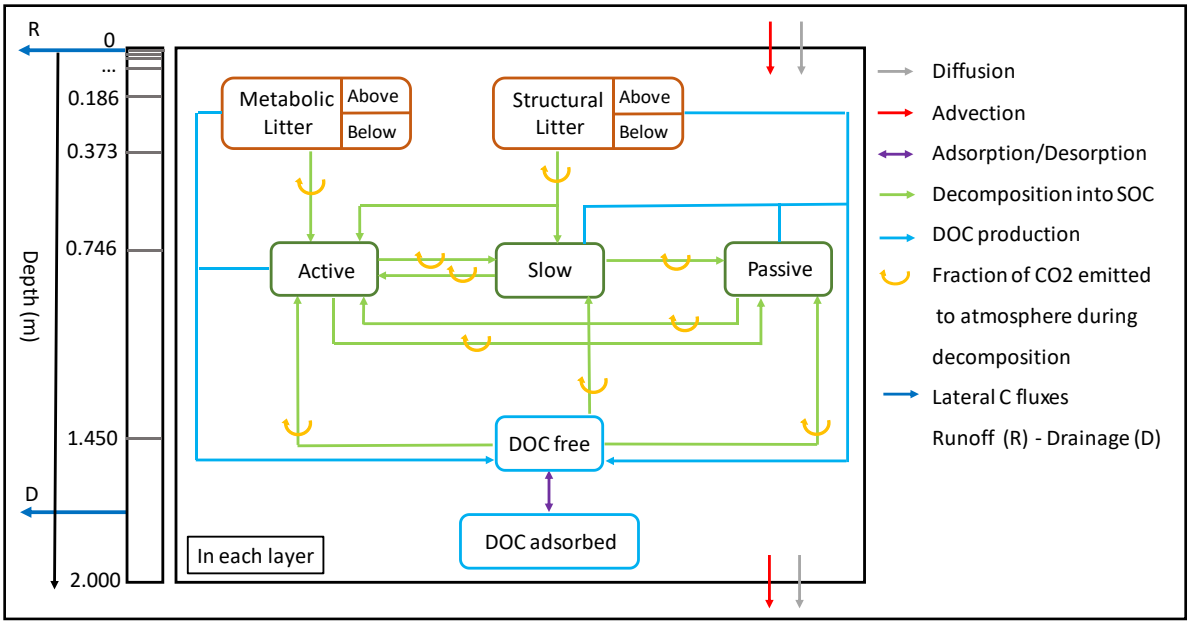

Figure 2.1 *The new version of the soil module of ORCHIDEE-SOM. The left box represents the discretization of the soil column and the transport processes between layers. The right box is a zoom of all the biogeochemical transformation processes that occur in each layer.*

Camino et al. (2018) updated this scheme with a vertical discretization of distinct SOC and litter pools over a 2 m soil profile represented by 11 layers, with geometrically increasing thickness from top to bottom (Figure 2.1; Lauerwald et al., 2017). Camino et al. (2018) further developed the soil C module by including an explicit representation of the fate of DOC along this vertically discretized soil profile. Processes accounted for are DOC production from the decomposition of SOC and litter, decomposition of DOC within the soil, sorption/desorption of DOC onto/from mineral surfaces, vertical advection and diffusion of DOC through the soil column, and lateral, advective leaching of DOC out of the soil profile, along with surface runoff (water flux from the topsoil surface) and drainage (water flux from the last layer soil at 2m depth). In each soil layer, ORCHILEAK explicitly simulates the fresh litter input (depending on the simulated vertical root distribution), decomposition of each organic matter pool (including litter and SOC), C transformation between different organic matter pools (showed by blue and green arrows between different pools in Fig. 2.1), C transport and diffusion between neighboring soil layers, and the loss of DOC due to leaching. For a specific organic C pool at each time step, only a fraction of the decayed C is respired as CO2 to the atmosphere (orange arrows in Fig. 2.1), the remaining being transferred to other organic pools (to mimic the microbial growth and mortality).

The DOC dynamics in the soil is simulated according to equation 2.1, which accounts for the dynamic interplay between by production, decomposition, transport and sorption- desorption processes along the discretized 2 m soil column (equation 2.1). All processes are simulated using a 30-minute time-step in following order: firstly,

production and decomposition of DOC are calculated, and DOC stocks for each layers and pool are updated accordingly. Secondly, vertical exchange of DOC between soil layers is simulated in two steps, first for the process of DOC advection with the flow of water through the soil column, then for diffusion of DOC. Lastly, the export of DOC through leaching from top- and bottom soil with runoff and drainage, respectively, are calculated.

$$\frac{dDOC_i}{dt} = \sum(Production_i - Decomposition_i) + F_{A,i} + F_{D,i} \quad (2.1)$$

In equation 2.1, i stands for the index of each layer. Each layer is connected to the adjacent layers by advective F_A and diffusive F_D fluxes. The total DOC transport flux is made of an advective component (equation 2.2) computed as the product of the water flux Q and the DOC concentration (in the i^{th} layer) and a diffusive component that follows Fick's first law (equation 2.3):

$$F_A = Q * DOC_i \quad (2.2)$$

$$F_D = -D * \frac{\partial^2 DOC}{\partial z^2} \quad (2.3)$$

where i stands for the ith layer, z is the depth along the discretized soil profile, and D stands for the molecular diffusion coefficient of DOC which is assigned a value of $1.06*10^{-5}$ m^2 d^{-1} (Ota et al., 2013).

The advective export of DOC to the river network is proportional to the top (first five layers, 4.5 cm) and bottom (11th layer) DOC concentrations, corresponding to water loss fluxes associated to runoff (for near surface) and drainage (for deep soil layer). Diffusion of DOC between adjacent soil layers is proportional to the gradient in DOC concentrations in the soil solution (eq. 2.3), moving towards an equilibrium. In addition, we apply a Fickian-type transport to represent the effect of bioturbation on SOC profiles. In this case, the transport is represented similar to eq. 2.3, but follows the gradient in SOC concentration relative to the volume of the soil layer. Representing bioturbation as diffusion-like process is the common approach in LSMs with vertically discretized SOC scheme (Camino et al., 2018). However, bioturbation is much slower than diffusion of DOC in the soil solution, with a diffusion coefficient D = $2.74x10^{-7}$ m^2 d^{-1} (Koven et al. 2013), compared to D=$1.06x10^{-5}$ m^2 d^{-1} (Ota et al., 2013). Therefore, bioturbation impacts the vertical SOC profile while it has only a marginal influence on the DOC dynamics.

The right hand-side of Fig. 2.1 summarizes the set of production/decomposition processes that occur in each layer. During litter decomposition, a fraction of the C is directly emitted back to the atmosphere as CO_2 while the remainder feeds the active and slow SOC pools:

$$CO_2\ respiration(Litter) = (1 - CUE) * k_L * (1 - \omega_L) * Litter \quad (2.4)$$

$$Litter\ decomposition = CUE * k_L * (1 - \omega_L) * Litter \quad (2.5)$$

where k_L is the kinetic rate for the litter decomposition (dependent on soil moisture and temperature (Camino et al., 2018)) and ω_L the fraction of litter that is channeled into DOC production (as opposed to particulate SOC). This approach of relating DOC production directly to the decomposing litter is inspired by Nakhavali et al., 2018 (following the ECOSSE model (Smith et al., 2010)) and is a major modification compared to the previous version of soil DOC and POC cycling from Camino et al., 2018. In equations (2.4) and (2.5), the partitioning between SOC production and respiration is defined by the carbon use efficiency (CUE).

In turn, active SOC is degraded into both slow and passive SOC and the respiration fluxes associated with these processes are also controlled by the CUE (Eqs 6 and 7, with k_{SOC} as the kinetic rate for SOC decomposition, which depends on soil moisture and soil temperature) and ω_{SOC} as the fraction of decomposed SOC that is transformed into DOC):

$$CO_2\ respiration(SOC) = (1 - CUE) * k_{SOC} * (1 - \omega_{SOC}) * SOC \quad (2.6)$$

$$SOC\ decomposition = CUE * k_{SOC} * (1 - \omega_{SOC}) * SOC \quad (2.7)$$

The decomposition of the litter and SOC pools produces a small amount of DOC according to equation 2.8. The DOC pool is thus fed by seven contributing sources, one for each of the four decomposing litter pools and three from the decomposing SOC pools:

$$DOC\ production = k_L * \omega_L * Litter + k_{SOC} * \omega_{SOC} * SOC \quad (2.8)$$

In ORCHIDEE-SOM (Camino et al. 2018), all decomposed litter and SOC which is not respired to CO_2, was first fed into the DOC pools, and only upon the decomposition

of that DOC, the non-respired fraction of the decomposed DOC could feed the other SOC pools. Such formulation is in contrast to the adaption of the RothC SOC model in ECOSSE (Smith et al., 2010) and JULES (Nakhavali et al., 2018) that we followed here, where the major exchange of C is between the different litter and SOC pools, and the production of DOC is related to these SOC and litter pools by empirical rate constants, which were fitted to reproduce observed DOC turnover times (Kalbitz et al., 2003, Turgeon, 2008) and DOC concentrations in the soil. The much higher DOC production rates simulated by ORCHIDEE-SOM in its original configuration during preliminary tests over Europe led us to implement the new approach (equations 2.4-2.7). While preserving the basic structure of ORCHIDEE-SOM, we thus adapted the model in a way that organic C exchange occurs mainly among the particulate litter and SOC pools, similar to the original Century model. The production of DOC is represented as a side product of this C exchange between pools of litter and SOC, with production rates as used in ECOSSE. In the modified soil carbon module, we used the parameter ω in Equations (2.4-2.7) as a scaling factor that determines how much DOC is produced by the decomposition of litter and SOC. This parameter was calculated after Smith et al. (2010) as the ratio of production of DOC from litter (p_{DOC_L}) and the SOC pools ($p_{DOC_{SOC}}$) to the decomposition rates of litter (k_L) and SOC (k_{SOC}). The initial values for ω were 0.5 % and 3 % for the litter and SOC pools, respectively. Further optimization with regard to reproducing observed soil DOC concentrations led to ω values set at 0.2% for the litter and 1.2% for the SOC pools.

Once produced, the free DOC can then be adsorbed to soil mineral particles, and the adsorbed DOC can again be desorbed and returns to the free DOC pool following a linear adsorption isotherm as described in Neff and Asner (2001) and Wu et al. (2014). We assume that equilibrium between the dissolved and absorbed phases is instantaneous. Moreover, the work by Kothawala et al. (2008) showed that this approach performed fairly well compared to the more complex approach of using Langmuir equations, and that it is based on a stronger empirical basis. The partitioning is controlled by K_D, the so-called equilibrium partition coefficient (equation 9), considered constant at 8.05×10^{-5} m³ water kg^{-1} soil (Moor et al., 1992). All constants used are listed in table S1.

$$DOC_{adsorption-desorption\ eq} = K_D * DOC \quad (2.9)$$

Finally, the DOC pool is subject to decomposition according to equation (2.10) and then partly feeds into the SOC pools (eq. 2.11), where k_{DOC} is the DOC decay rate, which also depends on soil moisture and soil temperature.

$$CO_2\ respiration(DOC) = (1 - CUE) * k_{DOC} * DOC \quad (2.10)$$

$$SOC\ production\ by\ DOC = CUE * k_{DOC} * DOC \quad (2.11)$$

2.2.1.3 Manure as an additional C source

In Europe, a large fraction of the landscape is dominated by agricultural and grazing activities and manure application represents a significant additional C - in particular DOC- source to the soil in regions dominated by grasslands and croplands. Studies have shown an increase in riverine DOC flux with runoff and of DOC concentration that is related to manure application, in particular they showed that the frequency and intensity of storm events in spring directly after manure application and exert an important control on the amounts of additional DOC leached to the river network (e.g., Royer et al., 2007; Delpla et al., 2011; Singh et al., 2014; Humbert et al., 2020). The type of manure input can be very different from one region to another, and the physicochemical properties (e.g. C:N ratio and the ratio of dissolved and particulate organic matter) depend strongly on the specific type of manure input. However, current forcing data of manure only provide the amount of total manure inputs, but without information regarding specific composition and/or physicochemical properties of the manure. To constrain the C flux from manure infiltrating into the soil, we used the gridded 0.5° resolution input of manure nitrogen (manure-N) applications produced by Zhang et al. (2017) as forcing file. Following the use of that forcing data in the model branch ORCHIDEE-CNP developed by Sun et al. (2021), we assumed that 90% of the total manure-N is in mineral form (i.e. NH_4^+ or NO_3^-) and the remaining 10% is in organic form. To convert the organic manure-N into a manure-C flux, a C:N stochiometric ratio of 13.7 was then applied (Vuichard et al., 2018). Finally, the particulate and dissolved organic manure-C were assumed to feed the litter and DOC pools, respectively (Fig. S.2.1). Consistent with ORCHIDEE-CNP (Goll et al., 2017), the fractions of particulate and dissolved manure-C were set to 0.9 and 0.1, respectively.

2.2.1.4 Hydrological processes

The representation of hydrological processes is handled in two distinct sub-modules. The first one, the hydrology sub-module, simulates the vertical exchange of water in the atmosphere-vegetation-soil system in each model grid cell, while the second one, the river routing module, simulates the horizontal transfers between grid cells. The hydrology is forced by several meteorological fields such as precipitation and air temperature. In the hydrology module, precipitation is divided into interception and throughfall, the latter being further subdivided into surface runoff and infiltration into the soil. The infiltration rate is controlled by the throughfall rate, the slope of the soil surface and the hydraulic conductivity of the soil which is a limiting factor for infiltration. The distribution of water within the soil is represented by the distribution

of soil moisture over the discretized soil profile (de Rosnay et al., 2002, d'Orgeval et al., 2008). The water budget within the soil is thus determined by the infiltration rate and runoff from the top soil, the evaporation and transpiration from the soil, runoff from the top soil and drainage at the bottom of the soil column. The infiltration rate and percolation through the soil profile are then used to compute the advective flux of DOC (equation 2.2)

The second module deals with river routing and represents the horizontal transfers of water from the soil column to the aquatic system though surface runoff and drainage, and further through the river network and adjacent floodplains (Vorosmarty et al., 2000). Meybeck (1993a,b) found that soils were the major source of DOC to rivers, while autochthonous DOC being negligible at the global scale. Furthermore, autochthonous DOC has a short turnover time and is quickly recycled within the river (Farjalla et al., 2009; Fonte et al., 2013) and thus does not contribute significantly to the net C budget of an entire river system. Since in this study the focus is on the role of fluvial DOC fluxes in the terrestrial C budget, autochthonous DOC is not accounted for. The representation of leaching processes in ORCHILEAK is simplified, the model represents flows of water from land to the stream network only through surface runoff and drainage from bottom soil. Leaching thus occurs either from the topsoil, which in our configuration represents the top 4.5 cm of the soil column, or from the bottom soil, i.e. the lowest 50 cm of the 2 m soil profile. DOC leaching from the top soil is controlled by two reduction factors, a general reduction factor and a reduction factor. The first accounts for the fact that some of the runoff represents excess throughfall that never entered the soil and thus corrects for the overestimated DOC concentration in the topsoil through. The second represents the connectivity between streams and their catchment through the extent of the water saturated riparian zone. Note that ORCHILEAK simulates the occasional inundation in the river's floodplains, where decomposition rates of the different carbon pools (litter, SOC and DOC) differ depending on whether the soil is flooded or not. For a detailed description of its features, please refer to Lauerwald et al. (2017).

2.2.2 Simulations

2.2.2.1 Model set-up

Model domain, land cover and forcing data. The simulated model domain extends over the area (4.1 10^6 km^2) between 35°N and 70°N latitude and 10°W and 30°E longitude (Fig. 2.2). This domain includes 5600 model grid cells at 0.5x0.5° resolution and encompasses 6 broad climate zones according to the Köppen-Geiger classification from Peel et al., 2017 (Fig. 2.2a). The dominant PFTs within Europe include croplands (20% mainly C3), grasslands (31% of which 24% are C3), and forests (39%, of which 16% and 9% are needleleaved evergreen and broadleaved summer-green, while temperate broadleaved summer-green, needleleaved and broadleaved

evergreen forests take 8%, 3% and 3% respectively) (Fig. 2.2b). The spatial distribution of manure application on grasslands and croplands is shown in Figure 2.2c. Finally, Figure 2.2d illustrates the actual river network derived from the HydroSHEDS DEM data (Lehner et al., 2008) and the one corresponding to our river routing scheme at 0.5 degree resolution, highlighting that the representation of the river network is not optimal due to the coarse spatial resolution of our model. This coarse resolution limits the possibility of model validation to the downstream parts of larger river networks. Note further that the mouth of the Rhine is more than 100 km too far east, which further limits model validation for that river.

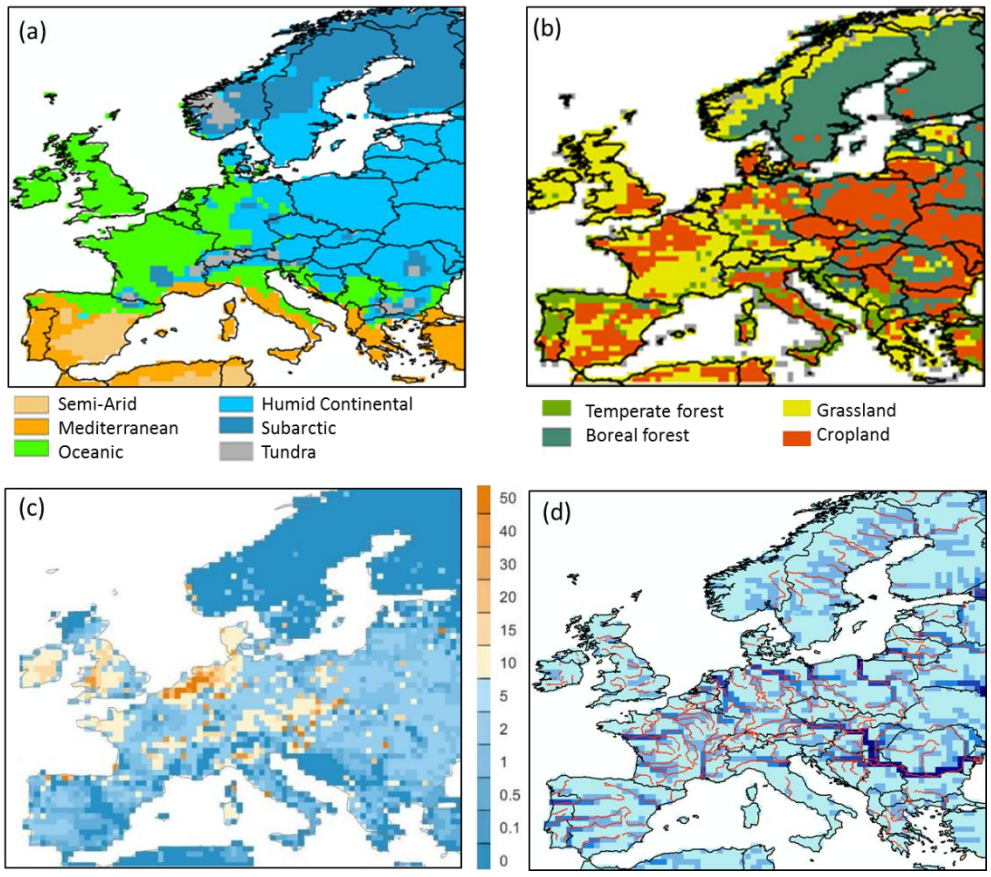

Figure 2.2 *Spatial distribution for each 0.5° grid cell of the continental European domain of (a) climate zones (according to the Koppen-Geiger classification); (b) dominant plant functional types (PFT) (c) manure application (in gC m^{-2} yr^{-1}); (d) the routing Network of ORCHILEAK (in blue). The real river network extracted from the European Environment Agency (https://www.eea.europa.eu/legal/copyright) is also shown.*

The forcing data applied in our study are listed in table 2.1. They are the same as those used in Lauerwald et al. (2017) except for the meteorological forcing data and the land cover. The WFDEI meteorological forcing dataset used in this study was derived by applying the methodology originally used to create the WATCH Forcing Data (WFD) from the ERA-Interim reanalysis data (Weedon et al., 2014). The dataset has a 0.5° spatial resolution and a 3-hourly time step from 1978 to 2014. The land

cover forcing data set, which gives the areal proportion of the 13 PFTs within each 0.5° grid cell, was taken from Peng et al. (2017). Note that the soil hydrology model in ORCHIDEE, which we adopted for ORCHILEAK, was developed and calibrated to work with the soil classes used in Reynolds et al. (1999). We thus kept that data source, while additional soil properties such as pH and specific soil classes which we defined as "poor soils" (Histosols, Podzols) with lower C turnover times and DOC filtering were taken from HWSD v1.1. A topographic index, which in ORCHIDEE controls the flow velocity in the river network of each cell is taken from Vorosmarty et al. (2000). "Floodplains", defined as the maximum areal proportion of a grid cell that can be flooded when the river exceeds its bankfull flow, and "Swamps" representing groundwater fed wetlands in the floodplain, were adopted from the Global Lake and Wetland database (Lehner and Doll, 2004). Depending on the areal extend of these swamps, a proportion of stream flow is simulated to feed into the soil moisture storage of the grid cell considered. Both parameters have an effect on the simulated river discharge and soil hydrology in the floodplains. For details, see Lauerwald et al. (2017).

Table 2.1 *List of the forcing files used for our simulations, along with their spatiotemporal resolution.*

VARIABLE	SPATIAL RESOLUTION	TEMPORAL RESOLUTION	DATA SOURCE
Rainfall, snowfall, incoming shortwave and longwave radiation, air temperature, relative humidity and air pressure, wind speed.	0.5°	3 hours	WFDEI_GPCC (WATCH Forcing Data (WFD) by making use of the ERA-Interim reanalysis data, Global Precipitation Climatology Centre; Weedon et al. (2014))
Soil texture class	0.5°	-	Reynolds et al., 1999
Soil pH, soil bulk density, poor soil	0.5°	-	HSWD v 1.1 (Fao et al., 2009)
Stream flow directions and topographic index	0.5°	-	STN-30p (Vörösmarty et al., 2000)
Floodplains and swamps	0.5°	-	Guimberteau et al., 2012
River surface area	0.5°	-	Lauerwald et al., 2015
10th, 50th, 90th percentile of the stream reservoir	1°	-	Derived from pre-runs with ORCHIDEE

Land cover	0.5°	-	Peng et al. (2017)

Parametrization of hydrological processes. ORCHILEAK was previously parametrized and validated for the Amazon (Lauerwald et al., 2017; Hastie et al., 2019; Lauerwald et al., 2020), Congo (Hastie et al., 2021) and Lena (Bowring et al., 2020) basins. In our study of the European river network, we updated ORCHILEAK with the more recent hydrology scheme of the recent standard version of ORCHIDEE (svn 5091). This hydrology scheme has been calibrated against observed runoff at a global scale (Ringeval et al., 2012; Yang et al., 2015). Furthermore, MacBean et al. (2020) has evaluated the model performance for simulating soil moisture in temperate ecosystem. This new hydrology scheme features a dynamic surface roughness of the vegetation, which decreases the aerodynamic resistance near the surface when vegetation cover is low, leading to lower ground temperatures and thus lower evaporation rates. This adjustment was deemed necessary in order to better capture the observed mean and seasonal variability of the discharge along the European river network. The two reduction factors controlling DOC leaching from the top soil to the headwaters streams were also adjusted (see 2.1.4).

Spin-up. Before the model can be used to simulate C dynamics over the past decades, a spin up is needed to reach an assumed steady state for the C fluxes during the pre-industrial period. This steady state is achieved by spinning up ORCHILEAK for 15000 years. The spin up was realized by recursively looping over 4 years of climate forcing using the WFDEI forcing dataset over the 1979-1982 period (because the first year of the forcing, 1978, is incomplete) and constant land cover and atmospheric CO_2 concentration of 286 ppm (Guimberteau et al., 2018) corresponding to year 1861. After the end of the spin-up, the soil C stock across the entire European continent changed by less than 1% over a century of simulation, which we considered close enough to steady-state.

Transient runs. Using the steady-state outputs as initial condition, the first part of the transient simulation (1861-1978) was carried out with increasing atmospheric CO_2 concentration, changing land use and land cover and with river routing activated while still looping over the 27 years (1979-2006) of the WFEDI forcing dataset. From 1979, the WFDEI atmospheric forcing data was applied over the entire period covered by this product with the changing land cover map and atmospheric CO_2 values applied for each year of simulation.

Model evaluation. Firstly, the simulated discharges were compared to times series of daily stream flow recorded at eleven gauging stations from "The Global Runoff Data Center (GRDC), 56068 Koblenz, Germany" dataset. For comparison, both observed and simulated discharges were aggregated at the monthly temporal resolution over

the years 1980 to 2006. Note that the river network in ORCHILEAK does not always match the real river network. The selected gauging stations were assigned to the cell best representing the parts of the river network to which the sampling location corresponds. However, important correction had only to be done for the most upstream station in the Rhine and the Elbe. The period 1980 to 2006 was chosen based on the GRDC data coverage.

Model performance was further evaluated with respect to several variables of the terrestrial C cycle. Firstly, simulated Net Primary Production (NPP) was compared to two different data products. The first one, the CARbon DAta MOdel fraMework (CARDAMOM; Bloom et al., 2015) built from model data fusion analysis at 1° resolution. The second one is the Global Inventory Modeling and Mapping Studies (GIMMS) at 0.5° resolution based on AVHRR and MODIS sensors. GIMMS uses several atmospheric forcing data set to derive NPP. Those are CRUNCEP version 4 P1 and P2 (Rainfall, cloudiness, relative humidity and temperature taken from the CRU (Climate Research Unit), while the other fields such as air pressure, longwave radiation, wind speed are directly derived from NCEP (National Center for Atmospheric Research)), ECMWF (European Centre for Medium-Range Weather Forecasts), MERRA2 (the Modern-Era Retrospective analysis for Research and Applications, Version 2) and NCEPR2 (https://www.esrl.noaa.gov/psd/). For our comparison, we calculated the average of the NPP obtained with these five atmospheric forcing files. The NPP values from ORCHILEAK and GIMMS were averaged over the period 1982-2006 while CARDAMOM only covers a shorter time period comprised between 2001 and 2010. Modeled NPP was then compared to the NPP data products at the European scale and at the scale of five large European basins for which we also evaluated the simulated river discharge and DOC fluxes, and which taken together, represent 19 % of the model domain (Fig.2.3): the Danube, Rhine, Elbe, Rhone and Seine.

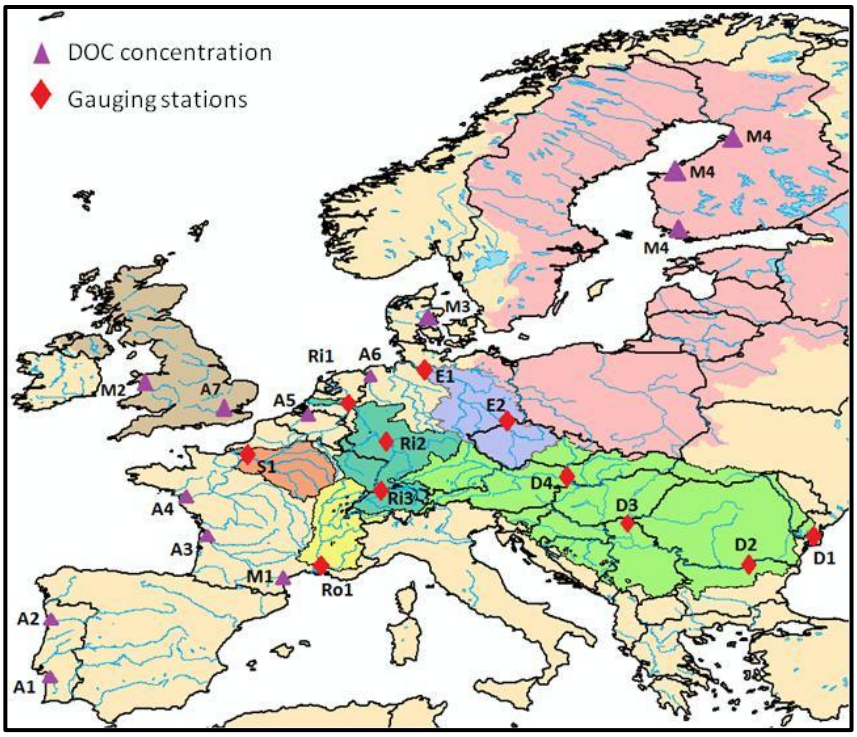

Figure 2.3 *Map of continental Europe delineating the (group of) catchments of focus in this study and the location of observed discharge and DOC concentrations. Catchments, from west to east are: All UK (light brown), Seine (orange), Rhone (yellow), Rhine (dark green), Elbe (violet), All Baltic (pink) and Danube (light green). Observations include GRDC stations (red diamonds) in the Seine (S1-Poses), Rhone (Ro1-Beaucaire), Rhine (Ri1-Lobith, Ri2-Main in Frankfurt, Ri3-Basel), and Danube (D1-Ceatal Izmael, D2-Svistov, D3-Tisza in Senta, D4-Bratislava) catchments, as well as river stations where DOC concentrations were measured (purple triangles): A1-Douro, A2-Sado, A3-Gironde, A4-Loire, A5-Scheldt, A6-Ems, A7- Wales, A8-Thames, M1-Tech, M2-Wales, M3-Denmark, M4-Finland (Abril et al 2002, Mattsson et al., 2008).*

All five basins are located in an oceanic or humid continental climate (Fig.2.3a) although the Rhone basin extends further into the Mediterranean climate zone. The basin characteristics according to land cover types are as follows: the Danube and the Elbe basins have both a high proportion of croplands (around 40%), the remainder being mostly covered by grasslands and boreal forests. The Rhone is covered by 50% of grasslands, while in the Seine basin croplands reach 50%. The Rhine has a more diverse land cover with a substantial proportion (about 30%) of boreal (10 %) and temperate (20 %) forests, 35% of grasslands and 25% of croplands. See table S2.2 for further details.

The soil temperature is compared to the soil temperature generated using data from the European Centre for Medium-Range Weather Forecasts reanalysis ERA5 dataset (Munoz-Sabater et al., 2021). The soil heterotrophic respiration (SHR) is compared against the data-driven global SHR dataset published by Yao et al. (2020). The global SHR data set was produced using a Random Forest algorithm, up-scaling from 455 data points from the Global Soil Respiration Database (SRDB 4.0) based on gridded

fields of climatic, edaphic and productivity related variables as predictors (Yao et al., 2020). We compared the results of ORCHILEAK with the average, minimum and maximum values of SHR estimated by Yao et al. (2020 SOC from the Harmonized World Soil Database (HWSD) was used to evaluate the simulated SOC stocks. HWSD is a global soil database that contains up-to-date information on a large range of soil properties. For instance, this dataset reports the organic carbon content in the soil as well as the soil bulk density. The bulk density in HWSD was calculated in two different ways. The first one follows the method described in Saxton (1986) where the bulk density is related to the soil texture - an approach tending to overestimate density in high porosity soils or in OC rich soils. The second method uses the SOTWIS database in which the bulk density is calculated as a function of soil type and depth. In this database, all variables are reported for the topsoil (0-30cm) and the sub-soil (30-100cm) horizons. For comparison purposes, our simulated SOC stocks were thus integrated over the same depth intervals. We further assessed the extent to which our model can reproduce the main features in observed soil DOC profiles. To that end, we compared our simulated DOC profile averaged over the entire European forest biome against the one established by Camino et al. (2014) on the basis of a synthesis of local measurements. Although there are many studies on DOC concentrations in the soil, we selected the one by Camino et al. (2014) because it provides a synthesis at the pan-European scale, and is thus ideal to extract "representative" concentration profiles over a sufficiently large domain, compatible to the regional scope of our study. Unfortunately, similar synthetic profiles based on observations have not been constructed for croplands and grasslands.

The key variables of interest in our study are the DOC leaching flux from the soil and the DOC export flux to the coast. These fluxes require accurate simulation of the water discharge fed by runoff and drainage as well as of DOC concentrations in the leaching flux and in the riverine flux. For the leaching flux, our simulation results were compared to measured fluxes reported by Kindler et al. (2011) across different locations in Europe. Because the observed DOC leaching fluxes from both top and bottom soil reported by Kindler et al. (2011) are based on local measurements that are not easily comparable to simulated fluxes at the coarse spatial resolution of our model (0.5° or about $2*10^3$ km^2 at the corresponding latitude), we nevertheless consider the comparison against measured river DOC fluxes more relevant for our purpose, as rivers are good integrators of mean, larger-scale catchment properties. For the riverine export fluxes, we assessed the modeled discharges and DOC concentrations separately. For evaluation of stream DOC concentrations, DOC data were extracted from the GLObal RIver CHemistry database (GLORICH, Hartmann et al., 2014) for the Rhine and Elbe basins and from the "Eau de France" database for the Seine and Rhone basins. These data were complemented by river DOC concentrations reported by Abril et al. (2002) for 9 river mouths (Sado, Thames, Ems, Scheldt, Gironde, Douro, Loire, Elbe and Rhine), and by Mattsson et al. (2008) for several river

basins located in Finland, Denmark, Wales and France.

2.3 RESULTS AND DISCUSSION

2.3.1 Model evaluation at pan-European and catchment scales

2.3.1.1 Discharge

Figure 2.4 compares the simulated discharge against observations for selected stream gauging stations (section 2.2). Those stations are located near the mouth of large rivers (Danube, Rhine, Rhone, Elbe and Seine) but also include a few locations further upstream the same rivers or at major tributaries (Fig. 2.3). The comparison is performed for the period 1990-2000, except for the Rhone at Beaucaire and the Danube at Svistov for which the observed stream gauge data cover only a shorter period. Overall, the model reproduces the observations well, both in terms of amplitude and seasonality, except for the Elbe at Neu Darchau, for which the temporal variability is well captured but the absolute discharge is overestimated.

Note that the simulated catchment area often diverges (by -25% to +30 %) from the observed value due to the coarse resolution (0.5°x0.5°) of ORCHILEAK (Table S3). As a result of the model resolution, smaller tributaries are not represented individually and each grid cell was fully assigned to one larger river basin. The effect of the resolution is also shown in Figure 2.2d which compares the observed and modeled river network. Discrepancies between model and real world catchment area will translate into proportional biases in discharge simulation. Furthermore the 0.5° resolution is too coarse to be able to represent perfectly the pathways of the river. Our model tends more often to underestimate the catchment area, while its yearly mean discharge is overestimated, except at the Beaucaire station along the Rhone River. The bias can be significant and cannot be explained by the model resolution alone.

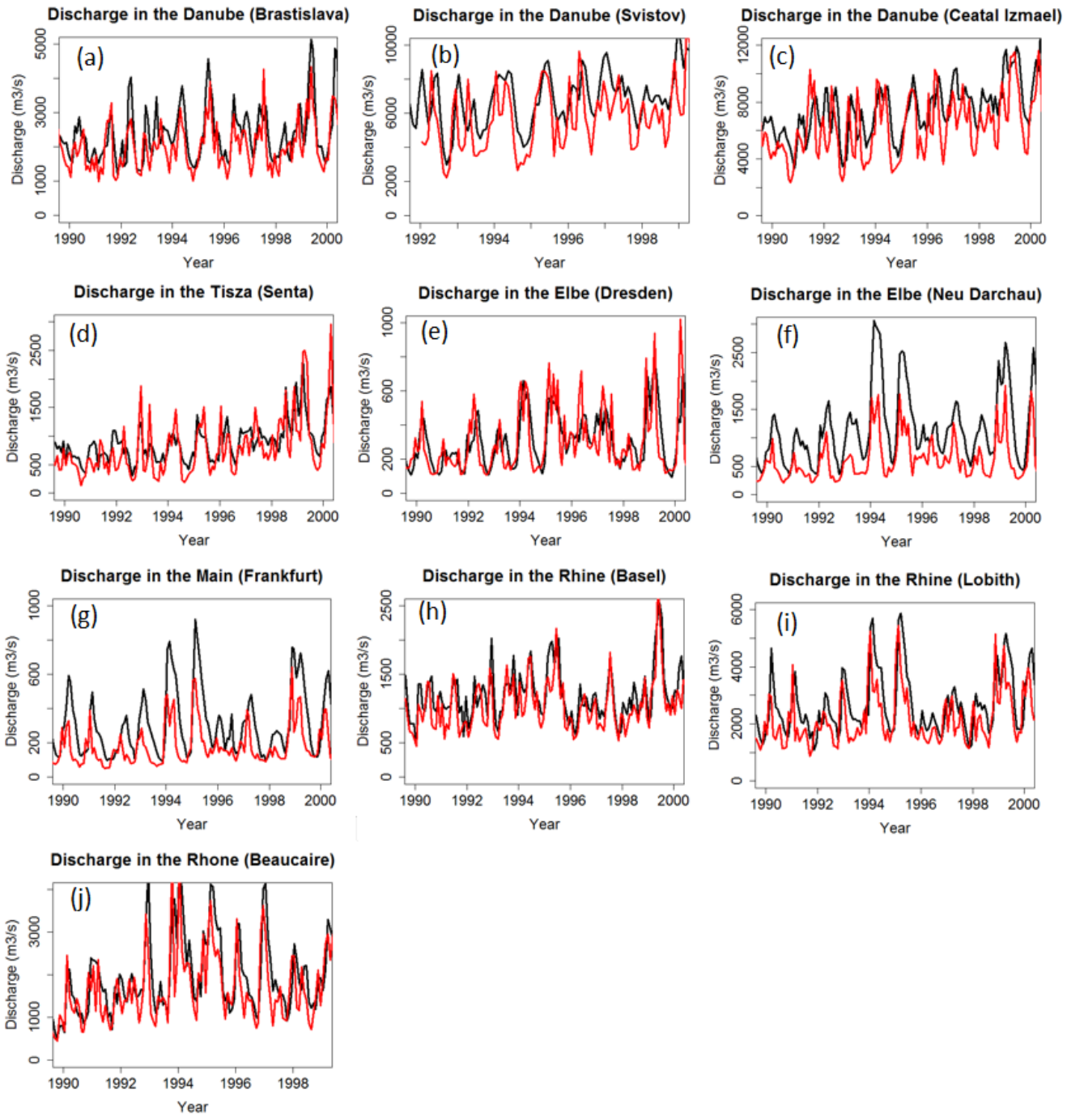

Figure 2.4 *Modeled (black) and observed (red) time series of discharge at the GRDC gauging stations in the Danube (a-c) and its tributaries (d), Elbe (e-f), Rhine and its tributaries (g-i) and Rhone (j). Note the different time periods of measurements. See figure 3 for exact location.*

To evaluate model performance for discharge, we used the Pearson's coefficient of determination (R^2) and the Nash Sutcliffe modeling efficiency (NSE, Nash and Sutcliffe

(1970)). The R^2 only accounts for the correlation with regard to the temporal variability. With R^2 values comprised between 0.43 and 0.62 for all stations, we conclude that the observed seasonality of the discharge along large European rivers is reasonably well reproduced by the model. The NSE not only accounts for the correlation between observed and simulated temporal signals, but also for the model's ability to reproduce absolute discharges. The statistics confirm our previous observation that the model generally overestimates discharges (low NSEs) except for stations Elbe in Dresden, Rhone in Beaucaire, Rhine in Basel and Danube in Bratislava where both the mean and temporality are well captured. Two stations have negative NSE values, which means that the error variance estimated by the model is significantly larger than the variance of the observations; in others words, model and observations are completely different. The mean error (%), that is the weighted difference between the average from the model and the one from observation, confirms that low NSEs are mostly due to overestimated discharges, which is further demonstrated by high mean errors. More results for other European catchments can be found in table S2.3.

2.3.1.2 NPP, biomass and soil organic C stocks

We briefly compare simulated NPP with the gridded observation-based products GIMMS and CARDAMON (section 2.2.2) as C fixation by the vegetation exerts an important control on DOC stocks in the soil and thus on DOC leaching. We first perform our comparison over a large domain comprised between -10° and 30° in longitude east and 35° and 70° in latitude north - covering the area from Ireland to the Western Black Sea (where the Danube flows into) and from the south of Spain to the north of Scandinavia. Over this area (referred to as "Europe" from here onwards), the modeled yearly averaged NPP amounts to 445 gC m^{-2} yr^{-1}, a value in remarkable agreement with both GIMMS and CARDAMOM estimates of 430 gC m^{-2} yr^{-1} and 460 gC m^{-2} yr^{-1}, respectively. Those two datasets are entailed with an uncertainty that we assume similar to that reported for the MODIS dataset, i.e. 20% (Turner et al 2006). The total living biomass in Europe is simulated at 15.5 PgC or 2.3 kgC m^{-2}. This value is in good agreement with the recent estimate by Avitabile and Camia 2018, which report a biomass stock at around 16 PgC. We estimate that the total soil carbon stock amounts to 58 PgC. Averaged over the first meter of the soil horizon, this corresponds to a value of 9.5 kgC m^{-2} which is comparable to that of HWSD (6 kgC m^{-2}) when using the SOTWIS method to compute the bulk density, but significantly lower when applying Saxton's method (22 kgC m^{-2}), plausibly because the latter overestimates the bulk density in OC-rich soils (Kochy et al., 2015).

Table 2.2 summarizes the yearly average NPP at the scale of the five selected European catchments. Simulated NPP is of the same order of magnitude as both observation based datasets, without any systematic bias towards an underestimation or overestimation. To provide error bounds for the observational products, we calculated the average standard deviation between yearly-mean values. For GIMMS, we also included the standard deviation induced by the use of the five distinct meteorological forcing files to assess the NPP (section 2.2.1). We find that our simulated catchment averaged NPP fall within the error bounds of the observational products for the Rhine and the Rhone while for the Danube, Elbe and Seine, simulated NPP is slightly above the upper error range.

Table 2.2 reports the biomass and soil carbon (SOC) stocks for the 5 river basins. SOC stocks are usually slightly overestimated compared to HWSD. Results have also been aggregated at the intermediate scale of broad climate zones to analyze how well our model performs for distinct climate regimes. Again the method to calculate the bulk density (section 2.2.2) leads to large uncertainties in observed SOC stocks. Nevertheless, we find that simulated SOC stocks for the warmer climates (Semi-arid and Mediterranean) match well the SOC stocks of the HWSD. However, for other regions, we systematically underestimate the SOC stock compared to HWSD using the Saxton Method, especially in the subarctic climate, but we are closer to the observed values relying on the SOTWIS method for the bulk density. This result is expected since the model does not represent peatlands, which contain important quantities of SOC (Leifeld and Menichetti 2018).

Table 2.2 *Comparison of modelled NPP (1982-2006) against estimates from the CARDAMOM (2001-2010) and GIMMS (1982-2006) datasets. The mean of the two datasets, along with an assessment of the uncertainty (based on MODIS) and of the standard deviation are also reported. In addition, the modeled biomass stock and soil organic carbon (SOC) content (first 1m) are compared with values reported in the HWSD database, using two methods (Saxton and SOTWIS) to calculate the soil bulk density. All variables and processes are reported for the large-scale basins of focus in this study (see fig. 3 for location), the main climate zones of continental Europe and the whole model domain.*

Basin	NPP gC m^{-2} yr^{-1}			Mean obs NPP	Uncer-tainty	Standard deviation	BIOMASS stock	SOC	HWSD SOC stock	HWSD SOC stock
	ORCHILEAK 1982-2006	CARDAMOM 2001-2010	GIMMS 1982-2006	gC m^{-2}yr^{-1}	20%	gC m^{-2} yr^{-1}	kgC m^{-2}	kgCm^{-2}	Saxton kgC m^{-2}	SOTWIS kgC m^{-2}
Danube	560	524	465	495	99	19	3.1	9.3	7.7	5.1
Rhine	527	601	482	542	108	55	1.5	9.5	9.1	5.7
Elbe	576	507	452	480	96	17	2	10.3	17.1	4.9
Rhone	497	593	504	549	110	38	1.4	8.2	5.3	4.5
Seine	667	484	485	484	97	0,5	1.3	9	4.4	3.6
Semi-Arid	264	199	246	222	44	32	0.4	3.3	3.9	4.1
ranean	390	383	386	385	77	21	1.7	5.3	5.1	4.6
Oceanic	561	535	511	523	104	2	1.7	10	23.1	5.6
continental	526	502	458	480	96	11	3.1	10.7	17.2	5.9
Subarctic	338	400	388	394	79	26	2.2	12.2	44.7	7.8
Tundra	344	451	347	399	80	18	2	9.1	5.2	4.3
Europe	445	460	430	441	88	11	2.3	9.5	22	6

Figure 2.5a shows the comparison of simulated vs. data driven estimates of soil

temperature. Soil temperature is overall well represented with a simulated mean temperature of 8.4° C against 9.3°C after ERA5. The overall slight underestimation is due to a substantial underestimation of soil temperatures in the northern regions. Furthermore, this underestimation is more important in the winter (January, February and March) with a difference relative to ERA5 values reaching 3.5°C, while in summer (July, August and September) this difference amounts to only 0.5°C. This underestimation is due to the poor representation of the isolating effect of the snow cover in ORCHIDEE (Wang et al., 2013).

The comparison of simulated SHR against Yao et al.'s estimate is shown in Figure 2.5b. Over Europe, ORCHILEAK underestimates the SHR compared to Yao et al.'s estimates by about 14%, with a simulated average of 312 gC m^{-2} yr^{-1} against an average of 363 gC m^{-2} yr^{-1} (range from 317 to 417 gC m^{-2} yr^{-1}) estimated by Yao et al. (2020) for the period 1985-2013. Looking at specific climatic regions, some regions are well represented in ORCHILEAK, as the Mediterranean and humid continental regions with a mean SHR of 371 and 363 gC m^{-2} yr^{-1}, against 385 and 354 gC m^{-2} yr^{-1} from Yao et al., respectively. SHR in semi-arid and tundra regions are on the contrary around 50% lower than Yao et al.'s estimate. For the tundra region the underestimation in SHR is consistent with an underestimation of the NPP (see table S2.4).

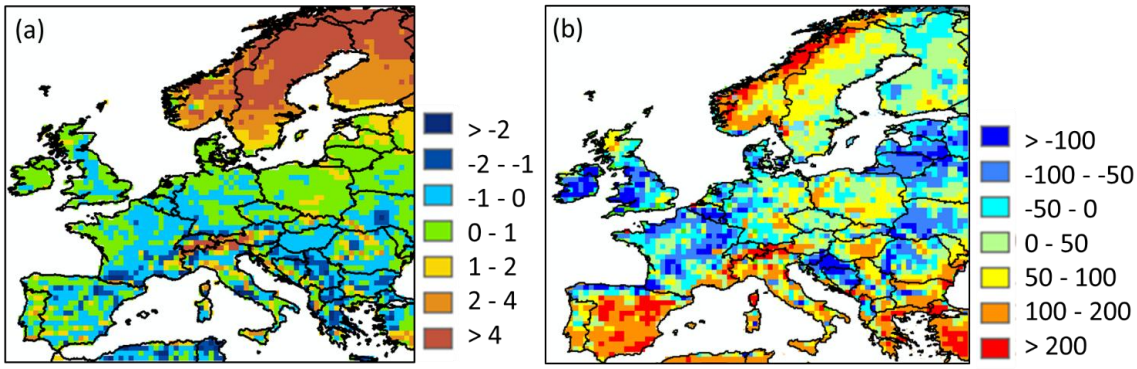

Figure 2.5 *Difference in (a) simulated soil temperature (in °C) against values reported by ERA5; (b) simulated soil heterotrophic respiration (in gC m^{-2} yr^{-1}) against values reported by Yao et al. (2020).*

2.3.1.3 Soil DOC stocks

Comparison between observed and modeled DOC stocks and fluxes is more difficult

than for biomass and SOC because those have not been assessed at large spatial scales. Nevertheless, representative soil DOC concentration profiles for coniferous and broadleaved forests of Europe have been compiled by Camino et al. (2014). These profiles were used to evaluate our model. Overall, we found that ORCHILEAK slightly overestimates DOC concentrations, especially in the very topsoil horizons with modeled values around 100 mg l^{-1} against 40-60 mg l^{-1} in the observations (Fig. 2.6). We also simulated higher concentrations in broadleaved forests than in coniferous forests while Camino et al. (2014) obtained the opposite. When integrated over the first meter of the soil horizon of forested ecosystems (28 % of the surface area), the modeled and observed DOC stocks amount to 22.2 and 11.3 gC m^{-2}, respectively. Above we have shown that over Europe SOC stocks were underestimated and now we observe that the average DOC concentrations in the soil over all European forests are overestimated. One explanation for the underestimation of SOC stocks and the likely overestimation of DOC stocks is that SOC decomposition rates in the new soil carbon module may be slightly too high. It is however difficult to generalize this conclusion because of the lack of synthesis data for other land cover types, especially croplands and grasslands which together represent about 50 % of the total European land area. Modeled DOC stocks averaged over broad climate regions reveal highest values for the oceanic climate with 32 gC m^{-2} and the Mediterranean climate with 26 gC m^{-2}. Semi-arid and humid continental climates have similar concentrations of respectively 17.5 and 20 gC m^{-2} and we find the lowest DOC concentrations around 8 gC m^{-2} in the coldest climates (subarctic and tundra).

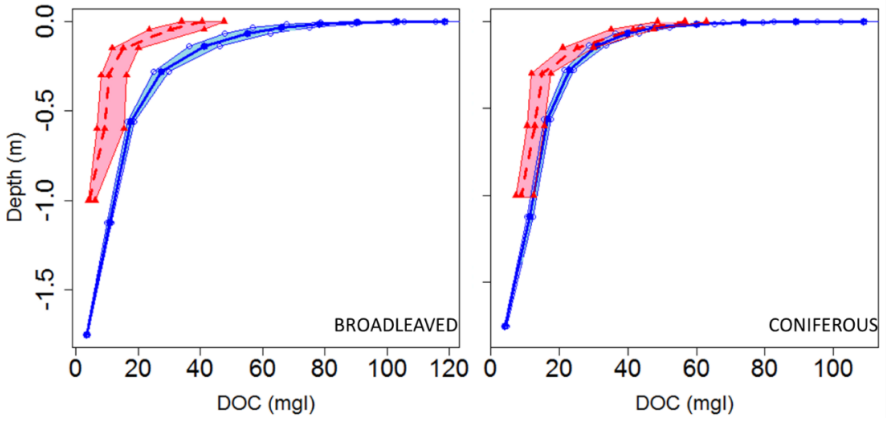

Figure 2.6 *Modelled (blue) versus observed (red dashed) DOC concentration profiles averaged over the soils of the European Coniferous and Broadleaved forest biome. Data from Camino et al. (2014). The shaded area represents the 95% bootstrap confidence interval for model and observations.*

2.3.1.4 DOC leaching fluxes

The model simulates a yearly-mean DOC leaching flux over Europe of 14.3 (±10) TgC yr^{-1} (Fig 2.7), the standard deviation being here coarsely approximated by spatial

variability. The average area specific flux rates is of 2.6 (±2.5) gC m^{-2} yr^{-1}. We compared DOC leaching fluxes with site level observations from Kindler et al. 2011, across 17 local measurements, each sampled fortnightly during the period October 2006 until March 2008. Comparing model results at 0.5° resolution to point measurement is complicated, and thus in this section, we compare our model-averaged result against the 17-site average from Kindler et al.. Our modeled average of 2.6 (±2.5) gC m^{-2} yr^{-1} is of the same order of magnitude as the observed one (4.2 gC m^{-2} yr^{-1}). Although the modeled mean is about 38 % lower than the one measured, the standard deviation representing the spatial variability in simulated DOC leaching fluxes over all our model grid cells encapsulate the observational mean, highlighting a significant heterogeneity that is difficult to embrace with local measurements alone. This comparison must be taken cautiously because of the limited number of observations and the resolution of our model. Furthermore, DOC leaching flux at the coast is generally not well represented. The reason is that DOC leaching fluxes are normalized by the area of the whole cell. This for cell located at the coast, where the entire cell is not covered by land, the DOC leaching flux is reduced according to the fraction of land that covers the whole grid cell. The area normalized flux at the coast is thus often lower.

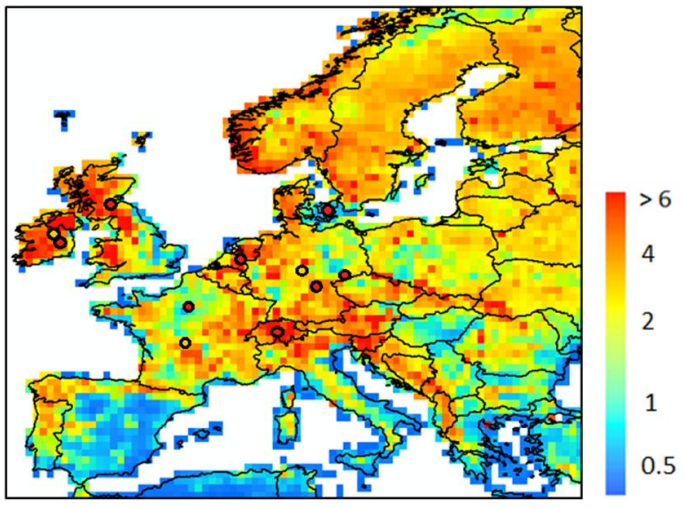

Figure 2.7 *Modelled yearly mean terrestrial DOC leaching flux (period 1979-2006) to the river European river network (in gC m-2 yr-1). The local observations from Kindler et al., 2010 are also reported, using the same scale. Note that the local observations cover a much shorter time period and may not be representative of the whole year.*

The seasonal distribution of the DOC leaching flux is shown in Fig. 2.8. On average, the leaching flux per season averaged over Europe amounts to 1.6, 1.3, 0.5 and 1.4 TgC $month^{-1}$ in winter, spring, summer and autumn, respectively. If we exclude the high latitude and high altitude regions (Scandinavia, the Alps), a clear seasonality is observed with the lowest fluxes in summer and spring and the highest fluxes in winter

and autumn. In the high latitude/altitude regions, the pattern is different with highest fluxes in spring which extends to the summer in the Alps, and corresponds to the snowmelt period. The highest fluxes per unit area are simulated in Scandinavia during the spring season, even though peatlands are not represented in the model. Some regions are leaching hotspots such as the Alps throughout the year, the West Balkans during autumn and the Western flank of the UK in autumn and winter. This is mainly due to the high local runoff and thus runoff rates in these regions.

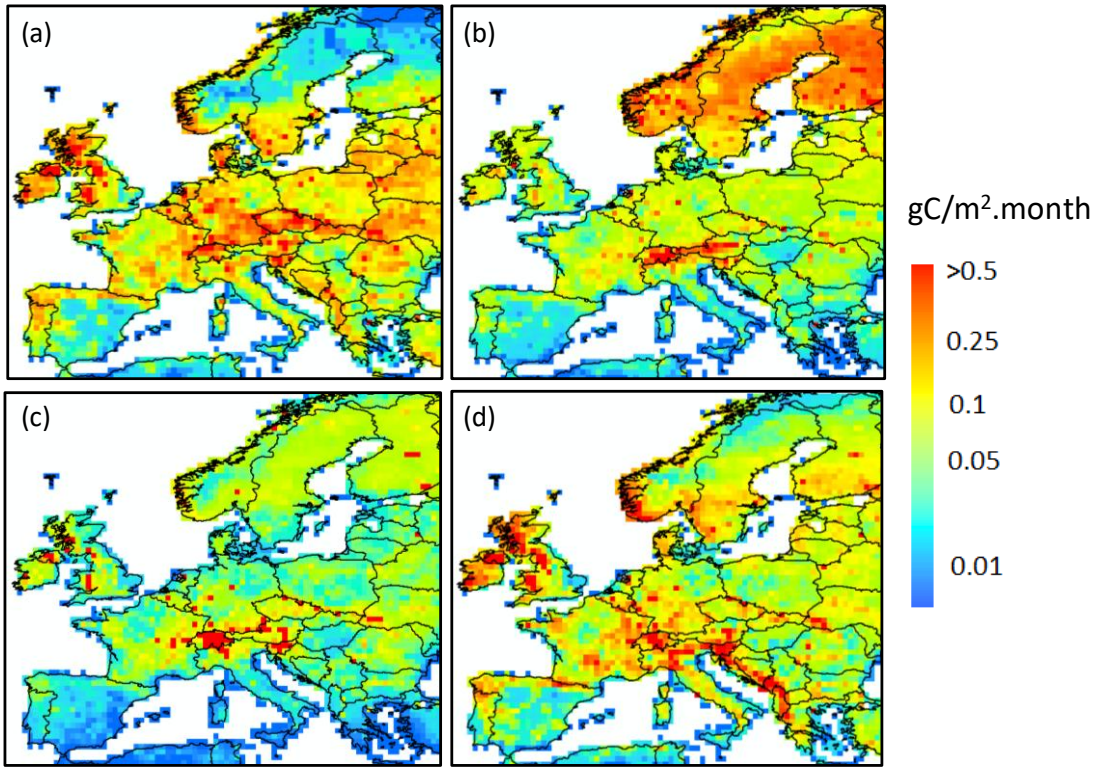

Figure 2.8 *Seasonal distribution of the terrestrial DOC leaching flux (gC m^{-2} $month^{-1}$), average over the period 1979-2006, (a) Winter, (b) Spring, (c) Summer and (d) Autumn. A logarithmic scale is used to better highlight the spatiotemporal gradients.*

2.3.1.5 Fluvial DOC decomposition and export fluxes

The export of DOC from the European river network to the coast is arguably the best monitored variable against which our model can be evaluated. Using this flux to build confidence in our estimate of the terrestrial DOC leaching requires an assessment of the DOC degradation within rivers, a process that is controlled by the hydrology and the half-lives of reactive DOC compounds. In the model, the first-order decomposition rates at a given temperature of 28°C are equal to 0.3 d^{-1} and 0.01 d^{-1} for the labile and refractory DOC pools, respectively. Based on those values and the simulated distribution of labile and refractory DOC, the estimated bulk decomposition rate constant averaged over the entire model domain is equal to 0.05 d^{-1}, which corresponds to a half-life for riverine DOC of about 14 days (Table 2.3). This rate constant varies across Europe but always remains within the same order of magnitude, with half-lifes ranging from 6 to 20 days (0.035-0.122 d^{-1}). These decomposition rates are in good agreement with the average rate reported by Berggren and Al-Kharusi (2020) of 0.037 d^{-1} based on field experiments carried out at multiple river sampling locations across Europe. We thus conclude that DOC decomposition rates used in ORCHILEAK are reasonable, and fluvial DOC fluxes are a valid proxy to evaluate simulated DOC leaching fluxes.

Table 2.3 *Estimated river DOC decay rates applied in ORCHILEAK. Values are reported for four large river basins and for the six dominant climate zones.*

REGIONS		**DECAY RATES (day^{-1})**
BASIN	Rhine	0.074
	Danube	0.043
	Meuse	0.056
	Rhône	0.072
CLIMATE ZONE	Semi-arid	0.035
	Mediterranean	0.046
	Oceanic	0.053
	Humid continental	0.048
	Subarctic	0.064
	Tundra	0.122

Figure 2.9 compares modeled versus observed multi-annual mean riverine DOC concentration at specific locations or within a group of small river catchments. Local

DOC measurements include data near the mouth of the Rhine, Elbe, Rhône and Seine rivers (discharge, DOC concentration and fluxes for the Rhine and Seine in figure 2.10). In addition, Abril et al. (2002) report DOC concentrations measured at nine river mouths discharging along the Atlantic façade and the North Sea, three of which (Rhine (NL), Scheldt (BE) and Gironde (F)) show the seasonality while the other six (Elbe (GE), Ems (GE), Thames (UK), Loire (FR), Sado (P), Douro (P)) only rely on a single measurement per year. Both GLORICH and Abril et al. (2002) report DOC concentrations at the mouth of the Rhine and the Elbe but their values diverge because in addition to analytical uncertainties, the sampling period and data density are not the same. Measured values are equal to 4.3 and 2.9 mg C l^{-1} for the Rhine and 4.6 and 6.1 mg C l^{-1} for the Elbe, respectively highlighting inherent variability in observational data. To complement these local samplings, we also compared our simulated DOC concentrations with those of Mattson et al. (2008) for several groups of catchments in Finland (9 spread over the whole country), Denmark (10 draining into Horsens fjord), the UK (10 draining into the River Conwy) and France (5 draining into the River Tech). All measured DOC concentrations ranged from 2.5 mg C l^{-1} to 10 mg C l^{-1} except in two regions in the north (Finland and basins flowing into the Baltic sea) where concentrations exceeded 10 mg C l^{-1}. For most of the data, the model slightly overestimated the river DOC concentrations. The model results also suggest that the concentrations broadly increase with latitude, with the higher values found in humid continental and subarctic climate and the lower ones in the Mediterranean climate, a result in agreement with the observations from Mattson et al. (2008). Such pattern possibly results from decreasing mean annual air temperature and runoff in Northern Europe that favor incomplete decomposition of litter and soil DOC, thus favouring DOC production in the soil, while at the same time DOC turnover rates in the soils are decreased. Also the increased abundance of forests, and in particular coniferous forests, is a valid explanation for higher DOC leaching (Lauerwald et al. 2012). However, it is important to keep in mind that peatlands are missing, suggesting that we could lack part of the DOC leaching in subarctic and tundra regions leading to even higher DOC fluxes further in the North. Finally, the comparison reveals that model performance tends to improve with catchment size, likely reflecting the difficulty to capture the DOC dynamics at the small scale with the current resolution of ORCHILEAK. But overall, our model is capable of reproducing observed yearly mean DOC concentrations for a wide range of river basins spread between Finland and Portugal.

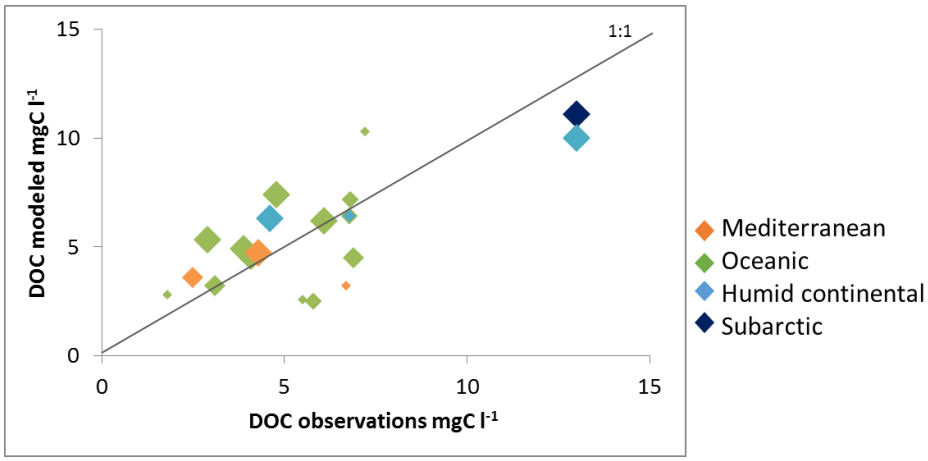

Figure 2.9 *Modelled river DOC concentration against observed values. The color code indicates the dominant climate zone for each catchment while the size of the diamond is proportional to the catchment area according to the following classes: < 10 000 km², < 50 000 km², < 100 000km² and > 100 000 km². See table S4 for further details.*

The temporal evolution of observed river DOC fluxes is only available at four stations (Rhine, Elbe, Rhône and Seine) where DOC time series have been recorded over multi-annual periods (Rhine and Seine illustrated in Fig. 2.10). In term of inter-annual variability (IAV), riverine DOC fluxes present the highest variability with a coefficient of variance (COV) of 0.62 for the Seine and 0.57 for the Rhine. For comparison, IAV of discharge and riverine DOC concentration shows COVs of 0.60 and 0.51 for the Seine and 0.40 and 0.45 for the Rhine, respectively. The higher IAV for the flux is due to a tendency of higher concentrations coinciding with higher discharge, which is due to the flushing effect where higher discharges follow higher amounts of runoff from top-soils rich in DOC. The multi-year mean modelled DOC fluxes are estimated for the Rhine, Elbe, Rhone and Seine at 11.9, 7.2, 8.8 and 3.2 kg s^{-1}, respectively. The observations amount respectively to 7.9, 3.6, 4.6, 1.6 kg s^{-1}. For all stations, the model thus slightly overestimates fluvial DOC fluxes, which is not surprising since the model tends to overestimate the discharge. At these four stations, ORCHILEAK also slightly overestimates river DOC concentrations except for the Seine where concentrations are largely underestimated and discharge largely overestimated. In terms of temporal correlation, the simulated DOC flux for the Rhone compared to the observed one yields a R^2 of 0.6 and a mean error of 92% (results for the Seine, Elbe and Rhine are reported in supplementary table S5). In figure 2.8, we clearly see a large overestimation of the temporal variability in DOC concentrations and this could lead to an overestimation in DOC fluxes since there is a positive relationship between concentrations and discharge. The overestimation of DOC concentrations and consequently of DOC fluxes could be due to high DOC leaching.

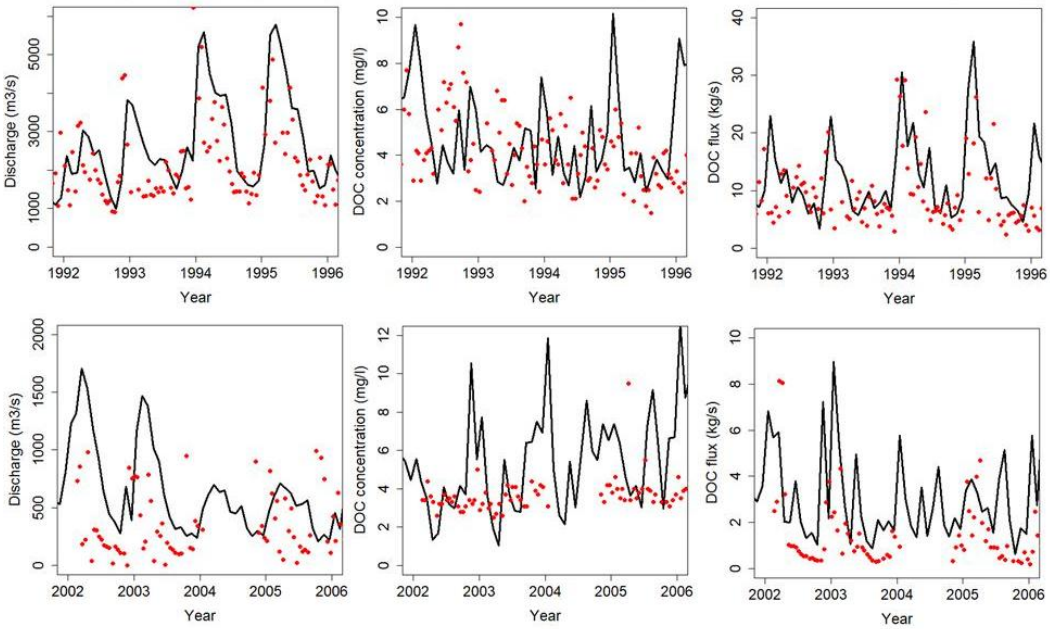

Figure 2.10 *Time series of discharge (left), DOC concentration (middle) and DOC fluxes (right) in the river Rhine at Lobith (top row, period 1992-96) and in the Seine at Poses (bottom row, period 2002-2006. See figure 3 for location of stations.*

The overestimation of DOC fluxes can also be due to the fact we choose to not recalibrate the hydrology scheme but instead we optimized the model for the discharge by adjusting the surface roughness of the vegetation (section 2.2.1). Since those four stations are all located in the same region with the same type of land cover (Western Europe), two other locations have been selected: England and the Baltic Sea. For those two locations, there are no time series data for DOC flux but some studies have measured DOC concentrations/fluxes. Worrall et al. (2012) estimated DOC concentration across UK and Fransner et al. (2016) reported modelled DOC concentrations for all the catchments flowing into the Baltic Sea (table S2.4).

Finally, although the model-data comparison points to a slight overestimation of the river DOC export flux, our pan-European estimate amounts to 12.3 TgC yr^{-1}. This estimate is in fact about 35 % lower than the one reported in another model study by Li et al. (2019), based on the TRIPLE-HYDRA, a process-based model for which the DOC export flux reaches 19.3 TgC yr^{-1}. Li et al. (2019) applied the model at the global scale and simulation results were primarily evaluated against observations in the world-largest rivers and for Europe only included the Volga River. Li et al. (2019) then applied the model for multiple rivers in Europe such as the Danube, the Po, and the Elbe. Despite these different scales of analysis, the export fluxes predicted by both models fall within the same order of magnitude.

2.3.1.6 Manure implementation

The implementation of manure significantly affects DOC leaching from grasslands

and croplands (Fig. 2.11) which cover more than half of the studied region. The average annual input rate of manure into the soil is around 2.5 gC m^{-2} yr^{-1} (Fig. 2.2c). With manure implementation, the DOC leaching rate increase drastically (average of +72% compared to the DOC leaching without manure), in particular in the oceanic and humid continental climate regions, where the average DOC leaching rate changes from 1.6 to 2.7 gC m^{-2} yr^{-1} and 1.7 to 2.5 gC m^{-2} yr^{-1}, respectively. In whole Europe, manure implementation leads to an increase of total DOC leaching into the river network from 9.8 to 14.3 TgC yr^{-1} (fig 2.10a-b). Figure 2.10d shows that the application of manure increases DOC leaching in particular in winter (January, February and March) while in summer (July, August and September) the increase is relatively low. In ORCHILEAK, the manure derived DOC first enters the topsoil. There, a part of it is decomposed, and the rest is transported to deeper soil layers with percolating water. Finally, a variable part of the DOC derived from manure is flushed out of the soil column with the surface runoff and belowground drainage. As manure enters first the topsoil, one could expect that it would increase mainly the DOC leaching from the top-soil. However, our results show that the application of manure does not influence the ratio of DOC leaching through surface runoff vs. belowground drainage. Over Europe, the average increase in top-soil DOC leaching due to manure is equal to half of the total increase, the rest of the increase being contributed by the drainage.

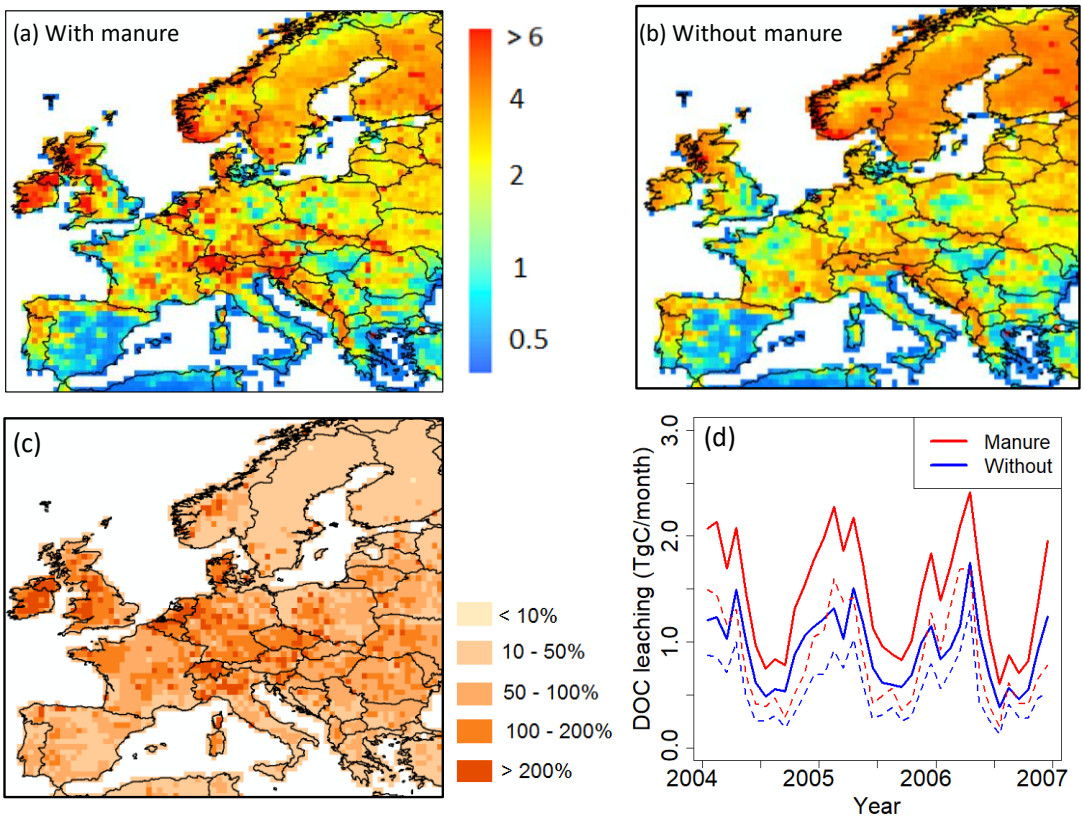

Figure 2.11 *Comparison of modelled yearly mean terrestrial DOC leaching flux (period 1979-2006) to the river European river network (in gC m^{-2} yr^{-1}), with (a) and without (b) the representation of manure application. (c) Increase of DOC leaching in percentage compared to DOC leaching without the manure implementation. (d) Comparison of DOC leaching (solid line) and DOC leaching through runoff only (dashed line) over all of Europe with and without the manure applicationin TgC per month for the years 2004-2006.*

2.3.2 European-scale DOC leaching dynamics

2.3.2.1 Drivers of DOC leaching

Here, we analyze what controls the spatial distribution and temporal variability in DOC leaching. While the grid cell and the basin scales were the most relevant for the evaluation, when searching for potential drivers of soil DOC leaching, such as temperature, runoff and drainage (driven by precipitation), a climatologic segmentation of the European domain can help to better explain the impact of these drivers. Figure 2.12 shows seasonal variability of DOC leaching and total runoff (surface runoff plus drainage) in different climate zones of Europe, revealing a clear and consistent relationship between those two fluxes. The seasonal peak in DOC leaching consistently occurs in winter while minimum values are found during summer. These results suggest that both spatial and temporal variability in leaching are correlated to total runoff.

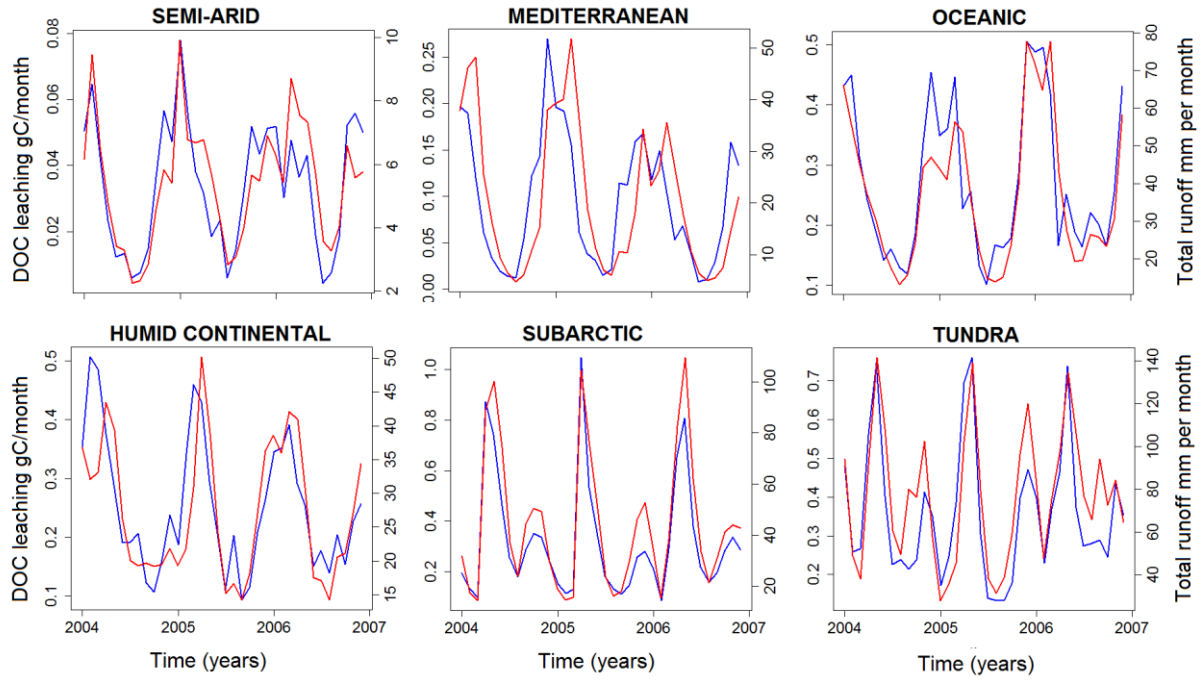

Figure 2.12 *Simulated DOC leaching flux (gC m^{-2} $month^{-1}$) (blue) and total Runoff (mm per month) (red) for the six largest climate zones (period 2004-2006).*

To further explore the environmental controls the DOC leaching, we calculate the partial correlation factor for surface runoff, drainage, temperature and NPP and they

are respectively 0.43, 0.54, -0.17 and 0.18, highlighting that surface runoff and drainage can explain most of the spatio-temporal variability in DOC leaching fluxes, temperature and NPP only playing a subordinate role. We decided to express DOC leaching as fraction of the annual terrestrial NPP (Figure 2.13). Doing this, we assume that NPP, which is undoubtedly the first indirect source for DOC production (since litter and SOC stocks, the sources of DOC, are fed by NPP), is as well an important control of the DOC leaching flux. Moreover, normalizing DOC leaching by NPP, we strive to show the possible influence of other controls, allowing for a more in-depth analysis of the effect of hydrology and climate on the DOC leaching flux. Figure 2.13 reveals that the fraction of terrestrial NPP lost to DOC leaching increases, as expected, with total runoff. Moreover, this fraction increases with the contribution of surface runoff to total water loss from surface runoff plus drainage (Fig. 2.13b). This can be explained by the general decrease in soil DOC concentrations with depth (Fig. 2.6), leading to higher DOC concentrations in surface runoff than in drainage. In fact, according to our simulations, 97% of the leached DOC is concentrated in the surface runoff. Note that higher total runoff is often associated with a higher contribution of surface runoff, which leads to a 'flushing effect' where high runoff events contribute a disproportionate high fraction of the long-term DOC leaching (Idir et al. 1999, Raymond and Saiers 2010). Finally, we found higher leaching to NPP ratios at lower temperatures (Fig. 2.13a), hinting at the fact that lower temperatures lead to longer turnover times of DOC in the soil, and thus higher concentrations in the leaching flux (section 2.1.2).

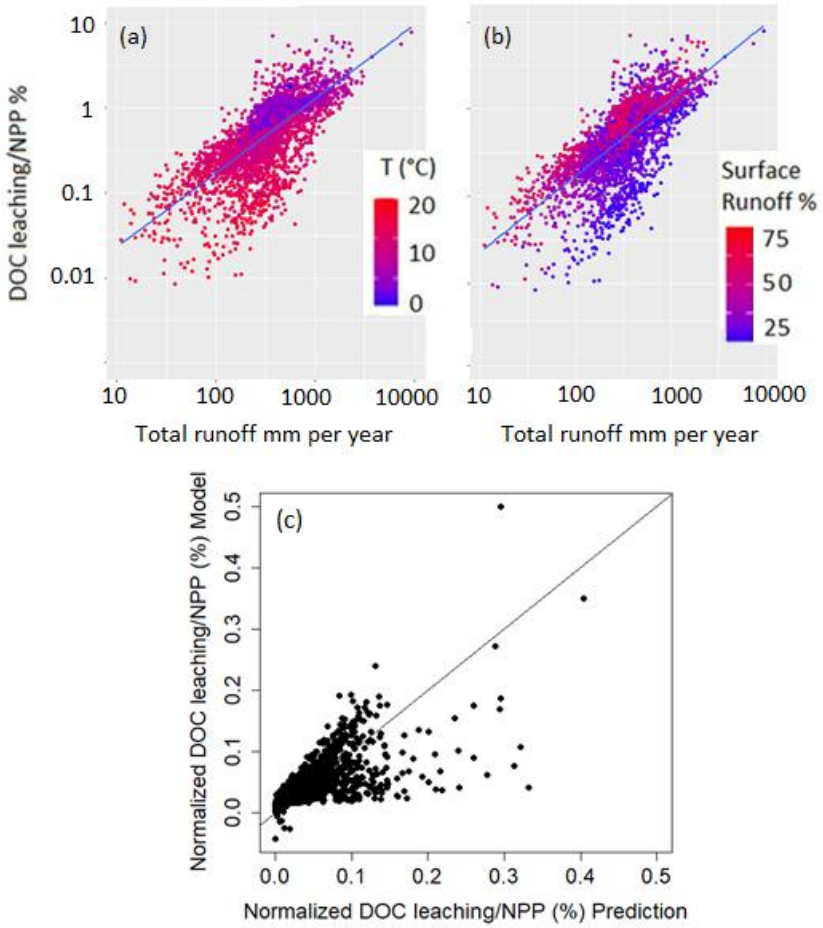

Figure 2.13 *Fraction (%) of terrestrial NPP that is leached as DOC in the river network as a function of total runoff. Each point represents the grid-cell average of both metrics for the entire simulation period (1979-2006). In panel (a) the color scale represents the grid-cell average temperature (°C) while in panel (b), the color scale represents the ratio of surface runoff to total runoff in percentage. Panel (c) the normalized predicted DOC leaching flux to NPP ratio (equation 2.13) against the normalized simulated values.*

To better quantify the effects of all these drivers on DOC leaching, we fitted a multi-linear regression model to predict the ratio of DOC leaching to NPP as a function of surface runoff, drainage and temperature at all grid points and for each month over the simulation period (eq. 2.12). The idea behind this rationale is to highlight that once normalized to the terrestrial NPP, we can directly analyses which physical drivers impact the fraction of NPP that is lost to leaching from terrestrial ecosystems. To compare the importance of each predictor for the spatiotemporal patterns of DOC leaching, we normalized all variables Vs of equation 2.12 according to equation 2.13 (where i is the cell index).

$$\frac{DOC\ leaching}{NPP} = \mathrm{K_0} + \mathrm{K_R} * Runoff + \mathrm{K_D} * Drainage + \mathrm{K_T} * e^{T(^{\circ}C)} \quad (2.12)$$

$$\mathrm{K_0} = 0.01 \pm 7 * 10^{-4}$$

$$\mathrm{K_R} = 0.342 \pm 0.009$$

$$\mathrm{K_D} = 0.276 \pm 0.014$$

$$\mathrm{K_T} = -0.055 \pm 0.013$$

(p-value < $2*10^{-16}$ except for temperature where p-value = $2.7*10^{-5}$)

$$\mathrm{V_{i,N}} = \frac{\mathrm{V_i} - \mathrm{V_{min}}}{\mathrm{V_{max}} - \mathrm{V_{min}}} \quad (2.13)$$

To rule out any significant multi-collinearity in the regression model, we calculated for each predictor the Variance Inflation Factor (VIF). The VIF evaluates the correlations among all predictors which could impact the robustness of the regression model (James et al., 2017). The closer the VIF is to 1, the more robust is the model. In our regression, VIF's of the runoff, drainage and temperature are respectively 1.13, 1.13 and 1.01, confirming that our prediction is robust and not biased by high multicollinearity. The partial correlation factor for surface runoff, drainage, temperature and NPP are respectively 0.43, 0.54, -0.17 and 0.18, highlighting that surface runoff and drainage can explain most of the spatio-temporal variability in DOC leaching fluxes, temperature and NPP only playing a subordinate role.

In Fig. 2.13c, the DOC leaching simulated by ORCHILEAK is compared with the one predicted by equation 2.13. Our simple regression model is able to reproduce the simulations with a residual standard error of 0.68% and a R^2 of 0.45. The coefficients of our regression model reveal that spatio-temporal variability in DOC leaching is mainly driven by the surface runoff (K_R) and drainage (K_D). Air temperature as third control of DOC leaching is of subordinate importance as reflected by its low predictor's coefficient (K_T).

Table 2.4 *Key physical and biogeochemical characteristics of the six dominant climate zones of the European domain.*

Variables	Unit	Semi-arid	Mediterranean	Oceanic	Humid continental	Subarctic	Tundra
Area	km^2	3.01E+11	8.74E+11	1.38E+12	2.11E+12	9.03E+11	1.56E+11
Leaching	$gC\ m^{-2}\ yr^{-1}$	0.35	1.01	2.73	2.5	2.84	4.2
NPP		264.1	389.9	561.3	526.4	338.3	344.2
HR		175.5	278.6	390.6	345.7	255.3	266.9
Harvest (crop)		74.7	68	111.8	112.6	15.7	30.5
Harvest (wood)		5.4	25	46.1	40.7	41	41.8
LUC		-0.04	-4.8	-5.3	-7.7	-15.9	-3.7
NEE calculated		87	107.5	160	175	82.1	73.7
Leaching/NPP	%	0.13	0.26	0.49	0.48	0.84	1.22
Leaching/NEE		0.4	0.94	1.71	1.43	3.46	5.7
Runoff	$Mm\ yr^{-1}$	30	63	82	91	236	404
Drainage		62	229	406	236	290	517
Temperature	°C	15	14.6	10.4	7.8	1.8	4.6

Table 2.4 summarizes for each climate zone in Europe the DOC leaching fluxes, in total numbers and normalized by NPP, as well as other important components of the terrestrial C budget. Since runoff and temperature were identified as the controlling factors of the DOC leaching flux, normalized DOC leaching fluxes are expected to be significantly different among climate zones. Indeed, the fraction of NPP lost to the river network as DOC is the lowest in the semi-arid region (0.13%) where annual precipitation is low (total runoff around 92 mm per year) and temperatures are high.

The highest fraction of NPP exported to rivers as DOC is found in the tundra climate and reach 1.22%. That can be explained by high runoff and drainage (reaching 920 mm per year) in this climate zone, but also by low temperatures lowering the fraction of DOC already decomposed within the soil column. The subarctic climate also presents a similarly high DOC leaching to NPP ratio with a value of 0.84%. The Mediterranean, Oceanic and humid continental climate zones present intermediate DOC leaching to NPP ratios of respectively 0.26%, 0.48% and 0.49%. Averaged over the whole of the EU-27, the DOC leaching flux normalized to the NPP amounts to 0.60 %.

2.3.2.2 Comparison with previous assessments of DOC leaching

In one of the first studies on the terrestrial C budget of Europe (Janssens et al., 2003) an imbalance (missing sink) between atmospheric CO_2 inversions and bottom up C stock change accounting was partly attributed to the loss of carbon from land to rivers in the form of DOC of around 4 gC m^{-2} yr^{-1}. Our results, 2.6 ± 2.5 gC m^{-2} yr^{-1}, support this hypothesis although we suggest a DOC leaching rate slightly lower than this early study. Our lower value may come from the fact that we did not simulate peatlands and organic soils which are known hotspots of DOC leaching (Leifeld and Menichetti 2018), in particular in areas such as the northern UK and Scandinavia. Uncertainties in the processes included or omitted in the model could also explain some of the discrepancy. In terms of temporal variability, we found the highest DOC leaching in winter averaged over the continent (8.9 TgC in total for the six months of winter October to March) and the lowest in summer (5.4 TgC over the period April to September), consistent with the findings of Kindler et al. (2011). In terms of drivers of the DOC leaching fluxes, our results are in line with empirical findings by Gielen et al. (2011) that identified hydrology as the main driver of the inter- and intra-annual variability in DOC leaching. Similar conclusions have also been drawn by other empirical studies (Michalzik et al., 2001, Neff and Asner 2001, Worrall and Burt 2007).

It is also interesting to compare our results with recent global and regional model studies of DOC leaching in tropical and boreal ecosystems. For the Amazon and Congo basins, Hastie et al. (2019, 2021) found that 12 and 4 % of the NPP is exported each year to inland waters in the form of DOC, respectively – much higher than the one we report for Europe as a whole (0.6%). Note that for these tropical lowland river basins extensive riparian wetlands are an important source of DOC, which are of lower importance in Europe. For the Lena river basin located in the boreal region, Bowring et al. (2020) found a DOC leaching of NPP ratio of about 1.5%. In our model assessment, this ratio reaches a very similar value of 1.2% for the boreal portion of Europe. For the temperate zone, a ratio of 0.35% for the East Coast of the US can be calculated when dividing the average DOC leaching flux of 2.7 gC m^{-2} yr^{-1} simulated by Tian et al., 2015 by the average NPP of 780 gC m^{-2} yr^{-1} estimated by Zhao et al., (2005). Further, our value is quite similar to the one extracted from the global study

by Nakhavali et al. (2020) that amounts to 0.5 % for the European domain only. Overall, this comparison highlights that in Europe, the fraction of NPP lost as DOC to the river network is significantly smaller than in other regions of the world. The lower value is likely due to the lower connectivity between terrestrial and aquatic systems due to the lack of extensive wetlands, which have been reduced by major regulation of the European river network.

2.3.2.3 Implications for the terrestrial carbon budget of Europe

The terrestrial carbon budget is controlled by NPP, heterotrophic respiration, crop and wood harvesting and land use change. Here we look at the net ecosystem exchange (NEE) which is the net C exchange between land and atmosphere (Kramer et al., 2002). However, this view neglects the leakiness of terrestrial ecosystems that permanently removes a fraction of the land C and export it to the river network. Moreover, we can argue that DOC leaching represents a fraction of NEE, while the remainder of NEE can be attributed to harvest, land use change and changes in biomass and soil C stocks. From 1979 to 2012, the average NEE in Europe is 860 TgC yr^{-1} (123 gC m^{-2} yr^{-1}), equaling about 28% of the total NPP (Fig. 2.14b). The ratio of DOC leaching to NEE shows drastic spatial variation, varying from an average value of 0.4% in the semi-arid regions to a value of 5.7% in the tundra. In whole Europe, the DOC leaching is about 3% of the NEE.

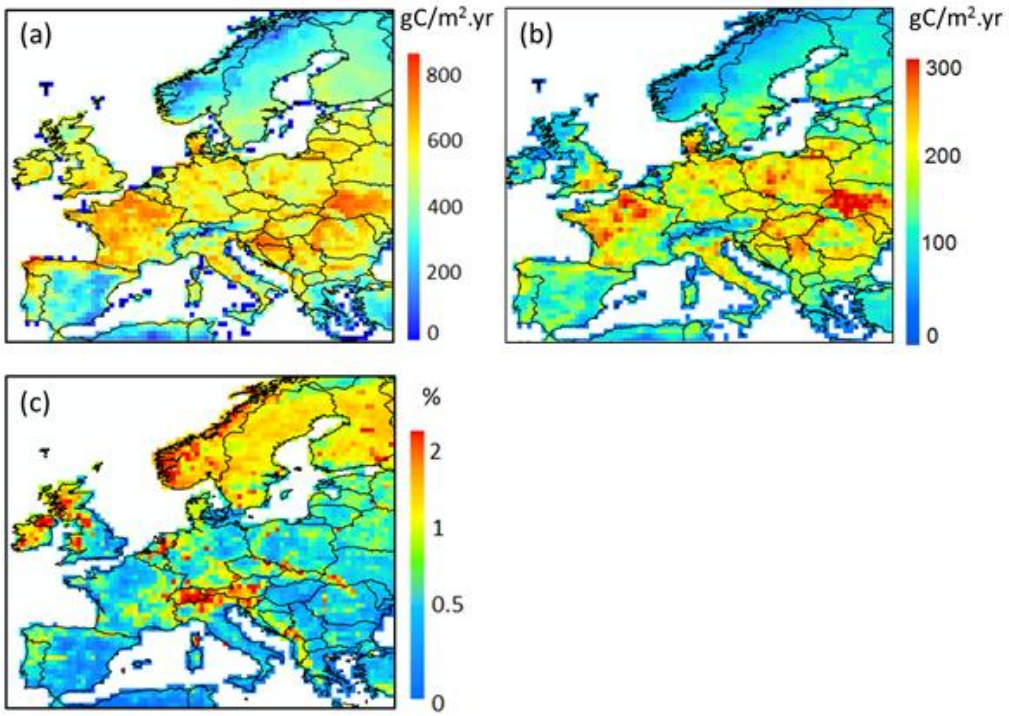

Figure 2.14 *Grid-cell average (a) Net Primary Production, (b) Net Ecosystem Exchange and (c) fraction of NPP leached to the river network as DOC (%) for the period 1979-2006.*

2.3.2.4 Model limitations

ORCHILEAK is a LSM that simulates riverine DOC transfers in the terrestrial C budget, but it still suffers from several limitations. In fact, ORCHILEAK cannot represented all biogeochemical transformation processes affecting DOC in the soil column and the river network (Lauerwald et al., 2017). For instance, environmental controls such as soil pH and ionic strength have been demonstrated to have an impact on DOC solubility in soils (Monteith et al., 2007) and thus affect DOC leaching to streams. Unfortunately, these parameters and processes are not represented in our model, as there are still no reliable methods and forcing data to simulate the dynamics of soil pH and ionic strength in the soil solution at large scale.

As mentioned before, peatlands are not included in the model, yet they cover a large part of the northern part of Europe. Peatlands are known to play an important role in the C cycle, and are an important source of DOC to the river network. One of the major next step would be to merge ORCHILEAK with ORCHIDEE-PEAT, a new branch of the land surface model ORCHIDEE (Qiu et al., 2019). Since this model has been developed for the northern peatlands at Holarctic scale, it could be directly merged with our version of ORCHILEAK.

Another source of DOC originates from wastewater treatments plants that are not included in the model due to the lack of forcing data related to the sewage water treatment. It has been shown that DOC concentrations in sewage are important (Griffith et al 2009). However, Meybeck (1986) showed that DOC from sewage is very labile and only affects the concentration within short distances downstream of water processing plants. Having avoided observation data from sites known to be impacted by sewage effluents directly, we assume that our model-data evaluation was not impacted by this potential DOC source. For assessing the role of soil DOC leaching in the terrestrial C budget, sewage is not a contribution of direct interest.

While riparian zones are a major source of DOC to the river network (Inamdar and Mitchell 2006, Grabs et al. 2012), the impact of riparian zones on DOC leaching through runoff to the river network is only implicitly represented in the model (as described in Lauerwald et al. 2017). Due to the coarse resolution of the model, riparian zones around small streams (order 1 to 3) are not explicitly represented in the model. It is assumed that the extent of the riparian zones, from which most of the DOC stems, scales linearly to the surface area of these small streams, both in time as well as in space (i.e. between different grid cells of our model grid). While the surface area of these small streams is not directly represented, Lauerwald et al. 2017 assumed that spatial and temporal variations in this stream surface area scale to the square root of discharge that is flowing through these streams (eqs. 1 and 2 below), roughly

in line with empirical scaling laws (e.g. Raymond et al. 2012). For the larger rivers, for which the surface area is explicitly represented in the model, it is assumed that the inundated riparian zone can temporally make up to 10% of the river water surface area, depending on the temporal variability of discharge.

ORCHILEAK could further be improved through the implementation of lakes and reservoirs. It has been showed that dams have a direct impact on C retention efficiency in the inland water river network (Maavara et al., 2017). The representation of methanogenesis and methane evasion could also be implemented, while it has been that wetland are a major source of methane and that this flux could be largely increased in the future due to climate change (Zhang et al., 2017), in Europe the representation of methane will likely not have a strong impact compared to tropical regions. So far, ORCHILEAK does not represent lateral transport of POC, yet its non-negligible role in the terrestrial C budget has been demonstrated (Zhang et al., 2018, Naipal et al. 2019). Finally, the effect of nutrient limitation on the C cycle is not yet taken into account in ORCHILEAK. It has been demonstrated that the implementation of nitrogen (N) and phosphorus (P) could reduce the simulated land C sink (Goll et al., 2012, Sun et al. 2021). It can be assumed that nutrient limitation would similarly affect DOC leaching, and could dampen its increase with rising atmospheric CO_2 levels predicted by previous studies with ORCHILEAK (Lauerwald et al. 2020, Hastie et al., 2021).

2.4 CONCLUSION

We reconstructed the terrestrial and riverine C fluxes in Europe during period 1979-2012 using the ORCHILEAK LSM. The total C leaching from soil to European rivers is 14.3 TgC yr^{-1} on average, about 0.6 % of the estimated NPP and 3% of the terrestrial net up-take of atmospheric C. This flux shows large spatial and temporal variations. In specific, DOC leaching overall increases from warm and dry regions to cold and wet regions. However, since the model does not represent peatlands yet, the simulation results for subarctic and tundra regions in northern Europe could be biased. In whole Europe, DOC leaching rate is the highest in winter and lowest during the summer, mainly controlled by the seasonal variation of runoff. The implementation of manure lead to a significant increase in DOC leaching over the oceanic and humid continental region where croplands and grasslands are dominant. Our results contribute to a better assessment of the land-ocean C fluxes in Europe and to a better understanding of the effects of lateral C transfer on the terrestrial C budget. Combined with recent large-scale studies in tropical and boreal biomes as well as along the east coast of the US, an emergent view regarding the global role of DOC leaching on the terrestrial C balance and its underlying drivers is progressively emerging.

2.5 SUPPLEMENTARY

Table S. 2.1 List of the parameters for the new soil carbon module of ORCHILEAK with their description, value, units, and the parameterization used for each parameter.

PARAMETER	DESCRIPTION	VALUE	UNIT	PARAMETRIZATION
D_DOC	Molecular diffusion coefficient of DOC	$1.06*10^{-5}$	$m^2\ d^{-1}$	Ota et al., 2013
D_bio	Diffusion coefficient used for Bioturbation litter and soil carbon	$2.74*10^{-7}$	$m^2\ d^{-1}$	Koven et al. (2013)
CUE	Partitioning between SOC production and respiration	0.3	-	This study
ω_L	Production of DOC by the decomposition of litter	0.2	%	This Study
ω_{SOC}	Production of DOC by the decomposition of SOC	1.2	%	This study
k_D	Equilibrium partition coefficient	$8.05*10^{-5}$	m^3 water kg^{-1} soil	Moore et al. (1992)

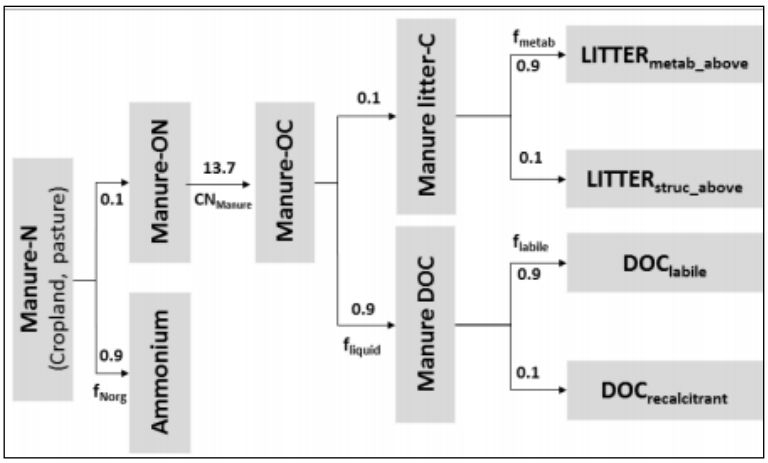

Figure S.2.1 Implementation of the manure scheme in ORCHILEAK.

Table S.2.2 Dominant pfts (%) for 5 large European river catchments.

Basins	Boreal Forest %	Temperate Forest %	Grassland %	Cropland %
Danube	27	8	22	39
Elbe	22	6	26	41
Rhine	10	20	35	24
Rhône	10	15	50	18
Seine	<0.1	12	35	49

Table S.2.3 *Hydrology results in multiple catchments across Europe. Comparison catchment areas, discharge observed vs modeled and statistics (Nash-Sutcliffe efficiency, mean error and coefficient of determination.*

Station	REAL Catchment area km^2	OBS average (m^3/s)	MODELED Catchment area km^2	MOD average (m^3/s)	NSE	mean error %	R^2
Frankfurt	24760	201	31900	335	-0.95	66	0.55
Basel	35900	1084	35770	1190	0.35	12	0.62
Dresden	53100	340	45830	342	0.54	2	0.55
Beaucaire	95590	1745	77270	1698	0.4	3	0.57
Bratislava	131330	2078	133830	2400	0.01	17	0.49
Neu Darchau	131950	704	137820	1216	-1.5	73	0.6
Senta	140130	809	106220	882	0.53	11	0.58
Lobith	160800	2345	152140	2767	0.04	20	0.48
Svistov	658340	5793	651980	6965	0.19	18	0.43
Ceatal	807000	6456	787530	7302	0.07	18	0.44

Table S.2.4 *Comparison of modeled (MOD) versus observed (OBS) DOC concentrations measured at specific locations along the European river network. The table also reports the location ID (see figure 3), the original reference, and the sampling period.*

RIVER	#ID	SOURCE	COVERED PERIOD	OBS mg C l^{-1}	MOD mg C l^{-1}
Douro	A1	Abril (2002)	09/1997	2.5	3.6
Sado	A2	Abril (2002)	04/1996 and 09/1997	6.7	3.2
Gironde	A3	Abril (2002)	11/1996 to 02/19998	3.1	3.2
Loire	A4	Abril (2002)	08/1998	3.9	4.9
Scheld	A5	Abril (2002)	07/1996 to 05/1998	6.8	7.2
Ems	A6	Abril (2002)	07/1997	6.8	6.4
Elbe	E1	Abril (2002)	04/1997	4.6	6.3
Rhine	Ri1	Abril (2002)	10/1996 to 03/1998	2.9	5.3
Thame	A7	Abril (2002)	09/1996 and 02/1999	5.8	2.5
Tech	M1	Mattsson (2008)	10/2001 to 09/2002	1.8	2.8
Wales	M2	Mattsson (2008)	01/2002 to 12/2002	5.5	2.6
Denmark	M3	Mattsson (2008)	10/2001 to 09/2002	7.2	10.3
Finland	M4	Mattsson (2008)	01/2001 to 12/2001	13	11.1
Rhine	Ri1	Glorich	1992 to 1996	4.3	4.7
Elbe	E1	Glorich	1998 to 2001	6.1	6.2
Seine	S1	Eau de France	2002 to 2006	6.9	4.5
Rhone	Ro1	Eau de france	1990 to 1995	4.1	4.4
England	-	Worrall 2012	2001 to 2007	4.8	7.4
Baltic	-	Fransner 2016		13	10

Table S.2.5 *Statistics for the simulated discharge, DOC concentration and DOC flux in four large rivers against measured values reported in the GLORICH dataset.*

River	Discharge RMSE %	Discharge R^2	Concentration RMSE %	Concentration R^2	Flux RMSE %	FLUX R^2
Rhine	45	0.43	70	0.43	84	0.35
Elbe	114	0.43	334	0.04	121	0.5
Rhone	37	0.6	117	0.1	122	0.6
Seine	202	0.08	64	0.4	147	0.5

3 INTRINSIC AND EXTRINSIC CONTROLS ON DISSOLVED ORGANIC CARBON DECOMPOSITION KINETICS: THE CASE STUDY OF THE UPPER-MEUSE CATCHMENT

Contribution: C. Gommet with inputs from S. Bonneville, L. Chou and P. Regnier

Abstract

Degradation of dissolved organic carbon (DOC) in freshwaters plays an important role in the carbon cycle. Understanding its reactivity in the river system is thus essential yet complex. The relationships between DOC reactivity, its composition and the environmental factors are still uncertain. Here, we investigated the link between DOC decay rate constant, the land cover of the catchment, the seasonality and the quality of the organic matter (OM). We sampled water in the upper Meuse and its tributaries in different locations across the catchment to isolate the effects of different land cover classes and during four different periods through one year to investigate the seasonality. We performed incubations in the dark to study the DOC biodegradation kinetics over one month and measured fluorescence properties (specific UV absorbance - SUVA and fluorescence index - FI). We described the biodegradation kinetics using a one-pool (FO) and two-pool (FOR) first order models as well as with a reactive continuum (RC) model. We observed that the one-pool first order kinetics did not adequately describe the DOC degradation in the river system and therefore should not be used in models. The two-pool first order kinetics and the reactive continuum (RC) proved to fit reasonably well the time-lapse DOC concentration in our incubations. Excluding data from the March campaign, the median half-life time determined by the FOR method is 10 days, value slightly lower than the estimated water residence time (WRT) of the entire Meuse catchment and the median initial decay coefficient for the same campaigns is around 0.02 day^{-1}. The SUVA index, which is a quantitative measure of the aromatic character of dissolved organic matter (DOM), proved to be a good proxy for DOC reactivity. The higher the index, the more aromatic is the DOM and the lower is the initial decay rate constant of DOC. Results on degradation for the Meuse show little seasonality and the land cover does not seem to have a strong impact on DOC reactivity, i.e., rate constants averaged over different seasons or land cover are not significantly different. Yet, we find that each land cover exhibits a specific SUVA *vs.* rate constant (k_{RC}) trend and that for cropland the DOC initial decay rate constant decreases the least with increasing SUVA and for grassland the greatest. Overall, we show that SUVA can provide a rough estimate for

DOC reactivity (within an order of magnitude), the advantage being that it is much less time-consuming to measure the SUVA than to conduct DOC incubations.

3.1 INTRODUCTION

Rivers convey large quantities of organic matter (OM) from terrestrial environments to the coastal zone (Bauer et al., 2013; Drake et al., 2018). Riverine OM comes from three main sources. Firstly, inland waters receive large loads of allochthonous OM of terrestrial origin through runoff and drainage of their catchment basin. The second source concerns autochthonous OM resulting from *in-situ* aquatic production via autotrophic and heterotrophic metabolic pathways (Guillemette and Del Giorgio, 2012). Allochthonous OM is generally considered to be more recalcitrant as it is derived from vegetation and soil organic matter while the autochthonous OM is associated with phyto- and bacterio-plankton activities (Tranvik, 1992; Jaffe et al., 2008). The third input is attributed to direct point and diffuse sources of anthropogenic origin, including those such as manure or sewage.

Riverine carbon (C) constitutes an important part of the carbon cycle (Battin et al., 2009) and is present as dissolved and particulate organic C (DOC and POC) and dissolved and particulate inorganic C (DIC and PIC). During transport in the river system, organic C is mineralized into CO_2 through an array of photoreactions and biodegradation pathways. DOC degradation can be influenced by factors such as the water temperature, microbial composition, and nutrient and oxygen availability as well as by the molecular properties of the organic matter (size, aromaticity, complexity) (Del Giorgio and Davis, 2003, Bastviken et al., 2004). Despite the increasing research focusing on DOC reactivity in inland waters (e.g., Koehler et al., 2012; Catalan et al., 2016), quantification of the decay rate constants and identification of the factors controlling the OM degradation are still uncertain and poorly constrained. Determining the ranges and the drivers of DOC reactivity in inland waters would help predict DOC dynamics and thus contribute to developing biogeochemical models (Arndt et al., 2013). In Chapter 2, the land surface model ORCHILEAK was used where DOC reactivity in the river network was represented as two distinct pools each following a first order kinetics. The goal of this chapter is to assess if a first order kinetics is the best representation of DOC degradation along the land-ocean aquatic continuum and, if not the case, to provide a better representation of DOC reactivity based on results from field and laboratory experiments.

Several experimental approaches have been used to determine the DOC decay rates in inland waters. Water samples are filtered through different pore size of pre-combusted glass fiber filters. In several experiments, the samples were filtered and an inoculum added (as in Servais et al., 1989, 1995; Koehler et al., 2012; Catalan et al., 2013, 2017; Lv et al., 2019). Other experiments only used filtered samples (Giorgio and Pace 2008; Benner and Kaiser, 2011; Hotchkiss et al., 2014; Soares et al., 2019; Lv et al., 2019). Also, some have directly incubated unfiltered waters (Attermeyer et al.,

2018). Closed-system incubation experiments carried out in the dark at a constant temperature have been performed to study the biodegradation (e.g., Servais et al., 1995; Vähätalo et al., 2010; Koehler et al., 2012; Attermeyer et al., 2018). Some studies also investigated the effect of photo-oxidation (Catalan et al., 2013; Lv et al., 2019). Lv et al. (2019) studied DOC degradation under three different conditions: microbial degradation only, photo-degradation only and a combination of both. DOC concentrations were found to decrease and stabilize rapidly (within a day of incubation) under UV-illumination alone, while in the presence of micro-organisms (in the dark or under UV-light) the degradation of DOM persisted over a longer duration (typically 5 to 6 days) (Lv et al., 2019). The duration of incubations differed greatly between studies, ranging from 7 days (Attermeyer et al., 2018) to 3.7 years in (Koehler et al. 2012). However, when investigating DOC microbial degradation, several studies have shown that an incubation of one month is often long enough to reach a relatively constant value of DOC concentration (Servais et al., 1989; Catalan et al., 2017).

As such, DOM bioavailability decreases with time because microbial communities selectively consume first the more labile substrates (Middelburg, 1989). DOM properties and characteristics have also been investigated as controls of decay rates. In particular, UV absorbance and fluorescence of DOM allow one to derive a series of indices illustrating, for instance, the aromaticity of DOM or its source from terrestrially-derived (i.e., plants and soil organic matter) to aquatic microbial by-products. Such intrinsic properties of DOM have been linked to its biodegradation kinetics (Attermeyer et al., 2018 and Soarse et al., 2019). More advanced studies on fluorescence of DOM have been conducted to characterize more precisely its chemical composition, with excitation-emission matrix (EEM) (Lv et al., 2019) or with liquid chromatography-organic carbon detection (LC-OCD) (Catalan et al., 2017). EEM is an effective method to identify protein-like and humic-like substances (Lu and Jaffé, 2013; Santin et al., 2009; Stubbins et al., 2014). LC-OCD allows one to differentiate three DOM chromatographic fractions: high molecular weight substances (HMWS), low molecular weight substances (LMWS), and humic substances (Graeber et al., 2015; Catalan et al., 2017).

Currently, different approaches are being used to model DOM biodegradation (Guillemette and del Giorgio, 2011; Koehler et al., 2012; Catalan et al., 2017) or photo-oxidation (Benner and Kaiser, 2011, Lv et al., 2019). DOM biodegradability is often described using a first order rate law where the decay rate constant is calculated only with the initial and final concentrations (e.g., Servais et al., 1995; Hotchkiss et al., 2014; Catalan et al., 2016; Attermeyer et al., 2018). This first order kinetics suggests that the DOM behaves as one compound characterized by a single decay rate constant while in fact DOM is composed of a variety of OM types, which exhibit a specific composition and thus reactivity. One possible improvement consists of including several pools of DOM, each following a specific first-order kinetic law; however, with increasing number of pools, it becomes difficult to estimate all the kinetic constants

(Hopkinson et al., 2002; Hotchkiss et al., 2014). To circumvent these difficulties, Boudreau and Ruddick (1991) introduced a new representation of OM bioreactivity based on the reactive continuum model to simulate the time-lapse evolution of DOC concentrations during incubations. This model relies on the same principle as the multiple first order kinetics but instead of having a finite number of pools, the RC model uses an infinite number of pools (Boudreau and Ruddick, 1991). Vähätalo et al. (2010) developed a new RC model that expresses the biodegradation as a probability, in other words, each OM pool has a certain probability of degradation between 0 and 1.

In the present study, we quantify the microbial DOC decay rates at the scale of a European catchment. The experimental work was carried out in the Meuse basin which exhibits several of the typical land cover types found in Europe. This catchment - in its upper portion – allows us to sample water that has not been strongly affected by human activities and, thus, to study the degradation of DOC coming from diffuse natural sources as opposed to point sources such as sewage. The first objective is to calculate the DOC decay rates according to different methods and to determine if the choice of methodology (first order kinetics versus reactive continuum models) has an impact on the interpretation of DOC reactivity. The second objective is to evaluate the spatio-temporal variability of DOC reactivity in relation to land use and, if possible, to unravel intrinsic DOM control on its reactivity via fluorescence properties. Finally, the implications of our results regarding the modelling of DOC degradation are briefly discussed.

3.2 MATERIAL AND METHOD

3.2.1 Study site

The Meuse catchment, with a total length of the main river of around 950 km, covers an area of 36,000 km^2 of which around 41% is located in Belgium, 26% in France, 22% in the Netherlands and the rest in Luxembourg and Germany. The source of the Meuse is situated in France (Haute Marne department) and flows into the North Sea in the south of the Netherlands. The Meuse catchment is under a pluvio-oceanic regime with an average discharge of 360 m^3 s^{-1}, controlled by rainfall–evapotranspiration (de Wit et al., 2007). The average annual discharge at the Belgium–Netherlands border amounts to 265 m^3 s^{-1}, with extremes of less than 10 m^3 s^{-1} during droughts and more than 2500 m^3 s^{-1} during floods (van Vliet and Zwolsman, 2008).

We have chosen to focus on the upstream part of the Meuse and its tributaries (in France and Southern Belgium) as downstream of Namur, the Meuse can be contaminated by industrial and sewage waters which would preclude any conclusions about DOM from diffuse sources. The upper Meuse catchment is covered by cropland (34%), grassland (20%) and temperate forest (35%). We use the map of the land use

(Global land cover 2000, Hartley et al., 2006) to select the sampling locations (Figure 3.1; Table 3.1). Three main land use types were investigated: grassland, cropland and forest. As sampling the Meuse after the confluence of the tributaries would mix diverse waters of distinct chemical composition (e.g., water from a catchment with different land cover), we sampled the Meuse mainly in its upstream part primarily covered by grassland and cropland. To sample water from the Meuse catchment with only one dominant land cover, we focused on the tributaries, in Strahler order from 2 to 6. For each station, we considered the upstream basin in the HydroSHEDS database (Lehner et al., 2008) to calculate the percentage of each land cover in the sub-basin (Table 3.1).

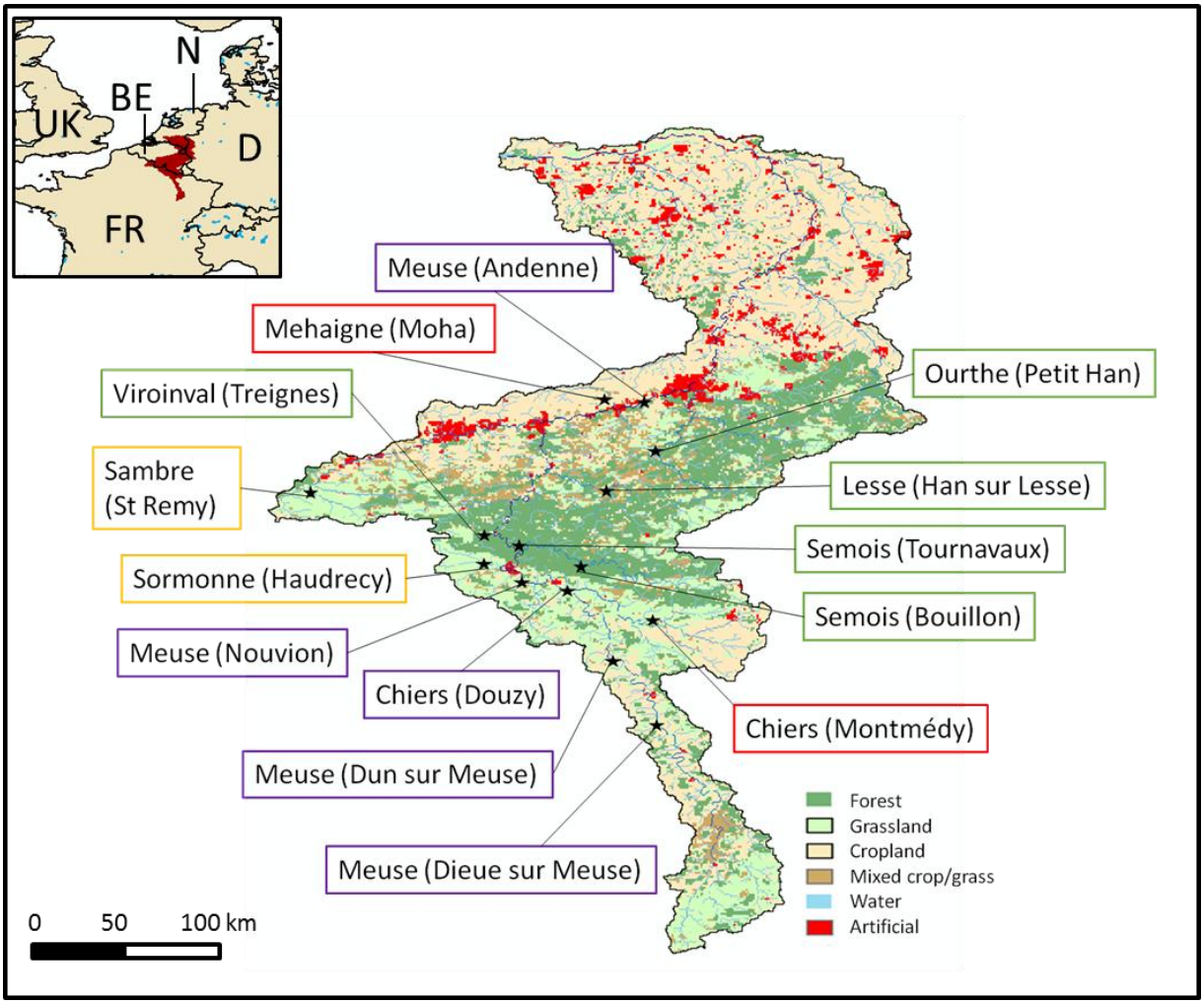

Figure 3.1 *Map of the Upstream Meuse (FR and BE). All sampling locations are represented with a star. The color code for the labelling of each location (the rectangles) represents the dominant land cover of the location and its upstream part: red for cropland dominant, yellow for grassland, green for forest and purple for mixed. (Adapted from the Global land cover 2000, Hartley et al., 2006).*

We classified individual stations according to their land cover percentage. If the percentage of one land cover type is equal to or higher than 50 %, then the station is classified as this one land cover (Cropland, Grassland or Forest). Several stations present similar percentages of both cropland and grassland (around 40 %), which are classified as mixed. The most downstream station (Andenne) is representative of the entire studied basin with equal percentage of the three land cover types (30 %).

Table 3.1 Sampling locations, ranked by land cover.

Locations	River	Latitude (°N)	Longitude (°E)	Land cover (%)			Classification
				Crop	Grass	Forest	
Moha	Mehaigne	50.55	5.19	95	4	0	Cropland
Montmédy	Chiers	49.52	5.37	58	25	16	Cropland
Douzy	Chiers	49.67	5.04	43	37	19	Mixed
Dun sur Meuse	Meuse	49.38	5.18	43	40	17	Mixed
Nouvion	Meuse	49.70	4.79	40	42	18	Mixed
Villers sur Meuse	Meuse	49.02	5.42	35	45	19	Mixed
Haudrecy	Sormonne	49.79	4.62	7	82	10	Grassland
St-Remy	Sambre	50.25	3.90	7	82	10	Grassland
Andenne	Meuse	50.49	5.10	31	30	31	All 3
Petit Han	Ourthe	50.34	5.43	14	37	50	Forest
Bouillon	Semois	49.79	5.07	10	31	58	Forest
Han sur Lesse	Lesse	50.13	5.19	8	12	80	Forest
Tournavaux	Semois	49.87	4.78	8	23	69	Forest
Treignes	Viroinval	50.09	4.67	8	25	54	Forest

3.2.2 Sampling strategy and experimental design

The first campaign (11th and 12th of March 2020) was carried out to obtain an overview of the basin, to examine how DOC concentrations and decay rates would vary within the basin and to explore whether there was a significant difference between stations and the various land cover types. For the subsequent campaigns, we decided to focus also on the reproducibility and reduced the number of sampling sites while collecting two samples at each location. Taking two samples per campaign at each station (for a total of 6 stations, 2 for each land cover type) allows us to assess the reproducibility of the experiment. The first expedition took place before mid-March 2020, corresponding to conditions of high discharge at the end of winter as illustrated by Figure 3.2, showing the discharges during the year 2020 at Amay, a location representative of the studied part of the Meuse (situated near Andenne, our most downstream station). For this first campaign, the discharge was high and reached 1120 m^3 s^{-1}.

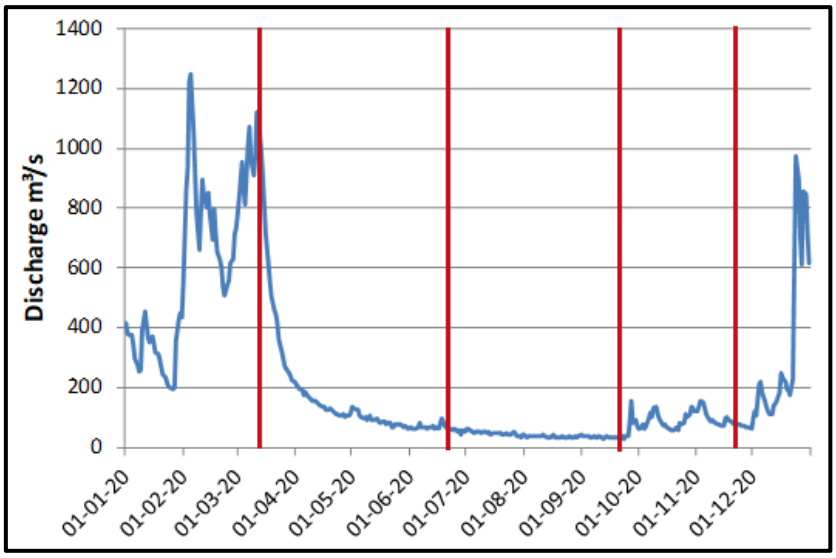

Figure 3.2 *Observed discharge for the year 2020 in Amay (Meuse). Data from " Service public de Wallonie (SPW), Direction générale opérationnelle de la Mobilité et des Voies hydrauliques". The vertical lines correspond to the dates of the four campaigns.*

The second field campaign was conducted right after the spring season on the 22nd of June, a period characterized by low discharge during which high phytoplankton productivity could be expected. The total precipitation for spring (April and May) 2020 amounted to 25 mm, which is significantly lower than the average value for a typical spring period (117 mm, IRM Belgium). As a result of these dry conditions, the discharge of the Meuse in Amay decreased drastically to 63 m^3 s^{-1}.

The third campaign took place at the end of the summer on the 21st of September, again characterized by comparatively low precipitation, 168 mm against 225 mm for the average summer, leading to the lowest discharge of 34 m^3 s^{-1}. This rendered water sampling from bridges or riverbanks very difficult and sometimes impossible.

As a result, the number of sampling stations was reduced from six to three with two samples per location. Finally, the last campaign occurred on the 25th of November with a discharge of 73 m^3 s^{-1}. The objective of this campaign was to perform DOC degradation experiments under conditions of increasing river discharge in late fall. This target was partly fulfilled, albeit the rise was not as high as potentially anticipated.

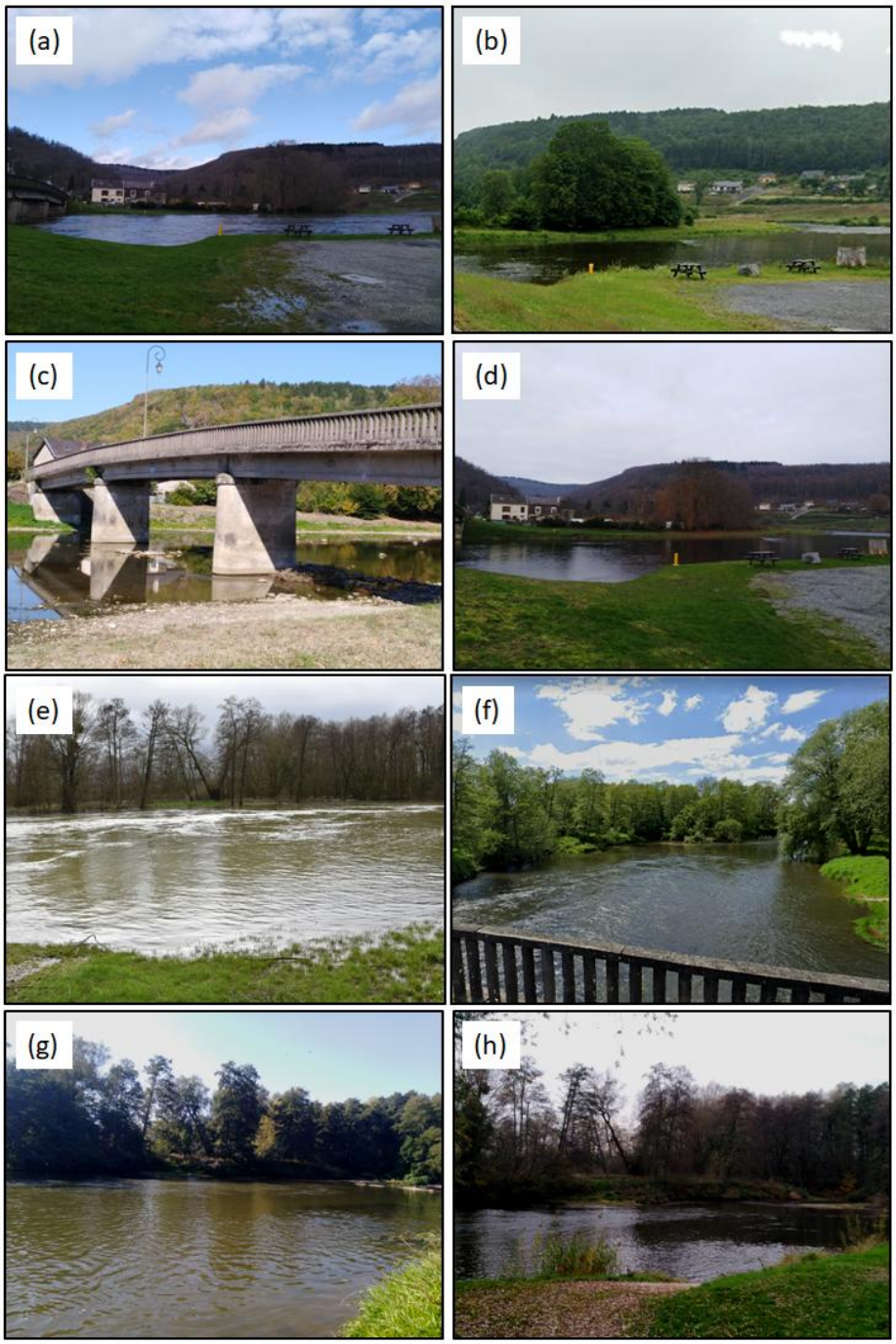

Figure 3.3 *Photography of sampling sites Tournavaux (a-d) and Douzy (e-h) for each season. (a) and (e) for March 2020; (b) and (f) for June 2020; (c) and (g) for September and (d) and (h) for November.*

Figure 3.3 shows for Tournavaux and Douzy (the two stations where all four seasons were sampled) the sampling locations during each campaign. For Tournavaux, the lack of discharge is easily noticeable while for Douzy the level of water reflected a higher discharge.

The water samples were collected with a pre-acid cleaned plastic bucket, preferably in the middle of the stream. The bucket was first rinsed with the water then thrown a second time to collect the first sample. Duplicates were sampled by repeating the operation. *In situ* water temperature and pH were measured immediately, and one or two 500-mL glass bottles (pre-combusted at 450°C) were filled. In the laboratory, water samples were filtered with pre-combusted GF/F filter (0.7 µm) into 0.5-L pre-combusted glass bottles. Incubation bottles were kept in the dark at ambient temperature on a shaking table (60 turns per minute). Over a one-month period, DOC samples were regularly collected (typically every day for the first 5 days then every 2 or 3 days for the following 10 days and finally 1 per week for the last 2 weeks). The samples were stored in pre-combusted 15-mL glass vials containing a small quantity of phosphoric acid (125 µL at 3M to reach a pH value inferior to 2 in order to eliminate the dissolved inorganic carbon in the sample). DOC concentrations were then measured in each sample by high-temperature combustion technique using an Analityk Jena TOC analyzer (Multi N/C 3100). Concentrations of DOC were calculated as the mean of three injections with a coefficient of variance of <5 %. The change in DOC concentration with time for each campaign and each location was then used to determine the rate constant of DOC degradation.

Figure 3.4 *The shaking table for the dark incubations of the samples (left) and the Analityk Jena TOC analyser (right).*

3.2.3 Determination of DOC decay rate constant

The DOC degradation rate constant (k) can be calculated according to different methods. In this study, two mathematical formulations were used to represent the process of DOC degradation: first order kinetic models and the reactive continuum model (Koehler et al., 2012; Catalan et al., 2017). For each sample, the statistical significance (significance F) with an analysis of variance (ANOVA test) was calculated.

This criterion when inferior to the p-value means that the regression model will be statistically significant.

3.2.3.1 First order kinetics

This simple formulation considers that DOC degrades according to a first order (FO) kinetic law as described by Eq. (3.1). Because of its simplicity, this model has regularly been applied to describe DOM degradation in aqueous systems, often using only initial and final concentrations. However, here, DOC concentrations were measured several times during incubation and, thus, the first order kinetic rate law is constrained using all data points of our incubation experiment. The FO model leads to the following evolution of DOC with time:

$$DOC_t = DOC_0 * \mathrm{e}^{-k_1 t} \tag{3.1}$$

where the parameter k_1 (h^{-1}) is the first-order kinetic constant. In order to compute the best possible fit for the first order kinetics with the data, the function solver in excel was used. The solver computes the best k_1 value by minimizing the Sum of the Squared Errors (SSE – defined as the sum of squared differences between predicted data points and observed data points). Using SSE and sum of Squares Total (SST), the coefficient of determinations (R^2) was calculated as 1-SSE/SST. Since k_1 is considered to be temperature dependant, it requires to hindcast back the kinetic constant corresponding to the *in-situ* temperature from the value obtained under the laboratory conditions. Assuming a constant air temperature during incubation of 20°C, the decay rate constant corrected for the *in-situ* water temperature (k_T) can be calculated according to the Arrhenius equation as follows:

$$k_{\mathrm{corr,T}} = \frac{\mathrm{k_1}}{\mathrm{q_{10}}^{\left(\frac{20-\mathrm{T}}{10}\right)}} \tag{3.2}$$

where k_1 (h^{-1}) is the decay rate constant derived from the first order kinetics in Eq. (3.1), q_{10} is a temperature coefficient (set at 2.0, Catalan et al., 2016) and T (°C) denotes the *in-situ* water temperature (Catalan et al., 2016). The calculated, temperature-corrected decay rate constant for the first order kinetics will from now on denominated as k_{FO}.

The second method assumes that a fraction of the DOM pool is non-degradable at the timescale of the incubation, as suggested by Westrich and Berner (1994), Koehler et al. (2012) and Lv et al. (2019). The first pool follows a first order kinetics for the "labile pool" with a decay rate constant k_2 and the second one, "refractory", is considered non-degradable for the timescale of the incubation experiment as described by Eq. (3.3):

$$DOC_t = DOC_L * e^{-k_2 t} + DOC_R \quad (3.3)$$

where DOC_L and DOC_R denote the initial concentrations of respectively the labile DOC and the refractory pool, and k_2 is the decay rate constant of labile DOC in the two-pool model.

Rearranging Eq. (3.3), one obtains:

$$\frac{DOC_t}{DOC_0} = f_L * e^{-k_2 t} + f_R \quad (3.4)$$

where $DOC_0 = DOC_L + DOC_R$ corresponding to the total initial DOC concentration of the two pools, and f_L and f_R are respectively the fraction of the "labile" and "refractory" pool. Note that the labelling "labile" and "refractory" are used here only to distinguish the two pools. f_L and f_R, along with the fast decay rate constant (k_2) are computed using the solver in excel in order to minimize SSE and to assure that the sum of f_L and f_R is equal to 1. For some samples, the best fit was found for f_L to be equal to 1, meaning that the first order kinetic model with a single pool (FO) outperformed the two-pool model. R^2 were computed in the same way as described before. Here, we also applied the temperature correction to the rate constant k_2 according to a formulation similar to Eq. (3.2) and the temperature-corrected decay rate constant for the first order kinetics with a refractory pool will from now on be denominated as k_{FOR}.

Additionally, half-life times for DOC in days (τ_{FO} and τ_{FOR} respectively for the FO and FOR methods) can be calculated following Eq. (3.5) and (3.6), with k in h^{-1}:

$$\tau_{FO} = \frac{\ln(2)}{k_{FO} * 24} \quad (3.5)$$

$$\tau_{FOR} = \frac{\ln(2)}{k_{FOR} * 24} \quad (3.6)$$

Figure 3.5 (a) illustrates the difference between the two first order kinetic models: one pool (FO) and two pools (FOR). Assuming that only a fraction of the initial concentration can be degraded, this leads to a higher k_{FOR} and a stabilization of the concentration with time while the FO model forces DOC concentration towards zero with increasing time.

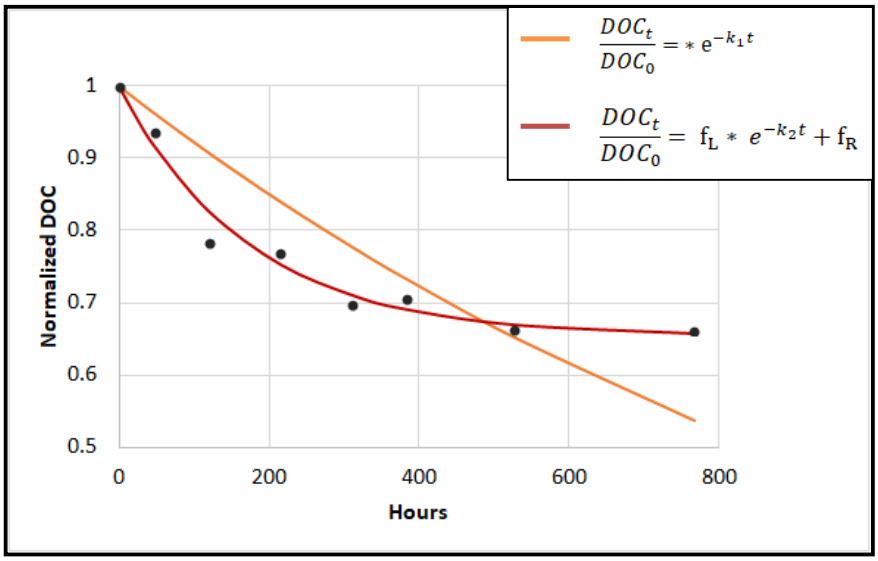

Figure 3.5 *Theoretical fit for the normalized DOC (i.e., DOC_t/DOC_0) as a function of time. Comparison of the two first order kinetics (FO and FOR) where k_{FO}= 0.0008 h^{-1}; k_{FOR}= 0.0058 $h^{-1}$with f_L= 0.35 and f_R= 0.65.*

3.2.3.2 Reactive continuum

DOC degradation kinetics can also be described by a reactive continuum (RC) model (Koehler et al., 2012; Catalan et al., 2017). This model assumes a continuous distribution of organic matter compounds in opposition to a first order kinetic model with a discrete number of pools (here, 1 for the FO and 2 for the FOR). Each compound of the complex organic matter has a different reactivity and thus follows its own first-order kinetics. Initial distribution of reactivities is determined using the gamma distribution which is characterized by two parameters, α and ν. The parameter α (in hours, h) is the average life-time of the more reactive components while ν is a dimensionless parameter related to the shape of the distribution (Boudreau and Ruddick, 1991).The ratio of the DOC concentration at time t (DOC_t) to the initial DOC concentration (DOC_0), corresponding to the remaining fractions of the initial DOC concentration at time t, can be described by Eq. (3.7), where α and ν are determined by the gamma distribution (using the solver function in Excel) to minimize the residuals between each measurement and model (minimum SSE):

$$\frac{DOC_t}{DOC_0} = \left(\frac{\alpha}{\alpha + t}\right)^{\nu} \tag{3.7}$$

The initial decay rate constant (k_3, h^{-1}) is calculated as ν/α and, in contrast to the first order kinetic model, k_3 will decrease through time during incubation following ν/(α+t). High ν and low α values characterize a DOM dominated by labile compounds while inversely, low ν and high α values reflect a refractory-dominated DOM. R^2 values were calculated with the method previously described. An example of this fit to data of the same incubation experiment reported for the first order models (Fig. 3.5) is shown by the red curve in Figure 3.6a. Compared to the FOR method where

DOC concentration stabilizes rapidly due to the "refractory" (in fact, unreactive) pool, the degradation here is slightly more important because the RC model allows for continuous decay of the most refractory DOM compounds. Figure 3.6 b shows the evolution with time of the corresponding k_{RC}, revealing that the rate constant decreases rapidly at the beginning of the experiment and then slows down after 200 hours of incubation. Again, we corrected the calculated k_3 with respect to the in-situ water temperature according to a formulation similar to Eq. (3.2). In the following sections, k_{RC} represents the temperature corrected initial decay rate constant of the reactive continuum model.

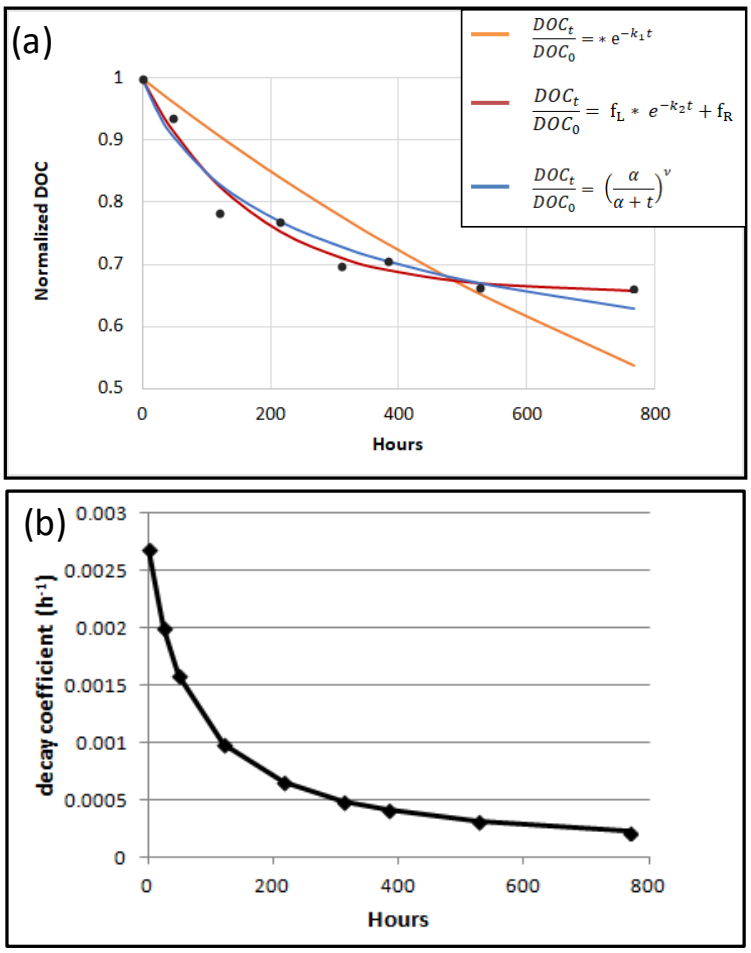

Figure 3.6 *(a) Theoretical fit for the normalized DOC (i.e., DOC_t/DOC_0) as a function of time. Comparison of the two first order kinetics (FO and FOR) and the reactive continuum (RC) method where k_{FO}= 0.0008 h^{-1}; k_{FOR}= 0.0058 h^{-1}, f_L= 0.35, f_R= 0.65; α= 70 h, v= 0.188. (b) Temporal evolution of the decay coefficient from the RC model (h^{-1}).*

3.2.4 Estimation of Water Residence Time

DOC reactivity has been shown to correlate with the Water Residence Time, WRT (Weyenmeyer et al., 2012; Catalan et al., 2016; Attermeyer et al., 2018). For instance, dissolved organic matter reaching the sea (with a long WRT) is likely to become more coloured, indicating a higher fraction of humic substances which is refractory (Weyenmeyer et al., 2012). In this study, we did not attempt to calculate the WRT for

each sampling station but instead we estimated an order of magnitude for the WRT in the Meuse river. This estimation allows us to compare the calculated half-life times based on the first order kinetic models to a typical, average hydraulic residence time. WRT is determined with Eq. (3.8) where A is the drainage area in km^2 (36,000 km^2 for the Meuse catchment) and Q the discharge in $m^3\ s^{-1}$ (average of 360 $m^3\ s^{-1}$ at the mouth), following the approach of Soballe and Kimmel (1987) which is after Leopold et al. (1964). Since the WRT depends directly on the discharge, it is important to note that this value will vary in time.

$$\mathrm{WRT} = 0.08 * \mathrm{A}^{0.6} * \mathrm{Q}^{-0.1} \tag{3.8}$$

3.2.5 Optical properties of Dissolved Organic Matter

An important goal of this study is to investigate the relationship between the DOC decay rate and the quality of organic matter. To do so, an aliquot of the filtered water was sampled at the beginning and at the end of the incubation experiments to evaluate the evolution of the quality of the organic matter. This assessment was performed via the Specific Ultraviolet Absorbance (SUVA) index and the fluorescence index (FI), both measured using a Horiba Duetta fluorescence spectrophotometer (Horiba-Jobin Yvone Scientific Edison, NJ) and the Horiba EzSpec v1.2.0.32 software. Each sample was analyzed individually in a 1-cm pathlength quartz cuvette. Absorbance spectra were blank-corrected using Milli-Q water.

SUVA is defined as the absorbance of UV-light by a water sample at 254 nm wavelength ($SUVA_{254}$) normalized by the DOC concentration in mg L^{-1} (Weishaar et al., 2003). The SUVA index allows us to evaluate the aromatic character of DOM, providing a quantitative measure of aromatic content per unit concentration of dissolved organic carbon (Karanfil et al., 2002), and the SUVA value is correlated with the molecular weight of OM (Johnson et al., 2002). DOM is generally considered as aromatic (i.e., high molecular weight, hydrophobic) and thus refractory when $SUVA_{254}$ exceeds 4 L mg^{-1} m^{-1} and conversely labile (i.e., low molecular weight, hydrophilic) when SUVA is below 3 L mg^{-1} m^{-1} (Karanfil et al., 2002). This index is often used to either characterize natural organic matter (e.g. Swietlik et al., 2005; Wolheim et al., 2015) or to investigate chemical composition for water treatment purposes (e.g. Fabris et al., 2008; Watson et al., 2018; Hua et al., 2020). The SUVA index has also been used to investigate DOC degradation, as in Lv et al. (2019) where the authors studied DOC degradation in the Changjiang river network in China. The authors showed that humic and aromatic substances (high SUVA) are typical examples of recalcitrant DOC compounds during biodegradation. This conclusion also holds for the study by Soares et al. (2019) who found a negative relationship between SUVA with WRT in Swedish waters, implying that during transit through continental watersheds, terrestrial DOM is transformed into less aromatic and more bioreactive forms.

Fluorescence index (FI) is calculated as the ratio of emission at 450 nm to that at 500 nm at an excitation wavelength of 370 nm. FI is inversely related to the lignin content as well as to the aromaticity of DOM. Thus, this parameter can be used to distinguish between diverse sources of DOM, varying from terrestrially derived (plant and soil organic matter, ~1.4) to microbial (bacteria and algae by-products, ~1.9) substances (McKnight et al., 2001). In 2017, Lambert et al. published a study for the Meuse basin where they investigated the impact of human activities on the concentration and composition of DOM and POM. The composition of DOM and POM was investigated through elemental (C:N ratios), isotopic ($\delta^{13}C$) and optical measurements, including FI. Lambert et al. (2017) reported typical FI values for the Meuse ranging from 1.3 to 1.9 with an average of 1.6. In this study, land use was found to be a major controlling factor of fluvial OM composition at the regional scale of the Meuse Basin, with the composition of both fluvial DOM and POM pools showing a shift toward a more microbial/algal and less plant/soil-derived character as human disturbance increased.

3.3 RESULTS

3.3.1 DOC concentrations and decay rates

3.3.1.1 March campaign

For the first campaign (11th and 12th of March 2020), we encompassed a large area with different land cover types (13 sampling locations). At the end of winter, water temperatures were low, with an average of 7.5°C. Initial DOC concentrations varied from 2.5 to 5.5 mg L^{-1} with the exception of St-Rémy (11 mg L^{-1}) (Figure 3.7a). Rivers draining forest ecosystems showed generally the lowest concentrations ranging from 2.5 to 3.5 mg L^{-1} (with the exception of Viroinval having 4.5 mg L^{-1}, see supplementary section) and grassland the highest in St-Remy with 11 mg L^{-1}. Unfortunately, due to COVID restrictions, the experiment had to be shut down after one week of incubation leading to only a few measurements of DOC concentrations over time. The final concentrations after one week of measurements ranged from 2.5 to 5.2 mg L^{-1} (8 mg L^{-1} for St-Rémy).

The restricted number of DOC measurements through time has limited the determination of decay constants via our three methods (FO, FOR, RC), half of the stations having the significance F higher than 0.05, meaning that the regression between DOC concentration and time will not give a good fit. Stations with too high significance F values are not reported here. Figure 3.8 shows the normalized DOC through time for the Douzy and St-Rémy stations and their three possible fits. The other stations exhibit a similar fit, as shown in the supplementary section. Due to the short duration of the experiment, less than 10% of the DOC for Douzy had been degraded within about one week. For the March campaign, the FOR method could not compute two distinct pools and thus the FO and FOR methods gave similar results (f_L=1 and f_R=0), with the exception of the kinetic experiment at St-Rémy where f_L=0.56. The fits for Douzy and St-Rémy with the FOR model are quite good with R^2

values respectively of 0.97 and 0.93. With the RC method, the fits are similar with R^2 values respectively of 0.98 and 0.93. For the other stations (in the supplementary section), the fits were not always as good with the FO(R) (e.g., R^2=0.6 in Bouillon), but overall the coefficients of determination are in general superior to 0.75. The good fit observed despite the experiment being shut down after 1 week can partly be related to the fact that there are only a few points in the incubation experiment. Nonetheless, with both FO(R) and RC, we were able to capture the evolution of DOC concentration with time.

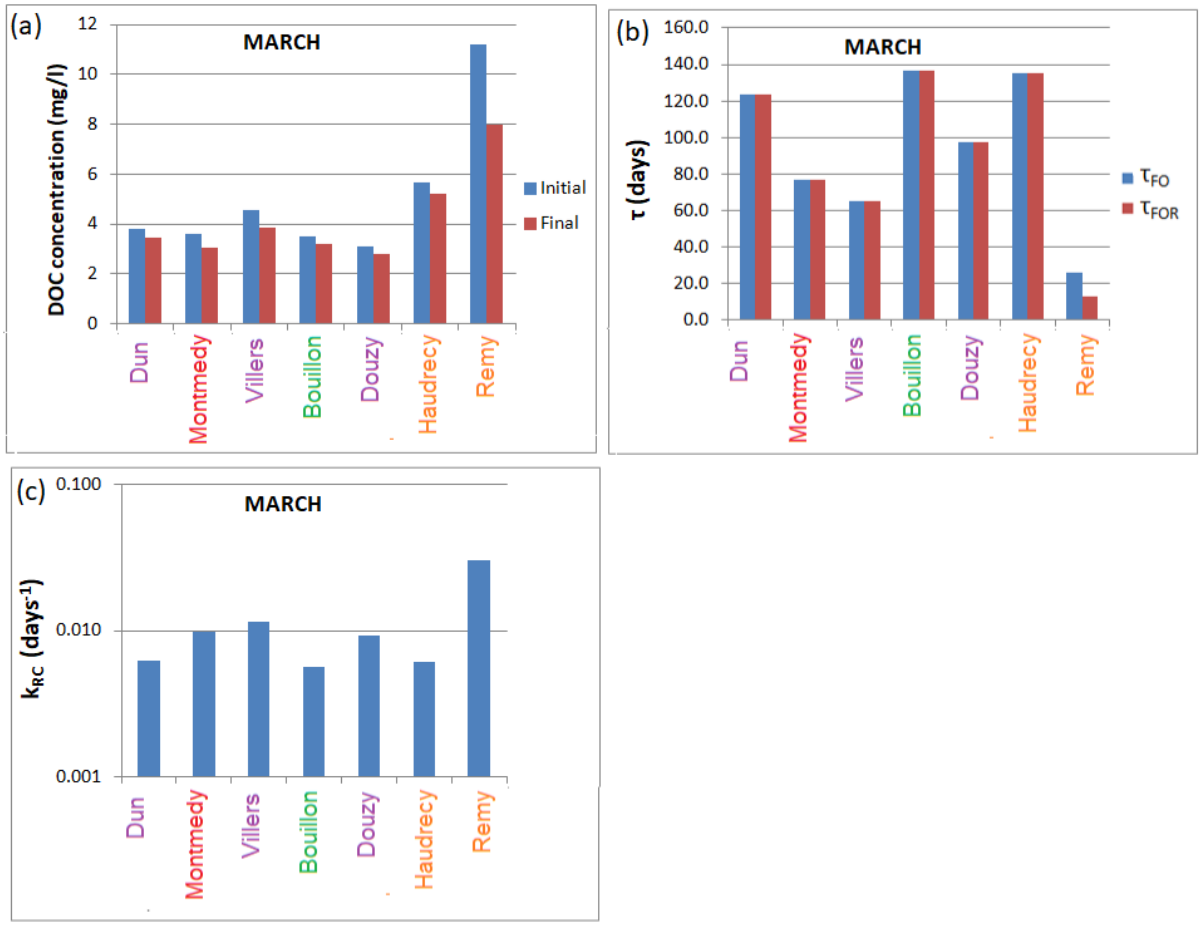

Figure 3.7 *Results of the DOC degradation experiments for the March 2020 campaign. Top panel, DOC concentrations at the beginning (initial) and the end (final) of the incubation experiments (mg L^{-1}); middle panel, half-life times (τ_{FO} and τ_{FOR} in days) calculated for the two first order kinetics); bottom panel, initial decay rate constant calculated with the RC method (day^{-1}). (Color code station: purple = mixed land cover; red = cropland; green = forests; orange = grassland).*

Calculated half-life times for all stations (Fig 3.7b) are disparate varying from 12 to 136 days. Our preliminary results suggest that half-life times for riverine DOC could be remarkably long, more than 60 days with the exception of St-Rémy with respectively 26 and 12 days for the FO and FOR method. The average WRT of the Meuse catchment is estimated to be about 24 days according to Eq. (3.8) and 21 days when accounting for the discharge on the sampling date. This suggests that only a small fraction of the DOC collected at our sampling stations could be decomposed before reaching the sea. Excluding St-Rémy, we find a median half-life time of 110 days for both first-order kinetic models. Initial decay rate constants from the RC model (Fig 3.7c) also show a high variability ranging from 4.8×10^{-3} to 2.8×10^{-2} day^{-1}. The highest value of k_{RC} is obtained for St-Rémy, which corresponds to the lowest half-life time in the FO/FOR models. Excluding St-Rémy, we obtain a median k_{RC} of 7.2×10^{-3} day^{-1}. As expected, high initial k_{RC} in the RC model corresponds to low half-life times in the first-order model. Overall, we note that during this campaign, the DOC decay was rather slow with typically less than 10 % degraded by the end of the experiment. However, the results for the March campaign should be taken carefully because one week of incubation is not long enough to capture the full picture of DOC degradation properly. The different fits are applied only to a few data points over a short period that does not represent, yet the stabilization of DOC concentration. These preliminary results nevertheless suggest that after a week of experiment, the DOC degradation is not complete and support the need to carry out the incubations over a longer period.

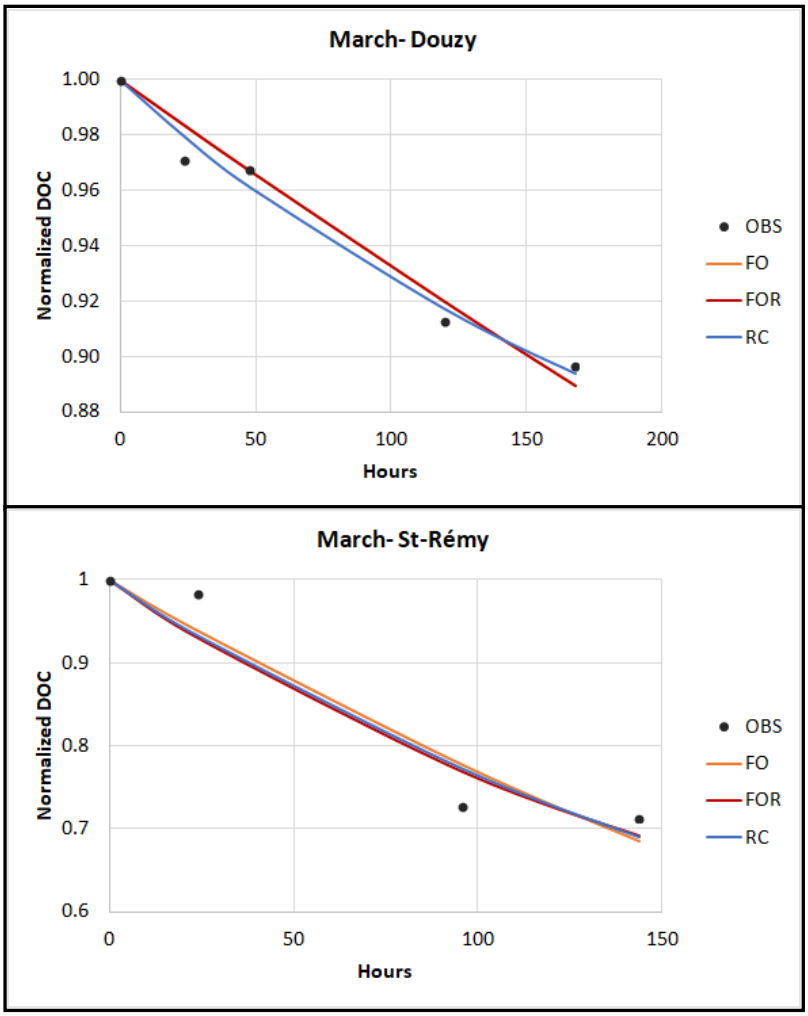

Figure 3.8 *Evolution with time of the normalized DOC concentrations in Douzy and St-Rémy (March 2020), fitted by the three models.*

3.3.1.2 June campaign

Compared to March, initial DOC concentrations in June did not show a trend with land cover and the concentrations varied from 1.7 to 4.3 mg L^{-1} (Figure 3.9 a). The water temperature had increased significantly since March with an average of 16.9 °C. We also noticed that the initial DOC concentrations at some stations (e.g., Dun, Douzy or Han) were quite variable between the two duplicate samples, while the final concentrations after 28 days of incubations were generally similar between duplicates. Final concentrations across stations ranged from 1.3 to 3 mg L^{-1}.

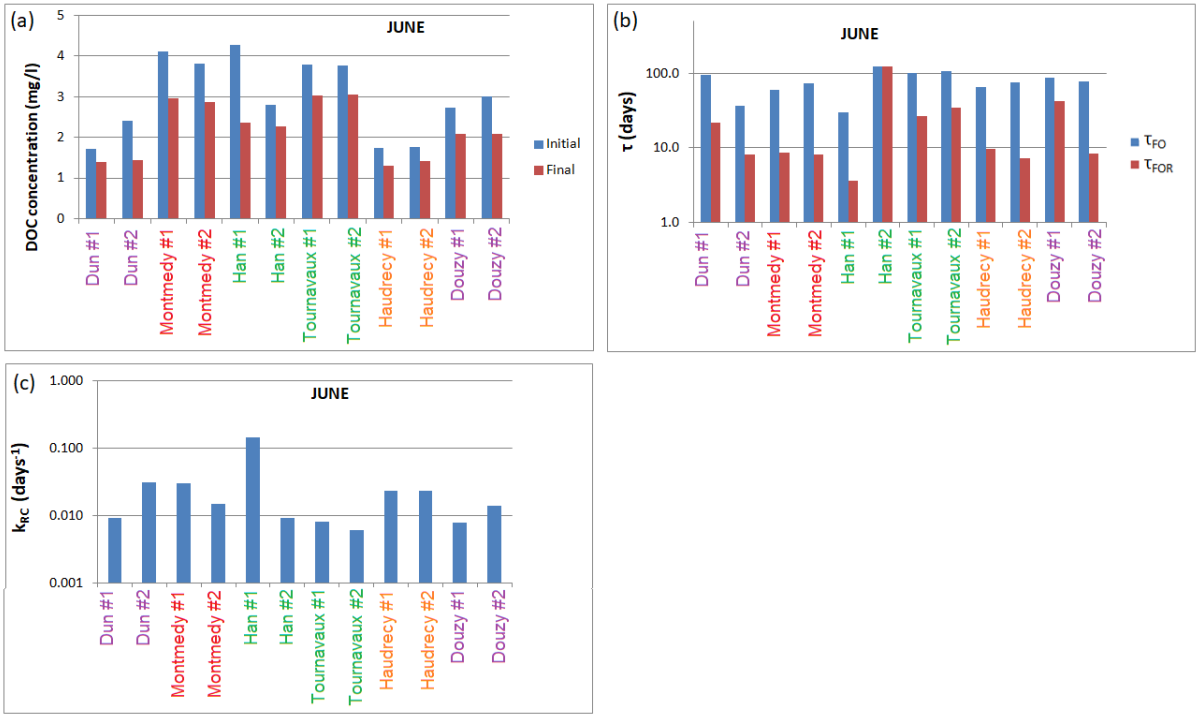

Figure 3.9 *Results of the DOC degradation experiments for the June campaign. (a) DOC concentrations at the beginning (initial) and the end (final) of the incubation experiments (mg L^{-1}); (b) half-life times (days) for the two first order kinetics (τ_{FO} and τ_{FOR}); (c) initial decay rate constant calculated with the RC method (day^{-1}). (Color code station: purple = mixed land cover; red = cropland; green = forests; orange = grassland).*

Figure 3.10 shows the DOC degradation kinetics throughout the experiment for Montmédy (see supplementary information for the kinetics at the other stations). For both replicates, around 30 % of the DOC is degraded by the end of the experiment (f_L of 0.28 and 0.25 respectively for Montmédy #1 and #2). It can be noted that the FO model (R^2= 0.80 for #1 and 0.84 for #2) does not allow one to capture the temporal evolution as adquately as the FOR (R^2= 0.96 for Montmédy #1 and 0.94 for #2) and RC (R^2= 0.96 for Montmédy #1 and 0.95 for #2) models. For one station only, Han #2, the FOR method yielded similar results to the FO method. However, one can note that having a non-degradable pool with the FOR method leads to a stabilization of the DOC concentration since the "labile" pool is almost entirely decomposed by the end of the experiment while the RC method suggests that DOC concentration will continue to slowly decrease.

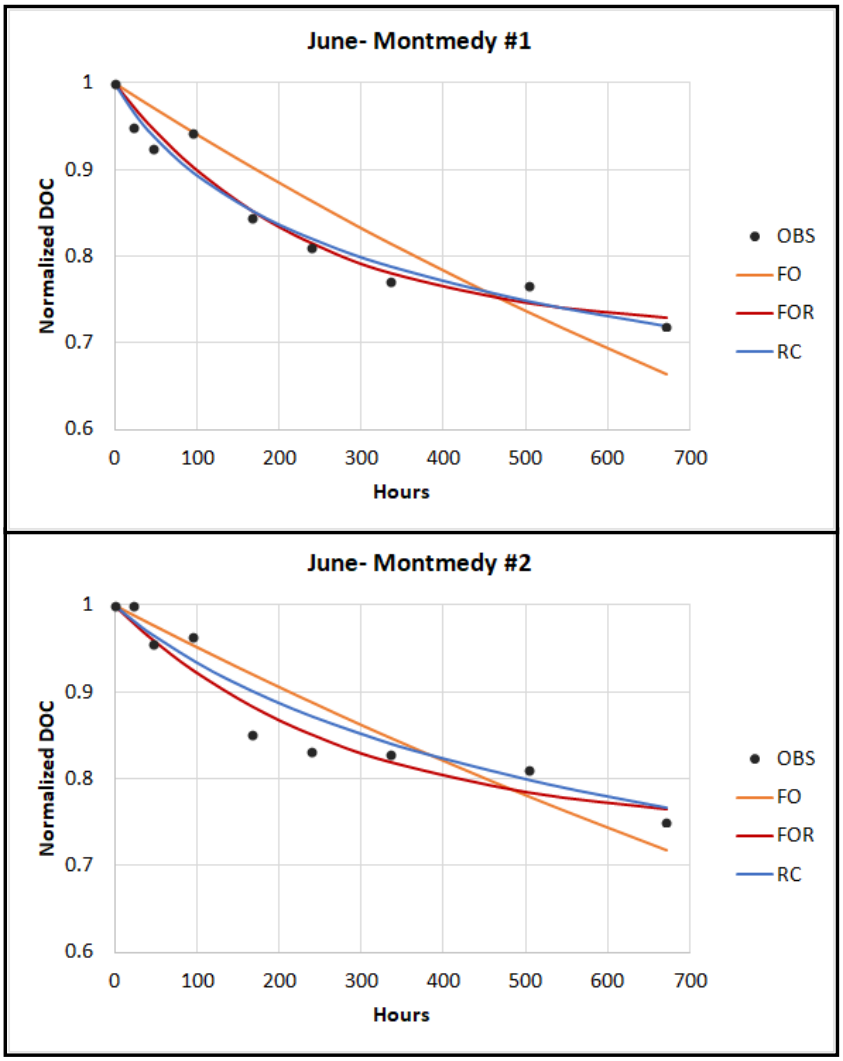

Figure 3.10 *Evolution with time of normalized DOC concentrations in Montmédy (June 2020), fitted by the three models.*

The half-life times of the two first-order kinetic models (Fig. 3.9b) are significantly lower than those in March and a striking difference between FO and FOR can be observed. The median half-life time for the FO is 74 days while with the more robust FOR method we obtain much lower half-life times with a median of 9 days (excluding Han #2), a value lower than the average WRT of the Meuse (24 days) or the estimated WRT for June (29 days), suggesting that a significant fraction of the DOC would likely be decomposed before it reaches the sea. Surprisingly, for a given location half-life times from the FOR method can vary significantly (from 8 to 43 days in Douzy for instance, or from 8 to 22 days in Dun), suggesting that the river water has variable composition even at the very local scale (i.e., one of the duplicate samples containing more labile DOC than the other). This may have been the case at Dun as the discharge was low, possibly preventing a good mixing of the water. The low water level could also be the reason for the distinct behaviour for one of the duplicate samples in Han, for which we found very long half-life time (125 days) and low k_{RC} (9.6×10^{-3} day^{-1}) compared to the rest of the samples during the June campaign. At Douzy, Dun and Han, the initial decay rate constants of the RC model between the

duplicate bottles differ by one order of magnitude. Excluding Han #2, a median initial decay rate constant of $1.4x10^{-2}$ day^{-1} is obtained. Overall, the time-lapse DOC concentrations are better fitted with FOR and RC models, suggesting that the FO method is not appropriate to describe the DOC dynamics. In particular, it leads to a substantial overestimation of the half-life times.

Compared to the March campaign, k_{RC} are all largely superior, suggesting that DOC decay is faster in June in the upper-Meuse catchment. However, as the March incubations lasted only for a week, this conclusion must be taken with caution.

3.3.1.3 September campaign

Due to the dry conditions in the summer of 2020, the discharge in the Meuse basin was very low during the third campaign in September and only a few stations could be sampled. Compared to June, the water temperature is slightly lower with an average across sampled stations of 16.4°C. Similarly to the June campaign, duplicate samples for a given station present sometimes differences in the initial DOC concentrations while the final concentrations at the end of incubations were relatively close. For instance, in Douzy the initial DOC concentrations were 3.0 and 3.5 mg L^{-1} while the final concentrations yielded 2.5 and 2.4 mg L^{-1} (Fig. 3.11a). This observation can be attributed once again to the low discharge of the river but the refractory pool seems in fact constant (i.e., similar final concentrations), that is, the labile pool is mostly responsible for the high variability.

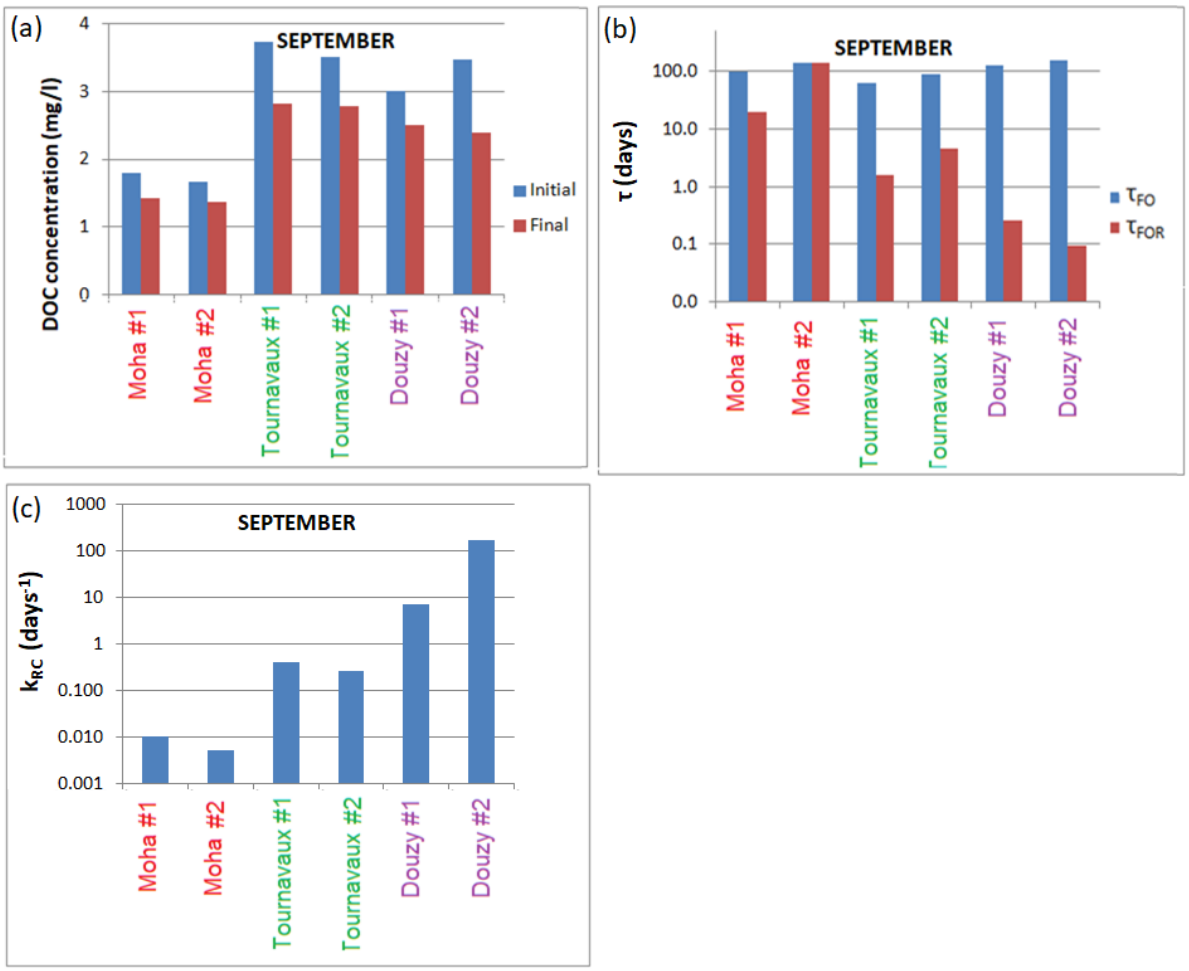

Figure 3.11 *Results of the DOC degradation experiments for the September campaign. (a) DOC concentrations at the beginning (initial) and the end (final) of the incubation experiments (mg L^{-1}); (b) half-life times (days) for the two first order kinetic models (τ_{FO} and τ_{FOR}); (c) initial decay rate constant calculated with the RC method (day^{-1}). (Color code station: purple = mixed land cover; red = cropland; green = forests; orange = grassland).*

Figure 3.12 shows the evolution with time of the normalized DOC for duplicates from Tournavaux for which the three kinetic fits present significant differences. The three fits for Douzy are also significantly different while for Moha, the three methods led to relatively similar results (paramenters for all fits can be found in the supplementary section). The worst fit is again obtained with the FO method (R^2 of 0.15 for Tournavaux #1 and 0.57 for #2). Both FOR and RC fit better the observations; the FOR has a R^2 of 0.97 for Tournavaux #1 and 0.81 for #2, while the RC has a R^2 of 0.93 for #1 and 0.98 for #2. With the FOR, the fraction of the "labile" pool amounts to 0.23 for Tournavaux #1 and 0.18 for Tournavaux #2. Both FOR and RC models capture equally well the observed temporal trends.

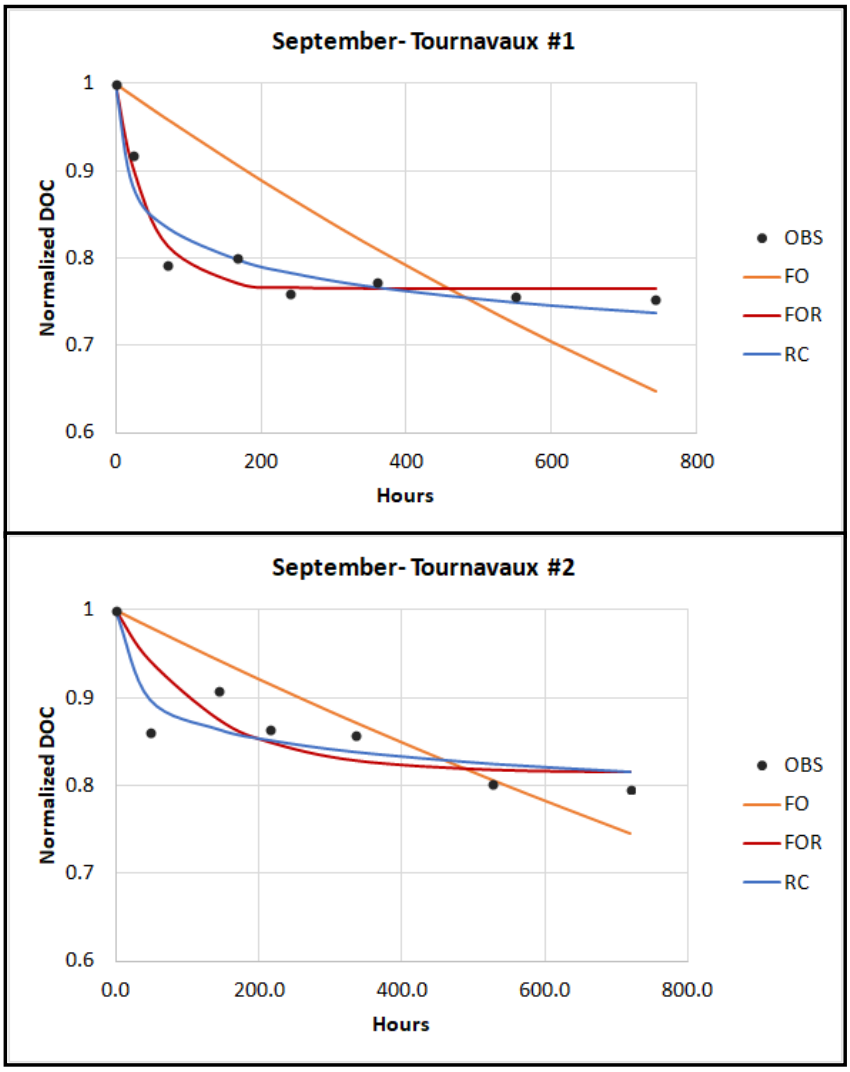

Figure 3.12 *Evolution with time of normalized DOC concentrations in Tournavaux (September 2020), fitted by the three models.*

Calculated half-life times (Fig. 3.11b) with the FO method have to be taken with great caution since the fits are generally poor. τ_{FO} values for the September campaign are similar to those of the March campaign, varing between 30 and 155 days. On the contrary, with the FOR, the degradation is much better captured and half-life times are ranging from 0.09 days in Douzy to 4.5 days in Tournavaux, values much lower than the average WRT (or the estimated WRT for September, 30 days). These results suggest that with high temperatures and low discharge, the complete degradation of the "labile" fraction of the DOC as defined in the FOR method will be achieved rapidly in the river system, i.e., this "labile" DOC pool will be degraded in transit before reaching the sea. The initial decay rate constants determined with the RC model are consistent with the results based on the FOR method and they imply a faster degradation in September compared to June and March. The results for this campaign also confirm that the FO method is not able to describe the DOC dynamics and leads to a significant overestimation of DOC half-life times. It can be noted that Douzy #2 has an extremely high value of k_{RC} reaching 168 day^{-1} and a τ_{FOR} of 6

minutes, suggesting a fitting issue with the RC method or a contaminated sample since τ_{FO} is surprisingly low compared to all other half-life times. In contrast, the initial decay rate constants in Moha are surprisingly low compared to the rest of the stations with values of respectively $7.2x10^{-3}$ and $1.4x10^{-2}$ day^{-1} for #1 and #2, two orders of magnitude lower than those for Tournavaux. The same conclusion holds for the FOR model results, although the spread in half-life times is not as significant. However, the Moha station was not sampled during other campaings and thus the results cannot be compared to the other seasons. Overall, the results for Tournavaux (and to a lesser extent, Douzy), suggest that the decay rate is the fastest in September.

3.3.1.4 November campaign

In November, the water level has risen again allowing us to sample the same locations as in June and the average water temperature is 8.6°C, about 8° lower compared to the late spring campaign. The initial DOC concentrations varied in incubations from 1.8 to 6.9 mg L^{-1} and the final concentrations from 1.6 to 5.1 mg L^{-1} (Fig. 3.13a). In this campaign, the difference in initial DOC concentration between duplicate samples is striking for most locations while again the final DOC concentrations at the end of incubation are comparable. However, for this campaign the variability in initial DOC concentration cannot be attributed to the very low discharge. One possible explanation for the highly variable initial concentrations observed in certain duplicate samples is the presence of a microlayer at the water-atmosphere interface enriched in bacteria that would increase the "labile pool". During the sampling, it is likely that part of this microlayer is sampled with the bucket. This would lead to a different fraction of the labile pool between a sample and its duplicate while the refractory pool remains relatively constant.

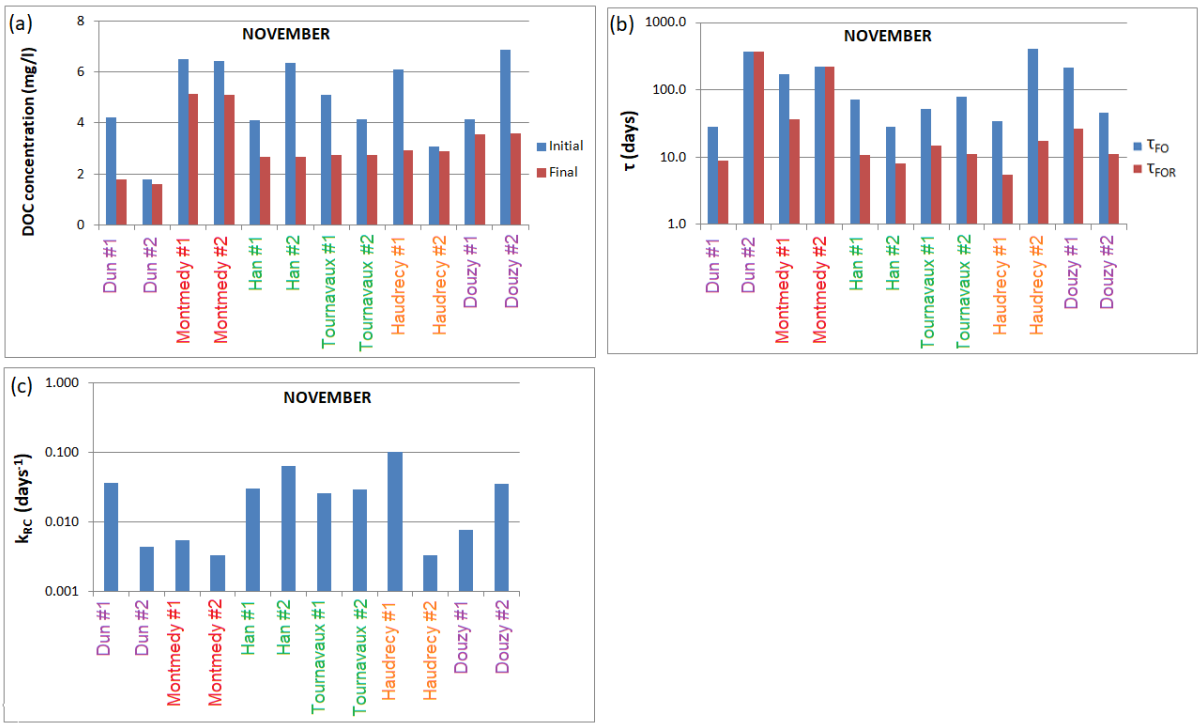

Figure 3.13 *Results of the DOC degradation experiments for the November campaign. (a) DOC concentrations at the beginning (initial) and the end (final) of the incubation experiments (mg L^{-1}); (b) half-life times (days) for the two first order kinetic models (τ_{FO} and τ_{FOR}); (c) initial decay rate constant calculated with the RC method (h^{-1}). (Color code station: purple = mixed land cover; red = cropland; green = forests; orange = grassland).*

The evolution with time of the normalized DOC concentration for Han sur Lesse is shown in Fig. 3.14 for both samples. The other stations exhibit in general a similar behaviour (except for Dun #2 and Montmédy #2 where the "labile" fraction is 1 in the FOR model and thus the results are the same as for the FO model). Again, the results for Han reveal that the single-pool first order kinetic model (FO) does not capture well the evolution of DOC concentration with time (R^2 of 0.7 for both samples) and yields half-life times of 29 and 71 days for the two incubations. With the FOR method, 38% of the total DOC is found to be labile with a τ_{FOR} of 11 days for Han #1 while for Han #2 the labile fraction is more important (0.62) with a τ_{FOR} of 8 days. The FOR (R^2 of 0.93 for both) and RC (R^2 of 0.90 for #1 and 0.88 for #2) models again match the observations very well. However, it can be noted as previously that with time the DOC concentrations stabilize in the FOR model while for the RC model, the concentrations seem to continue to decrease albeit at a very slow pace.

With the FO, the range of half-life times is very large and is comprised between 28 and 400 days (Fig. 3.13b). The two fitting methods for the first-order rate law yield very different results for all stations: a median half-life times of 75 days (FO) and of 11 days (FOR, excluding Montmédy #2 and Dun #2 where FOR=FO). With the FOR method, as in June, November half-life times are lower than the average WRT (28 days for the November WRT) in the Meuse and DOC decay behaviour is similar to that observed in June (where the median half-life time was 9 days). In agreement with

FOR, the initial decay rate constants determined by the RC model are quite comparable to those found for the June campaign with a median of 2.6×10^{-2} day^{-1}.

To conclude, June and November present similar results for the FOR method and RC, with a median half-life time of around 10 days obtained for both campaigns. In September, with the exception of Moha, DOC decay is much faster with half-life times ranging from 0.09 (Dun #2) to 4.6 (Tournavaux #2) days. The results of March are unfortunately difficult to compare to the other seasons because of the shortened experiments. However, these preliminary data would suggest that the decay is slower in March than in any other seasons sampled. Compared to the calculated WRT from ORCHILEAK, we see that in June and November, most of the "labile" DOC from the FOR method will not reach the sea, WRT being higher than the half-life time. Finally, the widely used FO method does not allow us to capture DOC degradation kinetics and therefore should not be used to describe the DOC dynamics while both the FOR and RC models fit well the observations.

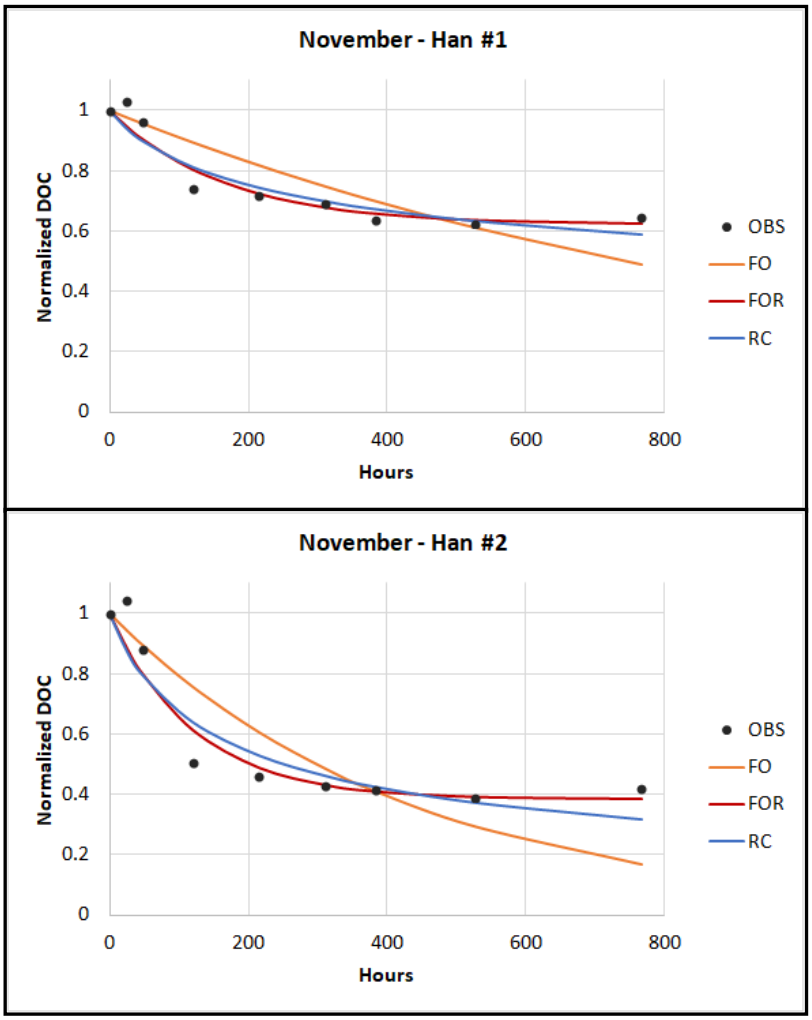

Figure 3.14 *Evolution with time of normalized DOC concentrations in Han sur Lesse (November 2020), fitted by the three models.*

3.3.2 DOM optical properties

Karanfil (2002) has established that a SUVA index of < 3 L mg^{-1} m^{-1} characterizes a DOM dominated by labile compounds. This is the case for the majority of our samples, with the exception of duplicate samples collected from Haudrecy and Douzy in November which exhibit a DOM dominated by recalcitrant compounds and aromatic DOM with SUVA > 3.5 L mg^{-1} m^{-1} (unfortunately, we do not have SUVA and FI measurements for September because the sample vials broke and for June, SUVA was measured only for one sample of each sampling location). In addition, our November SUVA results show that even duplicate samples from a given station can have variable SUVA indexes (Fig. 3.15; Table S.3.5). This observation is actually in line with our previous assessment of the large variability in initial DOC concentrations. For example, for both Douzy and Haudrecy (November), the sample with the lower DOC concentration correspond to the one with higher SUVA. This observation also holds for the other stations, such as for Dun (November) where DOC concentrations in the duplicate are 4.5 and 1.8 mg L^{-1} with SUVA indices respectively of 0.69 and 1.86 L mg^{-1} m^{-1}. During our incubations, the SUVA values tend to increase with respect to the initial ones (Fig. 3.15), suggesting that as the most reactive DOM compounds decompose, the proportion of the more "refractory" DOM will increase in the leftover DOM (except for one of the samples from Douzy and Haudrecy in November, and from Haudrecy in June for which SUVA index decreases with time). The decrease in SUVA during incubation is not expected since the "labile" pool is supposed to decompose first and thus the remaining DOM should become more refractory with time exhibiting higher SUVA values. One possible explanation for the decreasing SUVA may be related to a problem occurring during the course of incubation like bacterial growth that increases the "labile" pool, or can be due to partial degradation of the more refractory pool into labile compounds. It can be observed that in November and for the same location, the final SUVA values are usually similar although the initial ones can be quite different. This suggests that the duplicate samples can contain different amounts of more labile DOM initially; yet after one month of incubation, duplicates have roughly the same SUVA values, implying a similar amount of more recalcitrant DOM in both duplicate samples. Therefore, these results suggest that most of the variability across duplicate samples might rise from the sampling during which variable fractions of labile compounds were sampled.

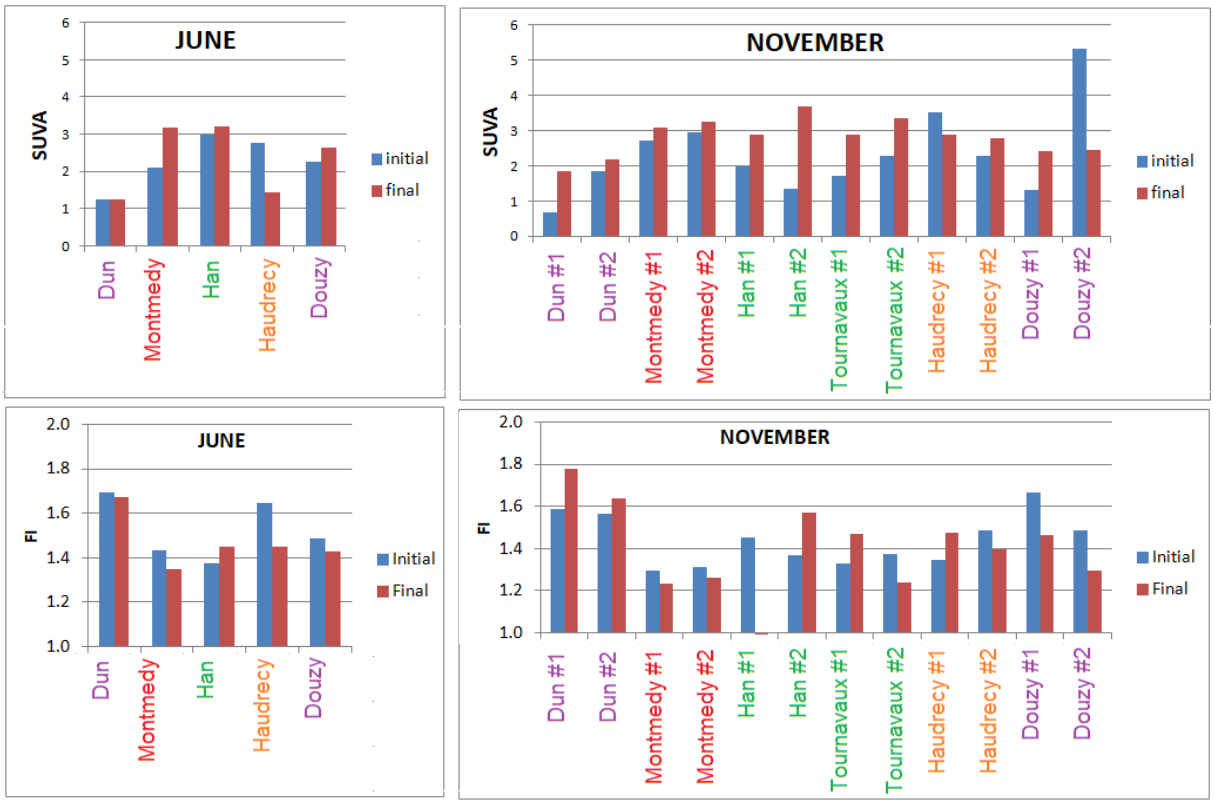

Figure 3.15 *SUVA (L mg^{-1} m^{-1}) and FI results (initial versus final) for the June and November campaigns. (Color code station: purple = mixed land cover; red = cropland; green = forests; orange = grassland).*

Fluorescence Index (FI) allows one to distinguish between terrestrial (<1.4) and microbial (>1.9) DOM (McKnight et al., 2001). All samples have FI values comprised between 1.2 and 1.8 indicating a mixture of both terrestrial and microbial DOM with a slight dominance of terrestrial organic matter. Our FI values fall within the same range as that reported by Lambert et al. (2017) on the Meuse (from 1.3 to 1.9). Over 17 incubations, nine showed decreasing FI over time while the other eight evidenced an increase in FI, with no clear trends of preferential decomposition of microbial or terrestrial sources (Fig. 3.15). Yet, for all incubations of June (with the exception of Han), FI decreased slightly indicating a preferential degradation of microbial DOM (autochthonous DOM). However, this trend is less clear in November, with half of the stations showing a decreasing FI while the other half exhibiting an increasing FI over time. In November, FI values are slightly more disparate, with generally lower values – an average of 1.4 in autumn - compared to 1.5 in June, indicating that in November the river contains slightly less autochthonous DOM. The higher discharge, meaning more precipitation, in November (compared to June) might have caused an increase in C export from soils into the river while in June, the spring bloom could explain the more autochthonous character of the DOM.

3.4 DISCUSSION

The high variability in initial decay rate constants between seasons, stations and even duplicates for a given station suggests that the OM quality is highly heterogeneous in the river, at least for the labile OM since the refractory pool seems relatively constant at each station. A plausible explanation for the variable amount of the more labile DOM could be the presence of a surface microlayer which is known to be enriched in bacteria and microalgae organic compounds (Liss et al., 1997; Wurl et al., 2004). The spatial and temporal dynamics of this microlayer are still unknown which makes it difficult for us to sample consistently (especially with an open recipient) (Jiang et al., 2010; Liu et al., 2014). Despite these methodological difficulties, our results allow us to draw several conclusions regarding the kinetic models of DOM degradation and the underlying controls of DOM degradability.

3.4.1 Models of DOC decay kinetics

The decay rate constant k in this study was calculated using three different models: two first order kinetics (FO and FOR) and the reactive continuum (RC). The FO method led to quite different results compared to the FOR and RC methods, as it assumes one single pool of DOC that will, given time, decomposes completely. This systematically leads to low values of k_{FO} and large half-life times (from 26 to 400 days). With this method, we calculated a median half-life time for DOC in the upper Meuse of 108 days, corresponding to a decay rate constant of 0.006 d^{-1}. This value is surprisingly high, especially compared to a typical water residence time in the Meuse of 24 days. In the Results section, we demonstrated that the fit obtained with the FO formulation does not describe well the time-lapse concentrations and we argued that this method should not be used to model the DOC degradation kinetics in rivers. Yet the FO method is often used to depict DOC degradation due to its simplicity, in particular when only fitting the first order kinetics with the initial and the final concentrations of an incubation experiment. In 2016, Catalan and co-workers published a study on the control of water residence times (WRT) on organic carbon decomposition rates determined by a first order kinetics. For that they compiled data of existing field and laboratory measurements of OC decay rates across the world: Sweden (from Langenheder et al., 2003; Berggren et al., 2010; Kohler et al., 2002; Tiwari et al., 2014), Spain (their study) and United States (Cory and Kaplan, 2012; Del Giorgio and Pace, 2008; McDowell et al., 1976). Their data, for rivers only, span two orders of magnitude from 0.0004 d^{-1} to 0.09 d^{-1}. Our value for the Meuse with the FO method falls into the same range, but our results also suggest that the river DOC degradability might also be underestimated with this approach.

The FOR is an improved method with respect to the FO. It includes a refractory DOC pool that does not degrade at least on the timescale of our incubations (about one month). Compared to the FO, the FOR generally fits much better the time-lapse DOC concentrations of our incubations. Yet, for some stations exhibiting slow DOC decay,

the FOR method could not produce two distinct pools and thus assumes one single pool as the FO formulation. Excluding these stations (mainly during the March campaign), the calculated half-life times range from 0.09 to 43 days. The lowest values, corresponding to the fastest decays, were obtained in September. Koehler et al. (2012) performed an experimental study on two Swedish lakes for two months and applied also the first order kinetics with a refractory pool. These authors obtained a labile pool of around 30% of the initial DOC concentrations and a half-life time of 533 days for one lake and 165 days for the other, showing that the degradability in rivers and lakes could differ significantly. Lv et al. (2019) applied the FOR method for rivers and lakes in China and obtained similar values for half-life time of around 3 days. Their value is however much lower than in Koehler et al. (2012) and falls into the same range as that found for our September results. However the ecosystem studied by Lv et al. (2019) is quite different; sampling in the Changjiang river took place down-stream of cities with millions of inhabitants (Anqing, Datong, and Wuhu) and thus organic-rich sewage water from these urban regions could explain the low values of half-life times.

Finally, the reactive continuum (RC) has a k_{RC} value decreasing over incubation time (see section 3.2, Fig. 3.16). There is high variability in DOC degradation between stations and seasons, with initial decay rate constants ranging from $3.4x10^{-3}$ to 167 day^{-1}. In particular, during the September campaign, the values for Douzy and Tournavaux were in general very high. Excluding data from this campaign, the range of k_{RC} can be narrowed down to that from $3.4x10^{-3}$ to $1.4x10^{-1}$ day^{-1}. Koehler et al. (2012) also applied the RC model in their study on lake water, and estimated a k_{RC} for one lake of $4.3x10^{-3}$ day^{-1} and a lower value for the other one of $9x10^{-4}$ day^{-1}, values lower than the ones obtained for the Meuse river. This result suggest that DOC biodegradability is lower in Swedish lakes than in rivers while in Lv et al. (2019), results for Chinese lakes and rivers were similar. The opposite conclusion can be explained by the urbanization, China being highly urbanized leading organic-rich sewage water while in Sweden population density is very low. Catalan et al. (2017) studied the biodegradability in a Spanish catchment, and reported results for rivers similar to ours with values for k_{RC} of $5.4x10^{-3}$ day^{-1} for the first site and $2x10^{-2}$ day^{-1} for the second one.

Based on our results, the best descriptions of DOC decomposition kinetics are obtained with the FOR and RC, both having usually similar R^2 values for the fits with a slight preference for the FOR method (two third of the fits had a slightly better R^2 with the FOR). Hyacinthe et al. (2006) have shown that when there are large differences in reactivity of the component under study between the two pools, the RC method tends to overestimate in the early stage of the incubations and the opposite towards the end, suggesting that the FOR method will in general perform better than the RC. However, further experiments should be performed in order to evaluate which method could better represent DOC degradation kinetics. Incubations carried out during one month gave similar results but maybe a longer incubation time (for

example, one year) could favour one method over the other. However, given the WRT estimated for the Meuse catchment, 24 days, it may not be relevant to study the fate of DOC in rivers at much longer timescales, contrary to lakes for which the WRT values are much higher (e.g., Koehler et al., 2012). To further investigate the behaviour of the FOR and RC models, an example of the evolution of k_{RC} and k_{FOR} with time for Han #1 and Han #2 in November is shown in Fig. 3.16. Initial k_{RC} values are lower than the constant value of k_{FOR}, which however only drives the fate of the labile pool. In contrast, the RC method applies the apparent initial decay coefficient to the bulk DOC pool. Figure 3.16b shows the evolution of the DOC decay rate, decay rate constant multiplied by the concentration (for the FOR method only the labile fraction is taken into account). The rate with the RC method is slightly higher than the one obtained with the FOR at the beginning of the incubation but the RC rate decreases faster in time, suggesting a continuous decay also of the less reactive and more refractory DOC.

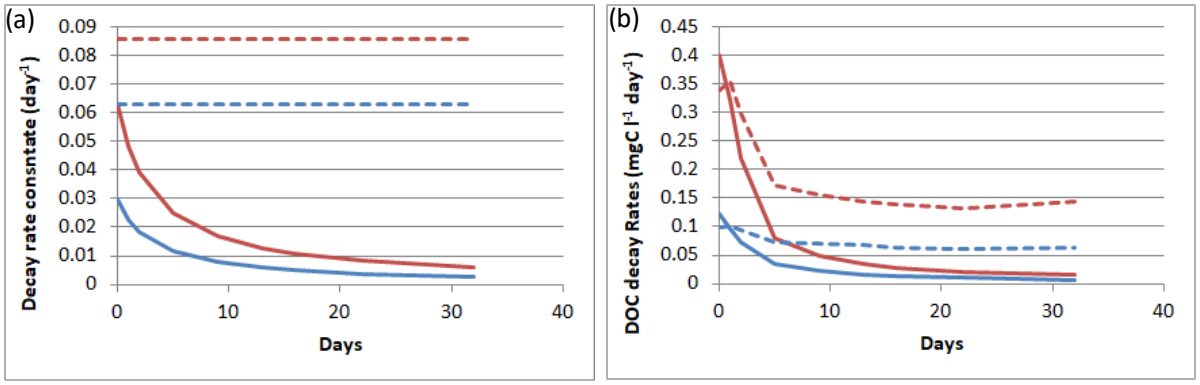

***Figure 3.16** (a) Evolution of the decay rate constants (day^{-1}) and (b) Evolution of DOC decay rate (mg C l^{-1} day^{-1}) for the FOR and RC models in Han #1 (blue) and #2 (red) during the November campaign. Solid line: RC model; dashed line: FOR model.*

3.4.2 Controlling factors of the variability in decay rate constants

This section aims to understand the factors controlling τ_{FOR} and k_{RC}. Previous studies have already related the decay rate constants to the water residence time (Catalan et al., 2016; Attermeyer et al., 2018; Soarse et al., 2019). Here, we investigate whether other variables could influence this parameter. We hypothesize that the land cover of the catchment can influence the DOM input, its nature and thus its degradation rate. We also sampled multiple times in a year to evaluate how the seasonality impacts the nature of the DOM and its biodegradability. Seasonality and land cover types are denominated as extrinsic properties. The other factors concern the intrinsic molecular properties of the DOM, in other words, the OM quality. A more refractory OM will evidently be more difficult to degrade and thus will lead to a lower decay rate constant. In this work, the OM quality was assessed through the measurements of SUVA and FI indices.

3.4.2.1 Extrinsic properties

We investigate first whether the land cover or the seasonality has an impact on k_{FOR} and k_{RC} value. Due to the change of sampling locations, especially in September, we only have data for the four seasons for Tournavaux and Douzy, and three for the rest of the stations. Several studies have already investigated the impact of seasonality on DOC and POC concentrations (e.g., Yukon river in North America in Wickland et al., 2012; Yellow river in China in Ran et al., 2013).

Figure 3.17a and 3.17b show the median and interquartile of the half-life times (days) and the initial decay rate constants (day^{-1}) for each season and land cover types. Looking first at the seasonality, one can note that March has the highest value of τ_{FOR} (97 days) while the other seasons have significantly lower values, 9 days for June, 4.5 days for September and 11 days for November. For these three seasons, the FOR model gave the same results as the FO model for a few stations only (Han# 2 for June; Moha #2 for September; Montmedy #2 and Dun #2 for November) and these stations were excluded when calculating the median half-life times. The interquartiles reflect the high variability between samples, rendering firm conclusions difficult. Furthermore, while the March campaign presents the slowest decays, results have to be taken carefully since the experiment was stopped after a week and only a few measurements could be collected. A similar seasonal trend can be observed with the RC method: the March campaign presents the lowest initial degradation rate constant with a median of $9.2x10^{-3}$ day^{-1} while the June and November campaigns yielded similar values, $1.5x10^{-2}$ day^{-1} and $2.7x10^{-2}$ day^{-1}, respectively, or about 1 order of magnitude lower than that found in March. The September campaign showed by far the fastest decay, a median k_{RC} of 0.4 day^{-1}, but this could be due to the sampling of the microlayer enriched in labile DOC reinforced by the low water level (stagnant water) or a fitting issue for Douzy leading to an extremely high value of k_{RC}.

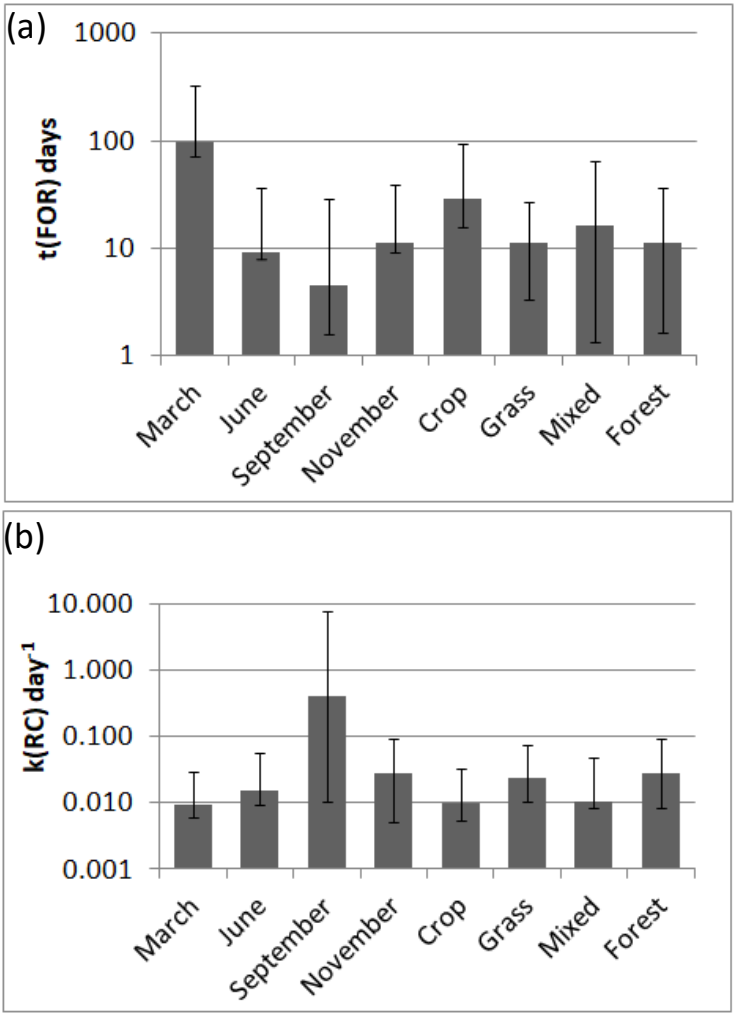

Figure 3.17 *Median and interquartile (a) half-life times (days) determined by FOR as a function of sampling season and land cover. (b) Initial decay rate constants (day^{-1}) determined by RC as a function of sampling season and land cover.*

We performed a Kruskal-Wallis test to check whether τ_{FOR} and k_{RC} values differ significantly between seasons (Table 3.2). The FOR method gives a value lower than the p-value of 0.05 only for the March campaign compared to June and November, a result to be taken with caution due to the experimental limitations mentioned above. Between June, September and November, all p-values are higher than the critical value and this is also the case for the RC method across all campaigns, indicating no clear seasonality. The reason why there is no statistically significant difference between seasons can be attributed to the high variability between stations and between a sample and its duplicate during each campaign. Although not statistically significant with both models, the lower decay rates found with the FOR and RC methods in March perhaps suggest that the degradation kinetics could decrease in late winter. More research will however be needed to clarify the potential effect of the seasonality on DOM reactivity.

Table 3.2 *Kruskal-test p-values calculated for τ_{FOR} and k_{RC} for each season.*

p-value	MARCH	JUNE	SEPT.	NOV.	MARCH	JUNE	SEPT.	NOV.
	FOR method				RC method			
MARCH	1	0.0057	0.1229	0.04252	1	0.1128	0.1675	0.4990
JUNE	0.0057	1	0.3356	0.2954	0.1128	1	0.2815	1
SEPT.	0.1229	0.3356	1	0.2059	0.1675	0.2815	1	0.1400
NOV.	0.04252	0.2954	0.2059	1	0.4990	1	0.14	1

We now look at the effect of the dominant land cover types of the sampling locations. As the seasonality, some studies have investigated the impact of land cover on DOC concentration (e.g., United States in Larson et al., 2014; China in Ma et al., 2018) but none for Europe and none on the DOC decay rate constant. Our results reveal that grasslands and forests present a similar median half-life time of 11 days. Mixed types and croplands on the other hand, show slightly slower decays with respectively 16 days and 28 days. Similar to the seasonal analysis, the variability within each land cover class is again high and the interquartile range is in fact systematically larger than the difference between each land cover class.

With the RC method, we obtain results that are similar to the FOR method, with the slowest decay for croplands (median of $1x10^{-3}$ day^{-1}) against $2.3x10^{-2}$ day^{-1} for grasslands (Douzy in September not accounted for) and $2.7x10^{-2}$ day^{-1} for forests. Again, k_{RC} is highly variable as evidenced by the interquartiles for all land cover types.

The Kruskal-Wallis test (Table 3.3) applied to τ_{FOR} and k_{RC} yields p-values that are all higher than the critical value, suggesting no significant variability in DOC decay rate constants between land cover types. In other words, land cover does not appear to be a dominant factor controlling the DOC degradability in the upper portion of the Meuse catchment.

Table 3.3 *Kruskal-test p-values calculated for τ_{FOR} and k_{RC} for each land-cover type.*

p-value	CROP	GRASS	FOREST	MIX	CROP	GRASS	FOREST	MIX
	FOR method				**RC method**			
CROP	1	0.2524	0.0640	0.2193	1	0.1161	0.1858	0.3621
GRASS	0.2524	1	0.4090	0.7924	0.1161	1	0.9062	0.5987
FOREST	0.0640	0.4090	1	0.6642	0.1858	0.9062	1	0.6642
MIX	0.2193	0.2954	0.6642	1	0.3621	0.5987	0.6642	1

3.4.2.2 Intrinsic molecular properties

Here we investigate if the aromaticity of the DOM exerts an important control of the DOM degradation kinetics. We work from the premise that the more aromatic the DOM is, the more difficult it is to degrade, leading thus to low decay rates (Karanfil et al., 2002).

The range of the SUVA index (from 1 to 6 L mg^{-1} m^{-1}) and FI values (from 1.3 to 1.7) for the June and November campaigns are consistent with other experimental studies (Attermeyer et al., 2018, Lv et al., 2019). We also found that the SUVA index tends to increase with time during the incubation experiment (Fig. 3.15), a result consistent with the work of Peacock et al. (2015). This study supports the view that the more aromatic DOC is, the more resistant it is to degradation but our results also indicate that the non-aromatic DOC would be preferentially degraded during the incubation, leading to an increase in the SUVA index.

Figure 3.18a and 3.18b show the half-life times calculated with the FOR method and the initial decay rate constant from the RC method against the SUVA index. While τ_{FOR} does not show any trend with the SUVA – whether linear or exponential -, Fig. 3.18b displays a general trend where k_{RC} decreases with increasing SUVA, the trend being better fitted with an exponential function. This observation agrees with what was previously found by Karanfil et al. (2002) who established a scale to describe OM composition on the basis of SUVA. An index greater than 4 L mg^{-1} m^{-1} corresponds to OM of high molecular weight while a value inferior to 3 L mg^{-1} m^{-1} can be attributed to OM of low molecular weight. One reason to explain why there is a correlation between SUVA and k_{RC} and not with τ_{FOR}, is that the SUVA characterizes the bulk of DOC and indicates if the DOC pool tends to be more refractory or more labile. In contrast, τ_{FOR} is calculated based exclusively on the 'labile' pool reactivity (defined by the FOR method) and thus based only on a fraction of the entire DOC pool. The advantage of using the RC model is that k_{RC} encompasses the entire spectrum of DOM reactivity and does not consider solely a portion of DOM - be it 'reactive' - as in

the case of k_{FOR}. Overall, SUVA could be proposed as a proxy for k_{RC} and providing at least an order of magnitude estimation of the rate of DOM degradation. Finally, no relationship could be established between τ_{FOR} and FI or k_{RC} and FI (Fig. 3.19), R^2 (for a linear or an exponential trend) being lower than 0.1 for FOR and RC.

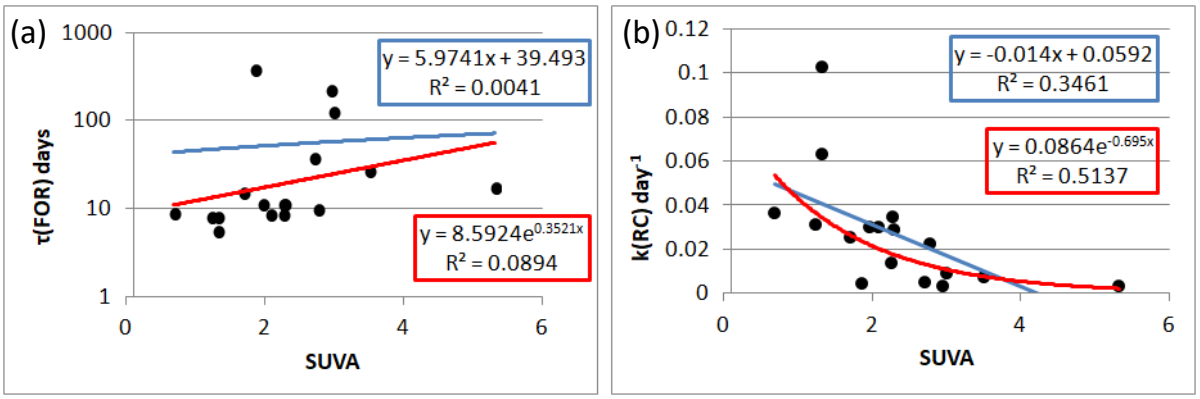

Figure 3.18 *(a) Half-life times (days) of the FOR model and (b) initial decay rate constants (day^{-1}) of the RC model as a function of SUVA (L mg^{-1} m^{-1}). Linear regression is shown in blue, exponential fit in red.*

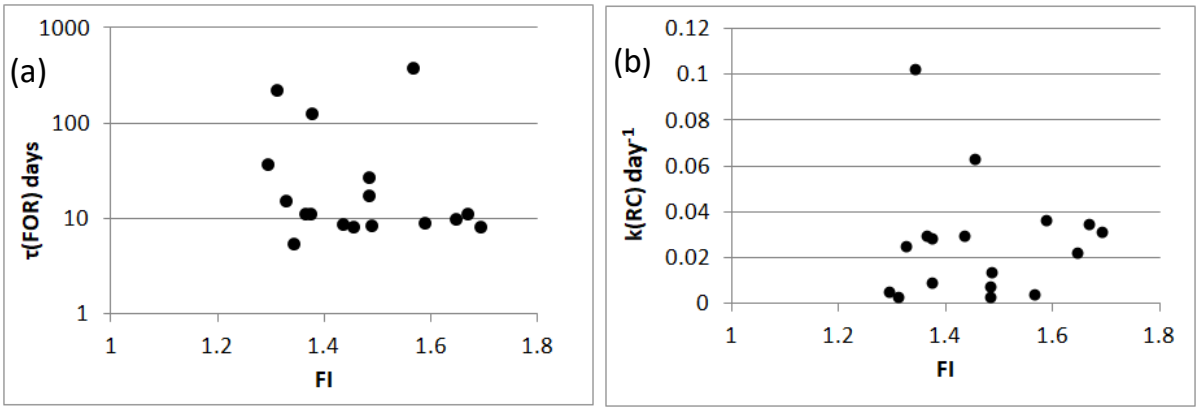

Figure 3.19 *(a) Half-life times (days) from the FOR method and (b) initial decay rate constant (day^{-1}) as a function of the FI index.*

When examining the relationship between k_{RC} and SUVA in more detail, our data tend to regroup along specific trends for a given land cover (Fig. 3.20). As discussed above, an exponential decrease of k_{RC} with increasing SUVA index provides reasonable fits for each land cover type. However, the results suggest that for croplands, k_{RC} decreases faster with increasing SUVA compared to the other land cover types. In addition, for a given SUVA index, k_{RC} appears to be lower for croplands than for grasslands. Figure 3.20 shows that for the experiments conducted at stations with a clear dominant land cover, the prediction is good (R^2 close to 0.9) for croplands, forests and grasslands, but when the catchment is under the influence of mixed land covers, a significantly lower R^2 is obtained. Thus, a diversity of land cover in a catchment could make it difficult to predict the initial decay rate constant with the

SUVA index. However this result need to be taken cautiously because a regression with only three or four points (cropland, grassland and forest) lacks robustness This hypothesis needs to be further tested with more data as we only have a few observations for each land cover.

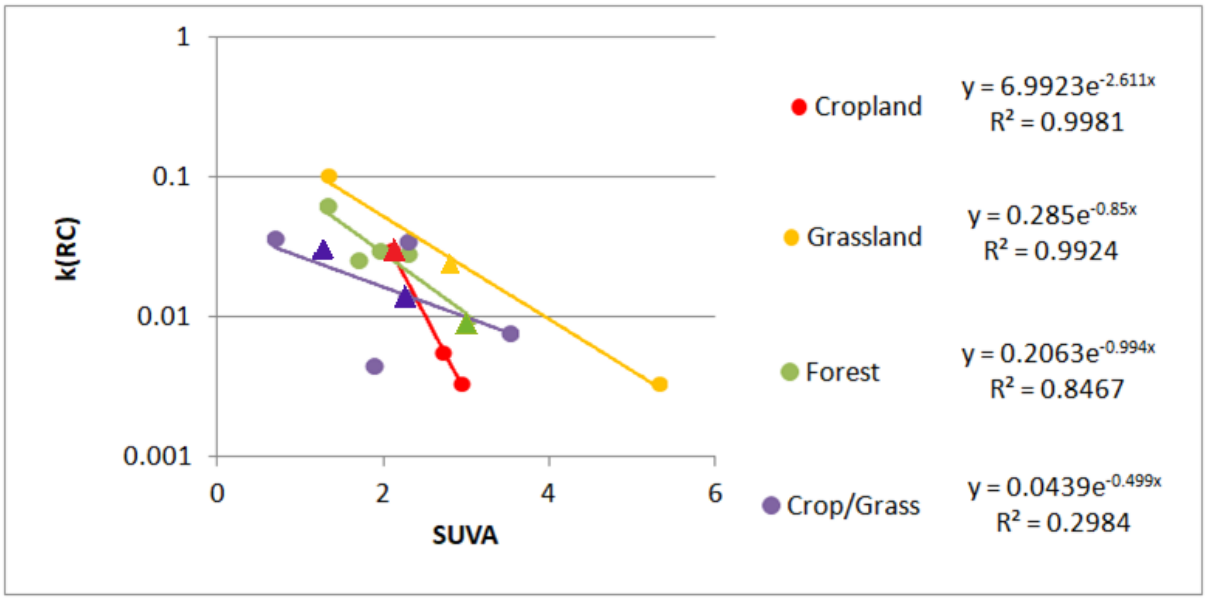

Figure 3.20 *Initial decay rate constant (day^{-1}) of the RC model as a function of SUVA (L mg^{-1} m^{-1}) for different land cover types and seasons (Triangles: June, Circles: November).*

3.5 CONCLUSIONS

Our experimental studies in the upper Meuse catchment reveal that the DOM decay rates are highly variable in space and time. This variability does not seem to be dominated by seasonal patterns or catchment properties such as land cover, the variability between duplicate samples often exceeding the one diagnosed for these environmental control factors. In contrast, our results show that the DOM reactivity, as constrained by the reactive continuum model, decreases with increasing SUVA, suggesting that the variability in DOM degradation kinetics can be related to the degree of its aromaticity.

Excluding data from the March campaign (for which calculated half-life times of DOC were high), values of the half-life times fall in the same order of magnitude as WRT of the entire Meuse catchment, which means that most of the DOC will be decomposed by the time it reaches the sea. The March results, although highly speculative, could in contrast indicate a much larger export of terrestrial DOC during later winter, a hypothesis that will require further investigation. In addition, the decay of DOC occurs at a much faster rate in September. Further studies could estimate the WRT at the sampling locations that can then be linked to the SUVA index and decay rate constants.

While single-pool first order kinetics is often used to describe DOC degradation, we

demonstrate here that this method is not able to capture well the DOC degradation kinetics in the river system. Instead, we recommend the use of either the FOR or the RC models calibrated on incubation experiments with multiple measurements through time to represent the DOC degradation kinetics. A possible improvement of the FOR method would be to assume that the "refractory" pool is not entirely inert but decays slowly with time; the model could also be extended to include multiple DOC pools as described in Vähätalo et al. (2010). However, the FOR or the RC method has been shown to provide already very good fits of the DOC degradation kinetics with R^2 superior to 0.8 for 70% of our incubations. Although both the FOR and RC models performed equally well in terms of degradation kinetics, we found that the variability in k_{FOR} could not be explained based on the intrinsic properties of the DOM (the SUVA or FI index) as k_{FOR} was determined by the reactivity of the "labile" pool only. On the contrary, the initial decay rate constant from the RC method characterizes the entire pool of DOM and the SUVA index has been illustrated to be a reasonably good proxy to estimate the initial decay rate constant (R^2 = 0.51). Furthermore, the resulting exponential relationship between k_{RC} and SUVA seems to be even improved if the analysis is performed within individual land-cover types. With further research on optical properties (EEM) and incubations, it may be possible to obtain a better description of DOM and their associated reactivities.

3.6 SUPPLEMENTARY MATERIAL

Table S.3.1 March campaign 2020

STATION	DOC initial ($mg\ l^{-1}$)	DOC final ($mg\ l^{-1}$)	pH	Water T (°C)	τ_{FO} (days)	R^2 (FO)	τ_{FOR} (days)	R^2 (FOR)	f_L	f_R	k_{RC} (day^{-1})	R^2 (RC)	α	ν
Dun	3.815	3.43	8.07	8	123.7	0.90	123.7	0.90	1.00	0.00	0.0063	0.89	602	0.358
Montmedy	3.61	3.045	8.2	7.2	76.8	0.78	76.8	0.78	1.00	0.00	0.0099	0.76	611	0.614
Villers	4.56	3.875	8	8	64.8	0.98	64.8	0.98	1.00	0.00	0.0115	0.98	600	0.662
Bouillon	3.485	3.21	7.31	6.5	136.7	0.60	136.7	0.60	1.00	0.00	0.0056	0.98	600	0.355
Douzy	3.09	2.77	8.04	7.7	97.1	0.97	97.1	0.97	1.00	0.00	0.0092	0.98	200	0.184
Haudrecy	5.66	5.205	7.82	7.6	135.0	0.77	135.0	0.77	1.00	0.00	0.0061	0.81	250	0.160
Remy	11.205	7.985	7.08	7.5	26.1	0.93	12.5	0.93	0.56	0.44	0.0303	0.93	457	1.357

Table S.3.2 June campaign 2020

STATION	DOC initial ($mg\ l^{-1}$)	DOC final ($mg\ l^{-1}$)	pH	Water Temperature (°C)	τ_{FO} (days)	R^2 (FO)	τ_{FOR} (days)	R^2 (FOR)	f_L	f_R	k_{RC} (day^{-1})	R^2 (RC)	α	ν
Dun #1	1.72	1.39	7.93	16.3	94.8	0.86	21.6	0.88	0.31	0.69	0.0093	0.88	676	0.355
Dun #2	2.42	1.43	7.93	16.3	36.5	0.80	8.0	0.93	0.42	0.58	0.0316	0.90	213	0.369
Montmédy #1	4.11	2.96	7.92	16.5	60.4	0.80	8.5	0.96	0.29	0.71	0.0301	0.96	98	0.159
Montmédy #2	3.81	2.86	7.92	16.5	74.3	0.84	10.3	0.94	0.26	0.74	0.0151	0.95	252	0.204
Han #1	4.28	2.36	7.19	16.5	29.5	0.53	3.6	0.91	0.40	0.60	0.1469	0.96	21	0.164
Han #2	2.80	2.27	7.19	16.5	124.9	0.70	124.9	0.70	1.00	0.00	0.0094	0.85	662	0.357
Tournavaux #1	3.80	3.02	8.51	17.5	101.2	0.87	26.4	0.88	0.33	0.67	0.0082	0.88	763	0.336
Tournavaux #2	3.76	3.05	8.51	17.5	106.7	0.93	34.8	0.93	0.38	0.62	0.0061	0.94	3340	1.030
Haudrecy #1	1.73	1.31	8.1	17	65.1	0.81	9.7	0.93	0.28	0.72	0.0234	0.83	159	0.186
Haudrecy #2	1.76	1.41	8.1	17	74.4	0.58	7.2	0.82	0.22	0.78	0.0234	0.67	98	0.118
Douzy #1	2.74	2.08	8.1	17.3	86.7	0.83	42.8	0.83	0.55	0.45	0.0080	0.92	2460	1.087
Douzy #2	3.00	2.09	8.1	17.3	78.7	0.55	8.4	0.74	0.22	0.78	0.0139	0.78	275	0.196

Table S.3.3 September campaign 2020

STATION	DOC initial (mg l^{-1})	DOC final (mg l^{-1})	pH	Water Temperature (°C)	τ_{FO} (days)	R^2 (FO)	τ_{FOR} (days)	R^2 (FOR)	f_L	f_R	k_{RC} (day^{1})	R^2 (RC)	α	ν
Moha #1	1.80	1.43	7.53	15.3	97.6	0.79	19.8	0.83	0.30	0.70	0.0104	0.82	448	0.281
Moha #2	1.66	1.36	7.53	15.3	137.5	0.92	137.5	0.92	1.00	0.00	0.0052	0.90	23500	6.350
Tournavaux #1	3.74	2.82	8.52	16.8	61.8	0.14	1.7	0.97	0.24	0.76	0.3980	0.93	2.6	0.054
Tournavaux #2	3.50	2.78	8.52	16.8	88.3	0.57	4.6	0.81	0.19	0.81	0.2712	0.98	2.6	0.036
Douzy #1	3.00	2.50	7.92	17.1	127.0	0.39	0.3	0.67	0.11	0.89	7.0255	0.75	0.038	0.014
Douzy #2	3.47	2.40	7.92	17.1	154.3	0.82	0.1	0.99	0.10	0.90	166.0668	0.95	0.001	0.009

Table S.3.4 November campaign 2020

STATION	DOC initial ($mg\ l^{-1}$)	DOC final ($mg\ l^{-1}$)	pH	Water Temperature (°C)	τ_{FO} (days)	R^2 (FO)	τ_{FOR} (days)	R^2 (FOR)	f_L	f_R	k_{RC} (day^{-1})	R^2 (RC)	α	ν
Dun #1	4.23	1.77	7.6	9	28.5	0.75	8.8	0.90	0.62	0.38	0.0369	0.93	244	0.809
Dun #2	1.77	1.60	7.6	9	374.9	0.80	374.9	0.80	1.00	0.00	0.0045	0.80	179	0.069
Montmédy #1	6.52	5.13	7.59	8.8	168.6	0.95	37.0	0.98	0.31	0.69	0.0055	0.97	525	0.284
Montmédy #2	6.45	5.12	7.59	8.8	220.3	0.75	220.3	0.75	1.00	0.00	0.0033	0.73	6150	2.031
Han #1	4.12	2.66	7.83	8	71.3	0.69	11.0	0.93	0.38	0.62	0.0303	0.90	77	0.223
Han #2	6.37	2.69	7.83	8	28.6	0.72	8.1	0.93	0.62	0.38	0.0637	0.88	79	0.481
Tournavaux #1	5.12	2.76	7.9	8.4	52.9	0.84	15.0	0.94	0.51	0.49	0.0258	0.92	190	0.453
Tournavaux #2	4.15	2.74	7.9	8.4	79.9	0.72	11.2	0.96	0.35	0.65	0.0290	0.94	70	0.188
Haudrecy #1	6.11	2.94	7.64	8.7	34.5	0.52	5.5	0.97	0.52	0.48	0.1031	0.92	172	0.116
Haudrecy #2	3.08	2.90	7.64	8.7	403.8	0.51	17.3	0.66	0.10	0.90	0.0033	0.79	124	0.394
Douzy #1	4.16	3.54	7.56	8.7	213.0	0.82	26.3	0.90	0.21	0.79	0.0077	0.90	28	0.263
Douzy #2	6.89	3.61	7.56	8.7	46.5	0.75	11.2	0.89	0.50	0.50	0.0351	0.87	785	0.247

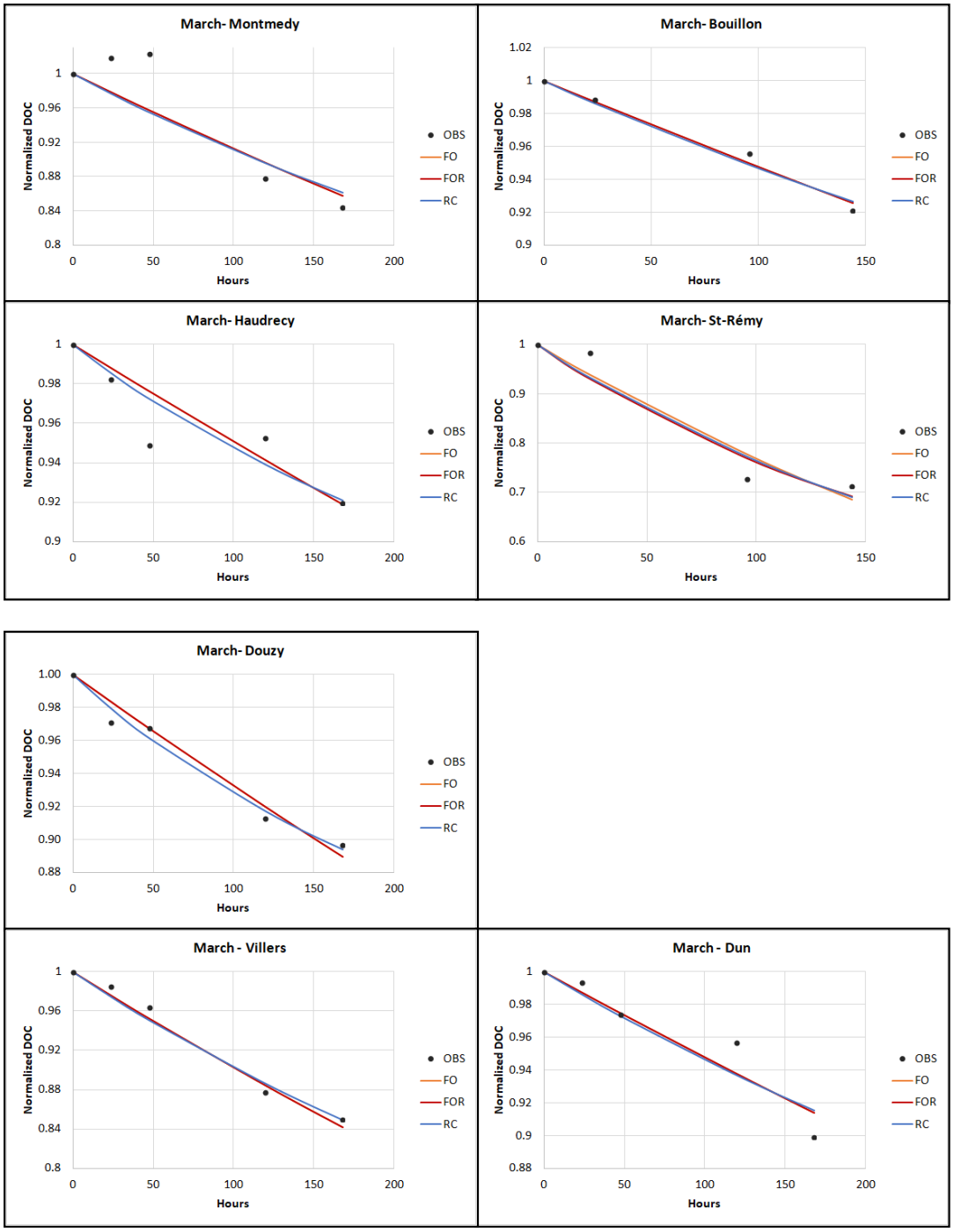

Figure S.3.1 *Evolution with time of DOC concentration normalized with respect to the initial concentration for all stations for the March campaign and the fits obtained with the three methods.*

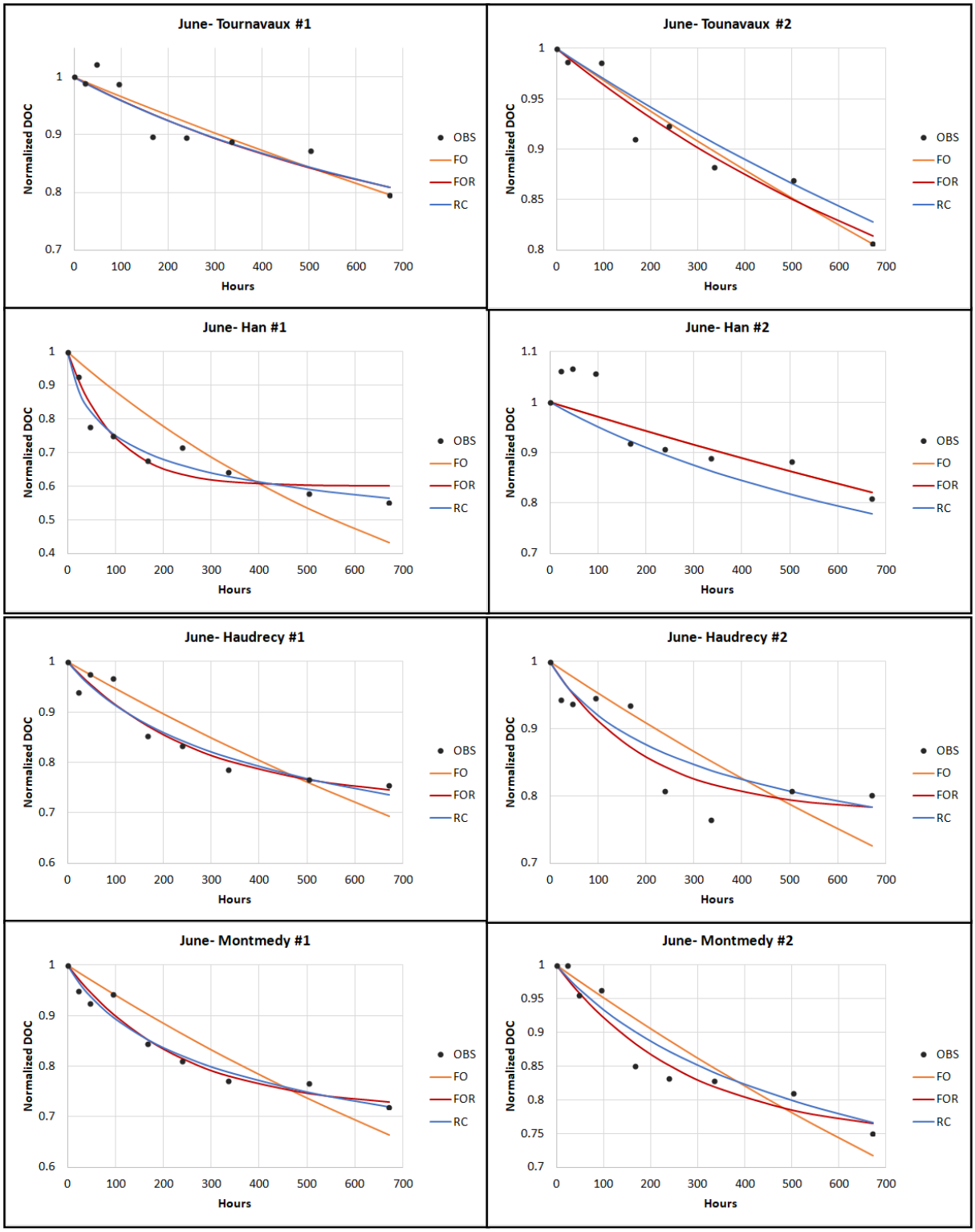
June- Tournavaux #1
Normalized DOC
Hours
OBS
FO
FOR
RC
June- Tounavaux #2
Normalized DOC
Hours
OBS
FO
FOR
RC
June- Han #1
Normalized DOC
Hours
OBS
FO
FOR
RC
June- Han #2
Normalized DOC
Hours
OBS
FO
FOR
RC
June- Haudrecy #1
Normalized DOC
Hours
OBS
FO
FOR
RC
June- Haudrecy #2
Normalized DOC
Hours
OBS
FO
FOR
RC
June- Montmedy #1
Normalized DOC
Hours
OBS
FO
FOR
RC
June- Montmedy #2
Normalized DOC
Hours
OBS
FO
FOR
RC

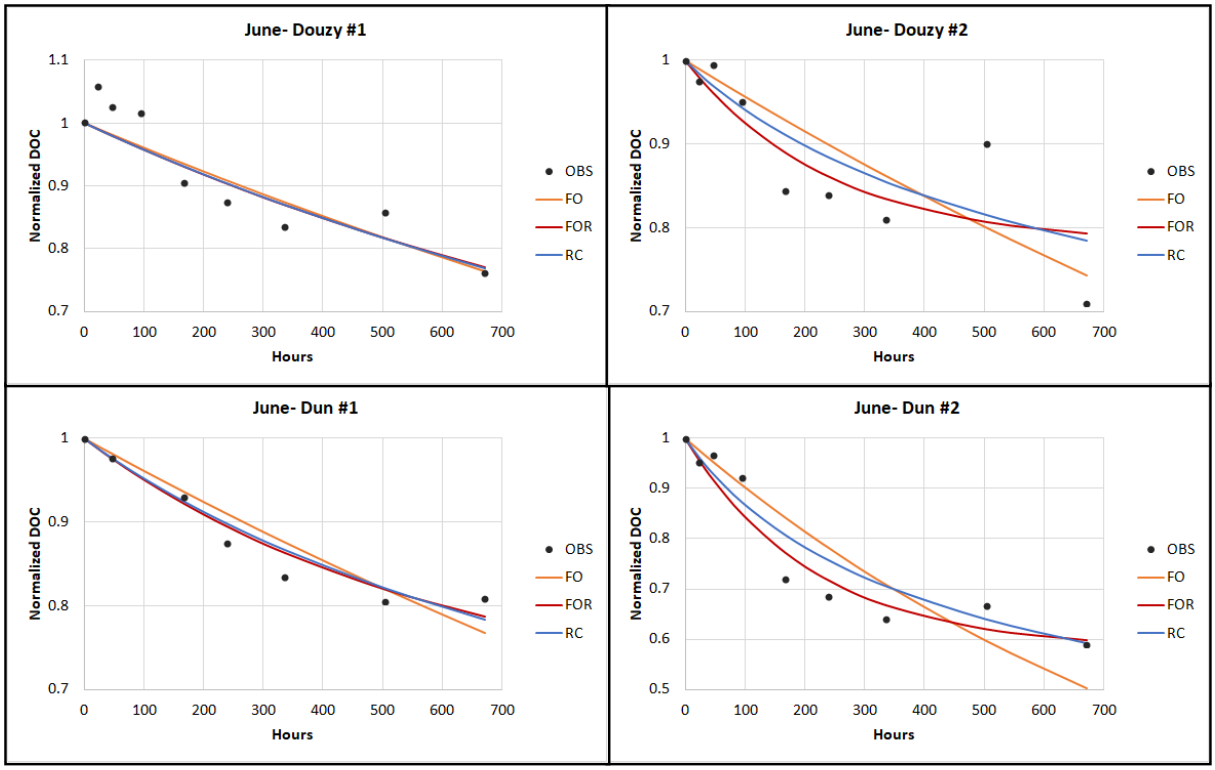

Figure S.3.2 *Evolution with time of DOC concentration normalized with respect to the initial concentration for all stations for the June campaign and the fits obtained with the three methods.*

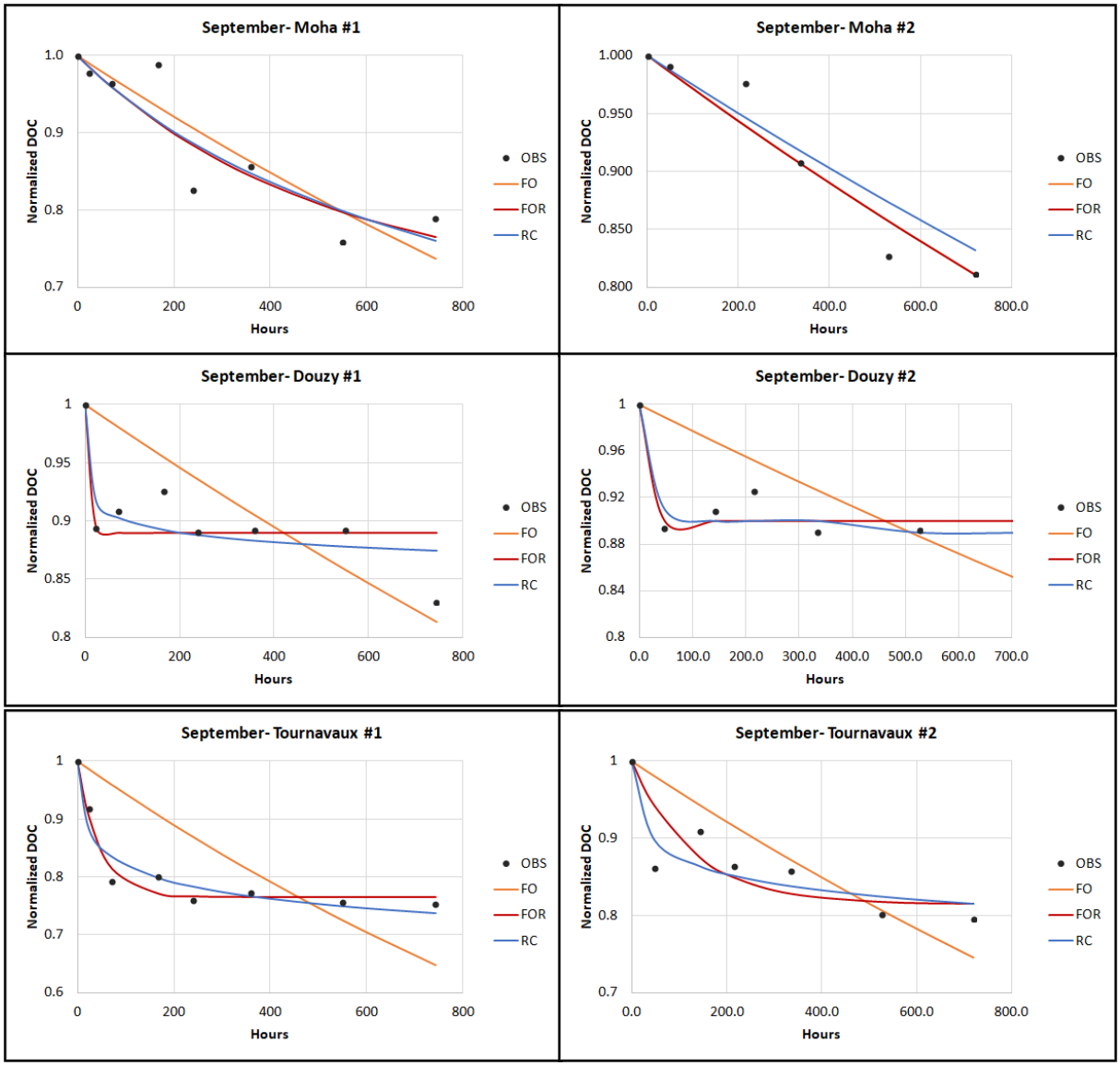

Figure S.3.3 *Evolution with time of DOC concentration normalized with respect to the initial concentration for all stations for the September campaign and the fits obtained with the three methods.*

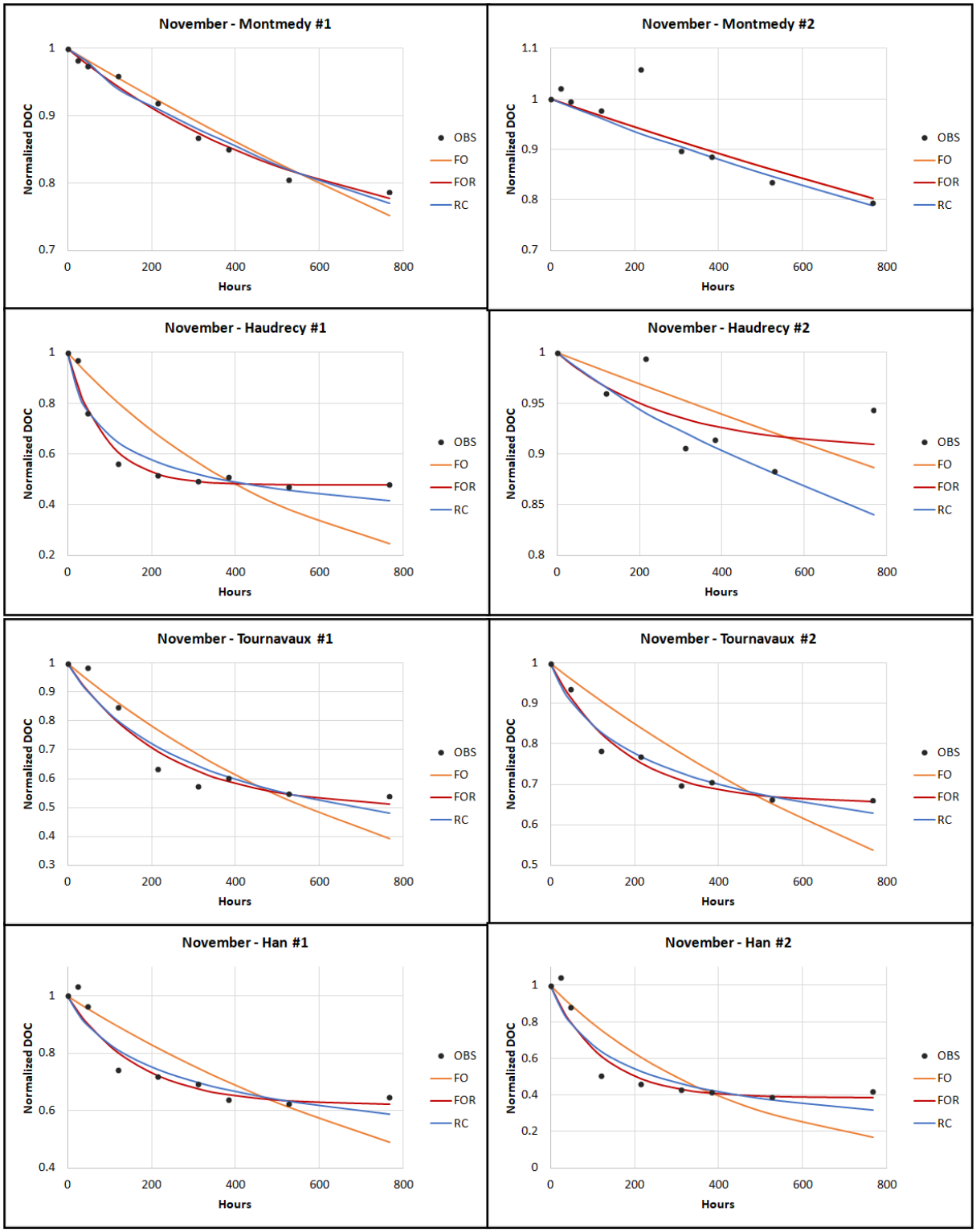
November - Montmedy #1
Normalized DOC
Hours
OBS
FO
FOR
RC
November - Montmedy #2
Normalized DOC
Hours
OBS
FO
FOR
RC
November - Haudrecy #1
Normalized DOC
Hours
OBS
FO
FOR
RC
November - Haudrecy #2
Normalized DOC
Hours
OBS
FO
FOR
RC
November - Tournavaux #1
Normalized DOC
Hours
OBS
FO
FOR
RC
November - Tournavaux #2
Normalized DOC
Hours
OBS
FO
FOR
RC
November - Han #1
Normalized DOC
Hours
OBS
FO
FOR
RC
November - Han #2
Normalized DOC
Hours
OBS
FO
FOR
RC

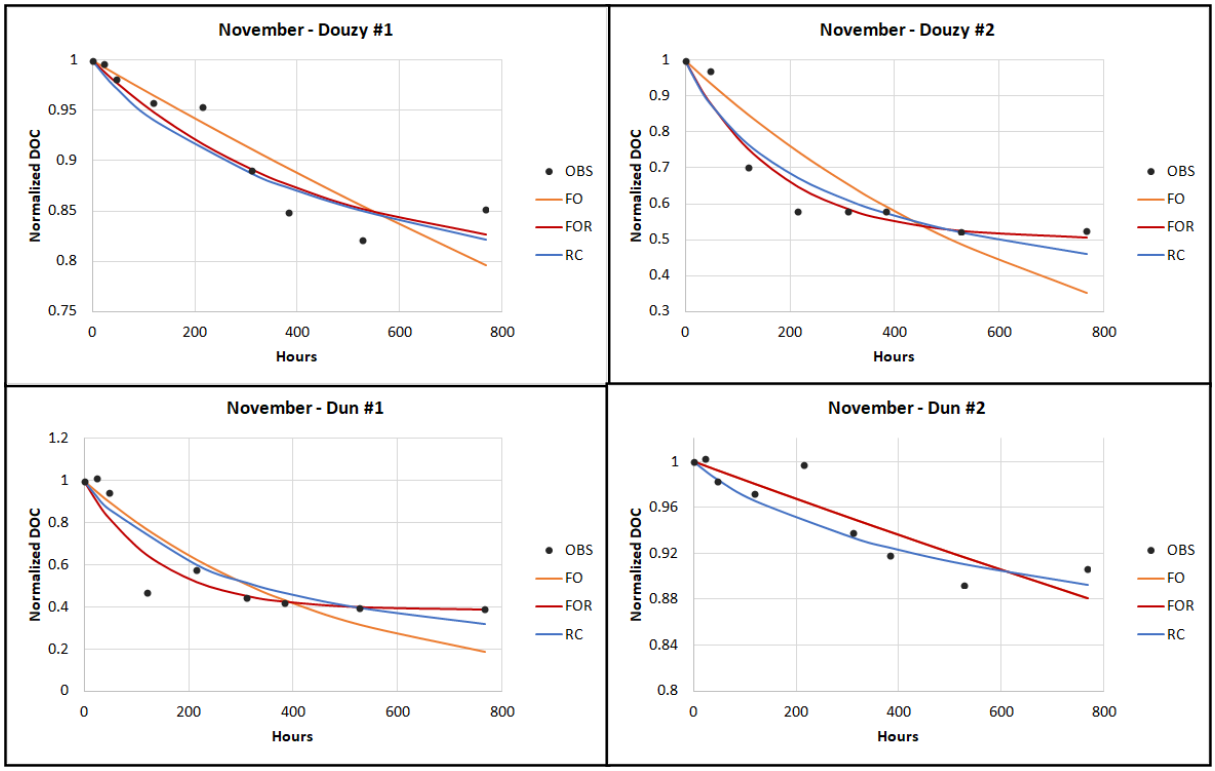

Figure S.3.4 *Evolution with time of DOC concentration normalized with respect to the initial concentration for all stations for the November campaign and the fits obtained with the three methods.*

Table S.3.5 *Result SUVA and FI for the June (top) and the November (bottom) Campaigns*

STATION	SUVA initial	SUVA final	FI(370) initial	FI(370) final
Dun	1.24	1.26	1.69	1.67
Montmédy	2.09	3.18	1.44	1.35
Han	3.00	3.22	1.38	1.45
Haudrecy	2.77	1.45	1.65	1.45
Douzy	2.27	2.63	1.49	1.43

Dun	0.69	1.86	1.59	1.78
Dun	1.86	2.19	1.57	1.64
Montmédy	2.71	3.08	1.29	1.23
Montmédy	2.95	3.24	1.31	1.26
Han	1.97	2.89	1.36	1.57
Han	1.33	3.68	1.45	NA
Tournavaux	1.70	2.90	1.33	1.47
Tournavaux	2.29	3.36	1.37	1.24
Haudrecy	1.33	2.41	1.34	1.48
Haudrecy	5.32	2.45	1.48	1.40
Douzy	3.51	2.88	1.48	1.30
Douzy	2.28	2.80	1.67	1.46

4 LATERAL CARBON FLUXES IN EUROPE: QUANTIFICATION AND IMPLICATIONS FOR NATIONAL CARBON BUDGETS.

Contribution: C. Gommet with inputs from R. Lauerwald, P. Ciais and P. Regnier.

Abstract

Large quantities of carbon (C) are transported by the river network from land to ocean and those fluxes have been demonstrated to be an important part of the C budget. When assessing national C budgets in Europe, the lateral C transfers by rivers from one country to another are not yet taken into account. Yet, rivers cross borders multiple times in Europe leading to C exchanges through this pathway. The goal of this chapter is to estimate by a mass balance approach the inland water C budget of European countries that includes imports from and exports to neighbouring countries. We calculate that on average over all of Europe, a flux density of 8.1 ± 2.7 gC m^{-2} yr^{-1} is leached from the soil to the inland water network, 5.2 ± 2.3 gC m^{-2} yr^{-1} out of this leached flux is emitted to the atmosphere as C dioxide (CO_2), and 0.8 ± 0.4 gC m^{-2} yr^{-1} is buried in the sediments. Looking at the fluxes between countries, 2.3 ± 7.5 gC m^{-2} yr^{-1} of C are imported from one country to another and 4.4 ± 7.6 gC m^{-2} yr^{-1} are exported either to the sea or to other countries. With this budget, a net river C balance (RNCB) is defined, which corresponds to the difference between C export and import. Most European countries export more C through rivers than they import. Few countries (the Netherlands, Portugal, Estonia and Ukraine) import more carbon. This lateral C component is then compared with other land-atmosphere fluxes of regional carbon budgets such as land use, land use change and forestry, total anthropogenic emissions and more specific emissions related to food and agriculture, in particular wood and crop trades that are also "lateral C fluxes". The comparison with other fluxes allows to estimate the relative importance of the RNCB for each European country individually. We found that half of the EU countries have a ratio RNCB to harvest trades greater than 10 % and a quarter of the EU countries have a ratio greater than 30 %. These results showed that the RNCB is for some European countries is a significant contributor to the lateral C fluxes and can even reach the same order of magnitude than the lateral fluxes caused by trade of crop and wood products. They should be carefully considered in national carbon budget of European countries, especially for reconciliation of atmospheric inversions fluxes and carbon storage change from national inventories.

4.1 INTRODUCTION

Rivers transport large quantities of carbon (C) from land to ocean (Tranvik et al., 2009; Regnier et al., 2013, Drake et al., 2018). This flux is an important part of the terrestrial C budget. It dominantly originates from C leaching and erosion from soil to the river network (Cole et al., 2007). Therefore, the processes of leaching and erosion decrease

the (*terra firme*) land C accumulation by transferring C to rivers. A large fraction of C leached by soils is emitted back to the atmosphere in inland waters. A recent study demonstrated that accounting for C emissions to the atmosphere from Swedish inland waters reduced the national land sink by more than 50 % (Lindroth and Tranvik, 2021). It is thus important to take riverine C fluxes into account in the assessment of the C uptake by land ecosystems, with regard to other fluxes. However, it is difficult to distinguish the natural component from the anthropogenic one in the fluxes related to river C transport.

Previously, the riverine C cycle was considered as a passive pipe transferring conservatively terrestrial C to the ocean. In a seminal contribution, Cole et al. (2007) showed that rivers are on the contrary active systems receiving considerably larger amounts of terrestrial C than their export to the sea, and losing the rest to the atmosphere. In inland water systems, C undergoes different transformation processes. A fraction is buried in the sediments, another is decomposed generating carbon dioxide (CO_2) and methane (CH_4) emissions to the atmosphere while the rest is exported to the coast. This natural riverine C cycle is affected by anthropogenic perturbations (Regnier et al., 2013) which add new inputs of C and nutrients to the river through land use changes and agricultural activities, and retain more C in sediments from damming and increased autotrophic production (Tian et al., 2015; Maavara et al., 2017, Ran et al., 2021). There are also indirect anthropogenic impacts induced by climate change, rising CO_2 affecting soil biogeochemistry and nutrient deposition (Lauerwald et al., 2020; Hastie et al., 2021).

Recently, studies on terrestrial C budgets started to include lateral C fluxes through the river system, to reconcile atmospheric C flux budgets with land storage budgets (Ciais et al., 2020) and to separate anthropogenic C fluxes from total fluxes, assuming that all river fluxes are natural (Le Quéré et al., 2013; Le Quéré et al., 2014;; Friedlingstein et al., 2020). In parallel, national inventories compile on a yearly basis national statistics of anthropogenic emissions and removals of greenhouse gases (GHG) (UNFCCC). These inventories include the contributions of different sectors: energy, industrial processes and product use, agriculture and land use, land use change and forestry (LULUCF) and waste emissions of CO, NMVOC and CH_4.

The accounting of lateral carbon through the inland water network has so far only been performed at continental to global scales. For national C budgets, accounting for lateral C fluxes needs to cope with the fact that rivers and watershed boundaries often cut through national borders. In inventories, lateral riverine C fluxes are implicitly included in the LULUCF sector through their reduction of soil C stock observed by stock-change inventories, but inland water C stock change from burial, C emissions to the atmosphere and lateral C export by rivers flowing out of each country are not reported. The inclusion of fluvial C transfers in national inventories would require to account for the non-conservative behaviour of C in inland waters. In addition, fluvial C transfers comprise a natural and an anthropogenic part, however

when accounting those transfer from one country to another into national inventories, only the anthropogenic part should be reported. This distinction is difficult to make, and was only attempted at the global scale (Regnier et al., 2013) with large uncertainties. In a first step towards a proper accounting of fluvial C transfers in country-scale C budgets, we propose to account for total river C fluxes in national budgets of European countries, and address the following questions:

- How much carbon is transferred from one country to another through the river system?
- How important are the fluxes of the riverine carbon cycle compared to other lateral carbon fluxes such as wood and crop harvesting and to other components of national greenhouse gas budgets such as land use change and anthropogenic emissions?

To address these questions, we use a mass balance approach to estimate each component of the riverine C cycle at country scale and the lateral C fluxes between countries. We compare these fluxes with those reported by national inventories to estimate their importance.

4.2 METHODOLOGY

We focus on the European region (EU-27 plus Albania, Bosnia and Herzegovina, Croatia, Iceland, Kosovo, Macedonia, Norway, Serbia, Montenegro, United Kingdom and Switzerland). Figure 4.1a shows the study domain with the main rivers and lakes compiled by the European Environment Agency (EEA). Figure 4.1b shows catchments areas, some of which spanning over multiple countries, e.g. the Danube. Figure 4.1c shows the percentage of total water surface area per country, a simple metrics of the potential importance of inland waters for national C budgets.

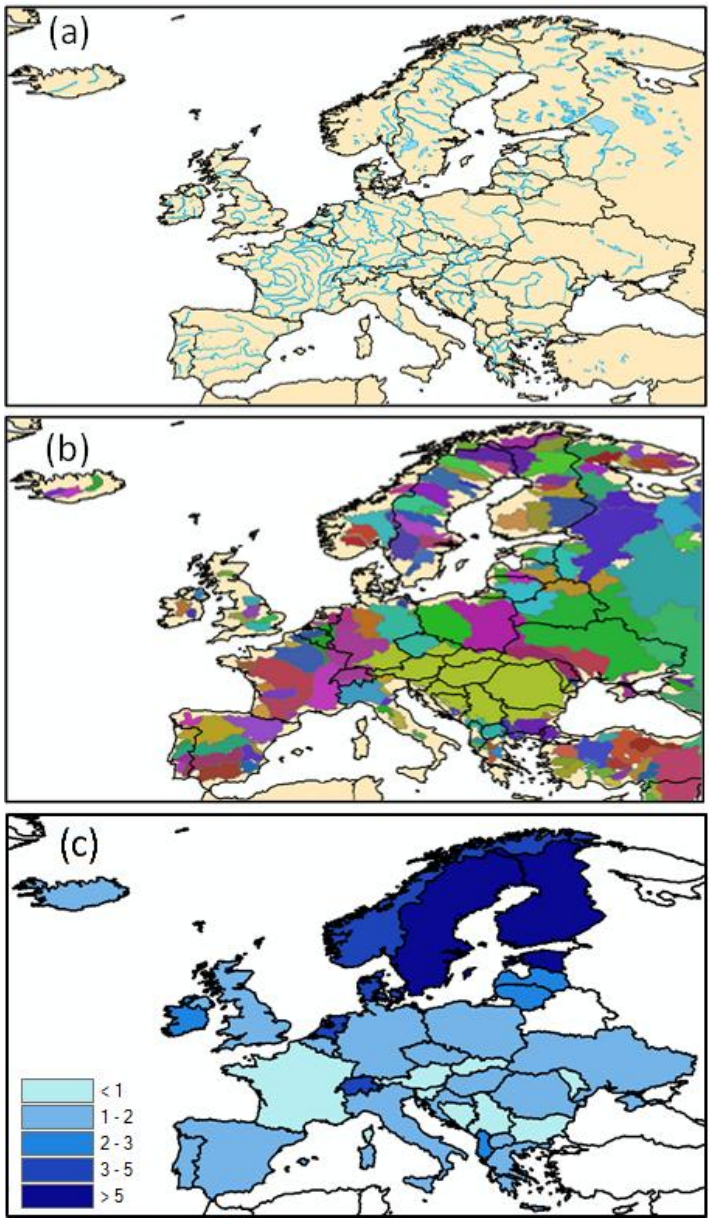

Figure 4.1 *(a) Map of Europe showing the major rivers and lakes and the country borders. Data from the European Environment Agency; (b) Map of the major European catchments from Global News 2 (area > 5000 km^2); (c) Proportion of water area per country (%).*

4.2.1 Datasets

We calculated the inland water carbon budgets of each country based on spatially explicit estimates of fluvial C exports to the coast, C burial in aquatic sediments and CO_2 emissions from the inland water surface. All data set are listed in table 4.1.

Table 4.1 *List of data sources used to assess the C budgets of the European inland water network.*

Variables	**Spatial Resolution**	**Method**	**Lake/River data set used**	**Reference**
Total Export (DOC+POC+DIC)	0.5°	Model	-	Global NEWS 2 data (Mayorga et al., 2010)
CO_2 Lake emissions (Boreal region)	0.5°	Empirical model	GLOWABO database (Verpoorter et al., 2014)	Hastie et al., 2018
CO_2 Lake emissions (Rest of Europe)	COSCAT	Regionalisation of observations	GLObal RIver CHemistry database (Hartman et al., 2014)	Raymond et al., 2013
CO_2 River emissions	0.5°	Empirical model	Hydrosheds (Lehner et al., 2008)	Lauerwald et al., 2015
OC burial in lake and reservoirs	COSCAT	Regionalisation of observations	COSCATs (Meybeck et al., 2006)	Mendonca et al., 2017

Terrestrial C is entering rivers as dissolved organic C (DOC), particulate organic C (POC) and dissolved inorganic C (DIC). All three forms are leached or eroded from the soil into the river. DIC comes also from chemical weathering of carbonate and silicate rocks. Organic carbon (DOC and POC) comes mainly from photosynthetically fixed C by terrestrial plants, while smaller inputs from direct additional anthropogenic sources such as sewage water and manure may have to be taken into account (Regnier et al., 2013). For the C export to estuaries, we used the estimates of Global NEWS 2 which is a global, spatially explicit, multi-element and multi-form model of nutrient and carbon exports by rivers (Mayorga et al., 2010). The river C export is represented as an average yield (kg C km^{-2} yr^{-1}) by basin (figure 4.2c). The CO_2 emissions (FCO_2) were taken from different spatially explicit estimates: For lakes and reservoirs, we used the results of Raymond et al. (2013) and Hastie et al. (2018) (figure 4.2b). Raymond et al.'s estimate is based on a regionalisation of observed pCO_2 and estimates of lake pCO_2 predicted from OC concentrations where observed pCO_2 were missing. Their scaling was performed using the COSCAT segmentation (COastal Segmentation and related CATchments, Meybeck et al., 2006), which represents groups of river catchments based on a coastal segmentation. Using lake and reservoir

surface area, the regional results from Raymond et al. (2013) were downscaled at 1° resolution (Zscheischler et al., 2017). Hastie et al.'s (2018) estimate is limited to the boreal region but provides a finer scale estimate of CO_2 evasion at 0.5° based on an empirical model relating lake pCO_2 to terrestrial NPP, rainfall, and lake size. The map of pCO_2 is combined with data on lake surface area and different estimates of gas exchange velocities to obtain an estimation of CO_2 emissions from lakes. We merged both datasets at 1° resolution and used Hastie's et al. results for the boreal region and Raymond et al. for the rest of Europe. The emissions of CO_2 from rivers are taken from the climatology of Lauerwald et al. (2015) (figure 4.2a). These river CO_2 water-air exchanges at 0.5° globally are based on spatially explicit application of empirical prediction functions for pCO_2, water surface area, and gas exchange velocity. Lakes, reservoirs and river CO_2 emissions were combined into a single climatology of CO_2 evasion from European inland waters.

For the C burial, we used the results of Mendonca et al. (2017) (figure 4.2d). This study compiled previously published burial estimates to generate a regional-scale assessment of this sink term in the river C cycle. Data gathered include 403 local measurements mainly located in Europe and North America, which were then upscaled globally through a predictive model that calculates burial rates per COSCATs. The in-situ measurements from Europe are located mainly in the United Kingdom, Denmark and Switzerland. The burial was first redistributed within each COSCATs based on a lake area map at 0.1° (from Hydrolakes data, Messager et al., 2016) and then re-aggregated to the 0.5° resolution, our working resolution for calculating the river C budget. All datasets correspond to the contemporary period. Some studies report the time period covered by their analysis, the C exports to the coast were estimated for the year 2000 (Mayorga et al., 2010), the CO_2 evasion from lakes from Hastie et al. (2018) are estimated over a 10-year period (1995-2004) and the OC burial was estimated based on a compilation of burial data, representing a much longer period (last century or so).

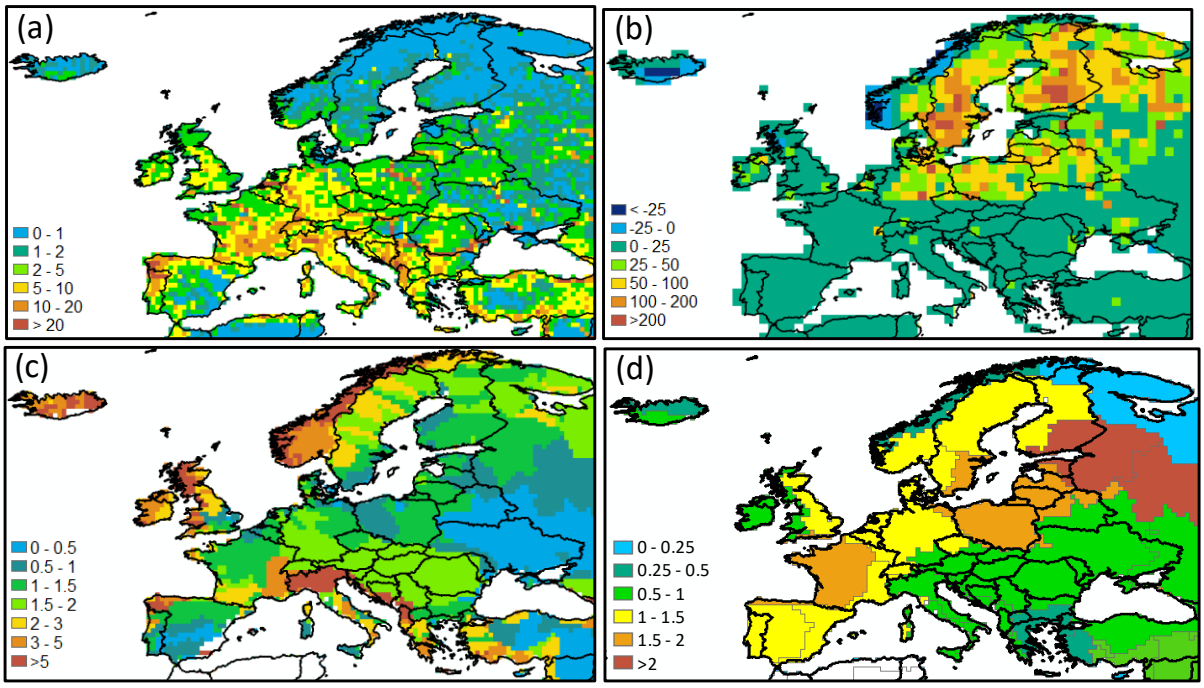

Figure 4.2 *Different datasets used to construct the European river C budget (units in gC $m^{-2}yr^{-1}$) (a) CO_2 evasion from rivers at 0.5° resolution from Lauerwald et al., 2015; (b) CO_2 evasion from lakes at 1° resolution from Raymond et al., 2013 and Hastie et al., 2018; (c) C yield export to the sea by catchment from Global News 2 (d) OC burial rate, from Mendonca et al., 2017. All flux densities are per unit total land area.*

4.2.2 River C budget at country scale

The first step is to determine the total C input of DOC, POC and free DIC from soil to inland waters network at basin scale, using Eq. (4.1) (fig 4.3a). All basin-aggregated components (evasion, burial and export to the sea) are from datasets in Table 4.1.

$$Lateral\ Input_{basin} = FCO_{2,basin} + Burial_{basin} + Export_{basin} \quad (4.1)$$

From the three terms on the right-hand side of Eq. (4.1), the total input can directly be calculated from equation 4.1. Next, this input was downscaled at 0.5° resolution. From all components at 0.5° resolution, we apply a country mask (at the 0.5° cell scale) to sum up all the grid-cell level inputs (arrow 5 in fig. 4.3b), burial (arrow 7 in fig. 4.3b) and CO_2 evasion (arrow 8 in fig. 4.3b) within each country. To determine the C import from upstream neighbouring countries (arrow 6 in fig. 4.3b) and the C export to downstream countries or to the sea (arrow 9 in fig. 4.3b), we specified the direction of the flow within each 0.5° cells from the STNp-30 river network (Vörösmarty et al., 2000) that was also used for the GlobalNEWS2 basins. With this routing scheme, we calculated C flows in / out of each country by summing across border cells (equation 4.2).

$$Import_{country} + Input_{country} = FCO_{2,country} + Burial_{country} + Export_{country} \quad (4.2)$$

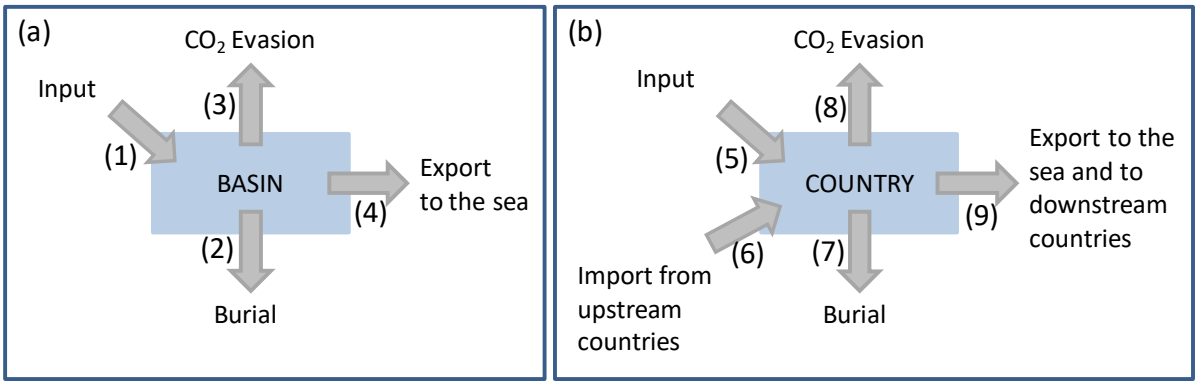

Figure 4.3 *Inland water carbon budgets at a (a) basin scale (b) country scale.*

4.2.3 Importance of the LOAC in the C budget

To evaluate if the riverine C horizontal exchange with neighbouring countries is significant compared to 'vertical' C fluxes within a given country, we defined the river net C balance (RNCB) index (eq. 4.3), as the difference between the export to the sea or other neighbouring countries minus the import.

$$RNCB = Export_{country} - Import_{country} = Input_{country} - FCO_{2,country} - Burial_{country} \quad (4.3)$$

As shown by eq. (4.3), the RNCB is also equal to the C inputs within the country minus inland water CO2 emissions and C burial.

We also aim to compare the river lateral fluxes the RNCB with other lateral fluxes between countries, due to wood and crop harvest trades. To do so, we used the biomass flow by country (crop and wood) from the BIOMASS project of the European Commission (Gurria et al., 2017). Not all countries of our studied region are listed in the BIOMASS project, which restricted our comparison to 26 countries. Imports and exports are expressed in ktonnes of dry matter (DM), converted to C with crop-specific conversion factors (Goudriaan et al., 2001; Ciais et al., 2007). Here we use the median factor which is equal to 0.48. For forests the conversion factor is 0.45 (Ciais et al., 2008). We define the net harvest trade as the difference between wood import and export for each country, a metric directly comparable to the RNCB.

We also compare the RNCB with other components of national C budgets averaged of the 2 last decades (2000-2019) in order to evaluate how important are the C fluxes in and out of a country via the river network. We compare the RNCB against the total land use, land use change and forestry (LULUCF) sink and the total non-LULUCF anthropogenic emissions (energy, industry, agriculture and waste related emissions) from the years 1990-2019 from the United Nations Framework Convention on Climate Change (UNFCCC). Then we look at more specific agricultural related emissions that are available on the Food and Agriculture Organization of the United Nations (FAO 2021): synthetic fertilizer (SF), burning crop residue (BCR), enteric fermentations CH_4 (EF), manure (soil and pasture) N_2O and CH_4 (M), on-farm energy

use (FE) and C emissions from drained organic soil (DOS). Those agricultural, forestry and other land use (AFOLU) emissions are an important part of the country-scale GHG budgets (Smith et al., 2014; FAO 2021). All emissions are expressed in ktonnes CO_2 equivalent, and we thus converted all fluxes originally expressed in ktonnes CO_2 per year into GgC per year by dividing them by 3.67.

4.3 RESULTS

4.3.1 National C budgets

Figure 4.4 shows the components of the inland water C budget by country. The average C input from soils to inland water (figure 4.4a) calculated as the area weighted average ± the standard deviation between all countries, equals 8.1 ± 2.7 gC m^{-2} yr^{-1}. The highest inputs, between 10 and 16 gC m^{-2} yr^{-1} are found in Slovenia, Italy, Finland and Sweden. The lowest input of 2.4 gC m^{-2} yr^{-1} is found in Iceland. High imports (figure 4.4 b) correspond to countries with large river inflows, such as the Netherlands with the Rhine or countries that are crossed by the Danube, like Slovakia, Hungary, Serbia, Bulgaria and Romania. Scandinavian countries have low imports because most rivers source inside their territory. Iceland and Spain have a zero import since no rivers flows into their territory. On average the mean import flux is of 2.3 ± 7.5 gC m^{-2} yr^{-1}, that is, 28 % of the inputs, indicating a significant fraction of river C coming from outside national borders. The CO_2 evasion and C burial shown in figure 4.4(c-d) equal 5.2 ± 2.3 gC m^{-2} yr^{-1} and 0.8 ± 0.4 gC m^{-2} yr^{-1}, respectively. C burial and CO_2 evasion are usually the most important in countries with largest water areas, such as Sweden, Finland and Estonia (figure 4.1c). Norway and Switzerland also have a high water area but low burial and CO_2 evasion, due to mountainous terrain leading to short water residence time to fuel burial and CO_2 evasion. Looking at the ratio of burial and evasion to the sum of inputs and import, we found that 7.7 ± 3.9 % of the input plus import is buried while 50 ± 22.5 % is emitted to the atmosphere. Finally, 4.4 ± 7.6 gC m^{-2} yr^{-1} of C is exported to the sea or other countries, corresponding to 42.3 ± 24.2 % of the total C generated by input plus import.

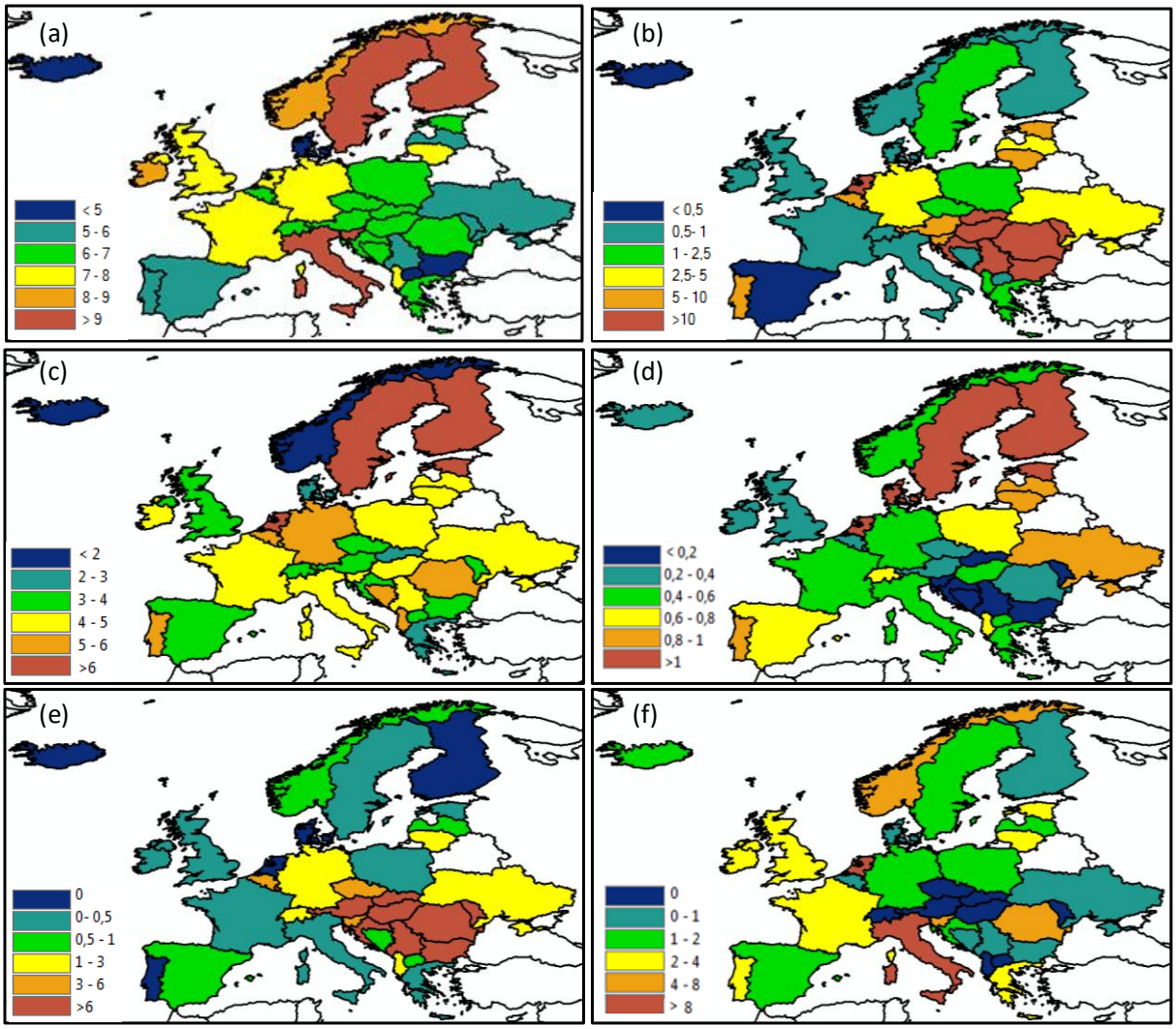

Figure 4.4 *Inland water C budget by country. (a) Input, (b) Import from neighbouring countries, (c) CO_2 evasion, (d) Burial, (e) Export to neighbouring countries and (f) Export to estuaries. All fluxes in gC m^{-2} yr^{-1} with area referring to total land area.*

4.3.2 Importance of the LOAC in national C budgets

In this section, we analyse the RNCB defined in section 2 (Figure 4.5). Only few countries have a negative RNCB (the Netherlands, Portugal, Estonia and Ukraine), that is, a RNCB for which the import is higher than the export. Most countries have a positive RNCB, so that CO2 emission and burial fluxes are lower than the C input into their territory. A high RNCB can either reflect a large export of C across borders or a low import from other countries. The highest RNCB for Italy and Norway are only mostly due to high exports to the sea, given small evasion and burial (Fig. 4.4). Norway and Italy are mountainous with steep catchments leading to a faster C transport from soils to estuaries and thus a limited time for C transformation.

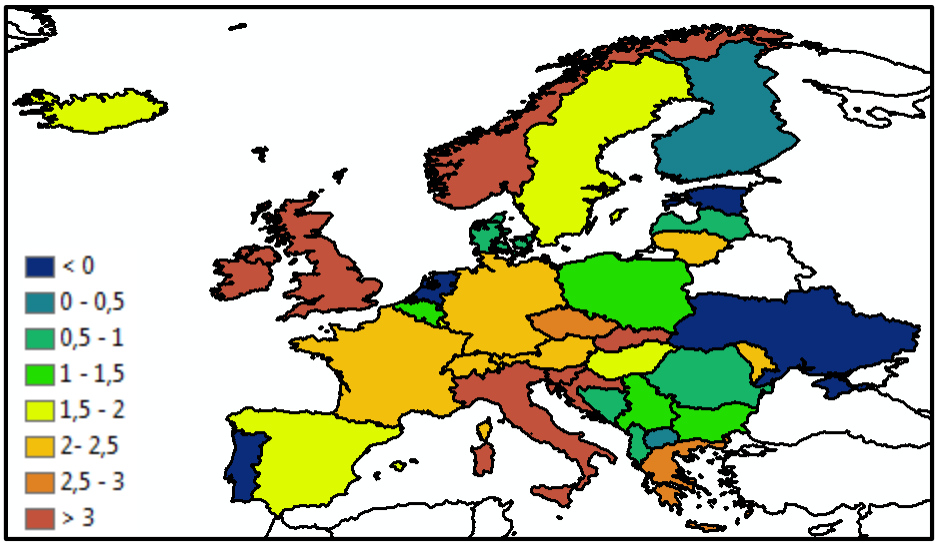

Figure 4.5 *River net C balance by country in gC m^{-2} yr^{-1}.*

Figure 4.6 (α) shows the proportion (α) of input to the sum of input and import (denominated as total source). As already shown in figure 4.4b, Iceland and Spain have no import from other countries. Half of the countries (Albania, Bosnia and Herzegovina, Czech Republic, Denmark, Finland, France, Iceland, Ireland, Italy, Macedonia, Norway, Poland, Spain, Sweden, Switzerland, United Kingdom) have α values > 90%, meaning that their river C budget is heavily dominated by national soil C leaching and erosion. In contrast, nine countries have α values < 50%, meaning that their river C budget is dominated by imports (Bulgaria, Croatia, Hungary, Luxembourg, Moldova, Netherlands, Romania, Serbia and Montenegro, Slovakia). These countries are downstream of large rivers (Netherlands with the Rhine and other countries with the Danube). Countries like Belgium, Portugal or Ukraine exhibit intermediate α values from 60 to 80%, still dominated by national C leaching and erosion. Figure 4.6 (β) shows the proportion (β) of the export to estuaries to the total export. As expected, countries with no border to the sea or the ocean have a β value of zero (Albania, Austria, Czech Republic, Hungary, Luxembourg, Macedonia, Moldova, Slovakia, and Switzerland). When the border with the sea is small, β values do not exceed 5% (Belgium, Bulgaria, Serbian and Montenegro, Bosnia and Herzegovina). Few countries only export to the sea (Iceland, Portugal, the Netherlands, Denmark and Finland) and have β values of unity. Both Ireland and the United Kingdom's export little C to one another, through Northern Ireland and have β value of 3.5% and 1%, respectively. Then for some countries, export is evenly distributed between exports to estuaries and to neighboring countries (Germany, Slovenia and Spain) and have β values around 50%.

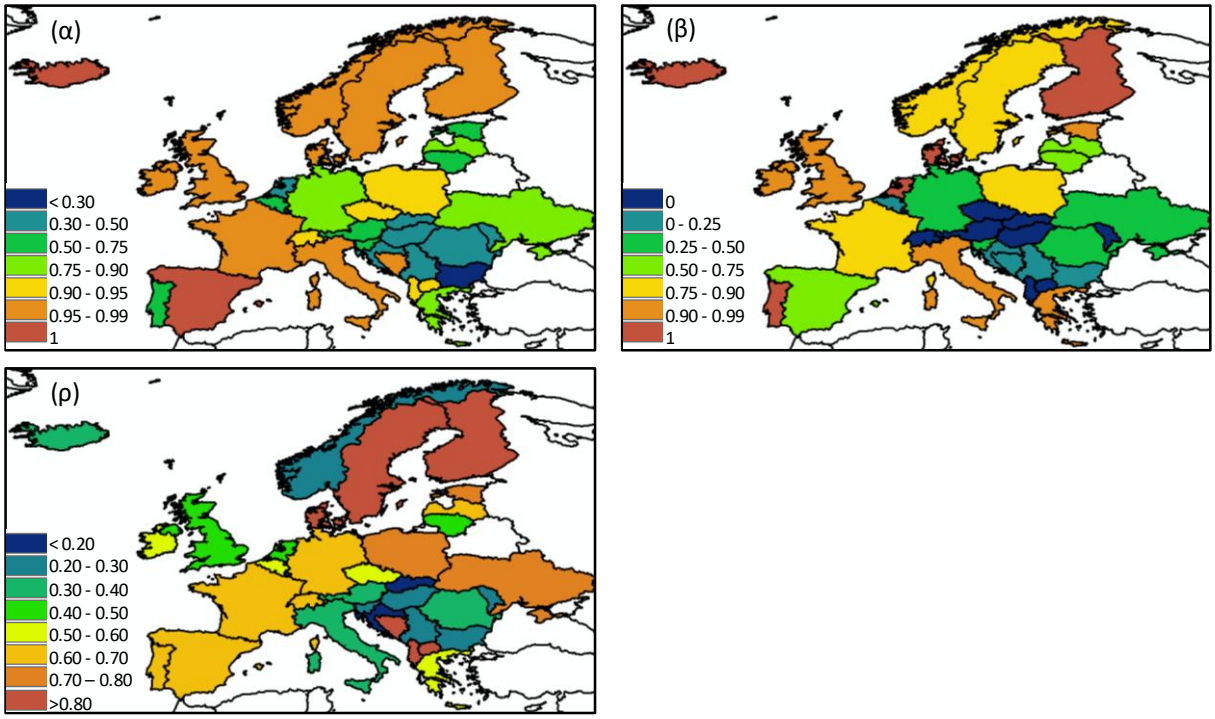

Figure 4.6 *α, Ratio input to total C sources (input and import from neighbouring countries); β, Fraction of the total C export that goes to estuaries; ρ, Ratio of burial and CO_2 emissions to total C sources.*

Figure 4.6 (ρ) represent the filtering efficiency ρ, as the ratio of input plus import to burial plus evasion. The value of ρ varies across Europe with high values in Scandinavia (except Norway) and in some Balkans countries. ρ is low in the Danube catchment which is somewhat surprising: given the length of the river, one might have expected to observe high burial and CO_2 emissions. We found countries with low ρ 33% (Bulgaria, Croatia, Hungary, Iceland, Luxembourg, Moldova, Norway, Romania, Serbia and Montenegro, Slovakia, Slovenia), intermediate ρ > 33 and < 66% (Austria, Belgium, Czech Republic, Germany, Greece, Ireland, Italy, Lithuania, Netherlands, Switzerland, United Kingdom) and high ρ > 66% (France, Portugal, Spain, Latvia, Poland, Ukraine, Estonia, Denmark, Albania, Bosnia and Herzegovina, Macedonia, Sweden, Finland).

4.4 Discussion

4.4.1 Implications for national C accounting

In this section, the RNCB is compared with LULUCF and non-LULUCF fluxes from inventories (Figure 4.7). For a few countries, data were unavailable (Albania, Bosnia & Herzegovina, Macedonia, Moldavia and Serbia & Montenegro). LULUCF ranges from a sink of -11300 GgC yr^{-1} in Italy to a source of 3700 GgC yr^{-1} in the Czech Republic. Most countries report LULUCF carbon as sinks and the ratio μ corresponding to RNCB to LULUCF varies from 0.02 (Finland) to 0.4 (Norway). Slovenia is an outlier with a high RNCB and a small LULUCF sink, leading to a μ of 5.3. High μ values are found when

RNCB is high such as in Norway (0.4) or when LULUCF are low as in Greece (0.37). Portugal and Estonia have a negative RNCB and a positive LULUCF, leading to μ values of 0.02 and 0.2, respectively. Seven countries report LULUCF as sources (Czech Republic, Denmark, Iceland, Ireland, the Netherlands, Ukraine and the United Kingdom's). For those countries, μ values vary from 0.04 (the Netherlands) to 1 (Ukraine).

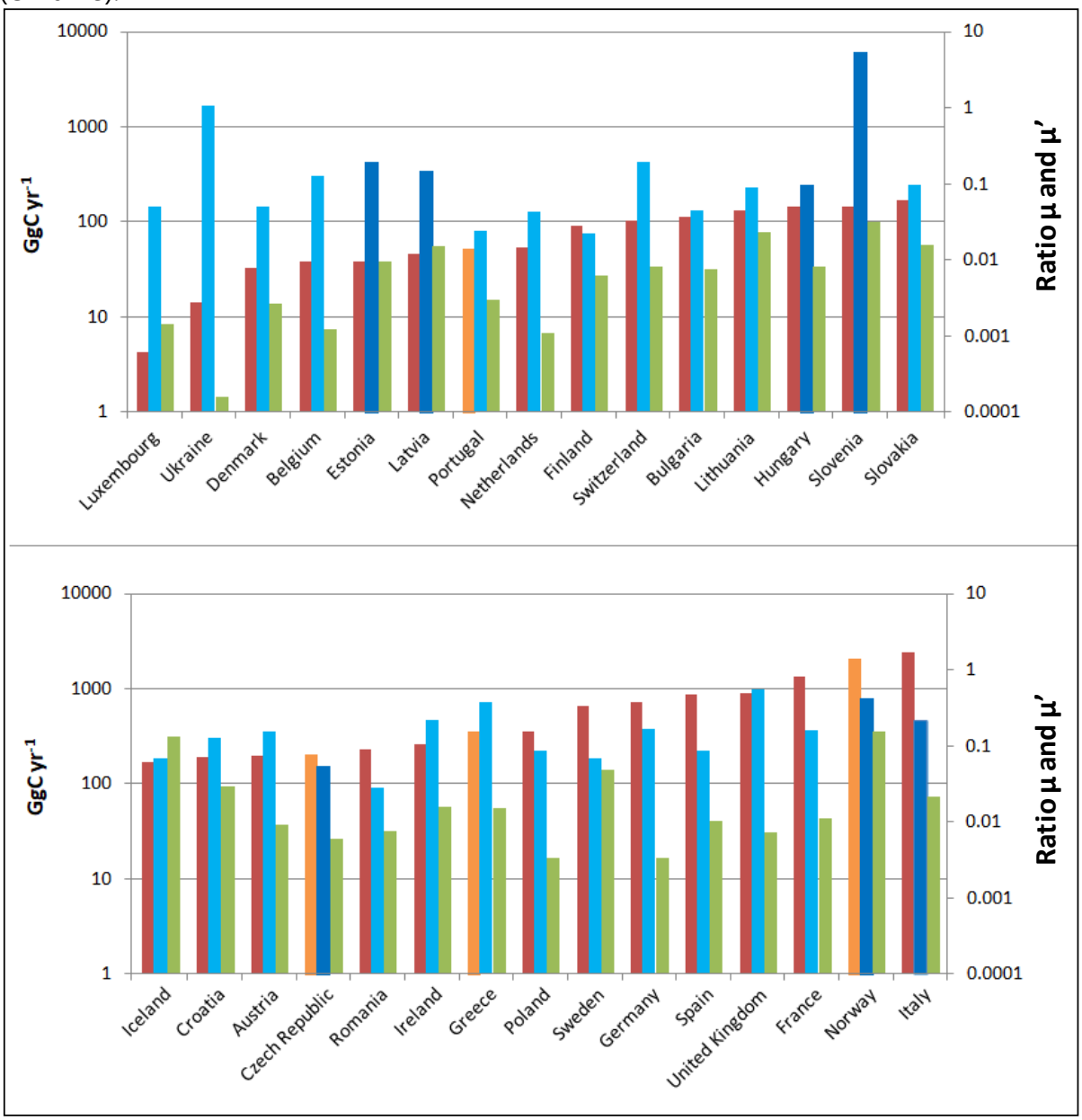

Figure 4.7 *Left y-axis, the RNCB in absolute value in GgC yr^{-1} (Red and Orange correspond to positive and negative RNCB, respectively). Right y-axis, the ratio RNCB to LULUCF (Light blue and dark blue correspond to positive and negative LULUCF, respectively) and the ratio RNCB to other anthropogenic (Non-LULUCF) emissions (Green) from the UNFCCC .*

We note that two of the countries have also a negative RNCB, Ukraine and the Netherlands. In summary, across Europe, the ratio of RNCB to LULUCF is highly disparate. For some countries, the RNCB is as important as LULUCF (Slovenia, Ukraine, Norway and UK) while for others the RNCB is relatively small, on the order of 0.1 or less (Romania, Finland and Portugal).

Non-LULUCF emissions are larger than LULUCF ones, and range from 1290 GgC yr^{-1} in Iceland to 220650 GgC yr^{-1} in Germany. The ratio μ' of RNCB to Non-LULUCF emissions ranges from $-2x10^{-4}$ (Ukraine) to 0.05 (Sweden), except for Norway and Iceland where μ' reaches 0.15 and 0.13, respectively. For Norway the high μ' is due to both a high RNCB and low anthropogenic emissions. For Iceland, the high value is due to low anthropogenic emissions.

The RNCB was also compared with specific agricultural emissions reported by the FAO (section 4.2.3) in Figure 4.1 (graphs for other countries are reported in figure S.4.1). Finland and France present similar ratios of RNCB to specific agricultural emissions of on the order of 0.5 or less except for burning crop residues for which the ratio > 10, and this despite the fact that Finland has a much lower RNCB (90 GgC yr^{-1}) than France (1330 GgC yr^{-1}). Norway and Slovenia have in general a higher ratio RNCB to specific agricultural emission above 1 than France and Finland, but again with a RNCB for Norway (2100 GgC yr^{-1}) much larger than for Slovenia (147 GgC yr^{-1}). The results for Portugal are also shown, one of the few countries with a negative absolute RNCB and a ratio of RNCB compared to specific agricultural emissions smaller than 0.3 except for burning crop residue for which the ratio is much higher. With the exception of 8 countries (Norway, Iceland, Slovenia, Italy, Slovakia, Croatia, Moldavia and Sweden, shown in figure S.4.1), the ratio RNCB to total FAO emissions is always smaller than 0.01, meaning that the RNCB is clearly much smaller compared to the sum of the emissions related to food and agriculture. The ratio nevertheless reaches 0.13 in Moldavia and Sweden, 0.18 in Croatia, 0.20 in Slovakia, Italy and Slovenia, 0.29 in Iceland and 0.45 in Norway.

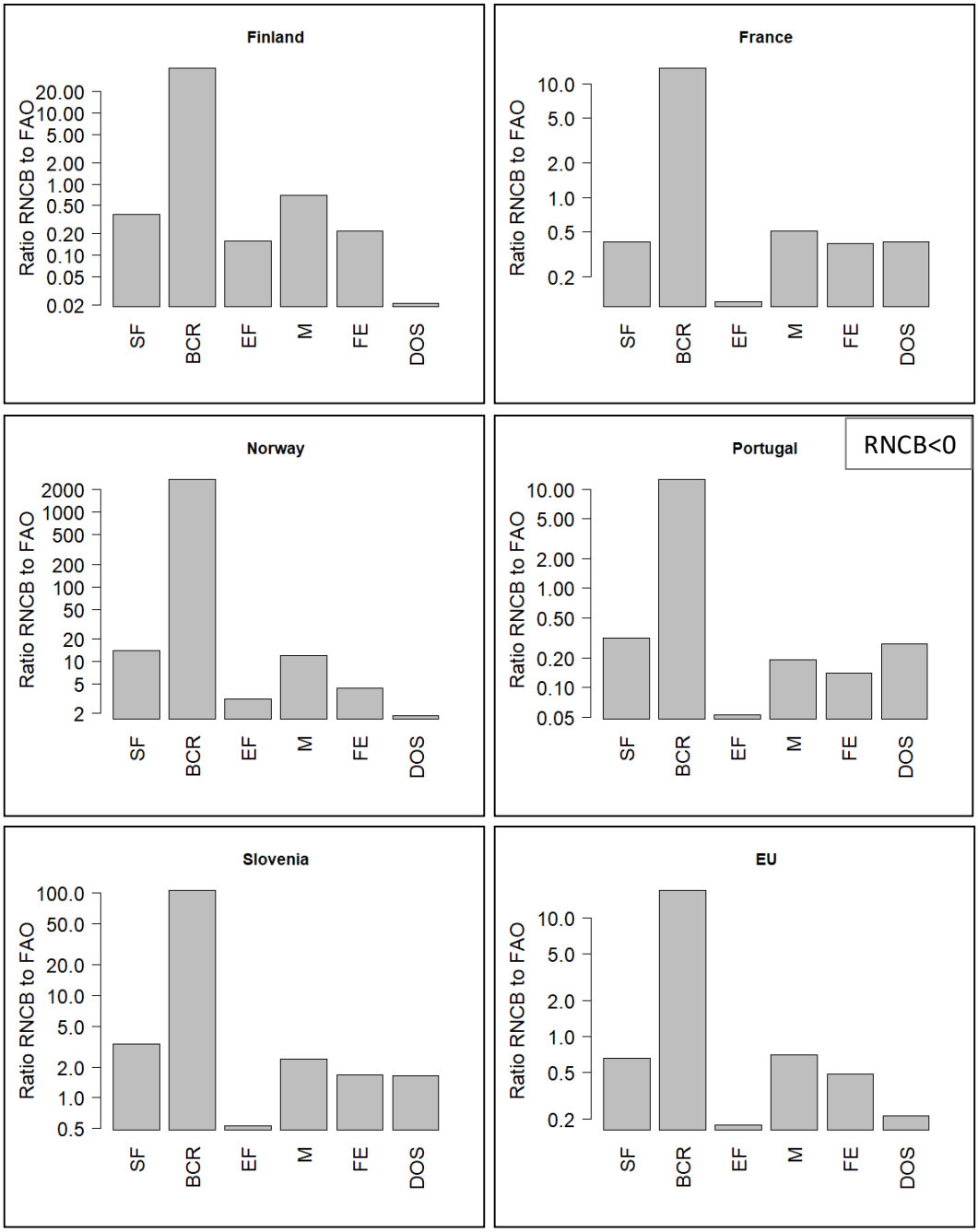

Figure 4.8 *Ratio of RNCB to national emissions due to of synthetic fertilizer use(SF), burning crop residue (BCR), enteric fermentation (EF), manure (M), on-farm energy (FE) and drained organic soil (DOS) for Finland, France, Norway, Portugal (RNCB<0), Slovenia and all of Europe).*

Between all agricultural emission fluxes in our comparison, we see that they are usually dominated by the contributions from enteric fermentation and drained organic soil. These two contributions are typically one order of magnitude larger than the RNCB. The first corresponds to a digestive process from animals that emits methane which is increased by agriculture and the second consists of nitrous oxide (N_2O) and carbon dioxide (CO_2) emissions associated with the mineralization and oxidation of the organic matter in organic soils that are drained for agriculture (FAO 2021). Synthetic fertilizer (production of N_2O from synthetic nitrogen additions to managed soils, FAO 2021), manure (applied to soils consist of direct and indirect N_2O emissions from nitrogen (N) of manure added to agricultural soils and left by grazing livestock on pasture, FAO 2021) and on farm energy use (carbon dioxide, methane and nitrous oxide gases associated with fuel burning and generation of electricity used in agriculture, including fisheries, FAO 2021) are also generally higher than the RNCB, but to a lesser extent, the ratio being typically comprised between 0.2 and 0.8. In contrast, the RNCB is typically one order of magnitude higher than burning crop residue, which consists in production of N_2O and CO_2 by the combustion of a percentage of crop residues burnt on-site (FAO 2021).

Finally, we compare the RNCB with other lateral fluxes, that is, wood and crop harvest trades from the "biomass flow" project of the European commission (Figure 4.9). Overall, wood and crop harvest trades are more important. Amongst the 26 countries analyzed, nine of them have negative net harvest trade meaning that those countries export more crop and wood carbon than they import (all values are listed in table S4.2). Ten countries have RNCB and trades fluxes going in the same direction (i.e. they have the same sign): Bulgaria, France, Hungary, Latvia, Lithuania, Poland, Romania and Slovenia (RNCB and harvest trades positive) and the Netherlands and Poland (RNCB and harvest trades negative). All other countries have opposite signs for RNCB and harvest trades (RNCB positive except for Estonia) suggesting that the RNCB could partly compensate the harvest trade flux in these countries. For most countries, the ratio RNCB to net harvest trades, Y, is smaller than 0.1 due to low RNCB and high net harvest trades (e.g. Belgium and the Netherlands which have the lowest Y's). Few countries have a high Y due to both high RNCB and low net harvest trades (Finland: 0.70, Croatia: 0.77 and Slovenia: 2.90). The average Y for the whole of Europe equals 0.29, but this value is pushed upward due to the outlier Slovenia. When the median Y is considered, a significantly lower (0.09) value is found. We note that almost half of the EU countries have a Y greater than 0.10 and a quarter of the EU countries have a Y greater than 0.30. These results show that the RNCB is for many European countries a non-negligible contributor to the lateral C fluxes and can even reach the same order of magnitude as the net harvest trades in several EU countries.

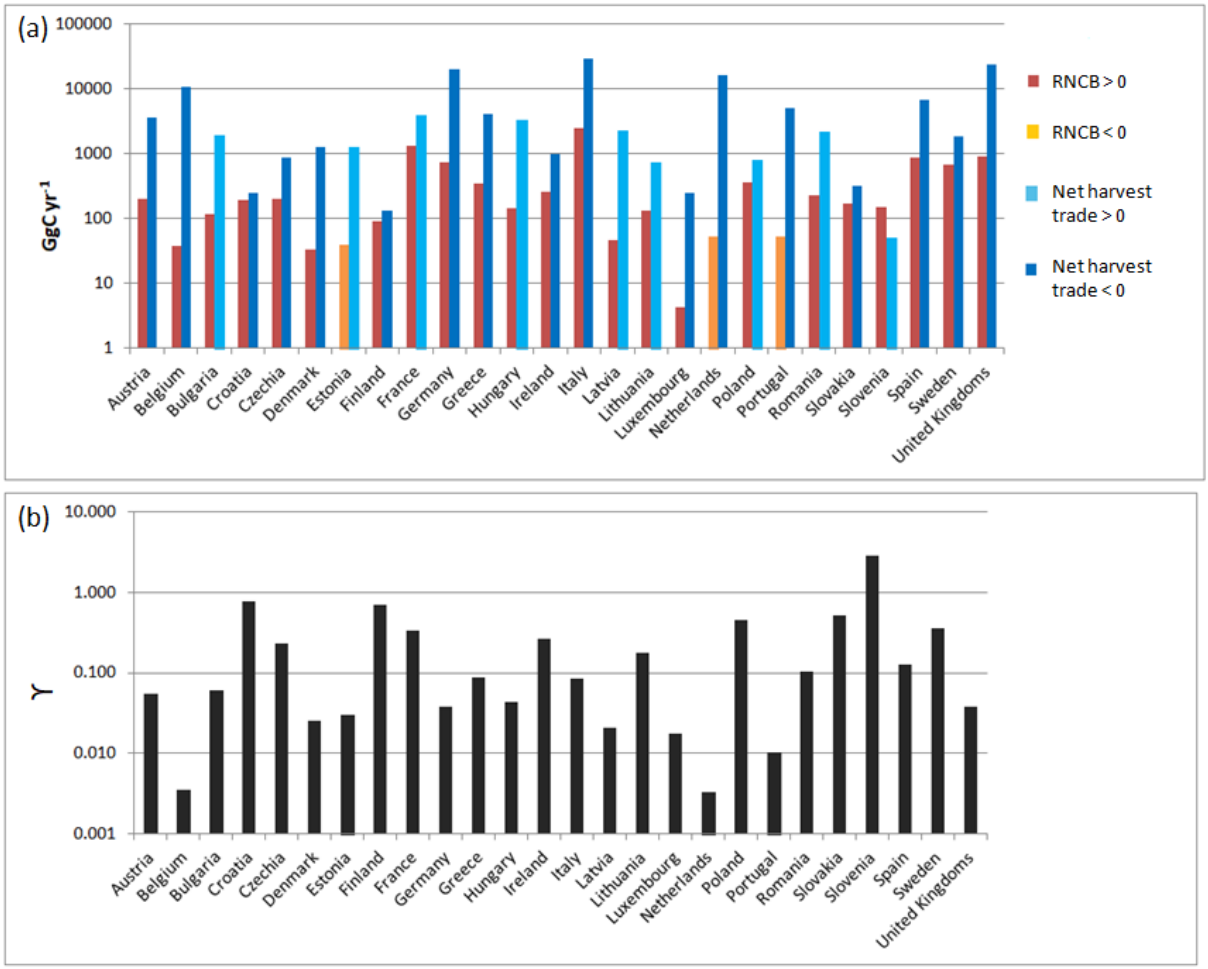

Figure 4.9 *Comparison between (a) the absolute values of the RNCB (negative RNCB are indicated by the orange color) and the net crop and wood harvest trades (defined as export-import) (negative net trades are indicated by the light blue color) (GgC yr^{-1}) for the countries for which data could be extracted from the "biomass flow" project of the European Commission (Gurria et al., 2017). (b) ratio ϒ of RNCB to net harvest trades.*

4.5 CONCLUSION

A methodology was developed to establish inland water C budgets at the country-scale for Europe, including rivers imports and exports through the country boundaries, evasion, burial and soil C loss to rivers headstreams. We have shown that the quantities of C transferred from one country to another or to estuaries can be significant, with their order of magnitude similar to other small components of the national GHG's budgets such as synthetic fermentation, manure, on farm energy use and burning crop residue. Further, we demonstrated that lateral C fluxes through rivers are generally one order of magnitude lower than wood and crop harvest. However, this ratio is significantly larger in Slovenia, Croatia, Finland, Slovakia, Poland, France, Sweden, Ireland and Lithuania. We thus recommend that the C transfer from one country to another through the river network should be reported for information in national inventories.

However, the RNCB cannot be separated into an anthropogenic component flux that should be part of the inventory scope and a natural flux that should not. Future work will require a new methodology to distinguish the natural part from the anthropogenic contribution. This is however not a simple task, as the decomposition of natural versus anthropogenic is currently impossible to achieve via observations. The new methodology needs to rely on modeling approaches as the one developed in chapter 2. In addition, CH_4 and N_2O emissions from inland waters should also be accounted although in the countries national GHG budgets. In the future, our methodology could also be applied to other regions of the globe and integrated in a global scale context. While this chapter aims to quantify the C fluxes between countries through rivers to account them in national C budget, it is important not to over interpreted or misused the results. Indeed, our results cannot directly be used for policy-making since the distinction between the natural and the anthropogenic fluxes is still missing.

4.6 SUPPLEMENT

Table S.4.1 *Calculated inland water C budget by country (GgC yr^{-1}), land area and proportion of water area (river, lake and reservoir).*

Country	Area km^2	Water Area %	Input	Burial	FCO_2	Import	Total Export	RNCB
Albania	2.86E+04	2.13	208.1	17.6	170.6	21.1	41.1	19.9
Austria	8.37E+04	0.93	507.5	22.1	288.1	395.8	593.2	197.4
Belgium	3.05E+04	1.37	201.1	9.9	152.9	78.2	116.6	38.3
Bosnia & Herzegovina	5.14E+04	0.78	315	8.8	258.6	5.8	53.4	47.7
Bulgaria	1.11E+05	0.72	519	21.3	382.9	1356.6	1471.4	114.7
Croatia	5.58E+04	1.01	374.8	10.8	173.9	665.8	855.9	190.1
Czech Republic	7.85E+04	1.06	488	23	263	50.7	252.7	202.0
Denmark	4.25E+04	4.71	178.6	55.1	90.5	2.7	35.7	33.0
Estonia	4.57E+04	5.66	295.1	54.1	279.5	140.5	102	-38.5
Finland	3.19E+05	10.31	4343.2	528.6	3724	137.8	228.4	90.6
France	5.47E+05	0.93	4125.7	292.9	2502	102.3	1433.1	1330.8
Germany	3.56E+05	1.71	2737.6	156.1	1848.1	499.8	1233.2	733.3
Greece	1.30E+05	1.05	799	67.8	380.8	95.7	446	350.4
Hungary	9.27E+04	1.48	569.1	39.8	383.9	1201.4	1346.8	145.4
Iceland	1.02E+05	1.83	246.6	20.5	55	0	171.1	171.1
Ireland	6.94E+04	2.2	596.4	26.3	309.9	21.6	281.8	260.2
Italy	3.00E+05	1.31	3890.9	120.6	1343.4	45.9	2472.8	2426.9
Latvia	6.43E+04	2.46	376	60.3	269.4	98.3	144.6	46.3
Lithuania	6.47E+04	2.2	502.1	53.7	317.8	241.3	371.9	130.6
Luxembourg	2.57E+03	1	16	0.6	11.2	98.6	102.8	4.3
Macedonia	2.54E+04	1.58	115.7	13.4	89.8	7.8	20.3	12.6

Moldova	3.36E+04	0.72	186	6.7	104.7	298.4	373.1	74.6
Netherlands	3.54E+04	4.18	254.3	37.6	269.9	453.5	400.3	-53.2
Norway	3.33E+05	3.32	2906.2	197.8	605.6	124.8	2227.7	2102.9
Poland	3.10E+05	1.85	2040	219.5	1467.9	203.9	556.5	352.7
Portugal	9.18E+04	1.23	548.8	81.7	519	347.2	295.4	-51.8
Romania	2.37E+05	1.16	1615.8	76.8	1309.2	2926.2	3155.9	229.8
Serbia & Montenegro	1.02E+05	0.69	576.6	8.1	445.7	1250.8	1373.6	122.8
Slovakia	4.88E+04	0.61	320.8	6.4	146.1	624.5	792.8	168.3
Slovenia	2.04E+04	0.45	239	1.5	90.8	88.6	235.3	146.7
Spain	5.06E+05	1.05	2855.2	398.5	1580.6	0	876.1	876.1
Sweden	4.43E+05	7.93	7218.9	920.7	5628.9	270	939.4	669.4
Switzerland	4.14E+04	3.58	283.5	32.7	149.3	17.7	119.2	101.5
Ukraine	5.96E+05	1.97	3302.1	565.8	2750.5	1092.6	1078.4	-14.2
United Kingdom	2.43E+05	1.57	1739.1	87	742.2	10.6	920.5	909.9

Table S.4.2 *Wood and Crop Harvest from the BIOMASS project from the European commission in ktonnes dry matter yr^{-1}. Calculated total import, export and net trades, conversion in GgC yr^{-1}using the forest and crop factors of respectively 0.45 and 0.48 (Goudriaan et al., 2001; Ciais et al., 2007; Ciais et al., 2008).*

COUNTRY	Wood Import	Crop Import	Wood Export	Crop Export	Total Import	Total Export	Net trades	RNCB
	(ktonnes dry matter yr^{-1})				(GgC yr^{-1})			
Austria	4946	5533	2825	0	4882	1271	3610	197.4
Belgium	2930	20226	0	636	11027	305	10722	38.3
Bulgaria	0	3180	963	6199	1526	3409	-1882	114.7
Croatia	0	2824	1544	860	1356	1108	248	190.1
Czech Republic	0	6449	2065	2717	3096	2233	862	202
Denmark	3679	2987	0	3757	3089	1803	1286	33
Estonia	0	437	2507	726	210	1477	-1267	-38.5
Finland	3801	2885	6303	270	3095	2966	129	90.6
France	1432	12558	2227	20073	6672	10637	-3965	1330.8
Germany	7048	38721	2008	2760	21758	2228	19529	733.3
Greece	520	8475	0	599	4302	288	4014	350.4
Hungary	0	2697	313	9305	1295	4607	-3313	145.4
Ireland	0	4411	412	1999	2117	1145	972	260.2
Italy	10536	49576	0	0	28538	0	28538	2426.9
Latvia	0	916	4260	1604	440	2687	-2247	46.3
Lithuania	112	2688	815	3549	1341	2070	-730	130.6
Luxembourg	126	416	26	0	256	12	245	4.3
Netherlands	2170	31856	218	0	16267	98	16169	-53.2
Poland	949	1264	274	3536	1034	1821	-787	352.7
Portugal	887	11142	1583	0	5747	712	5035	-51.8

Romania	1176	6395	2657	9627	3599	5817	-2218	229.8
Slovakia	0	3877	1577	1725	1861	1538	323	168.3
Slovenia	219	963	1359	0	561	612	-51	146.7
Spain	435	19051	1168	4076	9340	2482	6858	876.1
Sweden	4200	8265	8175	696	5857	4013	1844	669.4
United Kingdom	12596	38049	165	0	23932	74	23857	909.9

Table S.4.3 *RNCB comparison with other component of the EU C budget: RNCB; sum of emissions from FAO (synthetic fertilizer, burning crop residue, enteric fermentation, fires, manure, on farm energy and drained organic soil); Ratio RNCB to the sum of FAO emissions; LULUCF (UNFCCC); Ratio RNCB to LULUCF; total anthropogenic emissions without LULUCF (UNFCCC); Ratio RNCB to anthropogenic emissions All emissions in GgC yr^{-1} and all ratios in absolute values.*

COUNTRY	RNCB	FAO Emissions	RNCB /FAO	LULUCF	RNCB /LULUCF	Anthropogenic Emissions	RNCB /Anthro.
Albania	20	944	0.021	-	-	-	-
Austria	197	2050	0.090	-1263	0.156	21755	0.0091
Belgium	38	2790	0.014	-300	0.128	31785	0.0012
Bosnia & Herzegovina	48	670	0.068	-	-	-	-
Bulgaria	115	2051	0.054	-2605	0.044	15247	0.0075
Croatia	190	915	0.181	-1514	0.126	6432	0.0296
Czech Republic	202	1974	0.095	3696	0.055	33417	0.0060
Denmark	33	3153	0.010	657	0.050	12483	0.0026
Estonia	-38	2008	0.019	-195	0.197	4005	0.0096
Finland	91	5757	0.016	-4006	0.023	14447	0.0063
France	1331	24069	0.053	-8285	0.161	120704	0.0110
Germany	733	22586	0.032	-4486	0.163	220654	0.0033
Greece	350	3329	0.098	-949	0.369	23333	0.0150
Hungary	145	5169	0.028	-1517	0.096	17557	0.0083
Iceland	171	457	0.294	2472	0.069	1287	0.1330
Ireland	260	7281	0.035	1211	0.215	16288	0.0160
Italy	2427	10110	0.204	-11325	0.214	113973	0.0213
Latvia	46	2178	0.021	-314	0.147	3033	0.0153
Lithuania	131	4193	0.030	-1481	0.088	5550	0.0235

Luxembourg	4	174	0.024	-85	0.050	2927	0.0015
Macedonia	13	341	0.036	-	-	-	-
Moldova	75	532	0.127	-	-	-	-
Netherlands	-53	7668	0.007	1232	0.043	49131	0.0011
Norway	2103	3176	0.447	-5078	0.414	13715	0.1533
Poland	353	19396	0.018	-4099	0.086	106470	0.0033
Portugal	-52	1996	0.026	-2144	0.024	17294	0.0030
Romania	230	4245	0.052	-8234	0.028	30454	0.0075
Serbia & Montenegro	123	1941	0.061	-	-	-	-
Slovakia	168	713	0.201	-1728	0.097	10885	0.0155
Slovenia	147	597	0.208	-28	5.330	4650	0.0315
Spain	876	10507	0.079	-10239	0.086	85703	0.0102
Sweden	669	4867	0.125	-9670	0.069	13875	0.0482
Switzerland	101	1709	0.057	-527	0.193	12563	0.0081
Ukraine	-14	15153	0.001	13	1.065	90494	0.0002
United Kingdom	910	15758	0.055	1646	0.553	123461	0.0074

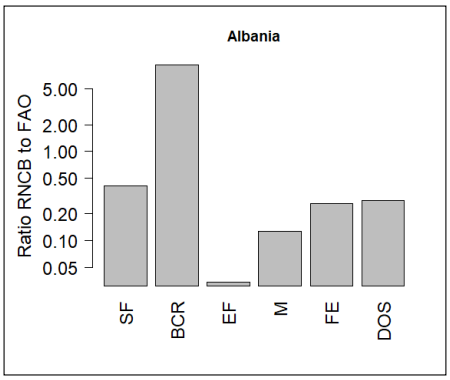
Albania
Ratio RNCB to FAO
5.00
2.00
1.00
0.50
0.20
0.10
0.05
SF
BCR
EF
M
FE
DOS

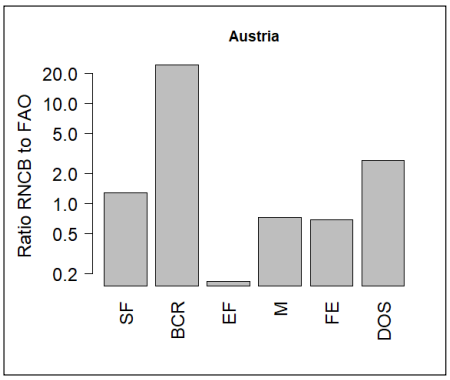
Austria
Ratio RNCB to FAO
20.0
10.0
5.0
2.0
1.0
0.5
0.2
SF
BCR
EF
M
FE
DOS

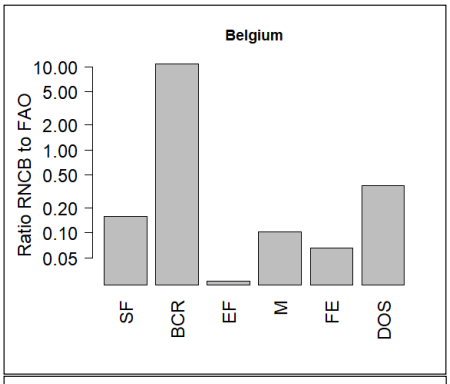
Belgium
Ratio RNCB to FAO
10.00
5.00
2.00
1.00
0.50
0.20
0.10
0.05
SF
BCR
EF
M
FE
DOS

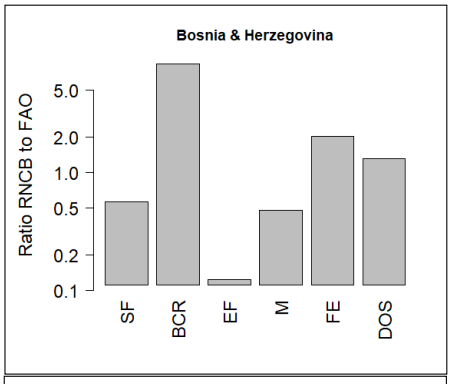
Bosnia & Herzegovina
Ratio RNCB to FAO
5.0
2.0
1.0
0.5
0.2
0.1
SF
BCR
EF
M
FE
DOS

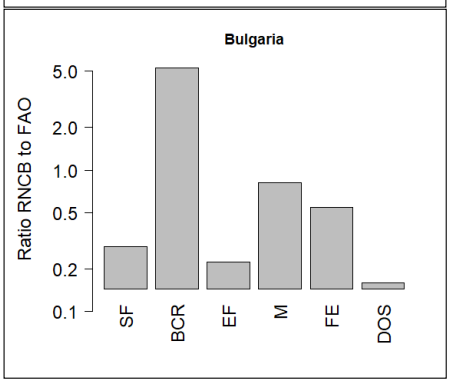
Bulgaria
Ratio RNCB to FAO
5.0
2.0
1.0
0.5
0.2
0.1
SF
BCR
EF
M
FE
DOS

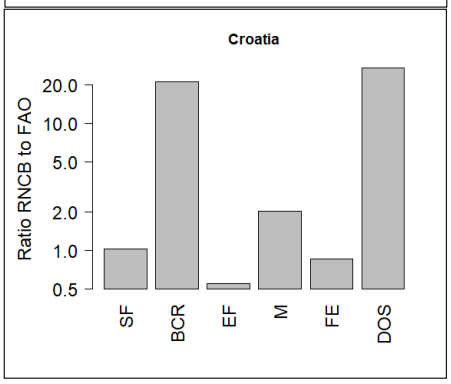
Croatia
Ratio RNCB to FAO
20.0
10.0
5.0
2.0
1.0
0.5
SF
BCR
EF
M
FE
DOS

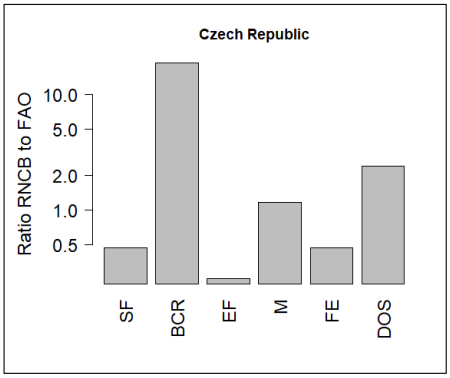
Czech Republic
Ratio RNCB to FAO
10.0
5.0
2.0
1.0
0.5
SF
BCR
EF
M
FE
DOS

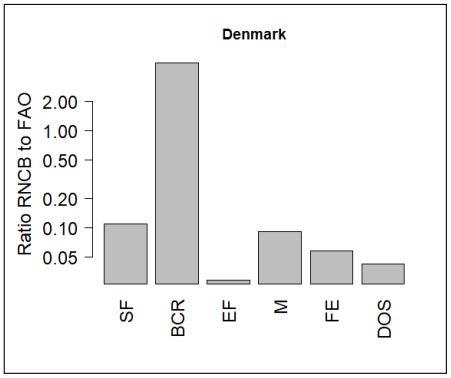
Denmark
Ratio RNCB to FAO
2.00
1.00
0.50
0.20
0.10
0.05
SF
BCR
EF
M
FE
DOS

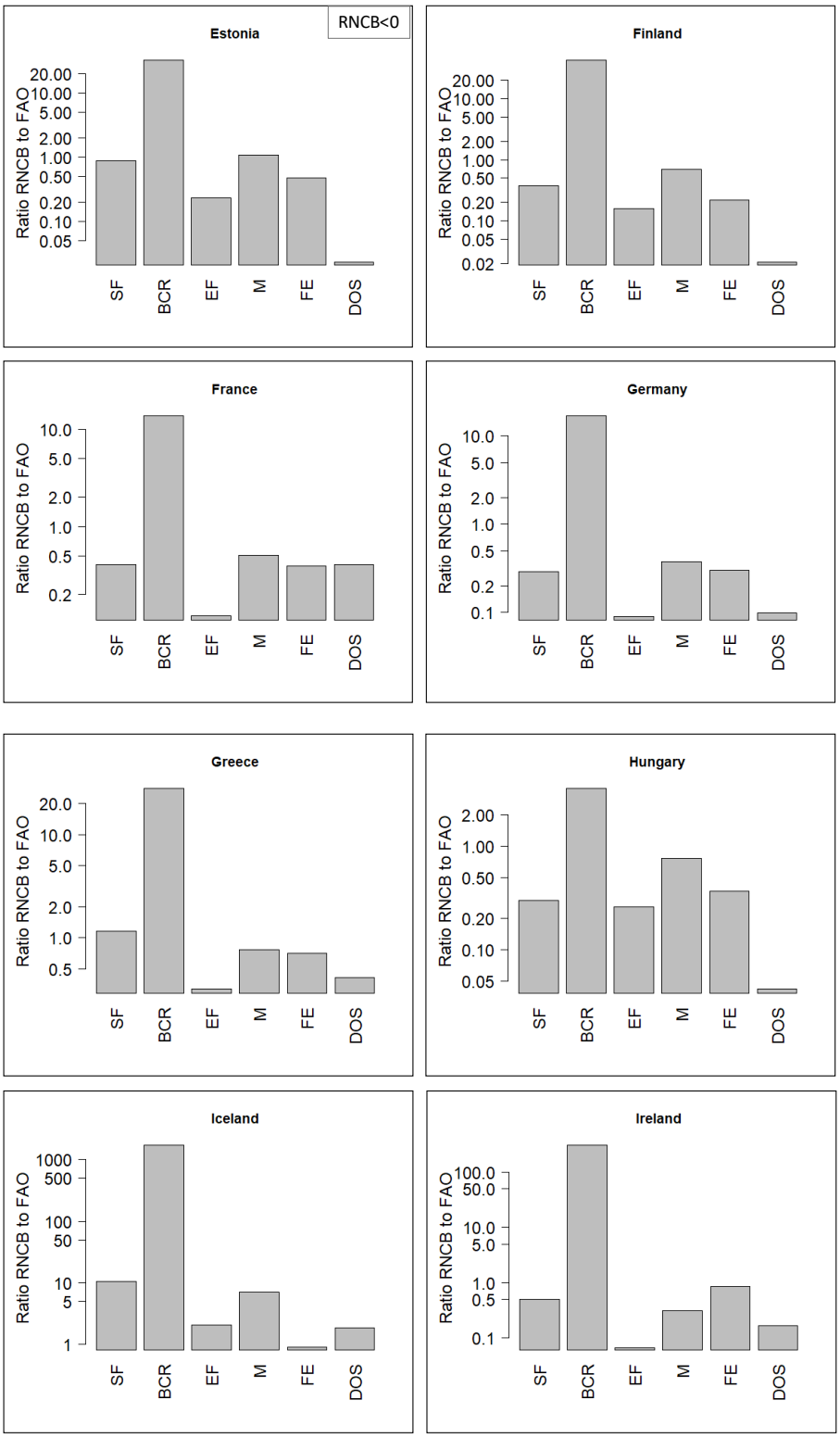
Estonia
RNCB<0
Ratio RNCB to FAO
20.00
10.00
5.00
2.00
1.00
0.50
0.20
0.10
0.05
SF
BCR
EF
M
FE
DOS
Finland
Ratio RNCB to FAO
20.00
10.00
5.00
2.00
1.00
0.50
0.20
0.10
0.05
0.02
SF
BCR
EF
M
FE
DOS
France
Ratio RNCB to FAO
10.0
5.0
2.0
1.0
0.5
0.2
SF
BCR
EF
M
FE
DOS
Germany
Ratio RNCB to FAO
10.0
5.0
2.0
1.0
0.5
0.2
0.1
SF
BCR
EF
M
FE
DOS
Greece
Ratio RNCB to FAO
20.0
10.0
5.0
2.0
1.0
0.5
SF
BCR
EF
M
FE
DOS
Hungary
Ratio RNCB to FAO
2.00
1.00
0.50
0.20
0.10
0.05
SF
BCR
EF
M
FE
DOS
Iceland
Ratio RNCB to FAO
1000
500
100
50
10
5
1
SF
BCR
EF
M
FE
DOS
Ireland
Ratio RNCB to FAO
100.0
50.0
10.0
5.0
1.0
0.5
0.1
SF
BCR
EF
M
FE
DOS

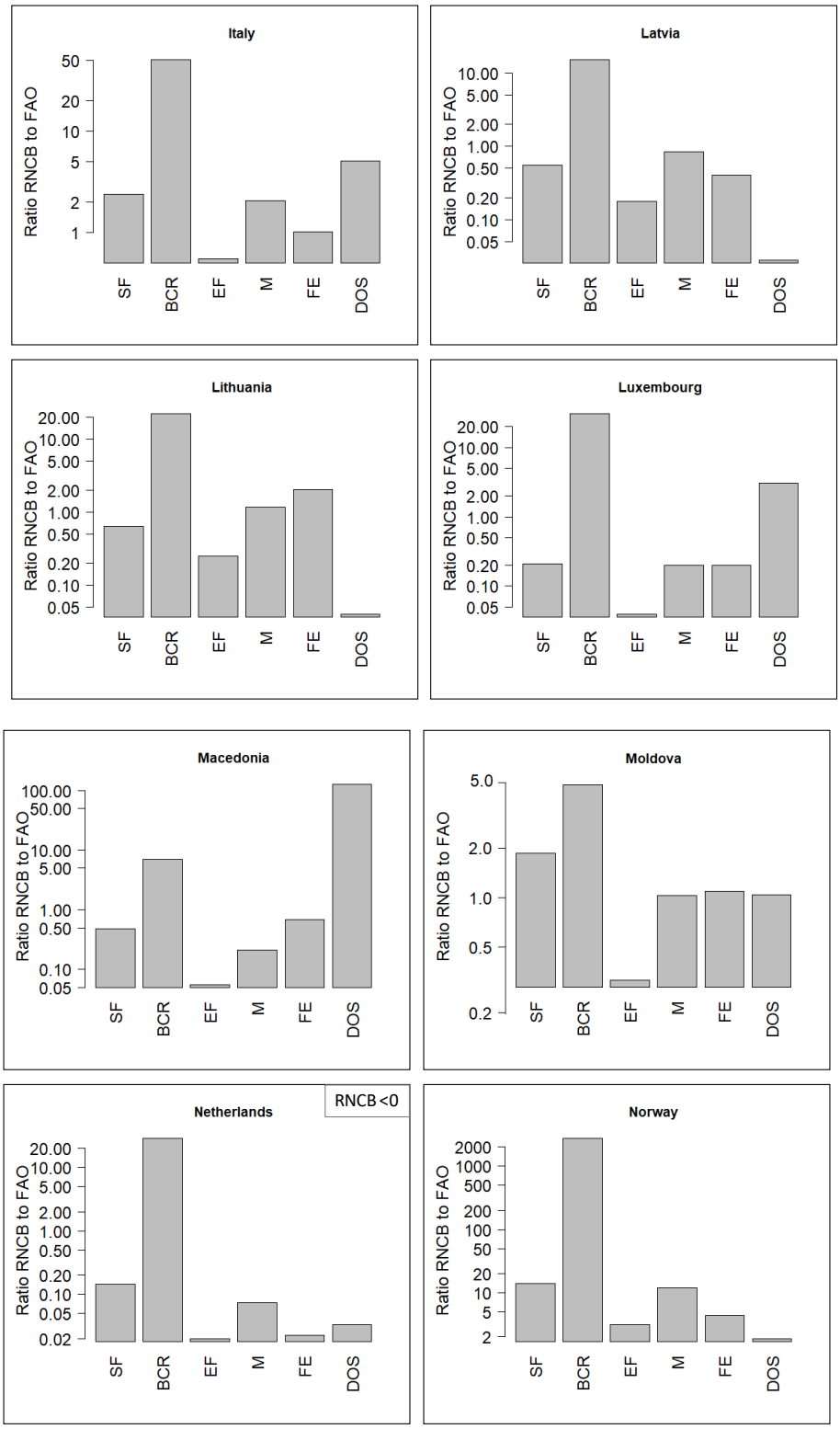
Italy
Ratio RNCB to FAO
50
20
10
5
2
1
SF
BCR
EF
M
FE
DOS
Latvia
Ratio RNCB to FAO
10.00
5.00
2.00
1.00
0.50
0.20
0.10
0.05
SF
BCR
EF
M
FE
DOS
Lithuania
Ratio RNCB to FAO
20.00
10.00
5.00
2.00
1.00
0.50
0.20
0.10
0.05
SF
BCR
EF
M
FE
DOS
Luxembourg
Ratio RNCB to FAO
20.00
10.00
5.00
2.00
1.00
0.50
0.20
0.10
0.05
SF
BCR
EF
M
FE
DOS
Macedonia
Ratio RNCB to FAO
100.00
50.00
10.00
5.00
1.00
0.50
0.10
0.05
SF
BCR
EF
M
FE
DOS
Moldova
Ratio RNCB to FAO
5.0
2.0
1.0
0.5
0.2
SF
BCR
EF
M
FE
DOS
Netherlands
RNCB <0
Ratio RNCB to FAO
20.00
10.00
5.00
2.00
1.00
0.50
0.20
0.10
0.05
0.02
SF
BCR
EF
M
FE
DOS
Norway
Ratio RNCB to FAO
2000
1000
500
200
100
50
20
10
5
2
SF
BCR
EF
M
FE
DOS

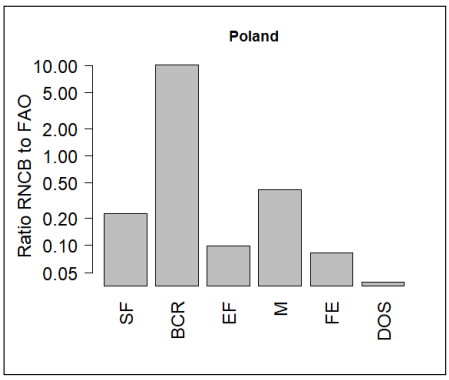
Poland
Ratio RNCB to FAO
10.00
5.00
2.00
1.00
0.50
0.20
0.10
0.05
SF
BCR
EF
M
FE
DOS

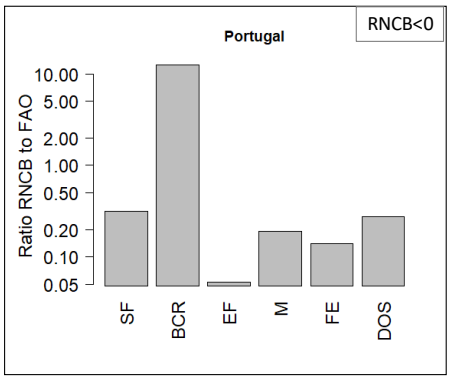
Portugal
RNCB<0
Ratio RNCB to FAO
10.00
5.00
2.00
1.00
0.50
0.20
0.10
0.05
SF
BCR
EF
M
FE
DOS

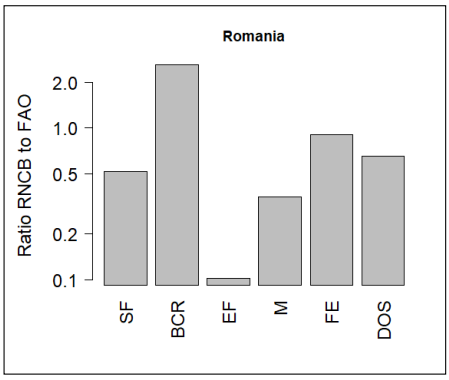
Romania
Ratio RNCB to FAO
2.0
1.0
0.5
0.2
0.1
SF
BCR
EF
M
FE
DOS

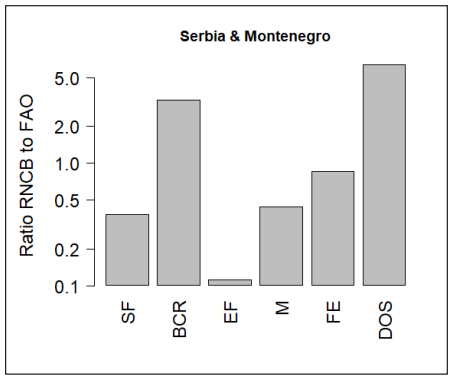
Serbia & Montenegro
Ratio RNCB to FAO
5.0
2.0
1.0
0.5
0.2
0.1
SF
BCR
EF
M
FE
DOS

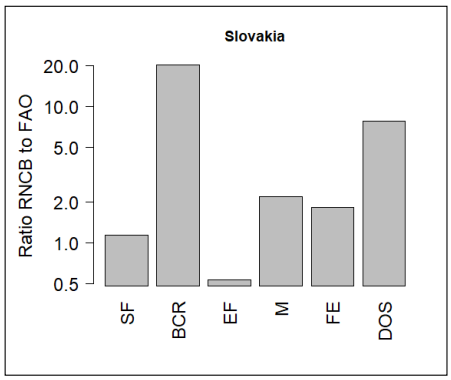
Slovakia
Ratio RNCB to FAO
20.0
10.0
5.0
2.0
1.0
0.5
SF
BCR
EF
M
FE
DOS

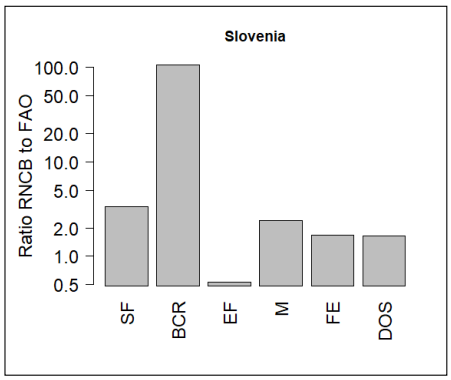
Slovenia
Ratio RNCB to FAO
100.0
50.0
20.0
10.0
5.0
2.0
1.0
0.5
SF
BCR
EF
M
FE
DOS

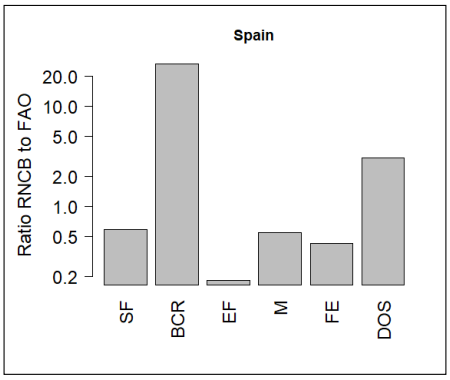
Spain
Ratio RNCB to FAO
20.0
10.0
5.0
2.0
1.0
0.5
0.2
SF
BCR
EF
M
FE
DOS

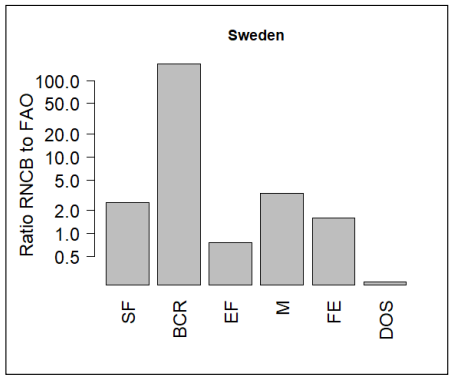
Sweden
Ratio RNCB to FAO
100.0
50.0
20.0
10.0
5.0
2.0
1.0
0.5
SF
BCR
EF
M
FE
DOS

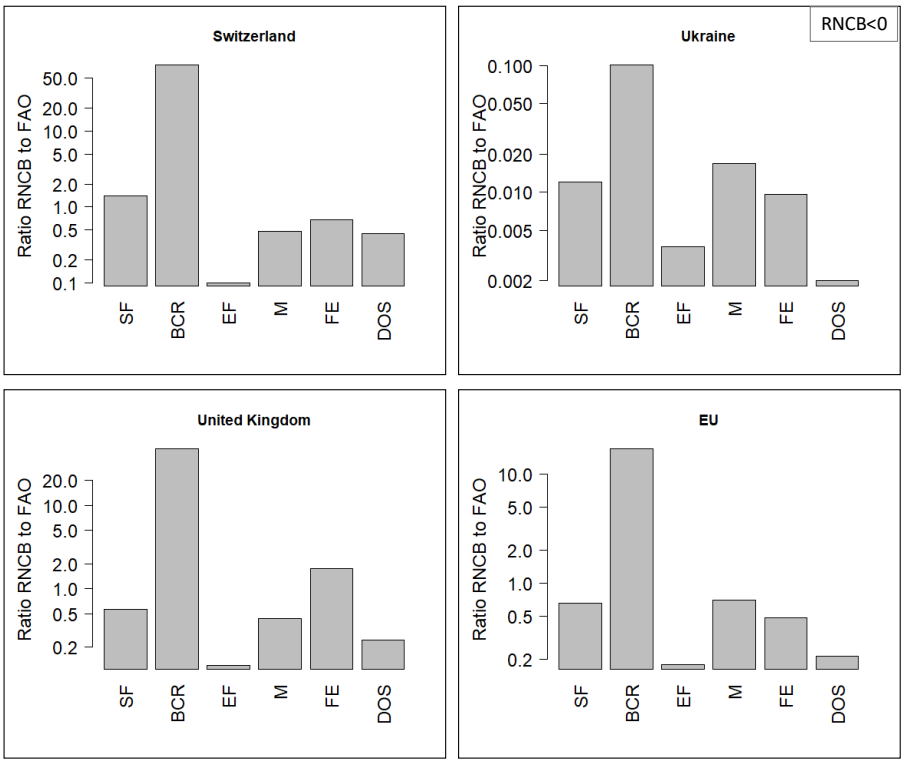

Figure S.4.1 *Ratio RNCB to the national emissions of synthetic fertilizer (SF), burning crop residue (BCR), enteric fermentation (EF), manure (M), on farm energy (FE) and drained organic soil (DOS) (%) for each EU country and the entire European region (countries where RNCB is negative is indicated in the figure).*

5 CONCLUSION AND PERSPECTIVE

5.1 SYNTHESIS

In my thesis, I applied three different approaches to improve our understanding of the role of rivers in the European C budget. In the first approach, the land surface model ORCHILEAK was used to estimate the DOC leaching from land to river at the European scale, its spatio-temporal variability, and its contribution to the terrestrial C budget. Using this model framework, I also quantified the DOC leaching for major climate zones in Europe, two potentially important drivers of the C fluxes at the terrestrial-aquatic system's interface. In the second approach, empirical work in the field and the laboratory was conducted to investigate the DOC degradation kinetics along the river network of the Meuse (FR-BE-NL). The Meuse is a typical example of a NW-European river basin with a mix of land-cover types ranging from near-natural forests to intensively used croplands. The objective of this empirical work was to explore the fate of terrestrial DOC in the river network and to investigate the potential impact of land cover on DOC lability. In this conclusion we investigate the extent to which these observational findings can be used to evaluate the simplified in-river DOC degradation scheme used in ORCHILEAK, and to discuss future improvements in model structure and parametrization. In the third approach, I re-assessed the inland water C budget for Europe based on recent literature data. Moreover, I went one step further and refined the analysis to quantify C losses to the aquatic system at national scale and fluvial transfers of C across country borders. This final study sets the foundation for including lateral C transfers through river networks into national C and greenhouse gas (GHG) budgets.

5.1.1 Chapter 2 : "Spatio-temporal patterns and drivers of terrestrial Dissolved Organic Carbon (DOC) leaching to the European river network."

5.1.1.1 Research questions

- *At the European scale, what quantities of DOC are leached for the soil to the river network and how does it vary in time and space?*

The LSM ORCHILEAK was applied and evaluated for the first time for Europe, defined in this thesis has the region comprised between 35°N and 70°N latitude and 10°W and 30°E longitude. According to my simulations from 1979-2012, it was found that on average 14.3 TgC yr^{-1} of DOC is leached from land to European rivers, which is about 0.6% of the terrestrial net primary production (NPP). Of the DOC leaching, on average 12.3 TgC yr^{-1} is exported to the coast via the river network, the rest being respired in transit. DOC leaching exhibits a large seasonal variability, with a maximum occurring in winter and a minimum in summer, except for the Northern most part of Europe where the maximum occurs in spring due to the snow melt. DOC leaching rate is generally lower in warm and dry regions, and higher in cold and wet regions of Europe.

- *What are the controlling factors of the spatio-temporal distribution of DOC leaching and how do they impact the leaching fluxes?*

The precipitation expressed by runoff and drainage and the temperature, both factors directly related to the climate region, were investigated. In order to evaluate only those factors, I normalized the DOC leaching by the NPP which is the indirect source of DOC in the soil. My results showed that DOC leaching to the river network is primarily controlled by the hydrology. While temperature has been discussed in the literature as an important control factor of SOC turnover rates, temperature only plays a secondary role in determining DOC leaching to the river network. Compared to other LSMs, ORCHILEAK represents SOC decomposition but also C losses through DOC leaching. Our results highlight that this leaching flux is mostly driven by surface runoff and by the drainage to surface runoff ratio, temperature having a less important role.

5.1.1.2 Model advantages and limitations

Land surface models such as ORCHILEAK allow us to work at regional and global scales with temporal variations, simulating the past as well as the future when applying different scenarios with defined forcing such as atmospheric CO_2, climate and land use change. Furthermore, the model I used, ORCHILEAK, has allowed me to connect the terrestrial C cycle with my thesis's subject, the aquatic C cycle. One of my major results is the significant spatio-temporal variability of DOC leaching from land to river at the European scale, result that would be difficult, if not impossible, to

achieve with only observations and field studies. The regional-scale control of the hydrological pathways (surface runoff versus deep drainage) on DOC leaching is another important finding that emerges from our simulations, a result that would not have been easily obtained from a few, local point measurements. Despite those advantages, models present some limitations. In fact, ORCHILEAK cannot represent all biogeochemical transformation processes of the C cycle in the water column of the inland water network (Lauerwald et al., 2017). As discussed in chapter 2, peatlands are not represented in the model, yet they cover a large part of the northern part of Europe (Scandinavia and Scotland). Previous research has proved that peatlands are an important part of the C cycle. One of the major next steps would be to merge ORCHILEAK with ORCHIDEE-PEAT, a new branch of the land surface model ORCHIDEE. This branch includes peatlands as an independent sub-grid hydrological soil unit in which peatland soils are characterized by a multilayered vertical water and carbon transport and peat-specific hydrological properties (Qiu et al., 2019). Since this model has been developed for the northern peatlands, it could be directly merged with our version of ORCHILEAK.

ORCHILEAK can also be improved with the implementation of lakes and reservoirs as important regulators of the inland water C cycle. It has been shown that dams have a direct impact on the C retention efficiency and the autotrophic production of C in the inland water river network (Maavara et al., 2017). The representation of methanogenesis and methane evasion could also be implemented. While it has been suggested that wetlands are a major source of methane and that this flux could increase significantly in the future due to climate change (Zhang et al., 2017), in Europe the representation of methane will likely not have a strong impact compared to tropical regions. So far, ORCHILEAK does not represent lateral transport of POC yet its role in the terrestrial C budget has been demonstrated (Zhang et al., 2018). Recently, POC transfers have been implemented in ORCHILEAK to form ORCHIDEE_C Lateral, and the model was then calibrated and evaluated for the Rhine catchment (Zhang et al., 2020). The effect of nutrient limitation on the C cycle is currently not taken into account in ORCHILEAK yet it has been demonstrated that the implementation of Nitrogen (N) and Phosphorus (P) could reduce the C uptake by the terrestrial sink (Goll et al., 2012) and significantly impact the inland water C cycle (e.g., Maranger et al., 2018). Only recently, Sun et al. (2021) applied and evaluated at the global scale a new version of ORCHIDEE that implements the couplings of the C, N and P first evaluated for tropical regions (Goll et al., 2017;2018) but regarding the ORCHILEAK model, such couplings remain to be done.

Finally, land-surface models are limited by their spatial resolution. For instance, the finest resolution achievable with ORCHILEAK is currently 0.5° because of the hydrology routing scheme. At this resolution, many fine scale features such as concentrations in headwater catchments or spatial heterogeneities induced by a complex topography are only very crudely represented, if at all (Lauerwald et al.,

2017). From a more technical point of view, LSMs cannot simulate processes at high spatio-temporal resolution for a large region for a long period. Therefore, even if LSMs will progressively be able to run at finer spatio-temporal resolution, the constrains imposed by the CPU times needed to carry large-scale simulations at the centennial scale will remain significant. Crucially, observations in the field and laboratory experiments will remain a priority for the calibration and validation of the outputs of process-based models such as ORCHILEAK.

5.1.2 Chapter 3: "Controlling factors of the degradation kinetics of dissolved organic carbon: An experimental study on the Meuse catchment"

5.1.2.1 Research questions

- *Do we observe any spatial or temporal patterns in DOC decay rate constants within the Meuse catchment?*

To answer that question, an experimental analysis covering several seasons was realized and decay rate constants were determined using three different methodologies. Calculated half-life times with the first order kinetic with a non-degradable pool method were found to be slightly lower than the estimated WRT for the Meuse river, ~24 days, with the exception of the late winter campaign. Furthermore, the September campaign presented surprisingly low half-life times. Consistent results were obtained with the reactive continuum with similar initial decay rate constants in June and November and high initial decay rate constants for September. In term of spatial variability between sampling locations and thus land cover, no trends were found, in fact the variability observed in decay rate constants were in the same order of magnitude than the variability observed between sample replicates.

- *How do the land use type, the seasons and the OM quality influence DOC decay rate constants in the river network?*

The results showed no trends between the different land cover types. A higher decay was observed in September. However there was a high variability of DOC decay rate constants between a sample and its duplicate and seasonality could not alone explain this variability. One possible explanation is that the OM quality influences in some way the degradation. The results for June and November showed an exponential relationship between the SUVA index and the initial decay rates determined by the RC method. Furthermore, for a catchment draining mainly croplands, initial decay rate constants decreased faster with increasing SUVA than for a catchment draining forests or grassland. In contrast, no clear correlation was found between the SUVA and the half-life times calculated with the two pools method.

- *How can we best represent DOC degradation in a model?*

Different methods for estimating the DOC decay rate constants were applied. We demonstrated that the first order kinetics is not able to capture well the temporal evolution of the DOC concentration. On the contrary, the first order kinetics with a refractory pool and the reactive continuum model were both valid methods to describe the DOC degradation in the river with R^2 superior to 0.8 for 70% of our samples. One advantage of the FOR method is that half-life times are directly comparable to WRT. The RC method provides another advantage, as the initial decay coefficients of the RC model were found to be correlated to the OM quality (measured with the SUVA index), a property that is easy and fast to measure in the laboratory. When modeling DOC degradation, we suggest to use either a multiple pools model or the reactive continuum model. In ORCHILEAK, DOC degradation is represented as a two pools model, one labile pool with a fast reactivity of 0.3 d^{-1} and one refractory with a slow reactivity of 0.01 d^{-1} (for a temperature of 28°C). My results in the Meuse show generally a slower decay constant of the labile pool, around one order of magnitude lower, but the decay rate constants from the Meuse were temperature corrected at 20°C, logically leading to lower values. Before decreasing the reactivity of the labile and refractory pools in ORCHILEAK, further work across other European catchments is needed to test whether the results for the Upper Meuse catchment could eventually be extrapolated to the entire EU domain. In order to implement the RC model, the two parameters (α and ν) should be estimated for different river basins in Europe but finding a suitable parameterization could prove difficult because at the scale of the Meuse, α and ν values are already quite disparate.

5.1.2.2 Advantages and limitations of empirical studies

Field observations and laboratory experiments, in addition to their essential role for calibrating and evaluating models, are the cornerstone of the scientific method. Unfortunately, observational studies present also limitations and my case study perfectly illustrates these limitations. First, sample representativeness can be challenging when analyzing streams and rivers. In my work, I have tried to partly circumvent this difficulty by collecting duplicate samples. This strategy has been useful in revealing the high heterogeneity of the medium under investigation, yet it has not allowed to provide robust results in the statistical sense. For the latter, more samples would have been required. Measurements in the laboratory rely on the instruments used, and in my case a calibration with control samples was needed to ensure accuracy and reliability in the measurements. For instance, one of the problem I faced was the difficulty to generate a control sample void of DOC contamination, the milli-Q water system being slightly contaminated. In addition to these technical issues related to sampling and laboratory work, field studies are also constrained by many logistical aspects such as climatic conditions or accessibility of sampling sites. This was the case during the September campaign when most of the sites could not be sampled due to very low river discharge. Last, but certainly not the least, field studies are comparatively much more expensive (in cost and human resources) than

modeling work, and these considerations often strongly limits the spatial and temporal extent of observations. Therefore, covering a large region during a long period of time at sufficiently high spatio-temporal resolution is generally challenging. In my case, performing monthly-scale kinetic experiments for a few (6-12) locations draining only a portion (about 1/3) of a medium-sized catchment and collected 4 times represented about 8 months of full-time work. In summary, process-based models and field studies present both advantages and limitations, but overall are highly complementary.

5.1.3 Chapter 4 : "Lateral carbon fluxes in Europe: quantification and implications for national carbon budgets."

- *How much is imported and exported through countries via the European river network?*

A new methodology has been developed to establish a fully closed inland water C budget at the country-scale for Europe, which includes the contributions from the imports and exports through the country boundaries. The European regions in this chapter corresponded to EU-27 plus Albania, Bosnia and Herzegovina, Croatia, Iceland, Kosovo, Macedonia, Norway, Serbia, Montenegro, United Kingdom and Switzerland. The different components of the inland water C budget were estimated through a mass balance approach based on literature data. We calculated, for the contemporary period, that on average over all of Europe, 8.1 ± 2.7 gC m^{-2} yr^{-1} is leached from the soil to the inland water network, 5.2 ± 2.3 gC m^{-2} yr^{-1} of CO_2 is emitted to the atmosphere and 0.8 ± 0.4 gC m^{-2} yr^{-1} is buried in the sediments. In terms of C fluxes between countries, on average 2.3 ± 7.5 gC m^{-2} yr^{-1} of carbon are imported from one country to another and 4.4 ± 7.6 gC m^{-2} yr^{-1} are exported either to the sea or to other countries. Most of the European countries export more carbon than they import with the exception of the Netherlands, Portugal, Estonia and Ukraine, which means that within the countries' borders, losses to the atmosphere and sediments are higher than the amount of terrestrial C mobilized into the river network. The methodology applied here at the European scale could be apply to other regions across the globe.

- *How important are the riverine carbon fluxes compared to the lateral carbon fluxes associated with wood and crop harvesting and to other components of the national greenhouse gas budgets such as direct anthropogenic emissions and land use change?*

The river net carbon balance (RNCB), which represents the net loss of C through river from one country to another, was compared to other components of the national GHG's budget. While overall anthropogenic emissions are generally much higher than the RNCB, I found that fluvial C transfers over country boarders are comparable to specific contributions of the budget such as synthetic fertilizer use, manure application and on farm energy use in many European countries. Moreover, the RNCB fluxes are found to be more important than, e.g., burning crop residue. Although this comparison can be used to highlight the extent to which inland water fluxes could eventually alter national C budget accountings, it should not be overinterpreted because the RNCB is not a GHG emission flux, nor is it a sole anthropogenic flux. In this context, the comparison is more straightforward with the other lateral C transfers through trade of carbon and wood products. I found that those are about one order of magnitude higher than the river fluxes, highlighting that in terms of lateral C exchange between countries, river C flows are not the dominant transport pathway in European catchments. Another interesting result is that for ten EU countries the RNCB and harvest trades are going in the same direction while for the remaining seventeen the lateral fluxes operate in opposite direction, the RNCB partly compensating the harvest trades.

- *Should lateral C flows through rivers also be accounted for in national C budget?*

My results showed that the RNCB can sometimes be a significant contributor to the lateral C fluxes and can even reach the same order of magnitude as other contributors of the C budget. If in general the RNCB was significantly smaller than the harvest fluxes for many countries, I also found several countries (Croatia, Finland and Slovakia) for which both fluxes reach the same order of magnitude. I anticipate that this conclusion could also hold outside of the EU, for countries that are crossed by large rivers such as the countries crossed by the Nile, the Niger or the Zambezi in Africa or the Mekong in Asia. Therefore, I recommend that the fluvial C transfers should also be implemented in national carbon accountings. However, in the classical budget accounting exercises at national level, countries are only accounting for the anthropogenic fraction of the C fluxes. In this chapter, there was no distinction between the natural and anthropogenic parts of the river C fluxes because we relied on datasets that only quantify the total fluxes. Future work should therefore focus on the decomposition of the natural and anthropogenic fraction of the fluvial C transfers. This can be achieved using a modelling approach such as the LSM ORCHILEAK as applied in chapter 2. ORCHILEAK would help to better constrain lateral C exchange through rivers across country boarders, as well as its seasonal, interannual and

decadal variability. Once DIC and POC transports are fully implemented in ORCHILEAK, the methodology used in chapter 4 to estimate a closed inland water C budget at the country-scale could then be applied based on the model results where natural and anthropogenic fluxes can be differentiated. The separation of natural C transport from the anthropogenic perturbation flux, will be of political relevance when evaluating how land and water management practices in one country might impact the C budget of the downstream country.

5.2 PERSPECTIVES

My work has answered several questions but has also opened new avenues for ongoing and future research. Recently, ORCHILEAK has been extended to study the evolution of the DOC and CO_2 evasion fluxes from European rivers during the historical period (1901-2014). The results highlight significant increase in DOC leaching fluxes (by 31%, figure 5.1a) and CO_2 evasion fluxes (by 30%) since the 1901-1910 period to the 2005-2014 period, as a combined result of climate change, atmospheric CO2 fertilization, and to a lesser extent, land-use change (Zhang et al., submitted). We note that the DOC leaching between 1980-2012 is higher than the one found in chapter two because the simulated domain is larger than in my work (figure 5.1b). These simulations therefore support the findings that the terrestrial-aquatic system's C cycle has already been significantly altered by human activities.

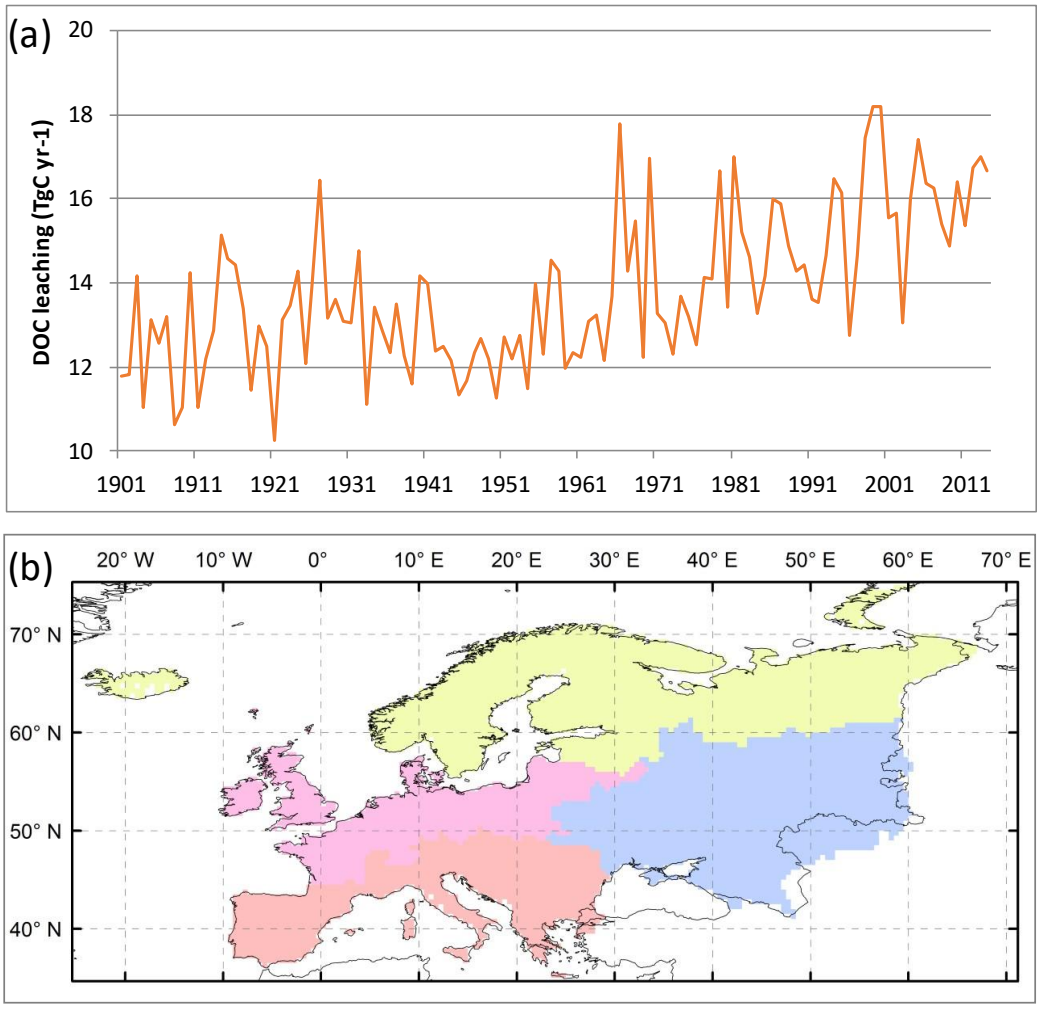

Figure 5.1 *(a) Historical evolution of the DOC leaching in European rivers from 1901 to 2014 (TgC yr^{-1}); (b) Simulated domain. From H. Zhang, pers. com.*

A next logical step would be to project these evolutions for the 21st century according to different socio-economic scenarios such as those building on the Representative Concentration Pathways (RCPs, Intergovernmental Panel on Climate Change (IPCC), Climate Change, 2013). Another logical direction is to continue to apply the model to other regions: So far ORCHILEAK was successfully applied to the two largest tropical catchments, the Amazon (Hastie et al., 2019; Lauerwald et al., 2017; 2020) and the Congo (Hastie et al., 2021), a modified version of ORCHILEAK was also applied to the Lena river in the Boreal/Arctic zone (Bowring et al., 2020) and my work has extended the applications to the continental scale of Europe. To complement regional studies, we suggest that North America, China and the Nile catchment could be priority areas, because of the presence large rivers that transport important quantities of C, with rivers such as the Mississippi-Missouri, the Mackenzie and the Saint-Laurent in Canada and the United States, and the Yangtze, the Heilong Jiang (the Amur) and the Yellow river in China, amongst others. Furthermore, like in Europe, North America and China are under the influence of a large variety of climate regions and a

heterogeneous anthropogenic pressure. Carrying simulations in these regions could help refine the results on DOC leaching from chapter 2. On the contrary, the Nile is mainly located in a arid climate zone for which ORCHILEAK has not yet been tested. The ultimate goal would of course be to run the model at global scale, which will require a model calibration step that allows to reach this goal. For example, the simulated river discharge could be calibrated using the GRDC database while the simulated riverine DOC fluxes could be evaluated against the GLORICH database (Hartman et al., 2009).

Following upon the work carried out in the third chapter, I recommend to collect more samples at the same location to achieve a more statistically robust treatment of the data. In this chapter, I also identified the possible role of a OM-rich micro-layer at the surface, which render the interpretation of the data difficult. I thus propose to develop a new sampling method based on a device that would open only when submerged. I also suggest pushing further the analysis of the DOM characterization. For instance, the excitation emission matrix fluorescence method allows to characterize more precisely the composition of the DOM (e.g. Koehler et al., 2012; Lambert et al., 2017; Hua et al., 2020).

More broadly, I recommend investigating the role of the water retention time on the DOC degradability as performed by, e.g., Catalan et al., 2016 in Spain and Soares et al., 2018 in Sweden. These authors found a negative relationship between the rate of organic carbon degradation and water retention time across systems (Fig 5.2), implying a decrease in organic carbon reactivity along the continuum of inland waters (Catalan et al., 2016). At the scale of the Meuse, I recommend to chose sampling locations for which the discharge is available and WRT could be derived, for instance in Belgium, several stations are monitored on a daily basis (http://aqualim.environnement.wallonie.be). Note that the span of WRTs values covered by such analyses in the Meuse (and in many other European rivers) would be significantly narrower than shown in Fig.5.2.

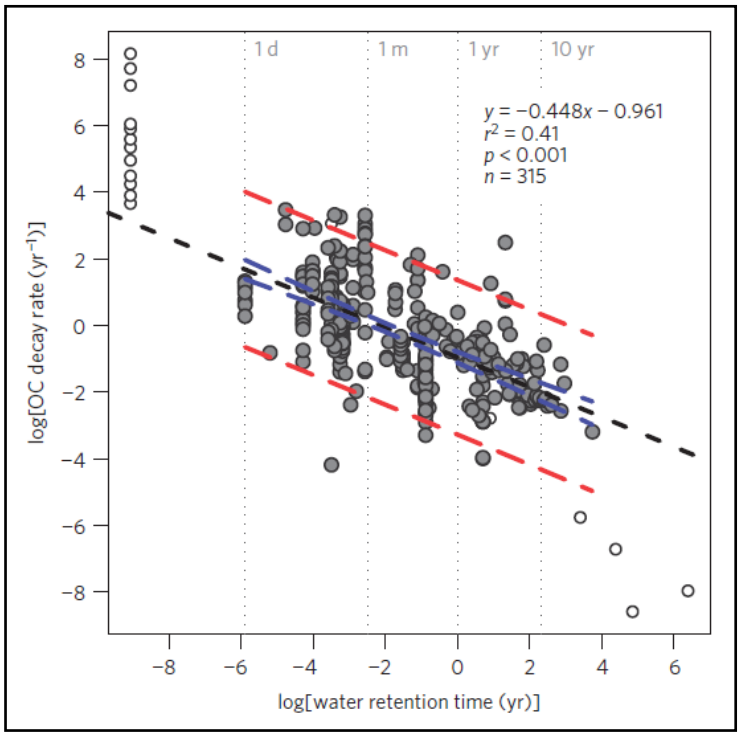

Figure 5.2 *Regression between the log-transformed water retention time (WRT) and decay rates of organic carbon (OC). The data set spans across a multitude of freshwater systems, including bioassays, field studies and several biomes. (Figure from Catalan et al., 2016)*

The inland water C budget from chapter four has allowed us to estimate how much C a country gains or losses through transfers via the river network. We have already identified the decomposition of the total river C fluxes into its natural and anthropogenic parts as the very top priority, a prerequisite before the inland water C cycle can be fully integrated into national C accountings. In this context, another important additional flux to focus on (in addition to lateral exchanges through the river network) would be the inland water C burial and the ecosystem service that freshwater ecosystems could play in sequestering anthropogenic C in their sedimentary reservoirs. In the meantime, our methodology could be extended to other regions of the globe or even at the global scale. Here, a central question would be to investigate the relative importance of lateral C fluxes through rivers in the regional C budgets as synthesized for instance by the Global Carbon Project in the framework of the REgional Carbon Cycle Assessment and Processes (RECCAP) initiative.

The results from chapter 3 could be used to improve the representation of DOC decay in ORCHILEAK, at least for the European river system. For that, a standard procedure should be established for the sampling, the laboratory set up and the methodology to calculate decay rate constants and then applied by European countries. This procedure would allow to obtain comparable results for decay rate constants across European rivers. The procedure could also be extended to DOC

decomposition in lakes and reservoirs in order to have a full representation of the DOC decay kinetics in inland waters. A European program could be installed in order to construct a common, comprehensive data repository on DOC concentrations and decay rates in the European river network, all following the same methodology. Concretely, figure 5.3 shows a selection of hotspots to investigate the DOC degradation kinetics further, with the aim to develop a network representative of European conditions. The idea would be to look first at regions where the population's density is not too high in order to minimize dircet anthropogenic perturbations such as those induced by sewage waters (figure 5.3a). Secondly, diverse land cover should be sampled. In the Meuse, I tried to isolate sub-catchments with specific land covers (a strategy partly resulting from the covid-pandemic), but it would be interesting to redo the analysis at larger scale, by investigating entire catchments with clear dominant land covers (boreal forest in Scandinavia, grassland in the west and north of the UK, temperate forests in the Iberia peninsula, figure 5.3b-c). Thirdly, different climate regions should also be investigated to cover the DOC dynamics in sub-arctic, wet continental, oceanic and semi-arid climates (figure 5.3d). Finally, I suggest that the catchments should also be selected where a wealth of data on DOC concentrations are already available, to maximize the exploitation of the kinetic experiments. For example, in chapter 2, DOC concentrations at the river mouth were compared to observations from literature (Abril et al., 2002, Mattsson et al., 2008). Worrall et al. (2004; 2012) compiled a comprehensive set of DOC concentration time series for the UK. Many studies have measured DOC concentrations in river and lakes (see chapter 3). Furthermore, several databases such as Glorich (figure 5.3e) and eau de France provide hydrochemical data, including DOC concentrations in rivers.

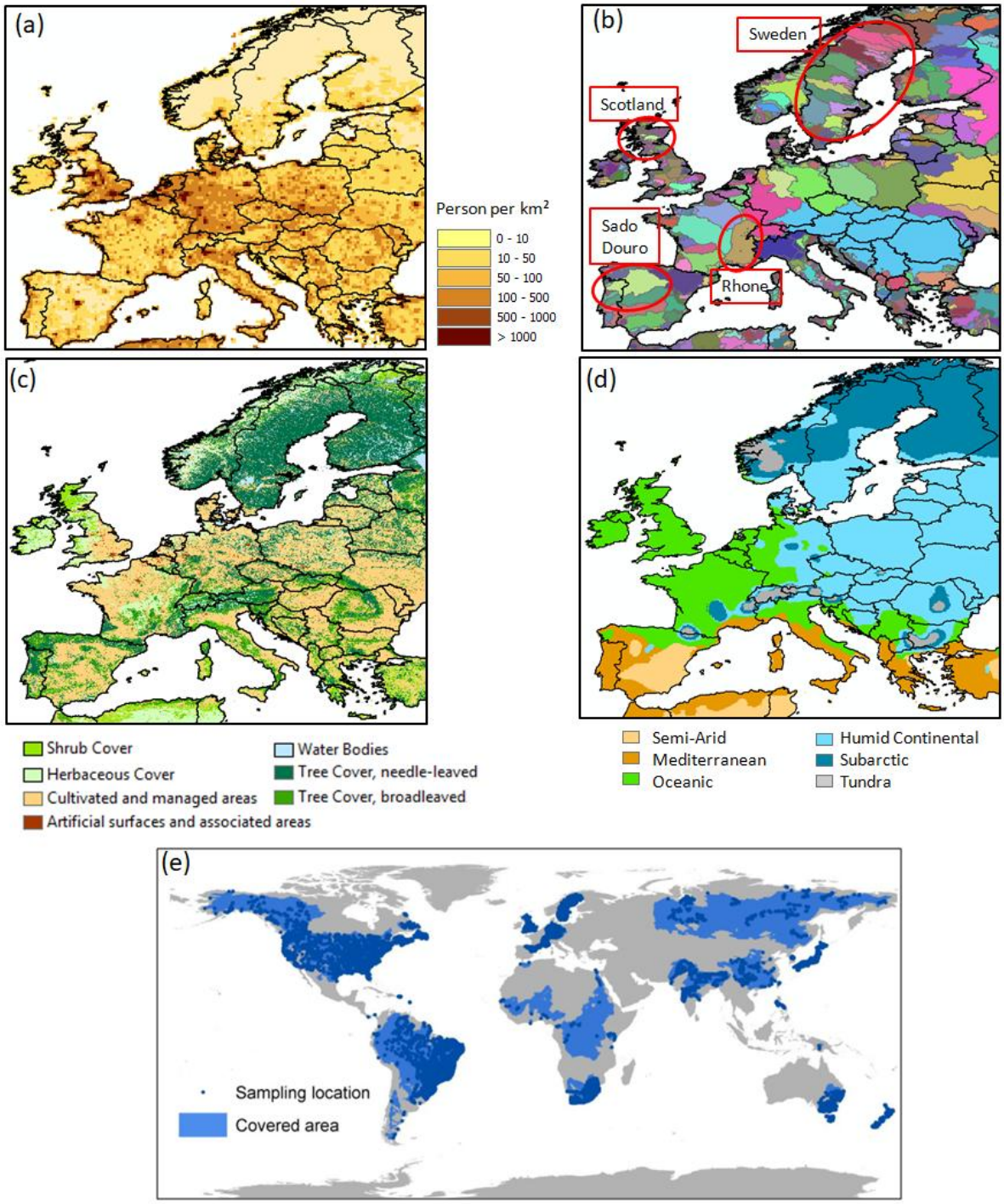

Figure 5.3 *(a) population density (person per km^{-2}) ; (b) delineation of European catchments; (c) dominant land cover types; (d) climatic regions according to the Koppen-Geiger classification (Peel et al., 2017); (e) Sampling locations and covered catchment areas of the monitoring stations included in GLORICH (figure from Hartmann et al., 2014).*

With all that in mind, several key locations can be selected (figure 5.3b). Catchments in Sweden, where riverine DOC concentrations are available for many of them, allow to cover the boreal forest biome and the humid continental and subarctic climates. River catchments in Scotland could also be investigated, as they are under the influence of an oceanic climate, are mostly draining shrub and herbaceous land covers and are represented in the Glorich database. For the semi-arid/arid and Mediterranean regions, the Sado and the Douro in Spain and Portugal could be key locations, these catchments being mainly covered by croplands in Spain and temperate forests in Portugal. The Rhône catchment could also be interesting because of the variety of climate zones crossed by the river and the influence of the Alps.

Eventually, those data could be used to evaluate simulations with an adequately upgraded version of ORCHILEAK, thereby improving the representation of DOC fluxes in the entire river network. The upgraded version of ORCHILEAK could be the perfect tool to integrate fluvial C fluxes into national inventories because it can separate the natural flux from the anthropogenic ones and furthermore it can help to understand how those fluxes will response to climate and environmental change.

6 BIBLIOGRAPHY

Abril G., M. Nogueira, H. Etcheber, G. Cabeçadas, E. Lemaire, M. Brogueira. Behaviour of organic carbon in nine contrasting European estuaries Estuar. Coast. Shelf Sci., 54 (2002), pp. 241-262

Arndt, S. et al. Quantifying the degradation of organic matter in marine sediments: a review and synthesis. Earth Sci. Rev. 123, 53–86 (2013)

Attermeyer, K., Catalán, N., Einarsdottir, K., Freixa, A., Groeneveld, M., Hawkes, J. A., … Tranvik, L. J. (2018). Organic carbon processing during transport through boreal inland waters: Particles as important sites. Journal of Geophysical Research-Biogeosciences, 123(8), 2412–2428.

Avitabile, V., Camia, A., 2018. An assessment of forest biomass maps in Europe using harmonized national statistics and inventory plots. For. Ecol. Manage. 409, 489–498.

Barrett, D. J.: Steady state turnover time of carbon in the Australian terrestrial biosphere, Global Biogeochem. Cy., 16., https://doi.org/10.1029/2002GB001860, 2002.

Bastviken, D., L. Persson, G. Odham, and L. Tranvik (2004), Degradation of dissolved organic matter in oxic and anoxic lake water, Limnol. Oceanogr., 49,109–116, doi:10.4319/lo.2004.49.1.0109

Battin TJ, Luyssaert S, Kaplan LA, Aufdenkampe AK, Richter A, Tranvik LJ (2009) The boundless carbon cycle. Nature Geoscience, 2, 598–600.

Bauer, J. E., W.-J. Cai, P. A. Raymond, T. S. Bianchi, C. S. Hopkinson, and P. A. G. Regnier (2013), The changing carbon cycle of the coastal ocean, Nature, 504(7478), 61–70, doi:10.1038/nature12857.

Berggren, M., Laudon, H., Jonsson, A. & Jansson, M. Nutrient constraints on metabolism affect the temperature regulation of aquatic bacterial growth efficiency. Microb. Ecol. 60, 894–902 (2010).

Berggren, M. Al-Kharusi, E.S. Decreasing organic carbon bioreactivity in European rivers. Freshw. Biol., 65 (6) (2020), pp. 1128-1138, 10.1111/fwb.v65.610.1111/fwb.13498.

Berner, R. A. (1964), An idealized model of dissolved sulfate distribution in recent sediments, Geochim. Cosmochim. Acta, 28(9), 1497–1503, doi:10.1016/0016-7037(64)90164-4.

Beusen, A. H. W., A. L. M. Dekkers, A. F. Bouwman, W. Ludwig, and J. Harrison (2005), Estimation of global river transport of sediments and associated particulate C, N, and

P, Global Biogeochem. Cycles, 19, GB4S05, doi:10.1029/2005GB002453.

Bloom, Anthony; Williams, Mathew. (2015). CARDAMOM 2001-2010 global carbon Model-Data Fusion (MDF) analysis, 2001-2010 [dataset]. University of Edinburgh. School of GeoSciences. https://doi.org/10.7488/ds/316.

Boudreau, B. P., and B. R. Ruddick (1991), On a reactive continuum representation of organic matter diagenesis, Am. J. Sci., 291(5), 507–538, doi:10.2475/ajs.292.1.79.

Bowring, S. P. K., Lauerwald, R., Guenet, B., Zhu, D., Guimberteau, M., Regnier, P., Tootchi, A., Ducharne, A., and Ciais, P.: ORCHIDEE MICT-LEAK (r5459), a global model for the production, transport, and transformation of dissolved organic carbon from Arctic permafrost regions – Part 2: Model evaluation over the Lena River basin, Geosci. Model Dev., 13, 507–520, https://doi.org/10.5194/gmd-13-507-2020, 2020.

Bowring, S. P. K., Lauerwald, R., Guenet, B., Zhu, D., Guimberteau, M., Tootchi, A., Ducharne, A., and Ciais, P (2019): ORCHIDEE MICT-LEAK (r5459), a global model for the production, transport, and transformation of dissolved organic carbon from Arctic permafrost regions – Part 1: Rationale, model description, and simulation protocol, Geosci. Model Dev., 12, 3503–3521, https://doi.org/10.5194/gmd-12-3503-2019, 2019.

Brye KR, Norman JM, Bundy LG, Gower ST (2001) Nitrogen and carbon leaching in agroecosystems and their role in denitrification potential. Journal of Environmental Quality, 30, 58–70.

Camino-Serrano, M., Gielen, B., Luyssaert, S., Ciais, P., Vicca, S., Guenet, B., Vos, B. De, Cools, N., Ahrens, B., Altaf Arain, M., Borken, W., Clarke, N., Clarkson, B., Cummins, T., Don, A., Pannatier, E. G., Laudon, H., Moore, T., Niemi- nen, T. M., Nilsson, M. B., Peichl, M., Schwendenmann, L., Siemens, J., and Janssens, I.: Linking variability in soil so- lution dissolved organic carbon to climate, soil type, and vegetation type, Global Biogeochem. Cy., 28, GB004726, https://doi.org/10.1002/2013gb004726, 2014.

Camino-Serrano, M., Guenet, B., Luyssaert, S., Ciais, P., Bastrikov, V., De Vos, B., Gielen, B., Gleixner, G., Jornet-Puig, A., Kaiser, K., Kothawala, D., Lauerwald, R., Peñuelas, J., Schrumpf, M., Vicca, S., Vuichard, N., Walmsley, D., and Janssens, I. A.: ORCHIDEE-SOM: modeling soil organic carbon (SOC) and dissolved organic carbon (DOC) dynamics along vertical soil profiles in Europe, Geosci. Model Dev., 11, 937–957, https://doi.org/10.5194/gmd-11-937-2018, 2018.

Campoy, A., Ducharne, A., Cheruy, F., Hourdin, F., Polcher, J., and Dupont, J. C.: Response of land surface fluxes and precipitation to different soil bottom hydrological conditions in a general circulation model, J. Geophys. Res.-Atmos., 118, 10725–10739, https://doi.org/10.1002/Jgrd.50627, 2013.

Carvalhais, N., Forkel, M., Khomik, M. et al. Global covariation of carbon turnover

times with climate in terrestrial ecosystems. Nature 514, 213–217 (2014). https://doi.org/10.1038/nature13731

Catalán, N., B. Obrador, M. Felip, and J. L. Pretus (2013), Higher reactivity of allochthonous vs. autochthonous DOC sources in a shallow lake, Aquat. Sci., 75(4), 581–593.

Catalán, N., J. P. Casas-Ruiz, D. von Schiller, L. Proia, B. Obrador, E. Zwirnmann, and R. Marcé (2017), Biodegradation kinetics of dissolved organic matter chromatographic fractions in an intermittent river, J. Geophys. Res. Biogeosci., 122, 131–144, doi:10.1002/2016JG003512.

Catalan, N., Marce, R., Kothawala, D. N., & Tranvik, L. J. (2016). Organic carbon decomposition rates controlled by water retention time across inland waters. Nature Geoscience, 9(7), 501–504. https://doi. org/10.1038/ngeo2720

Ciais P, Borges AV, Abril G, Meybeck M, Folberth G, Hauglustaine D, Janssens IA (2008) The impact of lateral carbon fluxes on the European carbon balance. Biogeosciences, 5, 1259–1271.

Ciais, P., Bousquet, P. Freibauer, A., and Naegler, T.: On the horizontal displacement of carbon associated to agriculture and how it impacts atmospheric CO2 gradients, Global Biogeochem. Cy., 21, GB2014, doi:10.1029/2006GB002741, 2007.

Ciais, P., et al. (2013), Carbon and other biogeochemical cycles, in Climate Change 2013: The Physical Science Basis. Contribution of Working Group I to the Fifth Assessment Report of the Intergovernmental Panel on Climate Change, edited by T. F. Stocker et al., Cambridge Univ. Press, Cambridge, U. K., and New York.

Ciais, P., Sabine, C., Bala, G., Bopp, L., Brovkin, V., Canadell, J., Chhabra, A., DeFries, R., Galloway, J., Heimann, M., Jones, C., Le Quéré, C., Myneni, R. B., Piao, S., Thornton, P., Willem, J., Friedlingstein, P., and Munhoven, G.: Carbon and Other Biogeochemical Cycles, in Climate Change 2013: The Physical Science Basis, Contribution of Working Group I to the Fifth Assessment Report of the Intergovernmental Panel on Climate Change, edited by: Intergovernmental Panel on Climate Change, Cambridge University Press, Cambridge, UK, 465–570, 2013.

Ciais, P., Sabine, C., Bala, G., Bopp, L., Brovkin, V., Canadell, J., Chhabra, A., DeFries, R., Galloway, J., Heimann, M., Jones, C., Le Quéré, C., Myneni, R. B., Piao, S., Thornton, P., Willem, J., Friedlingstein, P., and Munhoven, G.: Carbon and Other Biogeochemical Cycles, in Climate Change 2013: The Physical Science Basis, Contribution of Working Group I to the Fifth Assessment Report of the Intergovernmental Panel on Climate Change, edited by: Intergovernmental Panel on Climate Change, Cambridge University Press, Cambridge, UK, 465–570, 2013.

Cole, J.J., Prairie, Y.T., Caraco, N.F., McDowell, W.H., Tranvik, L.J., Striegl, R.G., Duarte,

C.M., Kortelainen, P., Downing, J.A., Middelburg, J.J., Melack, J., 2007. Plumbing the global carbon cycle: integrating inland waters into the terrestrial carbon budget. Ecosystems 10 (1), 171–184.

Cory, R. M. & Kaplan, L. a. Biological lability of streamwater fluorescent dissolved organic matter. Limnol. Oceanogr. 57, 1347–1360 (2012).

de Rosnay, P., Polcher, J., Bruen, M., and Laval, K.: Im- pact of a physically based soil water flow and soil- plant interaction representation for modeling large-scale land surface processes, J. Geophys. Res.-Atmos., 107, 4118, https://doi.org/10.1029/2001JD000634, 2002.

De Wit M.J.M. et al., 2007. Impact of climate change on low-flows in the river Meuse. Clim. Change, 82, 351- 372

Degens, E. T., Kempe, S. & Richey, J. E. 1991 Biogeochemistry of major world rivers, summary. In Biogeochemistry of Major World Rivers (Degens, E. T., Kempe, S. & Richey, J. E., eds). SCOPE 42. J. Wiley and Sons, New York, pp. 323–347.

Del Giorgio, P. A. & Pace, M. L. Relative independence of organic carbon transport and processing in a large temperate river: The Hudson River as both pipe and reactor. Limnol. Oceanogr. 53, 185–197 (2008).

Del Giorgio, P. A., and J. Davis (2003), Patterns in dissolved organic matter lability and consumption across aquatic ecosystems, in Aquatic Ecosystems—Interactivity of dissolved organic matter, edited by S. E. G. Findlay and R. L. Sinsabaugh, pp. 399–424, Academic, San Diego, Calif

Delpla I, Baures E, Jung AV, Thomas O. Impacts of rainfall events on runoff water quality in an agricultural environment in temperate areas. Sci Total Environ 2011;409(9): 1683–8. https://doi.org/10.1016/j.scitotenv.2011.01.033

Dlugokencky, E. and Tans, P.: Trends in atmospheric carbon dioxide, National Oceanic and Atmospheric Administration, Earth System Research Laboratory (NOAA/ESRL), available at: http://www.esrl.noaa.gov/gmd/ccgg/trends/global.html, last access: 16 November 2020.

d'Orgeval, T., Polcher, J., & de Rosnay, P. (2008). Sensitivity of the West African hydrological cycle in ORCHIDEE to infiltration processes. Hydrology and Earth System Sciences, 12, 1387– 1401. https://doi.org/10.5194/hess-12-1387-2008

Drake, T. W., P. A. Raymond, and R. G. M. Spencer. 2018. Terrestrial carbon inputs to inland waters: a current synthesis of estimates and uncertainty. Limnology and Oceanography Letters 3:132–142. http://doi.org/10.1002/lol2.10055

Ducharne, A.: Importance of stream temperature to climate change impact on water

quality, Hydrol. Earth Syst. Sci., 12, 797–810, https://doi.org/10.5194/hess-12-797-2008, 2008.

European Environment Agency https://www.eea.europa.eu

Fabris, R., Chow, C.W.K., Drikas, M., Eikebrokk, B., 2008. Comparison of NOM character in selected Australian and Norwegian drinking waters. Water Res. 42, 4188–4196.

FAO, 2021. FAOSTAT Climate Change, Emissions, Emissions Totals, http://www.fao.org/faostat/en/#data/GT

FAO/IIASA/ISRIC/ISS-CAS/JRC, 2012. Harmonized World Soil Database (version 1.2). FAO, Rome, Italy and IIASA, Laxenburg, Austria.

Farjalla VF, Marinho CC, Faria BM, Amado AM, Esteves FA, Bozelli RL, Giroldo D (2009) Synergy of fresh and accumulated organic matter to bacterial growth. Microb Ecol 57(4):657–666. doi: 10.1007/s00248-008-9466-8

Fonte ES, Amado AM, Meirelles-Pereira F, Esteves FA, Rosado AS, Farjalla VF (2013) The combination of different carbon sources enhances bacterial growth efficiency in aquatic ecosystems. Microb Ecol 66(4):871–878. doi:10.1007/s00248-013-0277-1

Fransner F, Nycander J, Mörth C-M et al (2016) Tracing terrestrial DOC in the Baltic Sea—a 3-D model study. Global Biogeochem Cycle 30:134–148. doi:10.1002/2014GB005078

Friedlingstein, P., O'Sullivan, M., Jones, M. W., Andrew, R. M., Hauck, J., Olsen, A., Peters, G. P., Peters, W., Pongratz, J., Sitch, S., Le Quéré, C., Canadell, J. G., Ciais, P., Jackson, R. B., Alin, S., Aragão, L. E. O. C., Arneth, A., Arora, V., Bates, N. R., Becker, M., Benoit-Cattin, A., Bittig, H. C., Bopp, L., Bultan, S., Chandra, N., Chevallier, F., Chini, L. P., Evans, W., Florentie, L., Forster, P. M., Gasser, T., Gehlen, M., Gilfillan, D., Gkritzalis, T., Gregor, L., Gruber, N., Harris, I., Hartung, K., Haverd, V., Houghton, R. A., Ilyina, T., Jain, A. K., Joetzjer, E., Kadono, K., Kato, E., Kitidis, V., Korsbakken, J. I., Landschützer, P., Lefèvre, N., Lenton, A., Lienert, S., Liu, Z., Lombardozzi, D., Marland, G., Metzl, N., Munro, D. R., Nabel, J. E. M. S., Nakaoka, S.-I., Niwa, Y., O'Brien, K., Ono, T., Palmer, P. I., Pierrot, D., Poulter, B., Resplandy, L., Robertson, E., Rödenbeck, C., Schwinger, J., Séférian, R., Skjelvan, I., Smith, A. J. P., Sutton, A. J., Tanhua, T., Tans, P. P., Tian, H., Tilbrook, B., van der Werf, G., Vuichard, N., Walker, A. P., Wanninkhof, R., Watson, A. J., Willis, D., Wiltshire, A. J., Yuan, W., Yue, X., and Zaehle, S.: Global Carbon Budget 2020, Earth Syst. Sci. Data, 12, 3269–3340, https://doi.org/10.5194/essd-12-3269-2020, 2020.

Gaillardet, J., B. Dupré, P. Louvat, and C. J. Allègre. 1999. Global silicate weathering and CO2 consumption rates deduced from the chemistry of large rivers. Chem. Geol. 159: 3–30. doi:10.1016/S0009-2541(99)00031-5

Garrels R.M. et Mackenzie F.T. (1971) — Evolution of sedimentary rocks. W.W. Norton, New-York, 397 p.

Gielen, B., Neirynck, J., Luyssaert, S., and Janssens, I. A.: The importance of dissolved organic carbon fluxes for the carbon balance of a temperate Scots pine forest, Agr. Forest Meteorol.,151, 270–278, https://doi.org/10.1016/j.agrformet.2010.10.012,2011.

Goll, D. S., Brovkin, V., Parida, B. R., Reick, C. H., Kattge, J., Reich, P. B., van Bodegom, P. M., and Niinemets, Ü.: Nutrient limitation reduces land carbon uptake in simulations with a model of combined carbon, nitrogen and phosphorus cycling, Biogeosciences, 9, 3547–3569, https://doi.org/10.5194/bg-9-3547-2012, 2012.

Goll, D. S., Joetzjer, E., Huang, M., and Ciais, P.: Low phosphorus availability decreases susceptibility of tropical primary productivity to droughts, Geophys. Res. Lett., 45, 8231–8240, https://doi.org/10.1029/2018GL077736, 2018. Qiu, C., Zhu, D., Ciais, P., Guenet, B., Peng, S., Krinner, G., Tootchi, A., Ducharne, A., and Hastie, A.: Modelling northern peatland area and carbon dynamics since the Holocene with the ORCHIDEE-PEAT land surface model (SVN r5488), Geosci. Model Dev., 12, 2961–2982, https://doi.org/10.5194/gmd-12-2961-2019, 2019

Goll, D. S., Vuichard, N., Maignan, F., Jornet-Puig, A., Sardans, J., Violette, A., Peng, S., Sun, Y., Kvakic, M., Guimberteau, M., Guenet, B., Zaehle, S., Penuelas, J., Janssens, I., and Ciais, P.: A representation of the phosphorus cycle for ORCHIDEE (revision 4520), Geosci. Model Dev., 10, 3745–3770, https://doi.org/10.5194/gmd-10-3745-2017, 2017.

Goudriaan J, Groot JJR, Uithol PWJ (2001) Productivity of agro-ecosys- tems. In: Terrestrial Global Productivity (eds Roy J, Saugier B, Mooney HA), pp. 303–314. Academic Press, San Diego.

Grabs, Thomas, et al. "Riparian zone hydrology and soil water total organic carbon (TOC): implications for spatial variability and upscaling of lateral riparian TOC exports." Biogeosciences 9.10 (2012): 3901-3916.

Griffith, David R., Rebecca T. Barnes, and Peter A. Raymond. "Inputs of fossil carbon from wastewater treatment plants to US rivers and oceans." Environmental Science & Technology 43.15 (2009): 5647-5651.

Guillemette, F., and P. A. del Giorgio (2011), Reconstructing the various facets of dissolved organic carbon bioavailability in freshwater ecosystems, Limnol. Oceanogr., 56(2), 734–748, doi:10.4319/lo.2011.56.2.0734.

Guillemette, F., and P. A. del Giorgio (2012), Simultaneous consumption and production of fluorescent dissolved organic matter by lake bacterioplankton, Environ. Microbiol., 14(6), 1432–1443, doi:10.1111/j.1462-2920.2012.02728.x.

Guimberteau, M., Drapeau, G., Ronchail, J., Sultan, B., Polcher, J., Martinez, J.-M., Prigent, C., Guyot, J.-L., Cochonneau, G., Es- pinoza, J. C., Filizola, N., Fraizy, P., Lavado, W., De Oliveira, E., Pombosa, R., Noriega, L., and Vauchel, P.: Discharge sim- ulation in the sub-basins of the Amazon using ORCHIDEE forced by new datasets, Hydrol. Earth Syst. Sci., 16, 911–935, https://doi.org/10.5194/hess-16-911-2012, 2012.

Guimberteau, M., Zhu, D., Maignan, F., Huang,Y.,Yue, C., Dantec- Nédélec, S., Ottlé, C., Jornet-Puig, A., Bastos, A., Laurent, P., Goll, D., Bowring, S., Chang, J., Guenet, B., Tifafi, M., Peng, S., Krinner, G., Ducharne, A., Wang, F., Wang, T., Wang, X., Wang, Y., Yin, Z., Lauerwald, R., Joetzjer, E., Qiu, C., Kim, H., and Ciais, P.: ORCHIDEE-MICT (v8.4.1), a land surface model for the high latitudes: model description and validation, Geosci. Model Dev., 11, 121–163, https://doi.org/10.5194/gmd-11-121- 2018, 2018.

Gurria Albusac P, Ronzon T, Tamosiunas S, Lopez Lozano R, Garcia Condado S, Guillen Garcia J, Cazzaniga N, Jonsson K, Banja M, Fiore G, Camia A and M`barek R. Biomass flows in the European Union The Sankey biomass diagram – towards a cross-set integration of biomass . EUR 28565 EN. Luxembourg (Luxembourg): Publications Office of the European Union; 2017. JRC106502

Harrison, J. A., Caraco, N., & Seitzinger, S. P. (2005). Global patterns and sources of dissolved organic matter export to the coastal zone: Results from a spatially explicit, global model. Global Biogeochemical Cycles, 19, GB4S04. https://doi.org/10.1029/2005GB002480

Harrison, J. A., Caraco, N., & Seitzinger, S. P. (2005). Global patterns and sources of dissolved organic matter export to the coastal zone: Results from a spatially explicit, global model. Global Biogeochemical Cycles, 19, GB4S04. https://doi.org/10.1029/2005GB002480

Hartley A., Pekel J-F., Ledwith M., Champeaux J-L., Badts E.De, and Bartalev S.A.. GLC2000 database, European Commision Joint Research Centre, 2006.

Hartmann, J et al. (2014): A Brief Overview of the GLObal RIver Chemistry Database, GLORICH. Procedia Earth and Planetary Science, 10, 23-27, https://doi.org/10.1016/j.proeps.2014.08.005

Hartmann, J., Jansen, N., Dürr, H. H., Kempe, S., and Köhler, P.: Global co2-consumption by chemical weathering: What is the contribution of highly active weathering regions?, Glob. Planet. Change, 69, 185-194, 2009.

Hastie, A., Lauerwald, R., Ciais, P., Papa, F., and Regnier, P.: Historical and future contributions of inland waters to the Congo basin carbon balance, Earth Syst. Dynam. Discuss., https://doi.org/10.5194/esd-2020-3, , 2021.

Hastie, A., Lauerwald, R., Ciais, P., Regnier, P (2019). Aquatic carbon fluxes dampen the overall variation of net ecosystem productivity in the Amazon basin: An analysis of

the interannual variability in the boundless carbon cycle. Global Change Biology,; 25: 2094– 2111. https://doi.org/10.1111/gcb.14620

Hastie, A., Lauerwald, R., Weyhenmeyer, G., Sobek, S., Verpoorter, C., & Regnier, P. (2018). CO2 evasion from boreal lakes: revised estimate, drivers of spatial variability, and future projections. Global Change Biology. https://doi.org/10.1111/gcb.13902

Holgerson, M. A. & Raymond, P. A. Large 628 contribution to inland water CO2 and CH4 emissions from very small ponds. Nature Geosci. 9 (3), 222–226 (2016).

Hopkinson CS, Vallino JJ, Nolin A (2002) Decomposition of dissolved organic matter from the continental margin. Deep Sea Res II 49:4461–4478

Hotchkiss ER, Hall RO, Baker MA, Rosi-Marshall EJ, Tank JL (2014) Modeling priming effects on microbial consumption of dissolved organic carbon in rivers. J Geophys Res Biogeosci 119:982–995. https://doi.org/10.1002/2013jg002599

Hua, G., Reckhow, D.A., Abusallout, I., 2015. Correlation between SUVA and DBP formation during chlorination and chloramination of NOM fractions from different sources. Chemosphere 130, 82–89.

Hua, L.-C., Chao, S.-J., Huang, K., Huang, C., 2020. Characteristics of low and high SUVA precursors: relationships among molecular weight, fluorescence, and chemical composition with DBP formation. Sci. Total Environ. 727, 138638. https://doi.org/10.1016/j.scitotenv.2020.138638

Humbert, G., Parr, T.B., Jeanneau, L. et al. Agricultural Practices and Hydrologic Conditions Shape the Temporal Pattern of Soil and Stream Water Dissolved Organic Matter. Ecosystems 23, 1325–1343 (2020). https://doi.org/10.1007/s10021-019-00471-w

Hyacinthe, Christelle, Steeve Bonneville, and Philippe Van Cappellen. "Reactive iron (III) in sediments: chemical versus microbial extractions." Geochimica et cosmochimica acta 70.16 (2006): 4166-4180.

Idir, S., A.Probst, D.Viville, and J. L.Probst (1999), Contribution of saturated areas and hillslopes to the water and element fluxes exported during a storm event: Tracing with dissolved organic carbon and silica. The Strengbach catchment case study (Vosges, France), C. R. Acad. Sci., Ser. II, 328(2), 89– 96, doi:10.1016/s1251-8050(99)80003-2.

Inamdar, Shreeram P., and Myron J. Mitchell. "Hydrologic and topographic controls on storm-event exports of dissolved organic carbon (DOC) and nitrate across catchment scales." Water Resources Research 42.3 (2006).

IPCC, 2021: Climate Change 2021: The Physical Science Basis. Contribution of Working Group I to the Sixth Assessment Report of the Intergovernmental Panel on Climate Change [Masson-Delmotte, V., P. Zhai, A. Pirani, S. L. Connors, C. Péan, S. Berger, N. Caud, Y. Chen, L. Goldfarb, M. I. Gomis, M. Huang, K. Leitzell, E. Lonnoy, J. B. R. Matthews, T. K. Maycock, T. Waterfield, O. Yelekçi, R. Yu and B. Zhou (eds.)]. Cambridge University Press. In Press

Jaffe, R., D. Mcknight, N. Maie, R. Cory, W. H. Mcdowell, and J. L. Campbell. 2008. Spatial and temporal variations in DOM composition in ecosystems: The importance of long-term monitoring of optical properties. J. Geophys. Res. Biogeosci. 113: G04032. http://dx.doi.org/10.1029/2008JG000683

James, Gareth; Witten, Daniela; Hastie, Trevor; Tibshirani, Robert (2017). An Introduction to Statistical Learning (8th ed.). Springer Science+Business Media New York. ISBN 978-1-4614-7138-7

Janssens, I. A., Freibauer, A., Ciais, P., Smith, P., Nabuurs, G. J., Folberth, G., Schlamadinger, B., Hutjes, R. W. A., Ceulemans, R., Schulze, E. D., Valentini, R., and Dolman, A. J.: Europe's terrestrial biosphere absorbs 7 to 12% ofeuropean anthropogenic CO2 emissions, Science, 300, 1538–1542, 2003

Jiang, Yu. "Comparison of the Water Quality between the Surface Microlayer and Subsurface Water in Typical Water Bodies in Sichuan." Journal of Water Resource and Protection 2010 (2010).

Johnson W.P., Bao G., John W.W. Specific UV absorbance of Aldrich humic acid: changes during transport in aquifer sediment. Environ. Sci. Technol. 36(4), 608, 2002.

Joos, F. and Spahni, R.: Rates of change in natural and anthropogenic radiative forcing over the past 20,000 years, P. Natl. Acad. Sci. USA, 105, 1425–1430, https://doi.org/10.1073/pnas.0707386105, 2008.

Kalbitz, K., Schmerwitz, J., Schwesig, D., and Matzner, E.: Biodegradation of soil-derived dissolved organic matter as related to its properties, Geoderma, 113, 273–291, 2003.

Karanfil T., Schlautman M.A., Erdogan I. Survey of DOC and UV measurement practices with implications for SUVA determination. JAWWA 94(12), 68, 2002.

Kempe, S. 1979. Carbon in the freshwater cycle, p. 317–342. In B. Bolin, E. T. Degens, S. Kempe, and P. Ketner [ed.], The global carbon cycle. Wiley.

Kicklighter, D.W., Hayes, D. J., McClelland, J.W., Peterson, B. J., McGuire, A. D., and Melillo, J. M.: Insights and issues with simulating terrestrial DOC loading of Arctic river networks, Ecol. Appl., 23, 1817–1836, 2013.

Kindler, R., Siemens, J., Kaiser, K., Walmsley, D. C., Bernhofer, C., Buchmann, N., Cellier, P., Eugster, W., Gleixner, G., Grunwald, T., Heim, A., Ibrom, A., Jones, S. K., Jones, M., Klumpp, K., Kutsch, W., Larsen, K. S., Lehuger, S., Loubet, B., Mckenzie, R., Moors, E., Osborne, B., Pilegaard, K., Rebmann, C., Saunders, M., Schmidt, M. W. I., Schrumpf, M., Seyfferth, J., Skiba, U., Soussana, J.-F., Sutton, M. A., Tefs, C., Vowinckel, B., Zeeman, M. J., and Kaupenjohann, M. Dissolved carbon leaching from soil is a crucial component of the net ecosystem carbon balance, Glob. Change Biol., 17, 1167–1185, https://doi.org/10.1111/j.1365-486.2010.02282.x, 2011.

Köchy, M., Hiederer, R., & Freibauer, a. (2015). Global distribution of soil organic carbon – Part 1: Masses and frequency distributions of SOC stocks for the tropics, permafrost regions, wetlands, and the world. Soil, 1(1), 351–365. https://doi.org/10.5194/soil-1-351-2015.

Koehler, B., VonWachenfeldt, E., Kothawala, D. N. & Tranvik, L. J. Reactivity continuum of dissolved organic carbon decomposition in lake water. J. Geophys. Res. 117, G01024 (2012)

Köhler, S., Buffam, I., Jonsson, A. & Bishop, K. Photochemical and microbial processing of stream and soil water dissolved organic matter in a boreal forested catchment in northern Sweden. Aquat. Sci. 64, 269–281 (2002).

Kramer K, Leinonen I, Bartelink HH et al. (2002) Evaluation of six process-based forest growth models using eddy-covariance measurements of CO(2) and H(2)O fluxes at six forest sites in Europe. Global Change Biology, 8, 213–230.

Krinner, G. et al. A dynamic global vegetation model for studies of the coupled atmosphere-biosphere system. Global Biogeochem. Cycles 19, 1–33 (2005).

Langenheder, S., Kisand, V., Wikner, J. & Tranvik, L. J. Salinity as a structuring factor for the composition and performance of bacterioplankton degrading riverine DOC. FEMS Microbiol. Ecol. 45, 189–202 (2003).

Lapierre, J.-F., Guillemette, F., Berggren, M. & del Giorgio, P.A. Increases in terrestrially derived carbon stimulate organic carbon processing and CO2 emissions in boreal aquatic ecosystems. Nat. Commun., 4, (2013).

Laruelle, G. G., Landschützer, P., Gruber, N., Tison, J.-L., Delille, B., and Regnier, P.: Global high-resolution monthly pCO2 climatology for the coastal ocean derived from neural network interpolation. Biogeosciences, 14, 4545-4561 (2017). doi: 10.5194/bg-14-4545-2017

Lauerwald, R., G. G. Laruelle, J. Hartmann, P. Ciais, and P. A. G. Regnier (2015), Spatial patterns in CO2 evasion from the global river network, Global Biogeochem. Cycles, 29, doi: 10.1002/2014GB004941.

Lauerwald, R., Hartmann, J., Ludwig, W. & Moosdorf, N. Assessing the nonconservative fluvial fluxes of dissolved organic carbon in North America. J. Geophys. Res. 117, G01027 (2012).

Lauerwald, R., Regnier, P., Camino-Serrano, M., Guenet, B., Guimberteau, M., Ducharne, A., Ciais, P. (2017). ORCHILEAK (revision 3875): a new model branch to simulate carbon transfers along the terrestrial--aquatic continuum of the Amazon basin. Geoscientific Model Development, 10(10), 3821–3859. https://doi.org/10.5194/gmd-10-3821-2017.

Lauerwald,R.,Regnier, P.,Guenet,B., Friedlingstein, P;Ciais, P: How simulations of the land carbon sink are biased by ignoring fluvial carbon transfers –A case study for the Amazon basin, Volume 3, Issue 2, 21 August 2020, Pages 226-236 https://doi.org/10.1016/j.oneear.2020.07.009

Le Quéré, C., Andrew, R. M., Friedlingstein, P., Sitch, S., Pongratz, J., Manning, A. C., Korsbakken, J. I., Peters, G. P., Canadell, J. G., Jackson, R. B., Boden, T. A., Tans, P. P., Andrews, O. D., Arora, V. K., Bakker, D. C. E., Barbero, L., Becker, M., Betts, R. A., Bopp, L., Chevallier, F., Chini, L. P., Ciais, P., Cosca, C. E., Cross, J., Currie, K., Gasser, T., Harris, I., Hauck, J., Haverd, V., Houghton, R. A., Hunt, C. W., Hurtt, G., Ilyina, T., Jain, A. K., Kato, E., Kautz, M., Keeling, R. F., Klein Goldewijk, K., Körtzinger, A., Landschützer, P., Lefèvre, N., Lenton, A., Lienert, S., Lima, I., Lombardozzi, D., Metzl, N., Millero, F., Monteiro, P. M. S., Munro, D. R., Nabel, J. E. M. S., Nakaoka, S., Nojiri, Y., Padin, X. A., Peregon, A., Pfeil, B., Pierrot, D., Poulter, B., Rehder, G., Reimer, J., Rödenbeck, C., Schwinger, J., Séférian, R., Skjelvan, I., Stocker, B. D., Tian, H., Tilbrook, B., Tubiello, F. N., van der Laan-Luijkx, I. T., van der Werf, G. R., van Heuven, S., Viovy, N., Vuichard, N., Walker, A. P., Watson, A. J., Wiltshire, A. J., Zaehle, S., and Zhu, D.: Global Carbon Budget 2017, Earth Syst. Sci. Data, 10, 405–448, https://doi.org/10.5194/essd-10-405-2018, 2018.

Le Quéré, C., Moriarty, R., Andrew, R. M., Peters, G. P., Ciais, P., Friedlingstein, P., Jones, S. D., Sitch, S., Tans, P., Arneth, A., Boden, T. A., Bopp, L., Bozec, Y., Canadell, J. G., Chini, L. P., Chevallier, F., Cosca, C. E., Harris, I., Hoppema, M., Houghton, R. A., House, J. I., Jain, A. K., Johannessen, T., Kato, E., Keel- ing, R. F., Kitidis, V., Klein Goldewijk, K., Koven, C., Landa, C. S., Landschützer, P., Lenton, A., Lima, I. D., Marland, G., Mathis, J. T., Metzl, N., Nojiri, Y., Olsen, A., Ono, T., Peng, S., Peters,W., Pfeil, B., Poulter, B., Raupach, M. R., Regnier, P., Rö- denbeck, C., Saito, S., Salisbury, J. E., Schuster, U., Schwinger, J., Séférian, R., Segschneider, J., Steinhoff, T., Stocker, B. D., Sutton, A. J., Takahashi, T., Tilbrook, B., van der Werf, G. R., Viovy, N.,Wang, Y.-P.,Wanninkhof, R.,Wiltshire, A., and Zeng, N.: Global carbon budget 2014, Earth Syst. Sci. Data, 7, 47–85, https://doi.org/10.5194/essd-7-47-2015, 2015.

Lehner, B., Verdin, K. & Jarvis, A. New global hydrography derived from spaceborne elevation data. Eos 89, 93–94 (2008)

Leifeld, J., & Menichetti, L. (2018). The underappreciated potential of peatlands in global climate change mitigation strategies /704/47/4113 /704/106/47 article. Nature Communications, 9(1). https://doi.org/10.1038/s41467-018-03406-6

Leopold, Luna B., M. G. Wolman, and J. P. Miller. "Fluvial processes in geomorphology WH Freeman and Co." San Francisco 522pp (1964).

Li, M., Peng, C., Zhou, X., Yang, Y., Guo, Y., Shi, G., & Zhu, Q. (2019). Modeling global riverine DOC flux Li, M., Peng, C., Zhou, X., Yang, Y., Guo, Y., Shi, G., & Zhu, Q. (2019). Modeling global riverine DOC flux dynamics from 1951 to 2015. Journal of Advances in Modeling Earth Systems, 11, 514–530. https://doi.org/10.1002/2018MS001363

Lindroth, A., Tranvik, L. Accounting for all territorial emissions and sinks is important for development of climate mitigation policies. Carbon Balance Manage 16, 10 (2021). https://doi.org/10.1186/s13021-021-00173-8

Liss, P. S., et al. "Report of group I–physical processes in the microlayer and the air-sea exchange of trace gases." The sea surface and global change. Cambridge University Press, Cambridge, p1 (1997).

Liu, Qing, et al. "Comparison of the water quality of the surface microlayer and subsurface water in the Guangzhou segment of the Pearl River, China." Journal of Geographical Sciences 24.3 (2014): 475-491.

Livingstone, D. A. 1963. Chemical composition of rivers and lakes. U.S. Government Printing Office

Lu X, Jaffe R (2001) Interaction between Hg(II) and natural dissolved organic matter: a fluorescence spectroscopy based study. Water Res 35:1793–1803

Ludwig, W., Probst, J.-L. & Kempe, S. 1996. Predicting the oceanic input of organic carbon by continental erosion. Global Biogeo- chemical Cycles 10, 23–41.

Luijendijk, E., Gleeson, T. & Moosdorf, N. Fresh groundwater discharge insignificant for the world's oceans but important for coastal ecosystems. Nature Communications 11, 1260 (2020).

Lv, S., Wang, F., Yan, W. et al. DOC fluorescence properties and degradation in the Changjiang River Network, China: implications for estimating in-stream DOC removal. Biogeochemistry 145, 255–273 (2019). https://doi.org/10.1007/s10533-019-00603-3

M. C. Peel, B. L. Finlayson, T. A. Mcmahon. Updated world map of the Köppen-Geiger climate classification. Hydrology and Earth System Sciences Discussions, European Geosciences Union, 2007, 4 (2), pp.439-473. ⟨hal-00298818⟩

Maavara, T., Lauerwald, R., Regnier, P., & Van Cappellen, P. (2017). Global perturbation of organic carbon cycling by river damming. Nature Communications, 8(May), 1–10. https://doi.org/10.1038/ncomms15347

Maranger, Roxane, Stuart E. Jones, and James B. Cotner. "Stoichiometry of carbon, nitrogen, and phosphorus through the freshwater pipe." Limnology and Oceanography Letters 3.3 (2018): 89-101.

Marx, A. et al. A review of CO2 and associated carbon dynamics in headwater streams: A global perspective. Rev. Geophys. 55, 560–585 (2017).

Mattsson T., P. Kortelainen, A. Laubel, D. Evans, M. Pujo-Pay, A. Raeike, P. Conan. Export of dissolved organic matter in relation to land use along a European climatic gradient. Sci. Total Environ., 407 (2009), pp. 1967-1976

Mayorga, Emilio & P. Seitzinger, Sybil & Harrison, John & Dumont, Egon & Beusen, A & Bouwman, Alexander & Fekete, Balazs & Kroeze, C & Van Drecht, Gerard. (2010). Global Nutrient Export from WaterSheds 2 (NEWS 2): Model Development and Implementation. Environmental Modelling & Software. 25. 837-853. 10.1016/j.envsoft.2010.01.007.

McDowell, W. H. & Fisher, S. G. Autumnal Processing of Dissolved Organic Matter in a Small Woodland Stream Ecosystem. Ecology 57, 561–569 (1976).

McKnight DM, Boyer EW, Westerhoff PK, Doran PT, Kulbe T, Andersen DT (2001) Spectrofluorimetric characterization of dissolved organic matter for indication of precursor organic material and aromaticity. Limnol Oceanogr 46(1):38–48

Meinshausen, M., Smith, S.J., Calvin, K. et al. The RCP greenhouse gas concentrations and their extensions from 1765 to 2300. Climatic Change 109, 213 (2011). https://doi.org/10.1007/s10584-011-0156-z

Mendonça, R., Müller, R.A., Clow, D. et al. Organic carbon burial in global lakes and reservoirs. Nat Commun 8, 1694 (2017). https://doi.org/10.1038/s41467-017-01789-6

Meybeck, M. 1982. Carbon, nitrogen, and phosphorus trans- port by world rivers. Am. J. Sci. 282: 401–450. doi: 10.2475/ajs.282.4.401

Meybeck, M. 1993a Riverine transport of atmospheric carbon: sources, global typology and budget. Water, Air and Soil Pollution 70, 443–463.

Meybeck, M. 1993b C, N, P and S in rivers: from sources to global inputs. In Interactions of C, N, P and S Biogeochemical cycles and global change (Wollast, R., Mackenzie, F. T. & Chou, L., eds). NATO ASI Series, 14. Springer-Verlag, Berlin, pp. 163–191.

Michalzik B., Kalbitz K., Park J.H. and Matzner E. 2001. Fluxes and concentrations of dissolved organic carbon and nitrogen – a synthesis for temperate forests. Biogeochemistry 52: 173–205

Middelburg, J. J. (1989), A simple rate model for organic matter decomposition in marine sediments, Geochim. Cosmochim. Acta, 53, 1577–1581, doi:10.1016/0016-7037(89)90239-1

Moore, T. R., de Souza, W., and Koprivnjak, J.-F.: Controls on the sorption of dissolved organic carbon by soils, Soil Sci., 154, 120– 129, 1992.

Nakhavali, M., Friedlingstein, P., Lauerwald, R., Tang, J., Chadburn, S., Camino-Serrano, M., Guenet, B., Harper, A., Walmsley, D., Peichl, M., and Gielen, B.: Representation of dissolved organic carbon in the JULES land surface model (vn4.4_JULES-DOCM), Geosci. Model Dev., 11, 593–609, https://doi.org/10.5194/gmd-11-593-2018, 2018.

Nakhavali, M., Lauerwald, R., Regnier, P., Guenet, B., Chadburn, S., & Friedlingstein, P. (2021). Leaching of dissolved organic carbon from mineral soils plays a significant role in the terrestrial carbon balance, (June 2020), 1083–1096. https://doi.org/10.1111/gcb.15460.

Nash, J. E. and Sutcliffe, J. V.: River flow forecasting through con-ceptual models, Part I - A discussion of principles, J. Hydrol., 10,282–290, 1970.

Neff J.C. and Asner G.P. 2001. Dissolved organic carbon in terrestrial ecosystems: a synthesis and a model. Ecosystems 4: 29–48.

Olson, J. S. (1963), Energy storage and the balance of producers and decomposers in ecological systems, Ecology, 44(2), 322–331, doi:10.2307/1932179.

Parton, W. J., Stewart, J. W., and Cole, C. V.: Dynamics of C, N, P and S in grassland soils: a model, Biogeochemistry, 5, 109–131, https://doi.org/10.1007/bf02180320, 1988.

Peacock, M., Freeman, C., Gauci, V., Lebron, I., Evans, C.D., 2015. Investigations of freezing and cold storage for the analysis of peatland dissolved organic carbon (DOC) and absorbance properties. Environ. Sci.: Processes Impacts 17, 1290–1301. http://dx.doi.org/10.1039/C5EM00126A.

Peng, S., Ciais, P., Maignan, F., Li, W., Chang, J., Wang, T., and Yue, C.: Sensitivity of land use change emission estimates to historical land use and land cover mapping, Global Biogeochem. Cy., 31, 626–643, https://doi.org/10.1002/2015GB005360, 2017.

Polcher, J.: Les processus de surface à l'échelle globale et leurs interactions avec l'atmosphère, Habilitation à diriger des recherches, University Pierre et Marie Curie, Paris, France, 2003.

Ran, L., Butman, D.E., Battin, T.J. et al. Substantial decrease in CO2 emissions from Chinese inland waters due to global change. Nat Commun 12, 1730 (2021). https://doi.org/10.1038/s41467-021-21926-6

Ran, L., Lu, X. X., Sun, H., Han, J., Li, R., & Zhang, J. (2013). Spatial and seasonal variability of organic carbon transport in the Yellow River, China. Journal of Hydrology, 498, 76-88.

Raymond PA, Saiers JE (2010) Event controlled DOC export from forested watersheds. Biogeochemistry 100(1–3):197–209

Raymond, P. A., Hartmann, J., Lauerwald, R., Sobek, S., McDonald, C., Hoover, M., .. . Guth, P. (2013). Global carbon dioxide emissions from inland waters. Nature, 503(7476), 355–359. Retrieved from https://doi.org/10.1038/nature12760

Raymond, Peter A., et al. "Scaling the gas transfer velocity and hydraulic geometry in streams and small rivers." Limnology and Oceanography: Fluids and Environments 2.1 (2012): 41-53.

Raymond. Peter A., Hartmann. Jens, Lauerwald. Ronny, Sobek. Sebastian, McDonald. Cory, Hoover. Mark, Butman. David, Striegl. Robert, Mayorga. Emilio, Humborg. Christoph, Kortelainen. Pirkko, Dürr. Hans, Meybeck. Michel, Ciais, Philippe, Guth, Peter : Global carbon dioxide emissions from inland waters Nature (2013) 503-355. Doi : 10.1038/nature12760

Regnier, P., Friedlingstein, P., Ciais, P., Mackenzie, F. T., Gruber, N., Janssens, I. A., Laruelle, G. G., Lauerwald, R., Luyssaert, S., Andersson, A. J., Arndt, S., Arnosti, C., Borges, A. V., Dale, A. W., Gallego-Sala, A., Goddéris, Y., Goossens, N., Hartmann, J., Heinze, C., Ilyina, T., Joos, F., Larowe, D. E., Leifeld, J., Meysman, F. J. R., Munhoven, G., Raymond, P. A., Spahni, R., Suntharalingam, P., and Thullner, M.: Anthropogenic perturba- tion of the carbon fluxes from land to ocean, Nat. Geosci., 6, 597–607, https://doi.org/10.1038/ngeo1830, 2013.

Reynolds, C., Jackson, T. & Rawls, W. Estimating available water content by linking 424 the FAO soil map of the world with global soil profile databases and pedo-transfer 425 functions. Am. Geophys. Union Fall Meet. EOS Trans. Spring Meet. Suppl. 80, S132 426 (1999).

Royer, I.; Angers, D. A.; Chantigny, M. H.; Simard, R. R.; Cluis, D. Dissolved organic carbon in runoff and tile-drain water under corn and forage fertilized with hog manure. J. Environ. Qual. 2007, 36, 855–863. doi: 10.2134/jeq2006.0355

Santin C, Yamashita Y, Otero XL, Alvarez MA, Jaffe R (2009) Characterizing humic substances from estuarine soils and sediments by excitation-emission matrix spectroscopy and parallel factor analysis. Biogeochemistry 96:131–147. https://doi.org/10.1007/s10533-009-9349-1

Sarmiento, J.L. and N. Gruber, 2002: Sinks for anthropogenic carbon. Phys. Today, 55, 30-36.

Saxton KE, Rawls WJ, Romberger SJ, Papendick RI (1986) Estimating generalized soil-water characteristics from texture. Soil Science Society of America Journal, 50, 1031–1036.

Schlesinger W.H, Melack J.M.. 1981. Transport of organic carbon in the world's rivers. Tellus 33:172–87.

Schulze, E. D., Ciais, P.,Luyssaert, S.,Schrumpf, M.,Janssens, I. A.,Thiruchittampalam, B.,Theloke, J.,Saurat, M.,Bringezu, S.,Lelieveld, J.,Lohila, A.,Rebmann, C.,Jung, M.,Bastviken, D.,Abril, G.,Grassi, G.,Leip, A.,Freibauer, A.,Kutsch, W.,Don, A.,Nieschulze, J.,BÖRNER, A.,Gash, J. H.,Dolman, A. J : The European carbon balance. Part 4: Integration of carbon and other trace-gas fluxes. Global Change Biology (2010) 16, 1451–1469, doi: 10.1111/j.1365-2486.2010.02215.x

Singh, S., Dutta, S., and Inamdar, S.: Land application of poultry manure and its influence on spectrofluorometric characteristics of dissolved organic matter, Agriculture, Ecosystems and Environment, 193, 25–36, https://doi.org/10.1016/j.agee.2014.04.019, 2014.Zhang, H., Goll, D. S., Manzoni, S., Ciais, P., Guenet, B., and Huang, Y.: Modeling the effects of litter stoichiometry and soil mineral N availability on soil organic matter formation using CENTURY-CUE (v1.0), Geosci. Model Dev., 11, 4779–4796, https://doi.org/10.5194/gmd-11-4779-2018, 2018.

Sitch, S. et al. (2003), Evaluation of ecosystem dynamics, plant geography and terrestrial carbon cycling in the LPJ dynamic global vegetation model, Glob. Chang. Biol., 9(2), 161–185, doi:10.1046/j.1365-2486.2003.00569.x.

Skopinstev, B. A., Recent advances in the study of organic matter in oceans, Oceanology, 11, 775-789, 1971.

Smith P., M. Bustamante, H. Ahammad, H. Clark, H. Dong, E. A. Elsiddig, H. Haberl, R. Harper, J. House, M. Jafari,O. Masera,C. Mbow, N. H. Ravindranath, C. W. Rice, C. Robledo Abad, A. Romanovskaya, F. Sperling, and F. Tubiello, 2014: Agriculture, Forestry and Other Land Use (AFOLU). In: Climate Change 2014: Mitigation of Climate Change. Contribution of Working Group III to the Fifth Assessment Report of the Intergovernmental Panel on Climate Change [Edenhofer,O.,R. Pichs-Madruga, Y. Sokona, E. Farahani, S. Kadner, K. Seyboth, A. Adler, I. Baum, S. Brunner, P. Eickemeier,B.Kriemann,J. Savolainen, S. Schlömer, C. von Stechow, T. Zwickel and J.C. Minx (eds.)]. Cambridge University Press, Cambridge, United Kingdom and New York, NY, USA

Smith, J., Gottschalk, P., Bellarby, J., Chapman, S., Lilly, A., Tow- ers, W., Bell, J.,

Coleman, K., Nayak, D., Richards, M., Hillier, J., Flynn, H., Wattenbach, M., Aitkenhead, M., Yeluripurti, J., Farmer, J., Milne, R., Thomson, A., Evans, C., and Smith, P.: Estimating changes in national soil carbon stocks using ECOSSE – a new model that includes upland organic soils. Part II. Application in Scotland, Clim. Res., 45, 193–205, https://doi.org/10.3354/cr00902, 2010.

Soares, A.R.A., Lapierre, JF., Selvam, B.P. et al. Controls on Dissolved Organic Carbon Bioreactivity in River Systems. Sci Rep 9, 14897 (2019). https://doi.org/10.1038/s41598-019-50552-y.

Soballe, D. M., and B. L. Kimmel. "A large-scale comparison of factors influencing phytoplankton abundance in rivers, lakes, and impoundments." Ecology 68.6 (1987): 1943-1954.

Stallard RF. 1998. Terrestrial sedimentation and the C cycle: coupling weathering and erosion to carbon storage. Global Biogeochem Cycles 12:231–7.

Stubbins A, Lapierre JF, Berggren M, Prairie YT, Dittmar T, del Giorgio PA (2014) What's in an EEM? Molecular signatures associated with dissolved organic fluorescence in boreal Canada. Environ Sci Technol 48:10598–10606. https://doi.org/10.1021/es502086e

Suchet PA, Probst JL. 1995. A global model for present-day atmospheric/soil CO2-consumption by chemical erosion of continental rocks (GEM-CO2). Tellus 47B:273–280.

Sun, Y., Goll, D. S., Chang, J., Ciais, P., Guenet, B., Helfenstein, J., Huang, Y., Lauerwald, R., Maignan, F., Naipal, V., Wang, Y., Yang, H., and Zhang, H.: Global evaluation of the nutrient-enabled version of the land surface model ORCHIDEE-CNP v1.2 (r5986), Geosci. Model Dev., 14, 1987–2010, https://doi.org/10.5194/gmd-14-1987-2021, 2021.

Swietlik, J., and E. Sikorska. "Characterization of natural organic matter fractions by high pressure size-exclusion chromatography, specific UV absorbance and total luminescence spectroscopy." Polish Journal of Environmental Studies 15.1 (2006): 145.

Tian, H., Q. Yang, R. G. Najjar, W. Ren, M. A. M. Friedrichs, C. S. Hopkinson, and S. Pan (2015), Anthropogenic and climatic influences on carbon fluxes from eastern North America to the Atlantic Ocean: A process-based modeling study, J. Geophys. Res. Biogeosci., 120, 752–772, doi:10.1002/ 2014JG002760.

Tiwari, T., Laudon, H., Beven, K. & Ågren, A. M. Downstream changes in DOC: Inferring contributions in the face of model uncertainties. Water Resour. Res. 50, 514–525 (2014).

Tranvik, L. J., Downing, J. A., Cotner, J. B., Loiselle, S. A., Striegl, R. G., Ballatore, T. J.,

Dillon, P., Finlay, K., Fortino, K., Knoll, L. B., Kortelainen, P. L., Kutser, T., Larsen, S., Laurion, I., Leech, D. M., McCallister, S. L., McKnight, D. M., Melack, J. M., Over- holt, E., Porter, J. A., Prairie, Y., Renwick, W. H., Roland, F., Sherman, B. S., Schindler, D.W., Sobek, S., Tremblay, A.,Vanni, M. J., Verschoor, A. M., vonWachenfeldt, E., and Weyhenmeyera, G. A.: Lakes and reservoirs as regulators of carbon cycling and climate, Limnol. Oceanogr., 54, 2298–2314, 2009.

Tranvik, L. J., J. A. Downing, J. B. Cotner, S. A. Loiselle, R. G. Striegl, T. J. Ballatore, P. Dillon, K. Finlay, K. Fortino, and L. B. Knoll (2009), Lakes and reservoirs as regulators of carbon cycling and climate, Limnol. Oceanogr., 54(6_part_2), 2298–2314, doi:10.4319/lo.2009.54.6_part_2.2298.

Turgeon, J.: Production and biodegradation of dissolved carbon, nitrogen and phosphorus from Canadian forest floors, McGill University, 2008.

Turner D.P., W.D. Ritts, W.B. Cohen, S.T. Gower, S.W. Running, M. Zhao, M.H. Costa, A.A. Kirschbaum, J.M. Ham, S.R. Saleska, D.E. Ahl. Evaluation of MODIS NPP and GPP products across multiple biomes. Remote Sens. Environ., 102 (3-4) (2006), pp. 282-292, 10.1016/j.rse.2006.02.017

UNFCCC. National greenhouse gas inventory data for the period 1990–2019. https://di.unfccc.int/global_map_content/map/index.html?year=growth_base_final&gas=Aggregate_GHGs&sector=to&zoom=2&lat=30&lng=15

Vähätalo, A. V., H. Aarnos, and S. Mäntyniemi (2010), Biodegradability continuum and biodegradation kinetics of natural organic matter described by the beta distribution, Biogeochemistry, 100(1), 227–240, doi:10.1007/s10533-010-9419-4.

Van Vliet MTH, Zwolsman JJG. Impact of summer droughts on the water quality of the Meuse river. J Hydrol 2008;353:1–17.

Verpoorter, C., Kutser, T., Seekell, D. A., & Tranvik, L. J. (2014). A global inventory of lakes based on high-resolution satellite imagery. Geo- physical Research Letters, 41(18), 6396–6402. https://doi.org/10. 1002/2014GL060641

Vinther FP, Hansen EM, Eriksen J (2006) Leaching of soil organic carbon and nitrogen in sandy soils after cultivating grass-clover swards. Biology and Fertility of Soils, 43, 12–19.

Vorosmarty, C. J., B. M. Fekete, M. Meybeck, and R. B. Lammers, Geo- morphometric attributes of the global system of rivers at 30-minute spa- tial resolution, J. Hydrol., 237, 17–39, 2000.

Vuichard et al., 2018, Accounting for Carbon and Nitrogen interactions in the Global Terrestrial Ecosystem Model ORCHIDEE (trunk version, rev 4999): multi-scale evaluation of gross primary production. Geosci. Model Dev. Discuss.,

https://doi.org/10.5194/gmd-2018-261

Wada S et al (2008) Bioavailability of macroalgal dissolved organic matter in seawater. Mar Ecol Prog Ser 370:33–44. https://doi.org/10.3354/meps07645

Watson, K., Farré, M.J., Leusch, F.D.L., Knight, N., 2018. Using fluorescence-parallel factor analysis for assessing disinfection by-product formation and natural organic matter removal efficiency in secondary treated synthetic drinking waters. Sci. Total Environ. 640–641, 31–40.

Webb, J.R., Santos, I.R., Maher, D.T. et al. The Importance of Aquatic Carbon Fluxes in Net Ecosystem Carbon Budgets: A Catchment-Scale Review. Ecosystems 22, 508–527 (2019). https://doi.org/10.1007/s10021-018-0284-7

Weedon, G. P., G. Balsamo, N. Bellouin, S. Gomes, M. J. Best, and P. Viterbo (2014), The WFDEI meteorological forcing data set: WATCH Forcing Data methodology applied to ERA-Interim reanalysis data, Water Resour. Res., 50, 7505–7514, doi:10.1002/2014WR015638.

Weishaar, J. L., Aiken G. R., Bergamaschi B. A., Fram M. S., Fugii R., and Mopper K. 2003. Evaluation of specific ultraviolet absorbance as an indicator of the chemical composition and reactivity of dissolved organic carbon. Environ. Sci. Technol. 37: 4702–4708.

Westrich, J.T., Berner, R.A., 1984. The role of sedimentary organic matter in bacterial sul- fate reduction — the G model tested. Limnology and Oceanography 29, 236–249.

Wickland, Kim P., et al. "Biodegradability of dissolved organic carbon in the Yukon River and its tributaries: Seasonality and importance of inorganic nitrogen." Global Biogeochemical Cycles 26.4 (2012).

Wollheim, W.M., Stewart, R.J., Aiken, G.R., Butler, K.D., Morse, N.B., Salisbury, J., 2015.Removal of terrestrial DOC in aquatic ecosystems of a temperate river network.Geophysical Research Letters 42, 6671–6679.

Worrall F. , Davies H., Bhogal A., Lilly A., Evans M.G. , Turner K., Burt T.P., Barraclough D. , Smith P. , Merrington G. The flux of DOC from the UK – predicting the role of soils, land use and in-stream losses. J. Hydrol., 448–449 (2012), pp. 149-160

Worrall, F., and T. P. Burt (2007), Flux of dissolved organic carbon from U.K. rivers, Global Biogeochem. Cycles, 21, GB1013, doi:10.1029/2006GB002709.

Wurl, Oliver, and Jeffrey Phillip Obbard. "A review of pollutants in the sea-surface microlayer (SML): a unique habitat for marine organisms." Marine pollution bulletin 48.11-12 (2004): 1016-1030.

Zhang, B., Tian, H., Lu, C., Dangal, S. R. S., Yang, J., and Pan, S.: Global manure nitrogen production and application in cropland during 1860–2014: a 5 arcmin gridded global dataset for Earth system modeling, Earth Syst. Sci. Data, 9, 667–678, https://doi.org/10.5194/essd-9-667-2017, 2017.

Zhang, H., Lauerwald, R., Regnier, P., Ciais, P., Yuan, W., Naipal, V., et al. (2020). Simulating erosion-induced soil and carbon delivery from uplands to rivers in a global land surface model. Journal of Advances in Modeling Earth Systems, 12, e2020MS002121. https://doi.org/10.1029/2020MS002121

Zhao, M., F. A. Heinsch, R. R. Nemani, and S. W. Running (2005), Improvements of the MODIS terrestrial gross and net primary production global data set, Remote Sens. Environ., 95(2), 164–176, doi:10.1016/j.rse.2004.12.011.

7 ANNEXE

7.1 RÉSUMÉ SUPPLÉMENTAIRE

Depuis la révolution industrielle, les émissions de dioxyde de carbone (CO2) dues à l'activité humaine ont fortement augmenté la concentration de carbone dans l'atmosphère, perturbant le cycle naturel du carbone (C). Cette augmentation a un effet direct sur le climat de la Terre et a de nombreuses conséquences telles que l'augmentation de la température, la modification des courants océaniques et l'augmentation du niveau des mers. Pour répondre à cette perturbation anthropogénique, les océans et la biosphère terrestre ont vu leurs stocks de C augmenter, agissant ainsi en tant qu'important atténuateur du changement climatique. La quantification et la compréhension de la variabilité spatiale et temporelle de ces puits océanique et terrestre sont donc essentielles. Une partie du C fixée par la photosynthèse n'est en réalité pas stockée *in-situ* mais est à la place transférée vers les eaux continentales. Cette perte de C terrestre se passe à travers le lessivage du C organique dissous (COD) et du C inorganique dissous (CID) ainsi que par érosion du C organique particulaire (COP). Lors de son passage dans ces eaux, le C peut être minéralisé et réémis vers l'atmosphère sous forme de CO2 et de méthane (CH4) ou enterré dans les sédiments, le reste étant amené jusqu'aux océans. Cependant la quantification et la variabilité spatio-temporelle de ces processus ne sont pas encore tout à fait comprises. Dans ma thèse, j'ai utilisé trois méthodes différentes afin d'améliorer notre compréhension de la dynamique du C dans le réseau hydrographique Européen, en me concentrant sur le destin du COD dans le système hydrographique.

Tout d'abord, j'ai évalué et appliqué ORCHILEAK, un modèle du système terre, à l'échelle Européenne pour estimer et étudier la variabilité spatio-temporelle du transfert du COD des terres jusqu'aux rivières. A ma connaissance, ceci est la première estimation paneuropéenne des flux de DOC à travers l'interface terre-eaux continentales. La performance du modèle est d'abord évaluée avec des observations de transfert de COD des terres jusqu'aux rivières, des observations de flux des COD et de réactivité du COD dans les rivières, permettant de prouver que les transferts de COD simulés sont réalistes. J'ai estimé qu'en moyenne environ 14.3 TgC sont transférés chaque année des terres vers le système hydrographique européen, ce qui représente environ 0.6% de la productivité primaire terrestre nette (NPP). J'ai observé également une importante variabilité spatio-temporelle avec un maximum en hiver et un minimum en été sauf dans les régions nordiques où le maximum a lieu au printemps lors de la fonte des neiges. J'ai étudié le lien entre la quantité de COD transféré des terres vers les rivières et différentes variables environnementales et mes résultats montrent que la fraction de NPP qui est transférée en tant que COD dans les rivières est principalement contrôlée par le ruissellement et le ratio de ruissellement de surface par

rapport au drainage alors que la température ne joue seulement qu'un rôle secondaire.
Ensuite, j'ai effectué des campagnes d'échantillonnage sur la Meuse en France et en Belgique afin d'étudier la biodégradation du COD dans un bassin tempéré. Pour cela, j'ai réalisé des expériences à l'échelle mensuelle en laboratoire et étudié comment la constante de vitesse de dégradation du COD (k) varie à travers les saisons, en fonction de l'occupation du sol du bassin ainsi que sa dépendance vis-à-vis de la qualité de la matière organique (MO). La qualité de l'MO est mesurée à l'aide du SUVA, l'absorbance ultraviolette spécifique à 254 nm, qui mesure l'aromaticité de l'MO. La biodégradation du COD est représentée une cinétique d'ordre 1 (FO), une cinétique d'ordre 1 avec une partie du COD considérée comme non-dégradable (FOR) et le modèle « reactive continuum » (RC). J'ai démontré que la méthode FO ne permet pas de bien représenter l'évolution de la concentration de carbone dans le temps à l'échelle mensuelle. Au contraire, la méthode FOR capture bien la cinétique de dégradation et, j'ai estimé un temps de demi-vie pour le COD à environ 10 jours, valeur inférieure au temps de résidence de l'eau de la Meuse estimé sur tout le bassin à 24 jours, ce qui signifie que la majorité du COD aura été décomposée avant d'atteindre la mer.
Cependant, la variabilité observée du k ne peut être expliquée par les variables étudiées (saisons, occupation du sol et le SUVA). La méthode RC permet tout autant de bien capturer la cinétique, et j'ai calculé un k initial qui vaut environ 0.02 jour-1 mais avec une importante variabilité. Cette variabilité dans k n'a pas pu être reliée avec les saisons ou l'occupation des sols mais une corrélation significative (R^2=0.5) a pu être trouvée entre le k du modèle RC et le SUVA, suggérant que cet index, facile et rapide à mesurer, pourrait être utilisé comme proxy pour la dégradation du COD.

Finalement, sur base de la littérature, j'ai construit un budget C pour les eaux continentales européennes et étudié comment les flux transnationaux de C à travers les rivières peuvent impacter les budgets et inventaires nationaux de C. Une méthodologie a été développée pour la quantification des transferts latéraux de C à travers les frontières et j'ai estimé que sur toute l'Europe en moyenne environ 2.3 gC m-2 an-1 sont importés d'un pays vers un autre et 4.4 gC m-2 an-1 sont exportés d'un pays vers un autre ou vers la mer, entraînant pour l'Europe, un budget net de C dans les rivières (RNCB) de 2.1 gC m-2 an-1. A l'exception des Pays-Bas, du Portugal, de l'Estonie et de l'Ukraine, tous les pays ont un RNCB positif, ils exportent plus de C qu'ils n'en n'importent dû aux apports de C des terres vers les rivières au sein du pays lui-même. J'ai comparé le RNCB avec d'autres composants du budget national de C et plus particulièrement aux flux latéraux de C attribués aux échanges de récoltes de bois et d'agriculture entre pays. J'ai montré que la moitié des pays européens ont un RNCB qui vaut plus de 10% que les échanges de récoltes et un quart plus de 30% montrant que le RNCB devrait être intégré dans les budgets nationaux de C. Dans le futur, notre méthodologie pourrait être appliquée à d'autres régions du globe et uniquement sur la partie anthropogénique du RNCB.